ATTRITION OF PARTICULATE SOLIDS

by

B.K.PARAMANATHAN

Keble College, Oxford

A thesis submitted for the degree of

Doctor of Philosophy at the

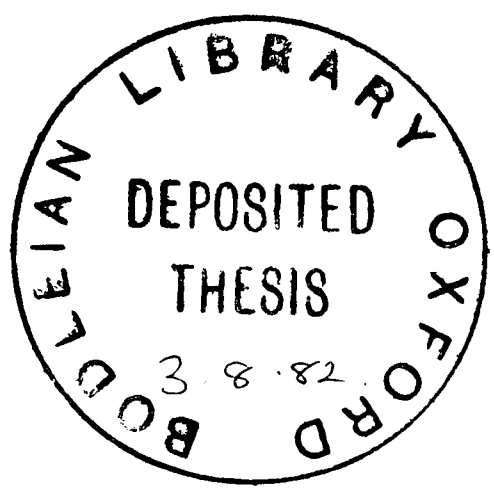
University of Oxford

Michaelmas 1981

Department of Engineering Science,

Parks Road,

Oxford.



To My Parents

ABSTRACT

Attrition of Particulate Solids

B K Paramanathan

Keble College

A thesis submitted for the degree of Doctor of Philosophy

at the University of Oxford.

Michaelmas 1981

Attrition occurs during the transport and storage of particles and leads to loss of material through dust formation and to environmental pollution. Standard tests are all specifically designed to cater for particular needs and are often indicators of relative hardness than of attrition rates. Since little progress has been made into understanding the mechanisms of attrition, the purpose here is to study one of the basic processes that determines the rate of grinding. The aim is thus to establish a fundamental framework within which past work and future developments can be assessed.

An annular attrition cell was designed, constructed and commissioned to permit one of the mechanisms of attrition, namely that in failure zones of deforming solids, to be considered in isolation. Sample weights of 100 gm were more than sufficient and the results were found to be reproducible, systematic and generally independent of sample size.

Several close-sized material in the size range 250-2000 μm of various shapes were studied including different grades of sodium chloride, sodium carbonate and molecular sieve beads. The mode of attrition, bodily fracture or surface grinding, was easily verified by microscopic examination of attrited product. Results followed Gwyn's empirical law $W = K_p t^m$ where W denotes the weight fraction attrited, t time and K_p, m are characterising parameters.

The reliable data permitted the development of simple kinetic models. One supposes first order loss of coarse material, another that attrition rate is dependent on radius reduction. It may be argued that the former applies to a fracturing mechanism, the latter to a surface grinding process. The first order approach has to be modified to allow for the initial high rate of attrition; the second model may be reduced to the Gwyn form.

The attrition cell is useful in characterising materials; it should, in future, permit assessment of equipment performance.

ACKNOWLEDGEMENTS

I wish to express my sincere thanks to my supervisor, Professor J Bridgwater, for giving me the privilege of his guidance, encouragement and patience throughout the course of this work.

I would like to thank Mr R A Ducker for his skill and enthusiasm in constructing the experimental equipment, and Mr S Walton for general maintenance.

I am grateful to the Science Research Council and ICI Mond Division for their financial support.

I am also indebted to Mr M N Nevin, Dr N Rolfe and Mr A I Thompson of ICI Mond Division for their helpful comments during frequent discussions and especially for their assistance in the preparation of the thesis.

I would also like to thank Mr R Bahu of AERE Harwell for making available the Silica Gel results.

Finally, I would like to thank Sharmini for all her help and for having been an enjoyable companion these last few years.

CONTENTS

		PAGE
CHAPTER 1	INTRODUCTION AND LITERATURE SURVEY	1
CHAPTER 2	THE ANNULAR ATTRITION CELL	30
	2.1 Equipment Selection	30
	2.2 Cell Design and Construction	32
	2.3 Control System	36
	2.4 Cell Operation	37
	2.5 Materials Used	38
	2.6 Experimental Procedure	38
	2.7 Sieving	39
	2.8 The Failure Zone	41
CHAPTER 3	MOLECULAR SIEVE	42
	3.0 Introduction	42
	3.1 Reproducibility	42
	3.2 Effect of Cell Revolutions or Shear Strain	44
	3.3 Effect of Normal Stress	45
	3.4 Effect of Cell Speed	45
	3.5 Effect of Sample Thickness	46
	3.6 Effect of Sample History	48
	3.7 Segregation of Particles	49
	3.8 Results According to Gwyn	50
	3.9 Mechanism of Attrition	51
CHAPTER 4	SODIUM CHLORIDE	53
	4.0 Introduction	53
	4.0.1 Granular Salt	53
	4.0.2 Pure Dried Vacuum Salt (PDV Salt)	54
	4.0.3 Laboratory Salt (Lab Salt)	54

PAGE

4.1 Granular Sodium Chloride 55

4.2 Pure Dried Vacuum Salt (PDV Salt) 61

4.3 Laboratory Salt 65

4.4 Mechanisms of Attrition 66

CHAPTER 5 SODIUM CARBONATE (SODA ASH) 67

5.0 Introduction 67

5.1 Experimental Runs 67

5.1.1 Correction of Data 69

5.2 Mechanism of Attrition 72

CHAPTER 6 THEORY AND DISCUSSION 74

6.1 Summary of Results from Gwyn Plots 74

6.1a Effect of Sample Thickness 75

6.2 Theory 77

6.2.1 Fracture Model (Mass Basis) 78

6.2.2a Surface Abrasion Model (Radius Basis) 82

6.2.2b Surface Abrasion Model (Radius Change Basis) 84

6.3 Effect of Normal Stress 94

CHAPTER 7 CONCLUSION 100

APPENDIX A
APPENDIX B
APPENDIX C
APPENDIX D
APPENDIX E
APPENDIX F

REFERENCES

CHAPTER ONE

INTRODUCTION AND LITERATURE SURVEY

Attrition of particulate solids is a common phenomenon in the chemical and allied industries, yet, despite its importance, little progress has been made in understanding the physical and chemical mechanisms. Consequently, prediction of attrition rates and the design of powder handling equipment relies largely on practical experience rather than on the understanding of basic principles. Undesired attrition in the process industries is both wasteful and expensive, and it is economically desirable to minimise particle degradation. Hence, knowledge of the fundamental principles of attrition would help in the reduction of unwanted damage to particulate solids in industrial environments.

Attrition or wear occurs when the surface of a body is stressed sufficiently to cause loss of material and this could transpire in a number of ways. In reviewing the early literature on sliding wear, Burwell and Strang (1952) report that, although wear rates are published extensively, they were in almost all cases the results on particular industrial materials run in tests designed to simulate specific operations in service. Thus, deducing general laws of wear were not possible and they argue that only two qualitative conclusions could be drawn concerning wear:

(a) wear increases with distance of travel but not linearly

(b) wear decreases with increasing hardness of the rubbing surfaces, but many exceptions can be found

They conclude that the lack of any laws of wear make it difficult to define a 'wear coefficient'. As a result, it was not possible to usefully apply dimensional analysis to such problems which meant that rational estimation of wear in actual machines or from scaled experiments was difficult.

They state that, for frictional wear to occur, two or more bodies needed to be in contact and these contacts were formed by the surface asperities found on each body. Attrition then occurred when these asperity junctions ruptured, giving rise to ground material. There were several ways in which asperity junctions could rupture:

(a) the interface could be weaker than both materials; dissimilar materials of similar hardness, e.g. cast iron on steel

(b) the interface could be stronger than one but weaker than the other, e.g. steel on lead

(c) the interface could be stronger than one but sometimes weaker than the other, e.g. steel on copper

(d) the interface is stronger than both materials; work-hardening on the surface, e.g. steel on steel

The most common methods of wear of metals were either by adhesion or abrasion, although diffusive, corrosive, fatigue and fretting wear were also found in practice. Adhesive wear occurs where the stresses are such that the two metals fuse at the asperities and external forces which cause them to slide cause wear. Abrasive wear occurs where two metals, one softer than the other, come into contact and the asperities present on the harder metal plough into the softer one.

Of these methods, adhesion wear is seen to be the least avoidable (Burwell and Strang, 1952), whereas the others could be eliminated or at least minimised with care in practice or under laboratory conditions.

Investigations have been carried out where attempts were made to link the wear rate to the properties of materials in contact. It was found that the wear rate was influenced by the applied stresses in sliding contact. Thus, surface asperities supported the load in localised regions where the highest asperities were actual contact. These asperities deformed until the area of contact was large enough to support the applied load. Thus the true area of contact between surfaces was much smaller than the apparent one and actual stresses around the actual contact areas correspondingly greater. Early work on the friction of solids indicated that the localised stresses were so high as to cause plastic deformation of the asperities and form areas of contact.

Hertz (1881) found that the deformation of a single spherical protuberance pressed against a flat plate required that if the load was truly elastic, the area of contact A was related to the load N by $A = kN^{2/3}$, where k was a constant depending on the local radius of curvature and elastic constants of the material. From this equation Amontons's laws of friction, which state that the friction is directly proportional to the load but independent of the apparent area of contact, could not follow. On the other hand, if the protuberances were permanently deformed by plastic flow, the total real area of contact would be proportional to the load and $A = N/p_m$, where p_m is the flow pressure of the softer material in contact

(Bowden and Tabor, 1964). An explanation of Amontons's law is thus provided.

When elastic contact of surfaces occurs at many small protuberances, Hertz's equation has to be modified to a more general form $A = k_1 N^n$, where k_1 depends on the assumed form of the surfaces and elastic constants of materials; n also depends on the form of the surfaces and takes a value between 2/3 and 1, depending on the height distribution of protuberances. Only when the asperities lie on a single plane and carry the same proportion of the total load does n equal 2/3. When the load makes the contacts increase in size whilst simultaneously bringing new asperities into contact, n assumes a higher value. Archard (1957) showed that the index, which was 2/3 for a perfectly smooth sphere, becomes 8/9 when one set of protuberances are superposed and 26/27 when two sizes of protuberances are present.

In contrast to a single region of contact, nominally flat surfaces touch at a number of widely separated regions. In the simplest model, a perfectly flat surface is in contact with a surface consisting of a number of spherical surfaces and Archard shows that the actual area of contact is given by $A \alpha N^{4/5}$.

If now an array of spherical protuberances is superposed to give a two scale model, the area of contact becomes $A \alpha N^{14/15}$, and for a three scale model, $A \alpha N^{44/45}$.

Thus, Archard shows that as the models are modified to represent a closer approach to the nature of the real surfaces, the true area of contact becomes very nearly proportional to the load and close conformity to Amontons's law is achieved. For example, Archard

conducted experiments with perspex and showed that Amontons's law was still valid for elastic deformation except when the load was highly concentrated.

Dyson and Hirst (1954) found that increasing the normal load tended to iron out the surface irregularities thus increasing the local number of contacts, rather than increase the size of existing contacts. Experimental corroboration led them to conclude that small asperities may be superposed on longer wavelength undulations and a two scale representation of surface irregularities was needed. Wear experiments suggest that the areas of contact are formed by elastic rather than plastic deformation. Each protuberance may be rubbed many times without being damaged (Burwell and Strang, 1952). Thus when materials of comparable hardness rub together, a protuberance may be plastically deformed at its first encounter with the other surface, but its relaxation would be elastic at its many subsequent encounters with the other surface. Archard's experiments with perspex show that when the load is increased these small protuberances are pressed flat and the multiple contacts merge to form larger areas; the coefficient of friction decreases as is expected if the deformation is elastic rather than plastic. This does not mean that plastic deformation is unimportant, but it is seen that elastic deformation can be consistent with an acceptable approximation to Amontons's law.

Archard (1953) described the wear of surfaces in terms of k which was a probability factor. He assumed that only one of the two surfaces contained asperities and that wear products were formed by lump removal through plastic deformation. He considers a

circle of contact of radius r, and thus of area πr^2, formed by one spherical protuberance. When plastic flow occurs, this contact supports a load $n = \pi r^2 . p_m$, where p_m is the flow pressure of the softer material. He assumed that during an encounter, either no wear particle was formed at all, or if it did, it was roughly hemispherical with a volume of $\frac{2}{3}\pi r^3$. Since the wear particle forms in the sliding distance 2r, wear per unit sliding distance is

$$\frac{1}{2r} \cdot \frac{2}{3}\pi r^3 = \frac{n}{3p_m}$$

As the same relation holds for every contact, total volume W per unit sliding distance is given by

$$W = \frac{N}{3p_m}$$

where N is the total load. If fraction k of encounters contribute to wear

$$W = \frac{kN}{3p_m} = \frac{KN}{p_m}$$

Archard and Hirst (1956) list values of K and hardness (measure of p_m). It is seen that for tungsten and mild steel, whilst the ratio of hardness is only sixfold, the corresponding ratio for K is 7000/1. Thus it would seem that whilst hardness was important in determining wear rates, the factor K is even more so. For fairly clean surfaces, K is of the order of 0.01. For plastic and oxidised surfaces, it could be as low as 10^{-7}.

It can be seen that $W \alpha N$ only when K is a constant. As surfaces rub together, the heat generated often alters the value of K. Thus, in practice, W is only approximately proportional to the load.

Holm (1946) assumed that the real area of contact is formed by the plastic deformation of contacting asperities and considered wear as an atomic process. He shows that the worn volume per unit sliding distance W is given by $W = ZN/p_m$, where Z is the number of atoms removed per atomic encounter and p_m the flow pressure of the material. If it was assumed that the total area of real contact consisted of S spots each of radius r, and considering the worn volume as consisting of p atomic layers removed from the contacting spots, then $Z = p\alpha/2r$, where α is the inter-atomic spacing. His theory could also be presented where the volume of material removed W is given by $W = k \cdot A \cdot L$, where k is the probability of removing an atom, A the true area of contact and L the sliding distance. Since for plastic flow $A = N/p_m$

$$W = (k \cdot N \cdot L)/p_m$$

If A_o is the apparent area of contact

$$h = kPL/p_m$$

where P is the average normal stress over the nominal contact area and h the depth of material removed.

As wear particles are normally removed as aggregates of atoms rather than as individual ones, it would seem that his assumption is not generally valid. However, if his theory is modified to incorporate wear particles rather than single atoms, then his equations involving k become the probability of removing a wear particle per unit distance of travel. Burwell and Strang (1952) applied his theory to the wear of steel surfaces as a function of load, distance of travel and hardness under controlled conditions which permitted

only adhesive wear. They found that at pressures less than a third of the hardness of the softer material, the amount of wear depended linearly on the resistance of travel and load and independent of the apparent area of contact. However, at average pressures higher than a third of the hardness, wear is still linear with distance of travel, independent of the apparent area of contact but increases very sharply for small increases in stress. It is claimed that this illustrates the characteristics of running-in processes.

One of the more recent theories on the wear of materials has been the delamination theory proposed by Suh (1973). It is based on the behaviour of dislocations at the surface of materials, sub-surface crack and void formation, and subsequent joining of cracks by shear deformation of the surface. This theory predicts qualitatively that the shape of the wear particle is likely to be thin plate-like sheets and that the surface layer can undergo large plastic deformation. Suh claims that this theory is more comprehensive since it considers the physical metallurgy of metal formation, makes less mathematical assumptions and provides insight into the wear of metals under different sliding conditions.

When particulate solids are considered, it is seen that various theories have been formulated to relate attrition, mainly by fracture, to particle strength but none have been able to predict the fracture rate of the material. It is not surprising that an overall model is lacking since the mechanisms of attrition can vary.

The effect of physical properties on the breaking stress of a particle has been explored theoretically by a number of investigators,

but the practical application of the theory is difficult to correlate in view of the overriding effects of particle interactions and the uncontrollable and unpredictable variable of crack length. Early work was aimed at trying to correlate fracture of the particle to the energy input into the system. The relationships developed were often called comminution laws (Schönert and Leschonski, 1975). Rittinger (1867) postulated that the amount of newly formed surfaces was proportional to the energy input. In general, it was found that this proportionality was not valid, and Rumpf (1973) developed a law which identified additional constraints needed to make the relationship feasible. Kick (1885) developed a hypothesis where he assumed that crack patterns for geometrically similar particles were the same, and found that the energy input for fracture was a constant independent of particle size. This indicates that energy requirement is inversely proportional to particle size, which is strictly correct for elastic material.

The energy input for crack propagation needs to be greater than is demanded by the specific surface energy since the material surrounding the edge of the crack is strained inelastically and elastic field energy is dissipated as heat. Essentially, crack propagation is due to an energy balance (Schönert and Leschonski, 1975) and Griffith (1920) considered this in terms of surface energy only. Irwin (1948) and Orowan (1949) extended this theory to include inelastic deformation.

Griffith (1920) sought the configuration for a crack system which minimised the total free energy; the crack would then be in a state of equilibrium and on the verge of extension. He considered

the individual energy terms which changed as a result of crack formation.

L_s = work done by the applied load in deforming body. This could be thought of as the reduction of potential energy stored in the loading system

E_s = Strain energy stored in the system must be sensitive to system geometry

E_f = Creation of new crack surface expends surface energy

Thus, total energy in system $E = (-L_s + E_s) + E_f$

As the crack extends, the composite term decreases and surface energy increases. Thus, the first term favours crack extension whilst the second opposes it. This is the Griffith energy balance concept given by the standard equilibrium requirement

$$dE/dc = 0$$

where c is the crack length.

This results in an expression for the breaking stress P where

$$P = \sqrt{\frac{2Eq}{\pi c}}$$

where E is the Young's modulus, q is the surface energy of the crack per unit area and P the breaking tensile stress normal to the crack.

Kendall (1978) attempted to show that when a compressed brittle body is made smaller, its fracture strength apparently increases until at a critical size crack propagation becomes impossible and particles below this size are ductile in compression. He considers

a solid block of material supported at one end and compressed by a narrow punch at the other. He describes how an existing fissure divides the block into two short struts and, from the geometry of the system, concludes that compression failure is only due to bending strains. He then invokes Griffith's energy criterion for crack propagation, obtaining an equation for the cracking force as a function of specimen size and material properties. He finds that the cracking force starts to rise as the specimen size is made smaller, and below a critical size given by

$$d_{crit} = \frac{32ER}{3Y^2}$$

where E is the Young's modulus of elasticity, R the fracture energy and Y the yield stress, gross yielding occurs. Kendall reports that if values of d below that of d_{crit} are used, the splitting force rises to infinity. Kendall's value for d_{crit} is obtained when the fracture equation, which is a quadratic function, is solved to give equal roots. Lowering the value of d_{crit} results in an imaginary solution which Kendall has confused with infinite stress.

Kendall (personal communication, 1981) states that at sizes below d_{crit} it was very difficult to observe visually whether further fracture had occurred and was convenient to assume that gross yielding had begun. Thus, it would seem that the value of d_{crit} does not have a sound theoretical basis.

Austin (1971) reviewed the existing literature on the breakage of particles during milling and attempted to show the similarities and differences between them in trying to lay a groundwork for common understanding. He and his co-workers (several papers) have carried

out extensive work in characterising the breakdown of particles in the milling processes.

Material properties of particles are important in the understanding of comminution and for designing crushers and mills. These properties could be called material comminution characteristics (Schönert and Leschonski, 1975) and include hardness, particle size, type of stress (compressive, impact or thermal shock), intensity of stress, loading velocity and environmental conditions (temperature). Impact attrition depends on the velocity of the particles (number of contacts) whilst shear attrition depends on the applied normal stress at a given shear strain.

Particle attrition is also seen in pneumatic handling systems, where dry bulk material is transported through pipelines by either negative or positive pressure gas streams. Pneumatic systems have several advantages in that they save space and are flexible, eliminate spillage and are safe and clean (Mason, 1975). The main disadvantages of such systems are that erosion of plant materials can occur and friable materials can suffer undesired particle degradation. The analysis of the problem represents a very difficult and complex task, for a large number of variables are involved with respect to both the product and plant. Mills and Mason (1978) show that particle attrition in pneumatic conveying can be quite considerable. In a series of sixteen tests on a batch of sand conveyed over a distance of 715μm which included approximately 140 bends, the mean particle size changed from 230μm in the original powder to about 200μm at the end of conveying. The original particles also had virtually no particles less than 60μm when charged, but about 10% of the total

mass had a mean particle size less than 60μm at the end of the tests. Mills and Mason conclude that the majority of the degradation was caused by the bends and isolate phase densities and conveying velocities as the two major variables for further study. Clearly there is scope for a great deal of work to be carried out in this field.

Erosion of pipe bends is another problem encountered in pneumatic conveying. Severe erosion of transport lines comprises two types of wear:

(a) that caused by repeated deformations during collisions

(b) that caused by the cutting action of free moving particles

The erosion of square section 90° bends by pneumatically conveyed alumina particles shows that the mechanism of wear largely depends on the angle of impingement of particles upon the bend material (Mason and Smith, 1972). It is seen that the erosion resistance of different materials changes as the angle of impingement changes. When particles are harder than the bend material, rapid erosion of the bend occurs at low angles of impingement (15° - 30°). Also, bend wear is not only a function of the velocity of particles but also dependent upon the solids to air ratio.

Agglomeration, which could be thought of as an inverse attrition process (Wei et. al., 1977), is seen to occur in grinding mills, for example, where the attrited fine particles coalesce to form larger particles (Schönert and Leschonski, 1975). Agglomerates can be formed by a number of mechanisms (Kapur, 1978; Capes, 1980; Sherrington and Oliver, 1981):

(a) Capillary forces due to negative capillary pressure (suction) and interfacial forces:

(1) liquid bridges or pendular bonds

(2) funicular bonds

(3) capillary pressure bonds

(4) liquid envelope (droplet) bonds

(b) Solid bridges between particles formed by:

(1) inorganic bonding agents (cementitious bonds)

(2) chemical reaction (chemical bonds)

(3) crystallisation of dissolved material

(4) melting of particle at points of contact by friction and pressure

(5) sintering

(c) Bridges with limited mobility:

(1) viscous binders

(2) absorbed layers

(d) Attractive forces between particles in the absence of liquid and solid bridges:

(1) molecular forces including valence and vanderWaals forces

(2) electrostatic forces

(3) magnetic forces

(e) Mechanical bonds due to interlocking, micro-contacts, friction and arching of particles.

Granular growth occurs in systems where liquid is present through successive stages: nucleation, transition and ball growth.

In the nucleation stage, particle-particle contact is established with liquid layers to form pendular bridges which, with further tumbling, become two-phase nuclei held by capillary forces. In the transition stage, the nuclei grow either by single particle addition (pendular bridging) or by the combination of two or more nuclei by reshaping. At the end of the transition period, a large number of small granules with a wide size distribution are obtained.

Ball growth can occur in several ways. Newitt and Conway-Jones (1958) show that large granules break up into two or three pieces which then join with the smaller granules and enlarge in size. Kapur and Fuerstenau (1966) proposed that larger granules were formed by the coalescence of two or more granules regardless of size. Capes and Dankwerts (1965) showed that a crushing and layering mechanism operates where selective comminution of smaller particles occurred, perhaps to their component particles, which then were distributed over the surface of the larger granules. A snowballing effect was also proposed by Sherrington (1969), which is also referred to as onion skinning or layering, where growth occurs by the deposition of tightly packed layers on the surface of the pellets.

Agglomeration also occurs in liquid suspensions. In the spherical agglomeration process, finely divided solids in liquid suspensions are agglomerated by agitating a small amount of a second immiscible liquid with the suspension to wet some or all particles preferentially. This results initially in voluminous floccs forming, which on collapse produce compact spheres, if the right amount of the second liquid is used.

Capes (1980) represents the mechanisms of size change in particulate processes by pairing nucleation with shattering, coalescence with breakage and layering with surface wear, the former in each pair being a granulation process and the latter an attrition process.

The kinetics of major growth mechanisms have been analysed by Kapur (1978) by means of statistical mechanics, but real situations are not adequately dealt with by the application of kinetic expressions derived analytically. Sherrington and Oliver (1981) summarise the recent empirical expressions obtained for specific systems.

In dry agglomeration in rotating drums, Meissner et. al. (1966) obtained an expression for the rate of disappearance of fines per unit bed weight, given by

$$\frac{dW_F}{dN} = \frac{-K\, d_B^2\, \rho_B\, V_B^3}{f(\rho_F)}$$

where

W_F - weight of fines per unit weight of bed

N - total number of revolutions of drum

d_B - diameter of granules

ρ_B - bulk density of granules

$V_B = (1-\varepsilon)$ where ε is the voidage

ρ_F - bulk density of fines

ρ_F was not established but shown that it increased linearly with decreasing W_F.

Kapur and Fuerstenau formed an expression for granulation in a rolling drum of the form

$$\ln\left[\frac{D_{max}}{D_{max_o}}\right] = \frac{N}{3\Delta N} \ln\left[\frac{6}{\pi} C_{max} K a\right]$$

where

$K = \frac{\overline{V}}{D_{max}}$

$\overline{V}$ - volume of average nuclei

D_{max} - size of largest nuclei in size distribution

D_{max_o} - size of largest nuclei when N = 0

N - number of revolutions of balling drum

ΔN - small number of drum revolutions over which C_{max} number of average nuclei combine

C_{max} - maximum number of nuclei combining in a given small number of drum revolutions

a - dimensionless volume shrinkage factor due to the reduction in porosity of agglomerates (assumed constant)

For a coalescence model, they suggest that D_{max} is sufficient to characterise the distribution and the equation would reduce to the form

$$\ln\left[\frac{D_{max}}{D_{max_o}}\right] = kN$$

where k is the rate constant for nuclei growth.

Sastry and Fuerstenau (1971) relate the weight median diameter (D_w) to the agglomeration time (t), thus

$$D_w = Kt^c$$

where c is an exponent.

An expression for particle growth in a rolling drum (Capes and Dankwerts, 1965) can be written as

$$\frac{n}{N} = \left[\frac{1 - (d/d_{max})}{(1-x)}\right]\beta$$

where

$$\beta = \frac{3(1-x)}{X}$$

$$x = \frac{d_{min}}{d_{max}}$$

n - number assigned to a given granule by counting from the largest granule in the charge in order of size

N - total number of granules in charge

d - diameter of n^{th} granule

d_{max}, d_{min} - diameter of largest and smallest granule

Timoshenko (1970) has extended the Hertzian analysis where he considers the stresses between two spherical bodies in contact. Molerus (1975) relates the applied hydrostatic stress to inter-particle forces in a particle bed. An alternative general formulation is presented later, where the stress transmitted through a powder bed is considered and is related to inter-particle forces.

A certain amount of work has been carried out in examining the obvious effects of attrition in solids handling processes. No link has been established between studies in mechanical engineering concerned with wear and those in chemical engineering concerned with dust formation, but it seems clear that most of the ideas mentioned must remain relevant. It is generally known that in moving bed systems, particle movement leads to a rounding of edges,

and material loss due to attrition has been far greater in circulating non-spherical particles than when circulating spheres of the same composition. Tests carried out in fluidised beds show that attrition rates decrease with time (USEPA, 1980) and bed samples exhibit greater sphericity than the particles originally charged. Submerged jet attrition tests show this edge wear very clearly.

Wei et. al. (1977) considered the attrition of catalyst particles in fluid catalytic cracking systems and found that both surface grinding and shattering of particles were present. In fluid bed systems, the ratio of impact energy to fracture surface energy was proportional to particle diameter and thus the larger the particle the greater the rate of attrition. Attrition data were formulated in terms of matrices and a population balance model was developed which was used to investigate optimal process conditions.

For geometrically similar particles, since the ratio of mass to cross-sectional area is directly proportional to particle size, it is evident that larger particles will be more prone to fracture than smaller particles. This is further reinforced since larger particles tend to have more defects in their structure. Submerged jet attrition tests have shown that larger sized particles in a mixture tend to grind down more slowly than the finer particles present, indicating that the rate of grinding is dependent on particle size.

Experiments conducted in grinding mills show that ground particles tend toward a skewed size distribution and when such a distribution is reached, the rate of grinding decreases unless selective additions or deletions are made to the batch to deliberately alter the size

distribution.

Historically, the theoretical development for processing equipment revolves largely around a fracture mechanism though in fluid bed tests all evidence points to a surface wear effect. The latter may well be a surface manifestation of the former and depends upon the structure of the particle.

A number of so-called standard attrition or hardness tests have been developed by various manufacturers, who are users of mainly catalyst particles, geared specifically to their own interests. In most instances, these give relative rather than absolute rates and are more indicators of hardness than of the rate of attrition. In all instances, where the tests involved batches of material as opposed to single particles, the variable of size distribution was not taken into account.

In standard crushing tests, a certain number of particles would be crushed by a plunger until a pre-set test pressure was reached and the number of undamaged partices as a percentage would indicate particle strength and hence susceptibility to attrition. Such tests have their limitations in that they may only be applied to spherical or regularly shaped particles, and since it reflects only a relative resistance to force as opposed strictly to hardness, resilient or elastic particles may not be used as they deform to spread the load.

The development of shaker tests is based on an accelerated form of the jostling which can occur in adsorbers during the desorption

or regeneration cycles. In these tests, 100 gm of material is placed on a 200μm sieve and shaken for 10 minutes and the amount passing through is termed primary attrition. The retained material is shaken for another 10 minutes and the amount passing through is claimed to be the true attrition. The first screening is used to separate the superficial dust which may adhere to the particles. This method was also adapted to investigate the effects of thermal shock where hot samples were dropped into a cool fluidised bed and the rate of attrition measured by recovering the samples from the bed and using the shaker test as in the previous instance.

Spouted jet attrition tests were developed to measure attrition rates in air lift moving bed processes where particles are subjected to high velocity accelerations at the lift pot as well as deceleration in free fall within the separator vessel. Tests have been developed where air at high velocity is passed through a bed of known weight and the particles are thrown against the walls of the bed. The air escapes through a fine mesh at the top of the bed along with any fine product caused by attrition. The experiment is usually run for one hour and the amount of fine materials passing through the fine mesh recorded. The attrition loss is then expressed as a weight percentage of the original charge.

Forsythe and Hertwig (1949) developed a system which simulated attrition occurring at the grid of a conventional fluidised bed where the bed depth exceeds the jet penetration length. The apparatus consisted of a 38 mm internal diameter tube 69 cm long fitted with a grid plate bearing three 0.4 mm holes as seen in Fig. 1.1. At its upper end, the tube expands to a diameter of 12.5 cm. A 100 gm sample of the material (usually catalyst particles) to be tested is charged to the 38 mm tube and high pressure air admitted to the plenum below the grid to yield near sonic velocities of about 275 m/s through the 0.4 mm holes. Despite this high velocity, the holes are too small to yield a significant jet penetration. In the expanded section the superficial velocity decreases to about 0.6 cm/s which is of the order just exceeding the terminal velocity of an approximately 20 μm particle, and hence all particles smaller than this size contained in the original charge or resulting from the attrition occurring in the bed are carried overhead and collected in a cyclone-filter arrangement. The weight collected after a fixed test period, of about 5 to 45 hours, is weighed and recorded as a percentage of the original charge.

Gwyn (1969) used this apparatus to measure the rate of attrition of close-sized catalyst samples. He expressed the rate of attrition as a simple function of time and initial diameter. He claimed that the initial rate was a function of initial diameter, whereas the decrease in attrition rate of a catalyst of a given size as it ages depended only on time. Attrition was expressed empirically by

$$W = K_p t^m$$

where W was the weight fraction attrited, t the time, m an exponent

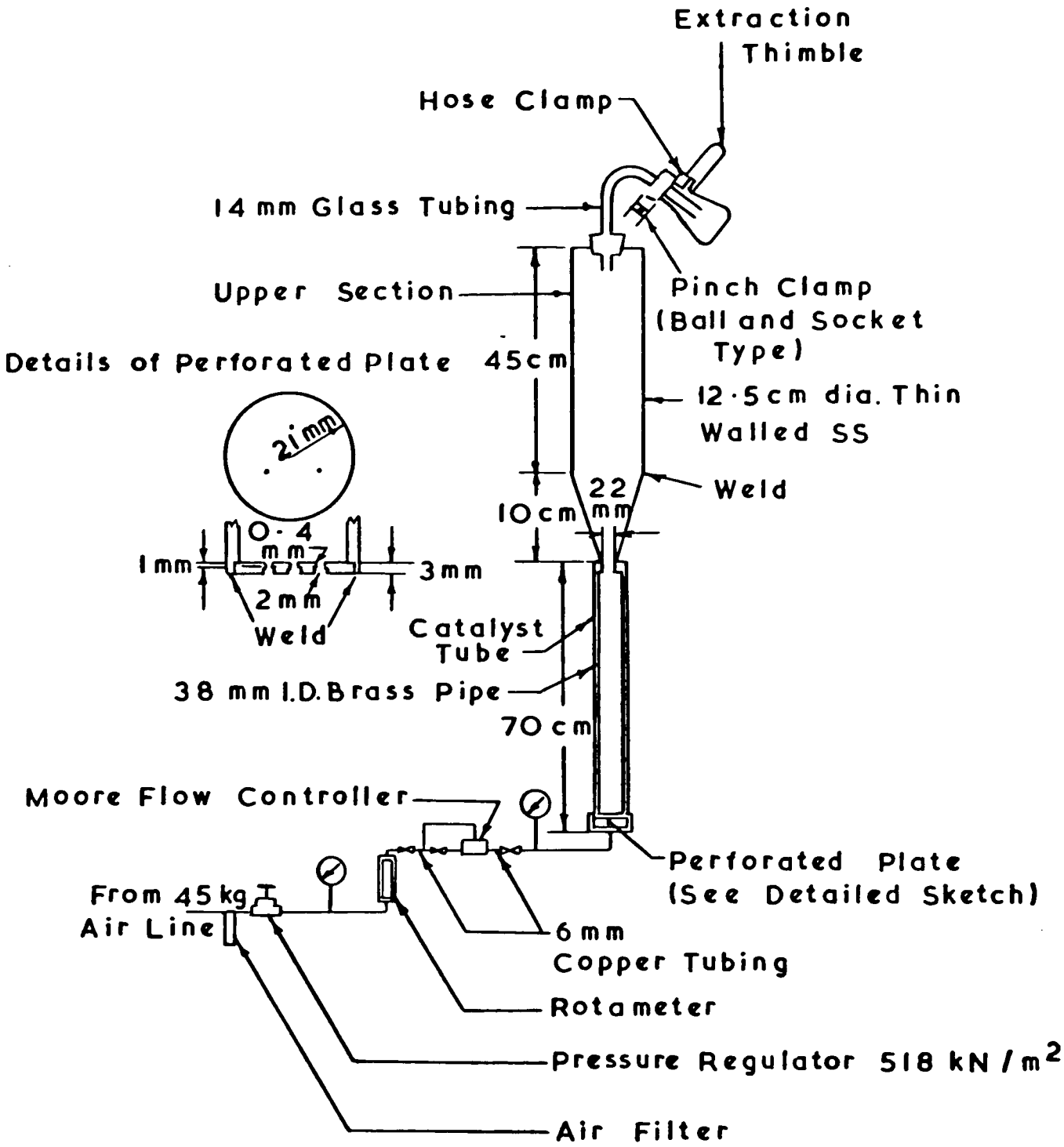


Fig. 1.1. Apparatus used by Gwyn

approximately constant for all catalyst particle sizes and K_p a constant which was a function of initial particle size. He showed that when the weight fraction attrited was plotted against time on a log-log plot, straight lines were obtained from which he was able to determine a value for m, a parameter he argues that characterises the attriting material.

Attrition in fluidised beds has recently been studied by the United States Environmental Protection Agency (USEPA, 1980) where the desulphurisation performance and attrition behaviour of limestone and dolomite in fluidised bed combustion systems were considered in detail. Attrition is seen to occur for a variety of reasons; abrasion, high energy collisions, thermal shock, chemical stress and internal gas pressure. Rounding of particles was seen when vigorous fluidisation took place especially at high temperature. The abrasion of particles was seen to decrease with time, probably as the defects found on the particle decreased with time. From theoretical studies, it was concluded that attrition rate in a bubbling zone of a fluidised bed varied inversely with particle strength. Definite conclusions as to the influence of particle size on attrition rate were not made as, although theoretical studies indicated that it was not important, analytical results showed a strong dependence.

Karabelas (1976) made a study of the attrition of particles in slurry flow. He suggested a kinetic type of formulation of particle dimunition in suspension flow which could serve as a framework for interpreting experimental data and for modelling particle attrition in slurry transportation and processing systems. He formulated a first order kinetic equation for brittle particles such as coal. He reports that these particles, in Couette flow, are reduced by loss

of surface protuberances which are much smaller than their mean diameter.

In reviewing the limited amount of knowledge of attrition in particulate systems, it is seen that the understanding of the mechanisms of attrition has been lacking, and tests have been geared mainly towards particular problems encountered in industry. The fracture mechanism has been traditionally explored but fluidised bed systems, for example, have shown that surface abrasion is predominant in such processes. Energy models have been considered but these have failed to produce an overall picture, probably because of the unpredictability of crack propagation, since attrition mechanisms vary. Uncertainty about detailed solids flow has also contributed to this situation. For these reasons, it is also difficult to find a system that accurately represents all types of attrition. This makes interpretation of results very complex.

The fundamental mechanisms of attrition can be examined by reducing the complexity of powder behaviour. This cannot be easily done using industrial equipment because of the interaction of the mechanisms controlling attrition. Hence, specifically designed equipment may enable particular aspects of attrition behaviour to be isolated. Fundamental studies can then provide a quantitative evaluation of the attrition process which can then be used, at least qualitatively, to aid in the design and operation of industrial systems.

The relationship between the shear stress and strain for a powder at a constant normal stress is well documented. The behaviour of

the powder is dependent on its initial voidage. If the voidage is less than its critical void ratio for that compacting stress, the powder is said to be densely packed. In an effort to attain this critical value the powder will expand when sheared, thus doing work against external forces. This produces a peak on the stress-strain curve. Once the shear strength of the powder is overcome, the powder fails and any further increase in strain occurs without the corresponding increase in shear stress. At high strain, the powder attains its critical void ratio. If the powder initially had a higher voidage than its critical value, then it is said to be loosely packed. On straining the void ratio decreases until the critical void ratio is reached when the powder fails. Here, there would be no peak on the stress-strain curve as the compact gradually rises to its maximum stress state. The limiting value of the shear stress for both powders will be the same if they were both compacted with the same normal load.

Hvorslev (1937) pointed out that the shear stress (τ) necessary to cause failure is a function of the normal stress (σ) and voidage (ε). The condition for failure was defined by a surface, known as the Hvorslev surface, in three dimensional space whose coordinates were σ, ε and τ. Roscoe (1958) extended this work by showing that when failure takes place, the path on the failure surface has an end point and when this point is reached, further strain takes place with no change in shear force or voidage under a given normal load. All such points lie on a single line on the failure surface known as the critical void ratio line. He also showed that when projected on to the τ,σ plane, this line gives a straight line passing through the origin.

A satisfactory failure criterion should express with reasonable accuracy the relationship between the principal stresses when the soil is in limiting equilibrium. The following criterion has been suggested for powders:

> Mohr-Coulomb criterion. The greatest principal stress difference at failure is some function of the mean of the greatest and least principal stresses:
>
> $$(\sigma_1 - \sigma_3)_f = F\,(\sigma_1 + \sigma_3).$$

The Mohr-Coulomb failure criterion is the one generally used in predicting failure in powder systems. This, however, does not take into account the dilatancy occurring in a densely packed material which has just failed.

Rowe's stress dilatancy relationship (1962) seeks to modify the Mohr-Coulomb failure criterion such that volume changes which occur when densely packed material is sheared are taken into account. He initially considered uniform packings of rods and spheres (later extended to non-uniform assemblies) and defined α (a geometrical property of packing or the average inclination to the major plane at which the particles are interlocked) and β planes (sliding angle in relation to the major principal plane) in the assembly. His theory is applicable to the peak and post-peak region of the stress-strain curve of a densely packed material, and states that β attains a critical value (β_c) at sliding as a result of the rate of dissipation of energy per unit rate of gross input energy being minimised.

The energy ratio can be presented as

$$E = \frac{\sigma_1'}{\sigma_3'\left[1 + \frac{\dot{dv}}{v\varepsilon_1}\right]} = \frac{\tan(\phi_u + \beta)}{\tan \beta}$$

where $\frac{\sigma_1'}{\sigma_3'}$ is the ratio of effective principle stressed, $\left(\frac{\dot{dv}}{v}\right)$ the unit volume expansion, ε_1 the increment of strain in the principal stress direction and ϕ_u the angle of internal friction. The critical value of β is obtained by minimising E, expressed by the condition

$$\frac{dE}{d\beta} = 0$$

and, as a result,

$$\beta = \left[45^\circ - \frac{\phi_u}{2}\right]$$

or when

$$\frac{\sigma_1'}{\sigma_3'\left[1 + \frac{\dot{dv}}{v\varepsilon_1}\right]} = \tan^2\left[45^\circ + \frac{\phi_u}{2}\right]$$

When Rowe extended his theory to random packings of irregular particles, he found it necessary to replace ϕ_u by ϕ_f, where

$$\phi_u < \phi_f < \phi_{cv}$$

ϕ_{cv} is the angle of internal friction at constant volume.

For the instance where there is no volume change, this reduces to

$$\frac{\sigma_1'}{\sigma_3'} = \tan^2(45^\circ + \phi_u/2)$$

which is the Mohr-Coulomb condition for failure.

The basic mechanisms of particulate attrition have both microscopic and macroscopic aspects. Macroscopic effects include particle impact on containing walls, particle to particle rubbing and attrition due to internal stresses within deforming bodies of solids. Microscopic aspects include particle structure, shape and size, adhesion, corrosion and fatigue behaviour. Lacey (1954) first described convective mixing where powder is seen to move in clumps or blocks when under strain. Between these moving blocks existed areas where the powder failed (Roscoe, 1970; Bransby et. al., 1973). These regions were known as failure zones and were up to twenty times the particle diameter in depth. Within these regions, particles moved relative to one another and was a suitable environment for particle to particle grinding to take place.

With the aim of developing a system that is close to the behaviour of powders in industrial systems and yet retaining sufficient control to enable basic information to be obtained, an annular attrition cell was designed and built. This cell is capable of infinite strain in one direction, thus enabling hard material to be tested. An estimate of the relationship between contact stresses and interparticle forces promoting attrition in such a cell has been derived and is presented in Appendix A.

The purpose of the work in this thesis is to develop a cell in which one of the mechanisms of attrition, namely that in failure zones of deforming solids, is considered in isolation. This work should be considered as a basic stage in the development from the fundamental study of particulate attrition mechanisms with a view to a thorough understanding of the attrition process. It aims to increase the range and value of basic information available as well as to provide an insight into attrition processes in industry.

CHAPTER TWO

THE ANNULAR ATTRITION CELL

2.1 Equipment Selection

To investigate the attrition of particles in failure zones, particle behaviour must be evaluated in such a region formed under known and controlled conditions. It was decided that such measurements would be best achieved in an annular shear cell. The design of the cell was based on previous models but significantly modified to suit present needs.

Jenike (1961) developed a shear box to measure shear strengths of powders, but this would not have been satisfactory for the present work due to its limited uni-directional displacement and poorly defined rate of strain. Consistent sample preparation was also difficult and the box was unsuitable for work at low normal stresses of less than 5 kN/m^2 (Carr and Walker, 1967/68). A simple shear cell was developed by Roscoe (1953) which was further modified by Scott (1974) for his powder mixing studies and Drahun (1978) in later work, where continued uniform strain could be applied to a powder by the repeated change of straining direction. One of the disadvantages of using the simple shear cell in attrition work was that powder would have become wedged in corners thus creating regions where particle attrition may not occur. The annular shear cell overcomes some of these difficulties in that unlimited strain can be applied to the powder sample in one direction. A wide range of normal stresses can also be applied successfully to the material and sample preparation and removal is straightforward.

The failure zone in the powder bed is readily established and attrition products can be easily sealed in to prevent loss of fines during experiments.

However, one disadvantage in the annular shear cell is the difference of strain rates experienced by the particles at the inner and outer walls of the annulus. The particles at the outer wall are displaced to a greater extent than those at the inner wall during revolution of the cell, and therefore undergo a correspondingly higher strain. It is possible to overcome this by using narrower annular rings.

Measurement of soil strength saw the initial development of equipment where the straining of material was controlled. Different types of apparatus have been used to determine the behaviour of material during initial failure which was of prime importance in the shear testing of particulate solids. Annular shear cells were developed to study the shear resistance that occurred in soils after continued straining in one direction (Hvorslev, 1939), but difficulties in sample preparation restricted their use. Primary interest with soils lay in initial failure but, with attrition, continuing behaviour of the particles after initial failure was also of great importance and this was readily investigated in an annular shear cell. Bishop et. al. (1971) have reviewed annular shear cells used to observe failure characteristics in soil and powder studies.

An annular shear cell was built by Novosad (1964), based on that of Hvorslev (1939), to evaluate the strengths and angles of friction of particulate solids. Bridgwater and Bagster (1969, 1972) built a similar cell of larger dimensions for powder studies. Both these cells had a split in the cell wall on a plane through the centre of

the powder sample, and movement of one half in relation to the other held stationary created a strain across it.

Powder studies have also been carried out by Carr and Walker (1967, 1968) and Scarlett and Todd (1968) using annular shear cells. These cells induced failure of the powder just adjacent to the cell lid but, although modifications were carried out to the design of the lid to overcome this problem, introduced cell effects which made evaluating powder behaviour difficult.

Stephens (1976) used an annular shear cell to study the mixing properties and segregation of solids in failure zones. He, again, used a cell with a split in the cell wall which, when one half was moved relative to the other, created a strain across the sample.

2.2 Cell Design and Construction (Fig. 2.2)

It was essential that the apparatus be constructed in such a way as to minimise cell effects. The cell was designed so that the attrition effected would be caused by true particle to particle grinding in a failure zone formed in the powder.

The overall size of the cell was determined by a combination of the following factors:

(i) the size of particles used in attrition studies
(ii) minimisation of the variation of strain rate across the annulus
(iii) minimisation of weight to lessen load on the motor

The attrition cell was constructed around a mild steel shaft (A1) press fitted into a stainless steel collar (Fig. 2.2A). The lower end

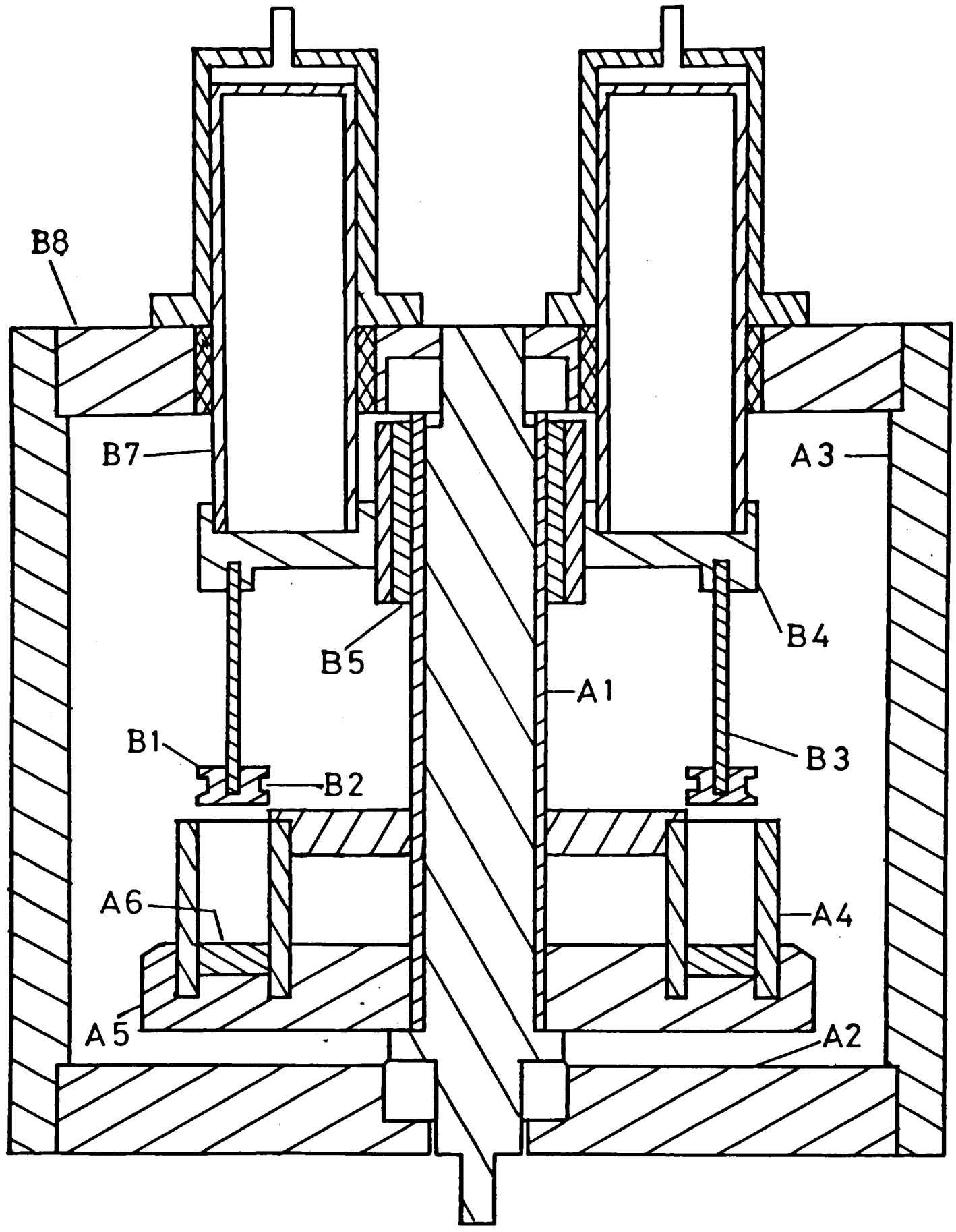


Fig. 2.2. Annular Attrition Cell (vertical section)

Notation as for following figures

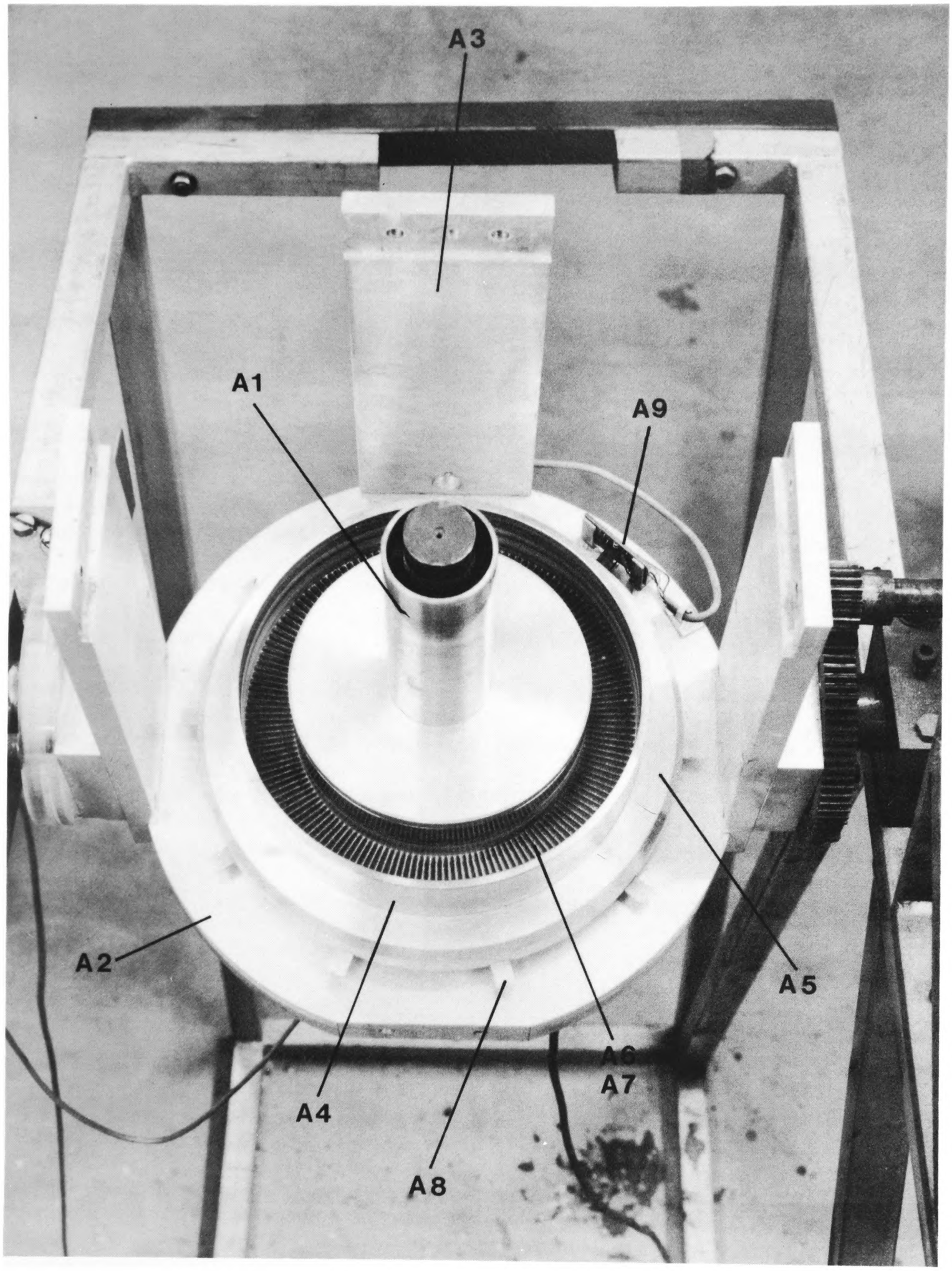


Fig. 2.2.A - Angled view of the annular attrition cell

of the shaft passed through a roller bearing housed in the base frame (A2) and coupled to the motor which rotated the shaft. The base frame had four supporting plates (A3) bolted to its four sides for added rigidity when the cell was fully assembled for operation.

The walls of the annulus (A4) were made from lengths of seamless stainless steel pipe which allowed abrasive powders to be used without damage, and to minimise corrosion problems. Both the inner and outer surfaces were accurately machined to ensure that a smooth finish was obtained to facilitate smooth operation and sealing. The annulus was 20 mm wide, having inner and outer diameters of 120 mm and 160 mm. This produced a strain ratio of 0.75 between the inner to outer wall. To ensure that a complete failure zone could form for the size of particles used, the cell was built to allow for a maximum bed depth of 20 mm, although this could be varied if necessary. The inner wall of the annulus was aligned securely to the centre shaft by means of a locking ring. The annulus was press fitted into an aluminium base plate (A5) which was, in turn, press fitted onto the central shaft.

A spherical interchangeable ring (A6), made of mild steel, was fitted into the recess at the bottom of the annulus, ie the aluminium base disc, and bolted into place from beneath. The ring contained a groove both on the inner and outer wall which housed a rubber 'O' ring. This served as an effective seal preventing any loss of minute debris which might otherwise have come between the walls of the ring and the annulus. The upper face of this ring was machined into radial grooves (A7) of a specific nature. The purpose of this ring was to present a sufficiently roughened face which

would grip the bottom row of sample particles firmly and not cause any slippage at the surface which might otherwise induce errors into any information obtained from the cell. A number of such rings were made to grip the different particles tested in the cell. The groove size chosen for a particular material depended entirely on the physical size and shape of the particles considered and is dealt with later.

An identical ring (Fig. 2.2B), made of an aluminium alloy, formed the top ring (B1). This ring also had a groove (B2) cut into its inner and outer walls to house the 'O' ring which efficiently sealed in the attriting powder sample and prevented the loss of fine particles. It also minimised any undesired attrition between the edge of the ring and the walls of the annulus, thereby avoiding anomalous edge effects. The bottom edge of the groove on the outer wall of this loading ring was cut back at an angle so that if any particles did get into the gap, they remained unground in the lip of the groove. The rubber rings were also specially machined to a knife-edge to minimise frictional drag which otherwise would have increased the load on the motor driving the cell (Fig. 2.2b).

The top of this loading ring was push fitted into a cylindrical brass plate (B3) which, in turn, was push fitted into an aluminium alloy disc (B4). A collar (B5) set into the neck of the alloy disc prevented the grooves cut into the top and bottom gripping rings from meshing together during operation, a necessary feature when very thin sample layers were used in the cell. The outer wall of the loading ring was finely machined to give a clearance of between 0.05 to 0.1 mm from the wall of the annulus.

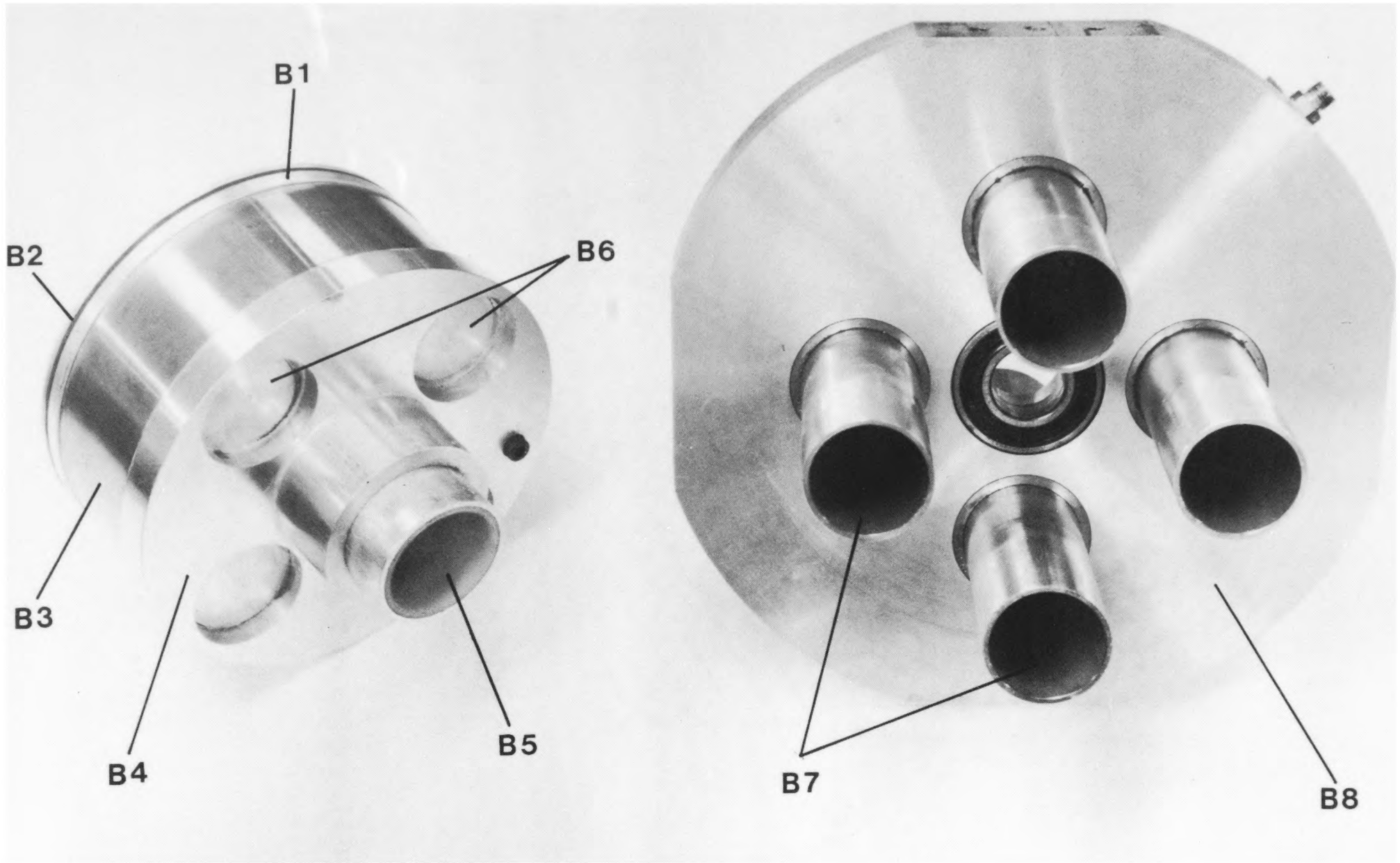


Fig. 2.2.B - View of the loading ring and the top frame incorporating the pneumatic plungers

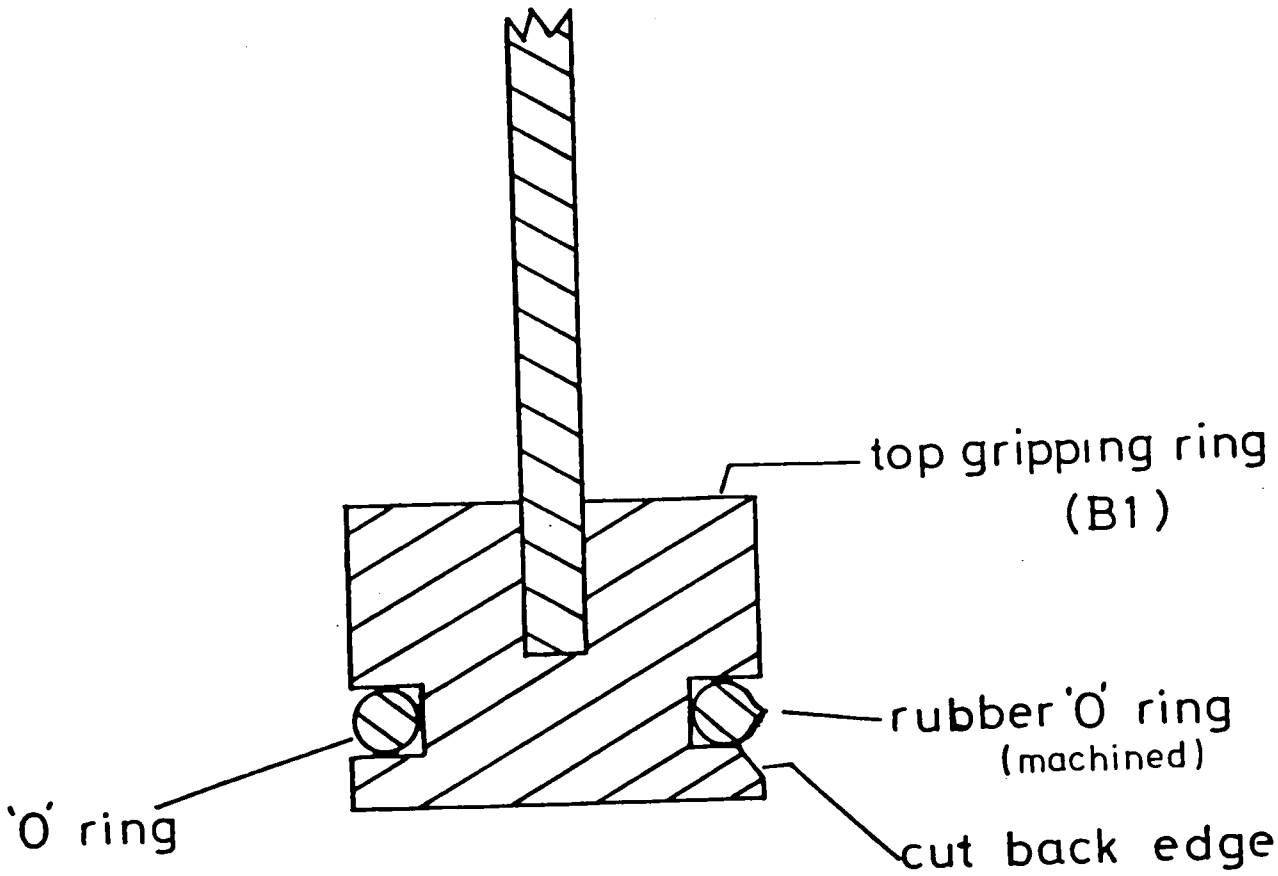


Fig 2.2.b Vertical section through top gripping ring showing the rubber seals

The top of the aluminium alloy disc (B4) had four cylindrical cut-outs (B6) into which fitted four stainless steel plungers (B7). These plungers were housed in the upper frame (B8) and were activated pneumatically from a measured air supply by means of a flexible air line. A roller bearing housed in the centre of the upper frame was used to locate the centre shaft of the annulus thereby vertically aligning the equipment. The upper frame was bolted to the side supports, and during operation of the cell the loading ring was held stationary by the plungers thus creating a strain across the powder sample.

The centre shaft (Fig.2.2C) was driven by a 0.25 hp constant torque DC series motor (C1) with a speed range of 5 to 3000 rpm. The drive was transmitted via a 50:1 reduction gearbox and further reduced by a 4:1 ring gear mounted in series producing a maximum cell speed of 15 rpm. The ring gears could be changed to adjust the torque to the cell required for attrition purposes.

A ring gear (C2) mounted on one of the side supports was connected to an AC series motor (C3) of fixed speed 3000 rpm and complete with an electro-magnetic brake. The drive was transmitted through a 48:1 reduction gearbox and this motor was used to swing the entire attrition cell through any desired angle. A system of micro-switches (C4) on another of the side supports allied to a system of cogs ensued that the cell always returned to the vertical position when re-inverted (Fig.2.2d). This option was included in case the cell had to be operated at different orientations to try and balance the effect of segregation of fine material produced during attrition.

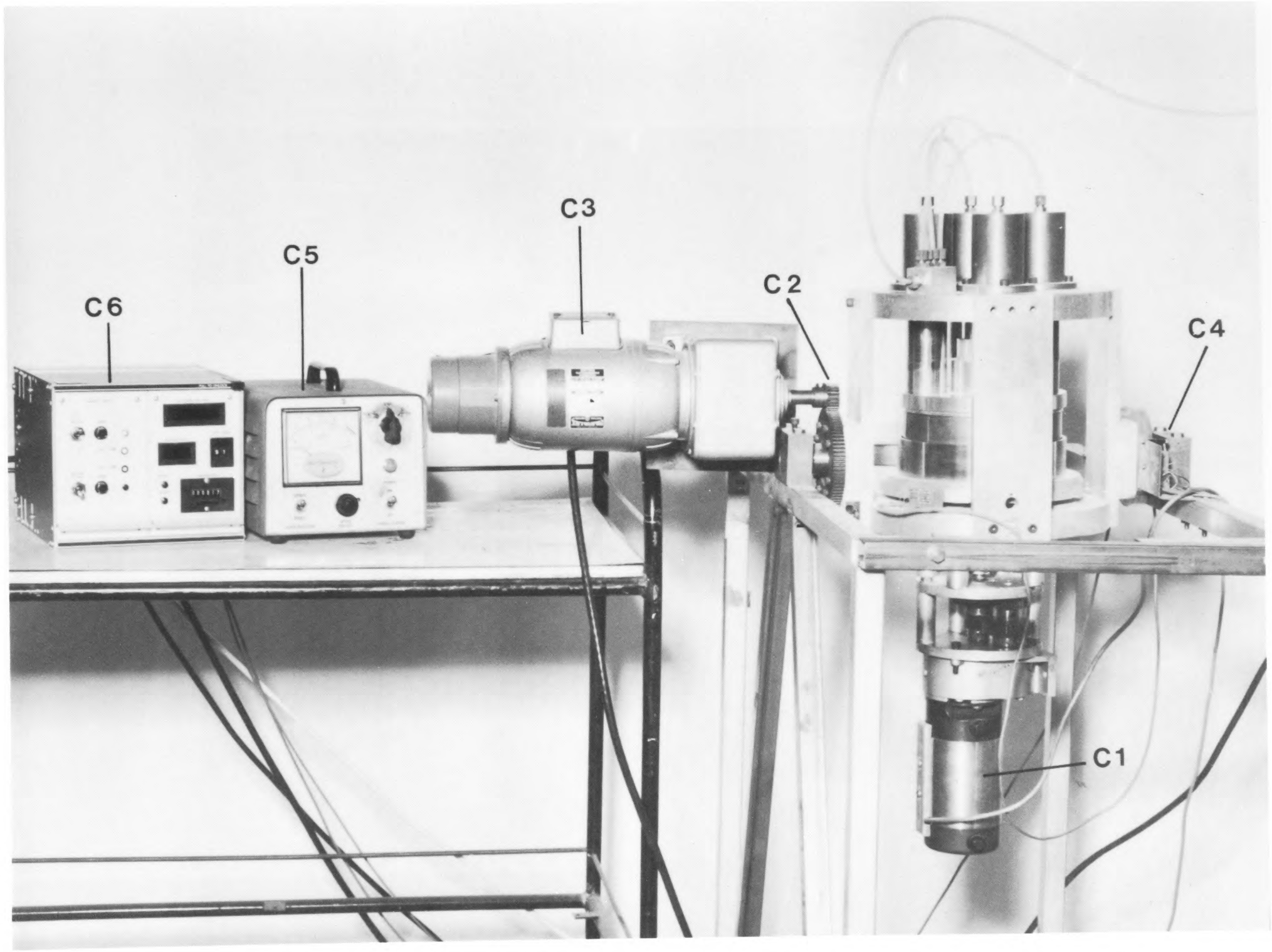


Fig. 2.2.C - Side view of the attrition cell and the control system

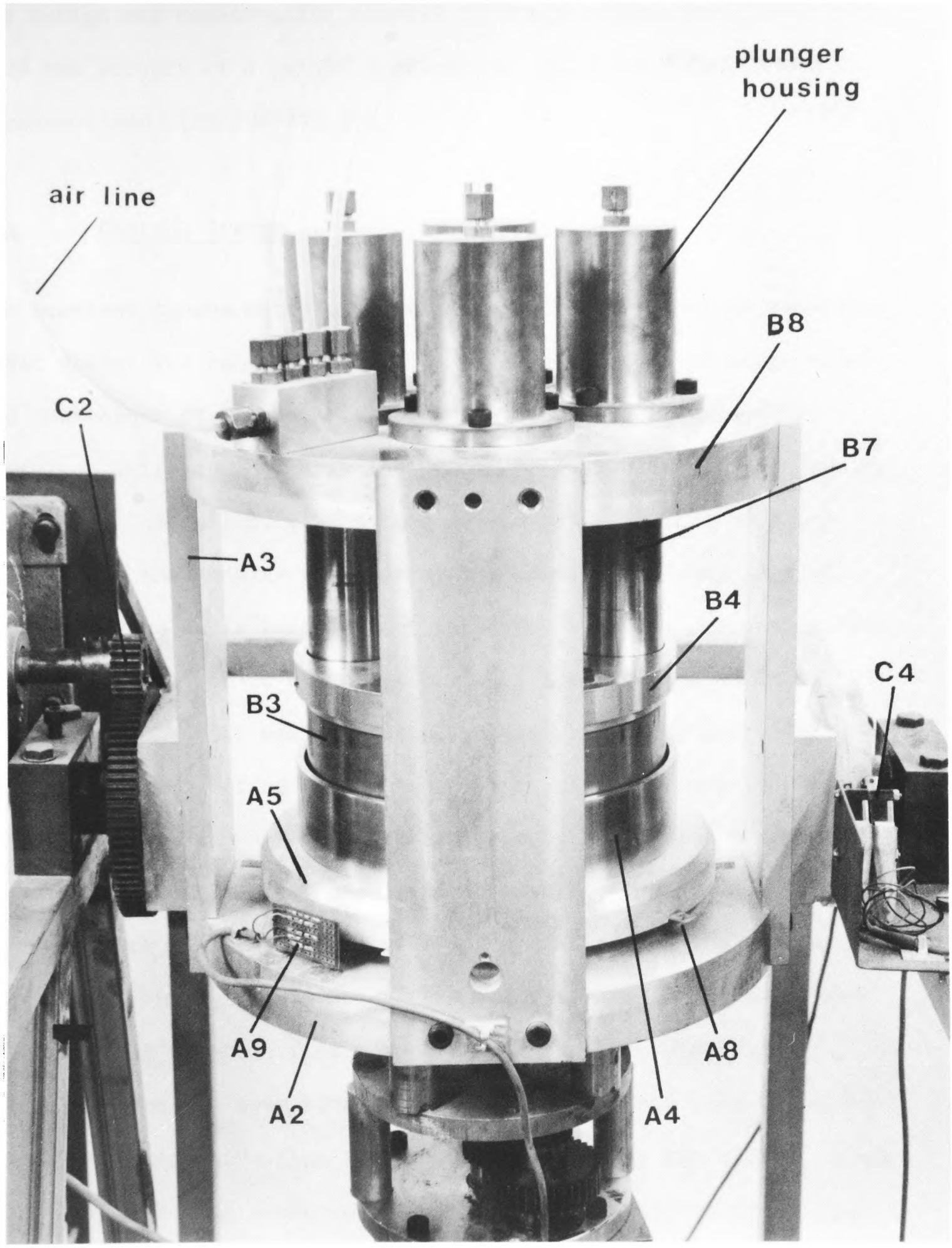


Fig. 2.2.D - The attrition cell set up for operation.
Notation as for previous figures.

The design and construction details of the attrition cell have been made the subject of a patent application; the patent was issued in November 1980 (GB 2047118 A).

2.3 Control System

The constant torque motor operated on a feedback signal to maintain a set speed. The control unit (C5) monitored the actual motor speed and the torque developed. Measuring the torque was practically useful as this gave an early indication of possible material jamming during cell operation. If the torque rose suddenly, the cell was stopped and the annular walls carefully examined for any sign of damage. If the walls were scored, they were smoothed over using fine emery paper, as, if it was neglected, the loading ring would be damaged and the cell would eventually seize.A display unit (C6) showed the number of revolutions of the annulus, the exact speed of the cell driven through the gearbox in use, the pre-set number of revolutions after which the cell would invert (if desired), and the number of such inversions. The speed of the cell was accurately monitored by using twelve metal fins (A8) set into the base of the annulus. Each of these fins passed through a photo-electric cell (A9) during normal operation, and the photo-electric cell timed the passage of successive fins to continuously display the overall speed of the annulus. The number of revolutions was monitored by a magnet housed on the underside of the annulus passing over another photo-cell attached to the stationary base frame. Every time the magnet passed over it, the number of revolutions was advanced by one on the display unit.

A signal was sent to the inversion motor when the pre-set number of revolutions was reached, and the cell then inverted. The cell always

stopped vertically under control from the micro-switches (C4) on one of the side supports which governed the angle of rest. The annulus continued to rotate and, when the pre-set number of revolutions was reached again, the cell re-inverted to its original position.

2.4 Cell Operation

The speed of the cell was set by running the annulus empty and adjusting the speed control on the control unit until the required speed was shown on the liquid crystal display window of the display unit. The cell was then filled by slowly pouring the powder into the annulus whilst it was revolving, until a fairly even surface was obtained. The surface was further levelled by holding a wedge on the moving surface of the powder and smoothing it over. The loading ring was then placed in the annulus on the powder and turned lightly a few times as a final levelling process. This provided a simple and consistent means of obtaining a level surface in the annulus without the occurrence of any undesired attrition. Since all powder samples were loaded in an identical manner without the use of normal loads, it was reasonable to expect the particles to be in a state of loose packing.

The top frame incorporating the plungers was then placed on top of the loading ring and bolted into place to the side supports. The cylinders were engaged into the cut-outs of the loading system, and the required normal stress set on the pressure gauge which was connected to the pneumatic pressurising system via a flexible air line.

The annulus was then revolved by the constant torque motor and the stationary upper loading ring created a strain across the depth of

the powder sample. After the required number of revolutions as shown on the display unit had been reached, the annulus was stopped and the loading system removed. The ground sample was extracted by using the inversion motor to vary the angle of rest of the cell and the powder carefully brushed out using a soft brush.

2.5 Materials Used

The following materials were used in the experimental programme. They were chosen since they were easily available and differed either in shape, size or structure.

(1) Sodium Carbonate (Heavy Soda Ash)

(2) Pure Dried Vacuum Salt (PDV Salt)

(3) Laboratory Salt (Lab Salt)

(4) Granular Sodium Chloride (ex. centrifuge)

(5) Granular Sodium Chloride (ex. crystalliser)

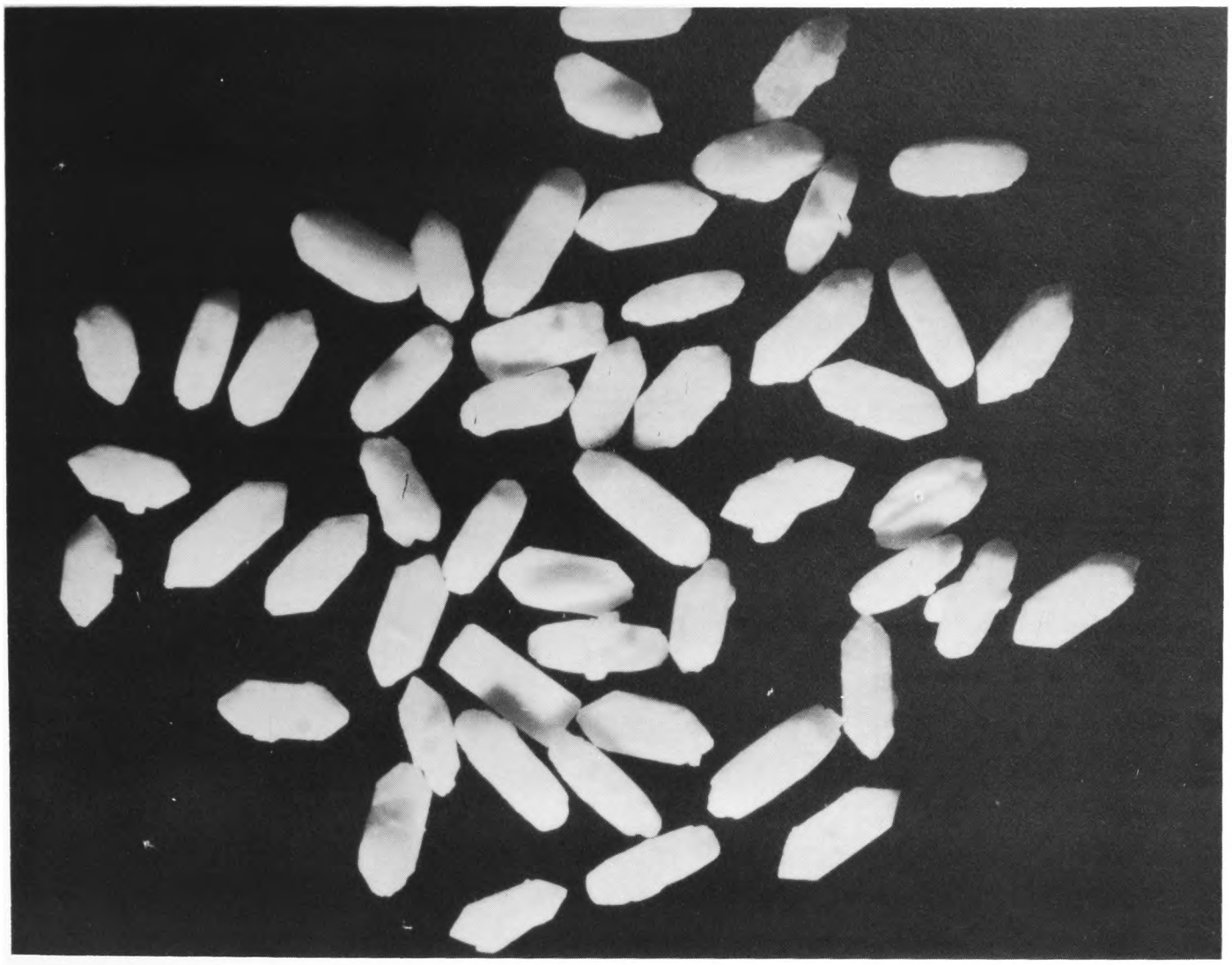
(6) Molecular Sieve Beads

(7) Silica Gel

Figs. 2.5a to 2.5e show the initial material used in the experimental programme. A detailed description of each material is presented later. Table 2.5.1 shows the initial size range and shape of the materials used, and the cumulative weight fraction of the materials is presented in Figs. 2.5.1 - 2.5.4.

2.6 Experimental Procedure

The required sieve-cut was isolated by hand-sieving bulk quantities of material using the desired size of sieves as shown in Table 2.5.1. 25-50 gm of original material was hand-sieved each time to isolate a sufficient weight for a series of runs. 100 gm samples



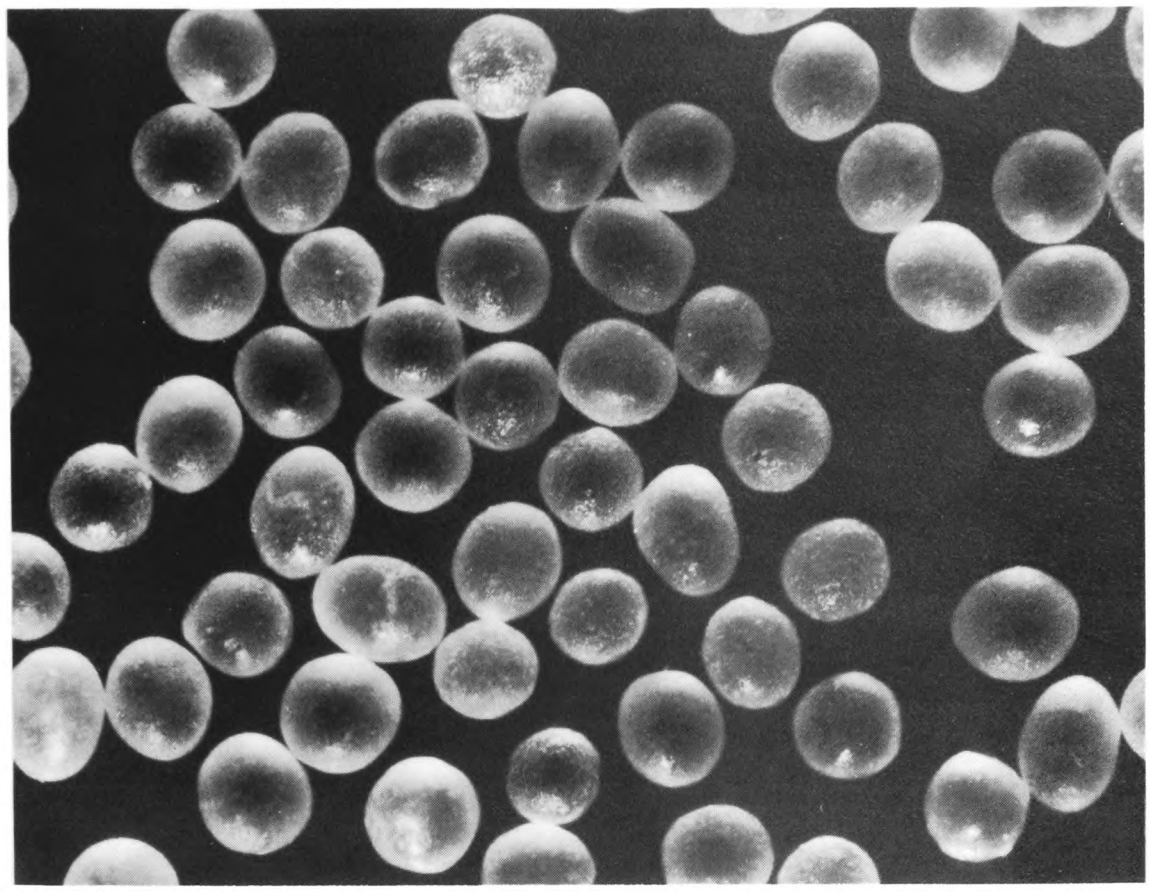
1 mm

Fig. 2.5.a - Sodium carbonate



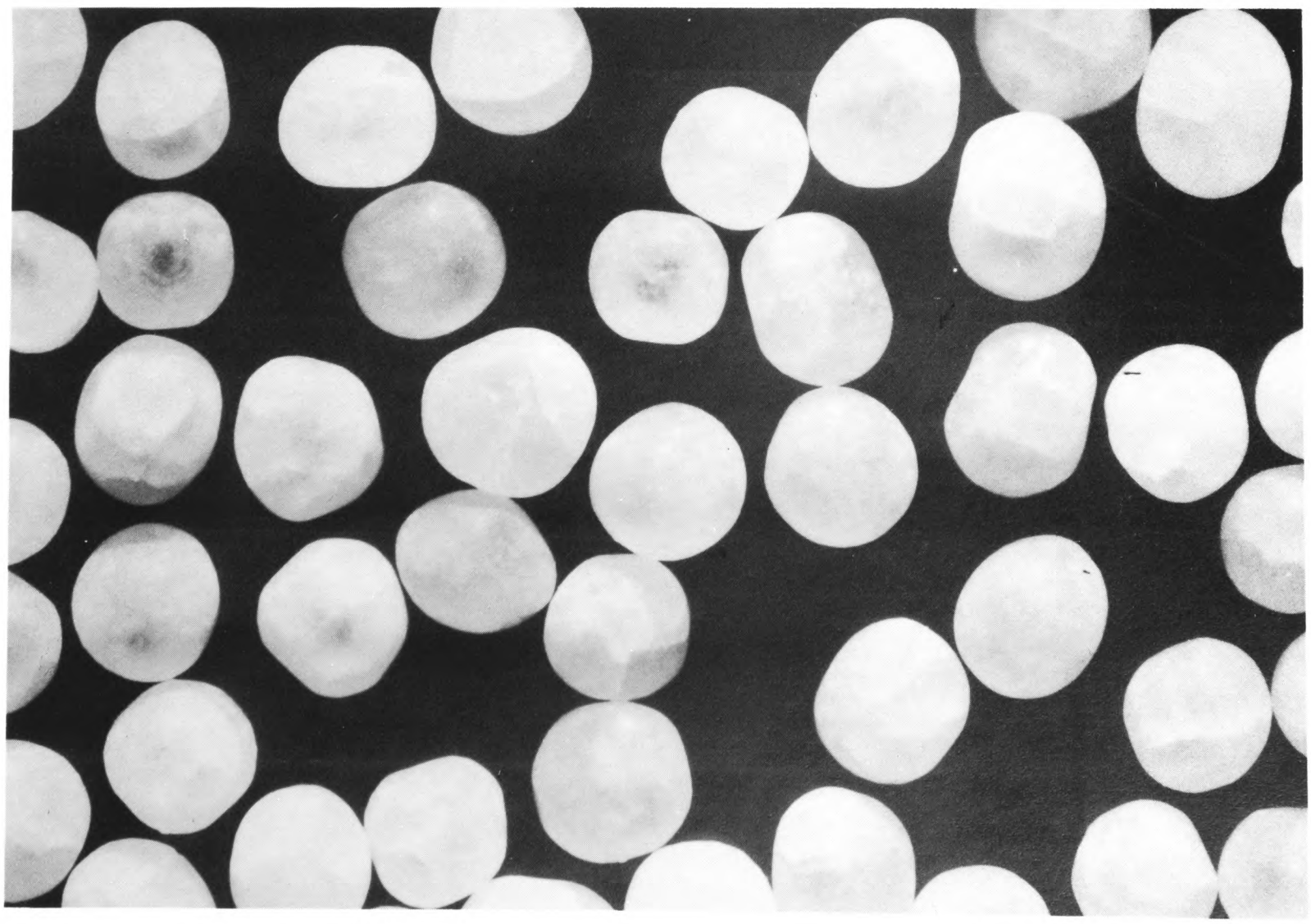
1 mm

Fig. 2.5.b - Pure dried vacuum salt (PDV Salt)



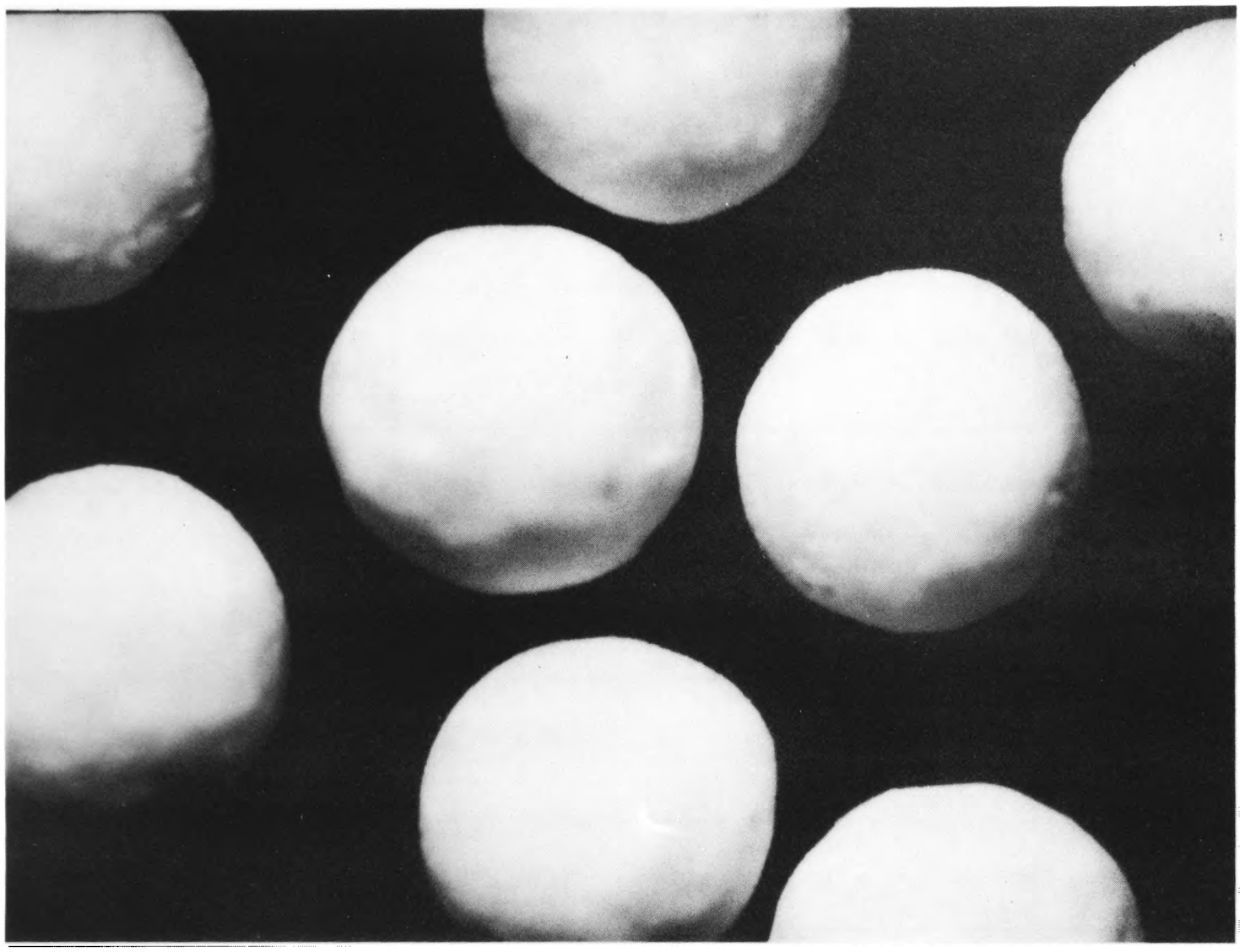
1 mm

Fig. 2.5.c - Laboratory salt



1mm

Fig. 2.5.d - Granular sodium chloride



1 mm

Fig. 2.5.e - Molecular Sieve beads

Material	Shape	Size range used (sieve-cut)
Sodium Carbonate (Soda Ash)	Hexagonal	250 - 355 μm
Pure Dried Vacuum Salt (PDV Salt)	Cubic	250 - 355 μm
Laboratory Salt (Lab Salt)	Spherical	355 - 500 μm
Pure Dried Vacuum Salt (PDV Salt)	Cubic	500 - 600 μm
Silica Gel	Cylindrical	1.4 - 1.7 mm
Granular Salt (ex centrifuge)	Spherical and half-spherical chips	1.7 - 2.0 mm
Granular Salt (ex crystalliser)	Spherical	1.7 - 2.0 mm
Molecular Sieve	Spherical	1.7 - 2.0 mm

Table 2.5.1 Materials Used

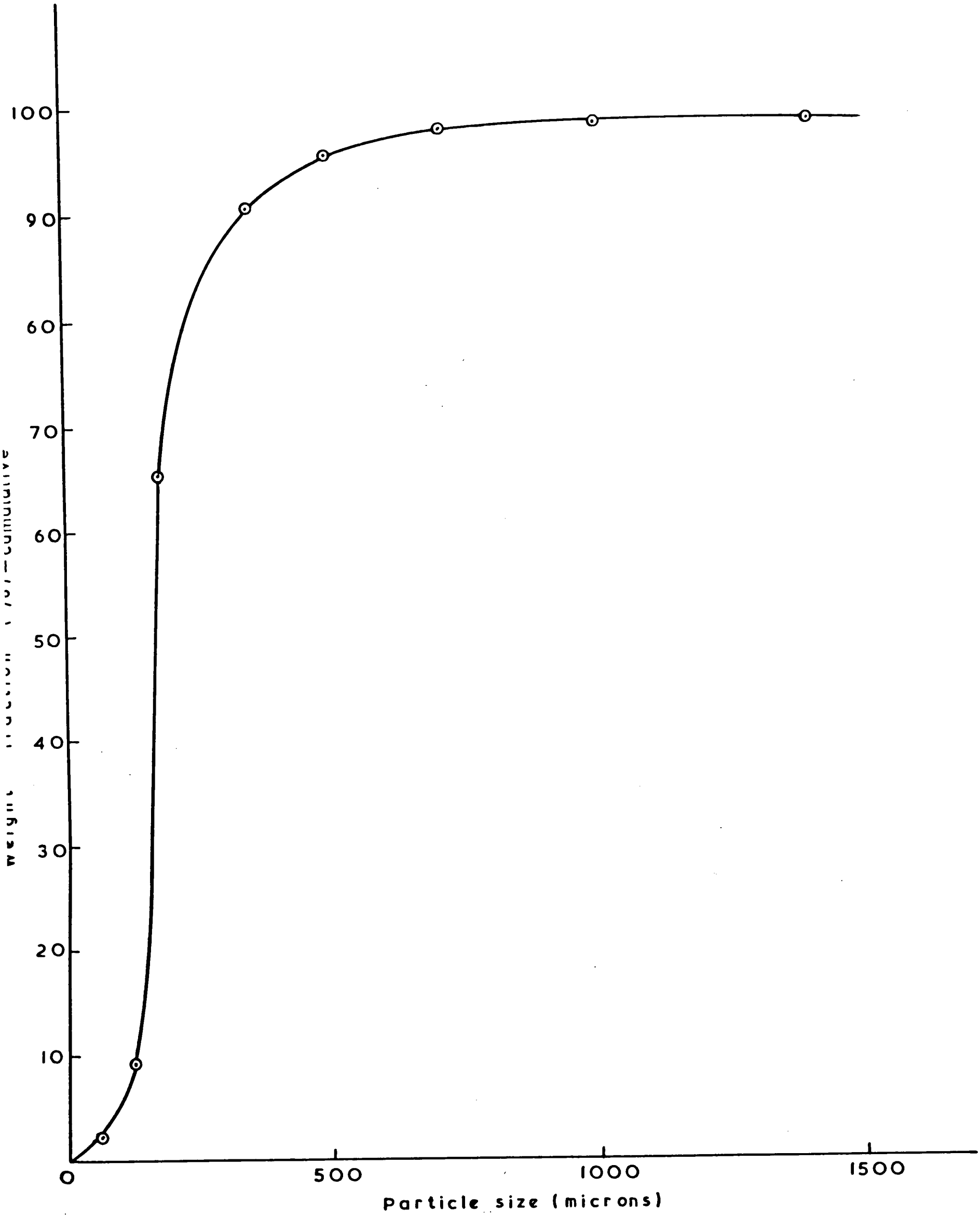


Fig. 2.5.1. Particle Size Distribution of Bulk Soda Ash

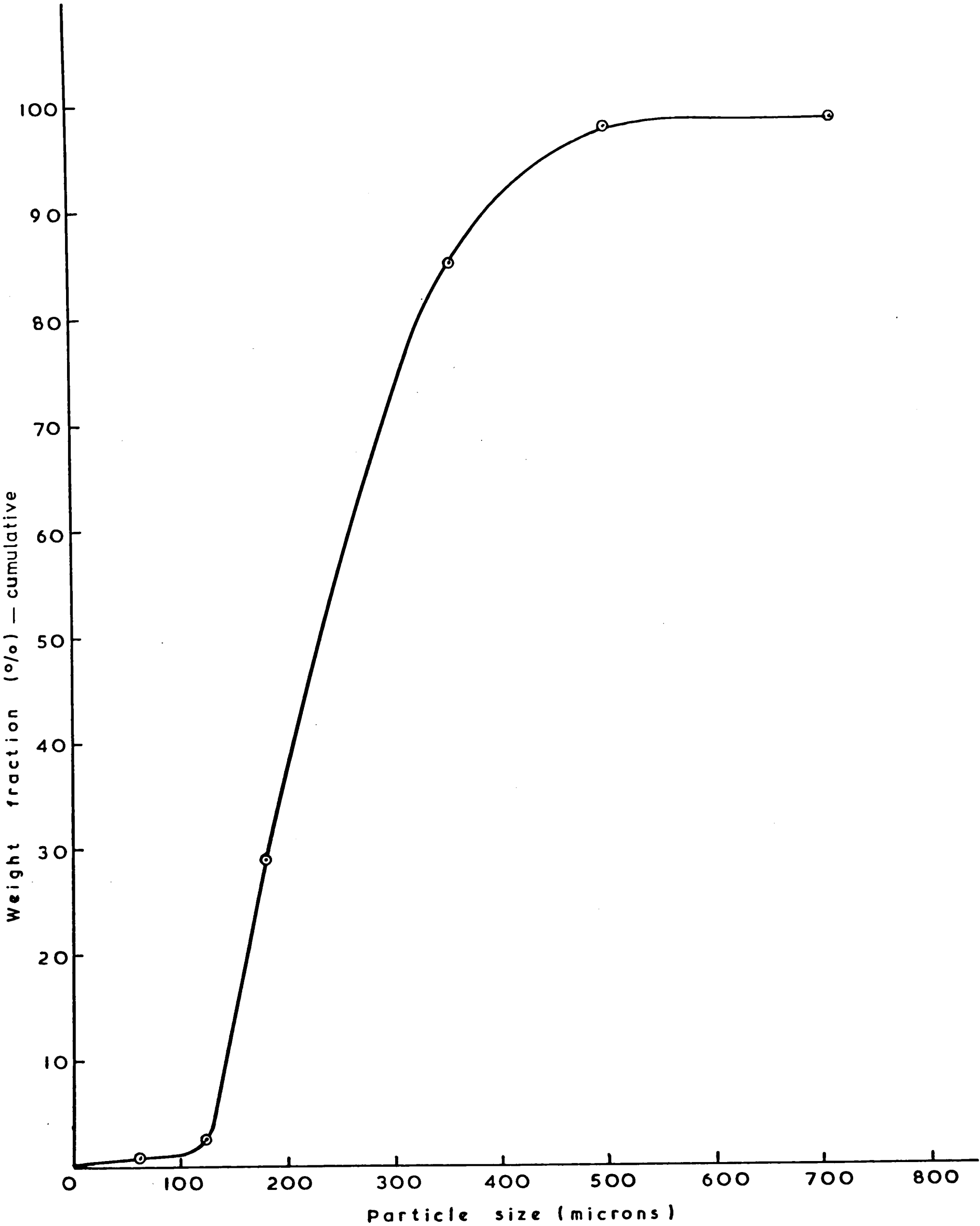


Fig. 2.5.2. Particle Size Distribution of Bulk PDV Salt

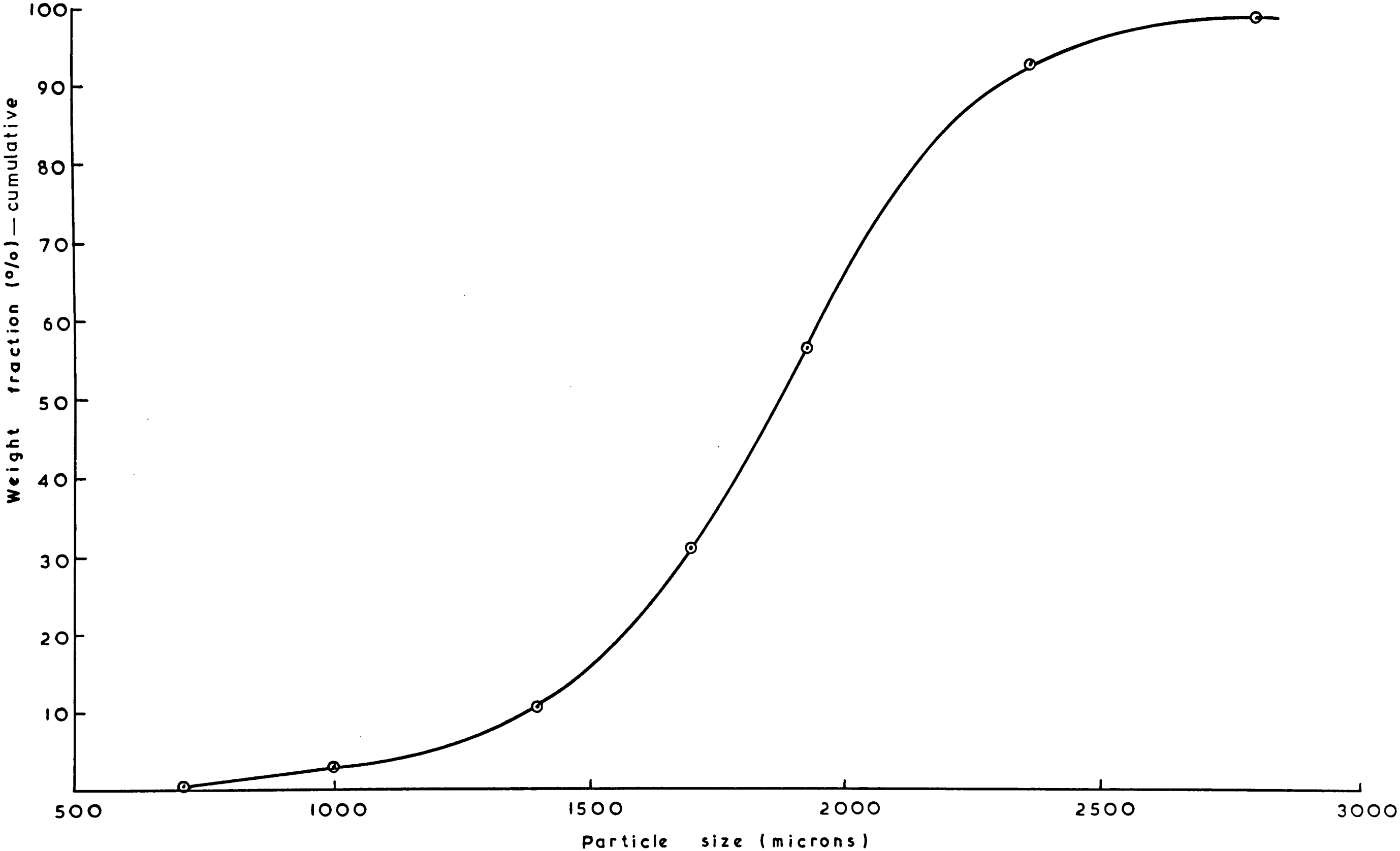


Fig. 2.5.3. Particle Size Distribution of Bulk Granular Salt

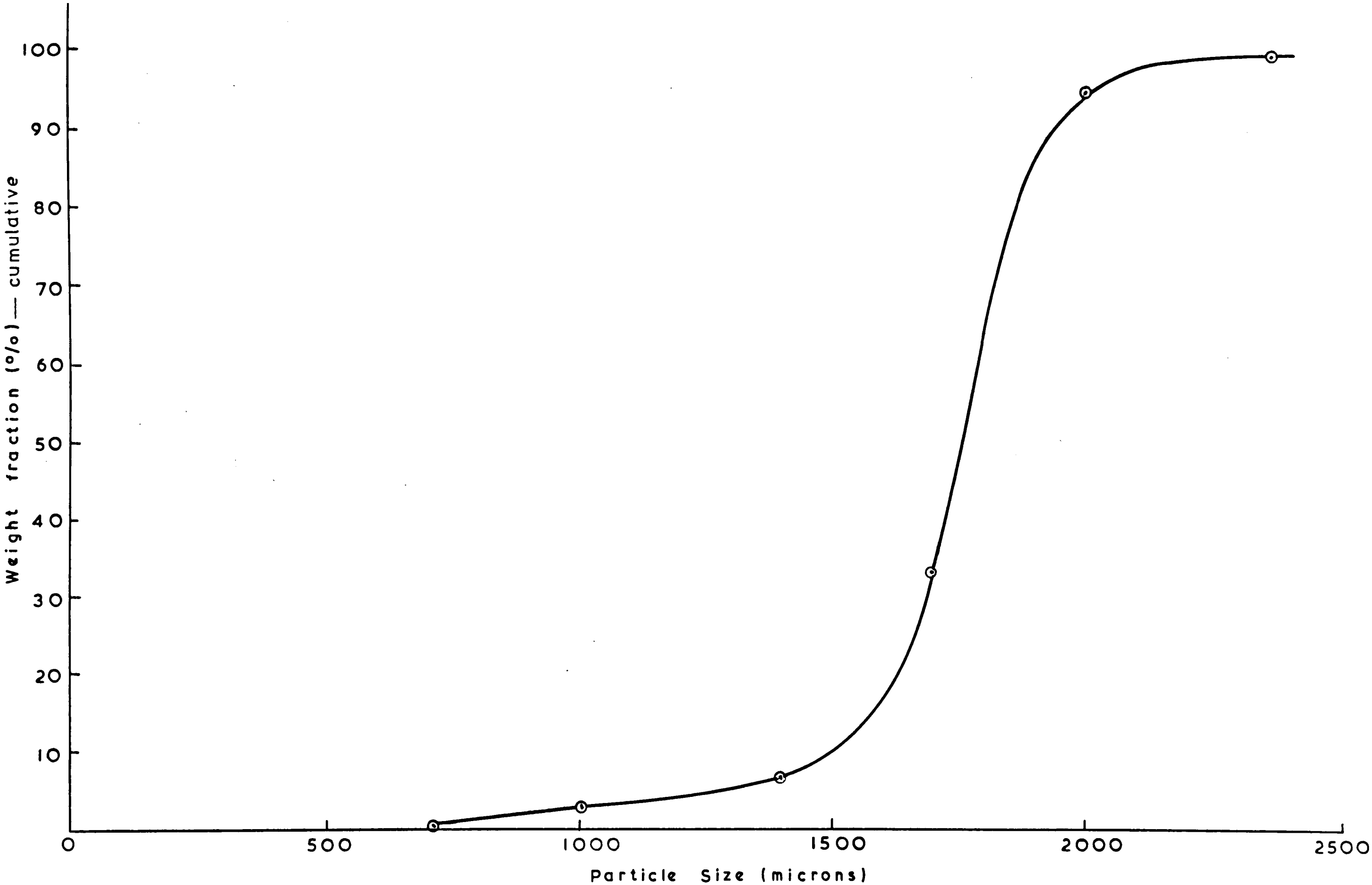


Fig. 2.5.4. Particle Size Distribution of Bulk Molecular Sieve Material

were normally used to carry out each test in all standard runs.

The cell was set up for operation and the sample attrited as described in Section 2.4. The attrited material was then analysed using a nest of 8 inch diameter sieves of the appropriate size range (See Table 2.7.1). The sieves were always mechanically vibrated for five minutes by using an Endecott sieve shaker.

2.7 Sieving

It was found that the procedure of hand-sieving bulk material to isolate the initial sieve-cut of a particular powder worked satisfactorily for all the particles used except for sodium carbonate. For sodium carbonate, it was found that if the hand-sieved material was further sieved on a sieve shaker, significant amounts passed through the 250 μm sieve. A full analysis of the work carried out to allow for this effect is described in detail at a later chapter.

The end-point for sieving attrited product on the sieve shaker was also analysed rigorously. BS 1796 (1976) states that the end-point for non-friable materials may be reached when the quantity passing through the sieve in one minute is less than 0.1% of the charge. The rate test for sieving states that the end-point is reached if less than 0.2% of sample by weight passes through the mesh in any five minute sieving period (ISO 2591, 1973).

Shergold (1946) investigated the effect of sieving time and load by using specially prepared sand and recorded the time taken for 50% of the charge to pass through a 75 μm sieve. He concluded that, in general, there was no end-point for sieving although the approach to true percentage was quicker for smaller sieve apertures.

Whitby (1958) and Kaye (1962) tried to predict sieving efficiency by mathematical treatment. Whitby found that, when the rate at which particles pass through a sieve is plotted as a function of time on a log-log scale, sieving could be divided into two distinct regions with a transitional area in-between. He suggested that the end-point would occur at the beginning of the second region. As this point was difficult to obtain in practice, a very good estimate was obtained at the intersection of the line through region one and the curve through region two.

The attrition products obtained in the preliminary experiments were studied using the above criteria and a sieving time of five minutes was adopted in practice for all materials.

A variety of sieve aperture ranges are currently used, the most popular being the German Standard, DIN 1171; ASTM Standard E 11-61; the American Tyler series; the French series AFNOR; the Institute of Mining and Metallurgy Standard and the British Standard, BSS 410 (1976). The International Organisation for Standardisation has been attempting to standardise these ranges (ISO 565, 1972) and some of their recommendations have been implemented in the British Standard. All sieves used in the present work were correct to British Standard BSS 410, except for the following which were of the American Tyler series.

(1) 1.7 mm

(2) 500 μm

(3) 250 μm

All sieves used have been listed in Table 2.7.1.

Materials Used				Sieves used in Analysis of Attrited Product (BSS 410)											
Sodium Carbonate											250 µm	180 µm		90 µm	45 µm
PDV Salt											250 µm	180 µm		90 µm	45 µm
Lab Salt									355 µm			180 µm		90 µm	45 µm
PDV Salt							500 µm		355 µm			180 µm		90 µm	45 µm
Silica Gel		1.4 mm	1.0 mm	850 µm		600 µm		425 µm		300 µm			106 µm		
Granular Salt (ex centrifuge)	1.7 mm	1.4 mm	1.0 mm		710 µm				355 µm			180 µm		90 µm	45 µm
Granular Salt (ex crystalliser)	1.7 mm	1.4 mm	1.0 mm		710 µm				355 µm			180 µm		90 µm	45 µm
Molecular Sieve	1.7 mm	1.4 mm	1.0 mm		710 µm				355 µm			180 µm		90 µm	45 µm

Table 2.7.1 Sieves used in Particle Size Analysis of Ground Product

All sieves were in the BSS series, except the 250 µm, 500 µm and 1.7 mm ones which were from the Tyler series.

2.8 The Failure Zone

To identify the shape and position of the failure zone, the cell was filled with powder and strained for a few revolutions under fixed operating conditions. A vertical column of coloured tracer particles, otherwise identical to the bulk, was then placed in the bed by inserting a hollow tube into the powder bed, filling it with tracer and then removing it, thus leaving the tracer in the bed. The cell was then run for one revolution and the powder carefully stripped down in layers. At each level, the circumferential position of the tracer particles was noted.

It was seen that the initially vertical column of tracer was displaced such that the tracer particle in the bottom layer of powder had travelled one complete revolution, whilst the position of the tracer in the top powder layer was relatively unchanged. The tracer particles in the intermediate powder layers had undergone corresponding circumferential displacement. Examples of failure zone identification experiments are presented in Appendix B.

CHAPTER THREE

MOLECULAR SIEVE

3.0 Introduction

Molecular sieve beads were tested in the cell and used to assess its performance. The primary particles are agglomerated and are made of crystalline metal aluminosilicates in a three dimensional interconnecting network structure of silica and alumina tetrahedra. The beads are porous and spherical in shape, made up of concentric layers and shell-like in composition. The bulk density of the material is 950 kg/m^3. Experimental runs were carried out with beads of initial diameter between 1.7 and 2.0 mm, and the ground product analysed using a nest of sieves of the following sizes: 1.7 mm, 1.4 mm, 1.0 mm, 710 μm, 355 μm, 180 μm, 90 μm, 45 μm. The effects of varying the number of revolutions of the cell, the normal stress, the cell speed and sample thickness were assessed in turn.

3.1 Reproducibility

The first aspect of cell operation to be investigated was the reproducibility of results under constant operating conditions. If a fixed weight of initial material was attrited under fixed process conditions, successive runs would be expected to produce the same particle size distribution of the ground product provided the cell behaved in a consistent manner.

Tables 3.1.1, 3.1.2 and 3.1.3 show the product particle size distributions under varying cell revolutions, normal stress and cell speed respectively, where all other process conditions were held constant. Experiments were repeated to assess reproducibility of results as shown in the Tables. Examination of data clearly shows that the results were reproducible in all cases.

A statistical analysis was also carried out on the values. A partial F-test (details given in Appendix C) was performed on each column in the tables where the standard deviation for each reproducible group of runs was obtained. For Table 3.1.1, these were as follows:

> 1.7 mm	standard deviation 0.90
1.4 - 1.7 mm	standard deviation 1.17
1.0 - 1.4 mm	standard deviation 0.118
710 µm - 1.0 mm	standard deviation 0.108
355 - 710 µm	standard deviation 0.197
180 - 355 µm	standard deviation 0.404
< 180 µm	standard deviation 0.395

The standard deviation of a set of reproducible runs was a measure of the variability in that group; as seen, the variance was small.

A similar procedure was carried out for values in Table 3.1.2 and Table 3.1.3 and the figures are as follows:

>1.7 mm	standard deviation 0.998
1.4 - 1.7 mm	standard deviation 0.792
1.0 - 1.4 mm	standard deviation 0.437
710 µm - 1.0 mm	standard deviation 0.096

Torque (Nm)		Number of Revs (Initial Weight)	Particle Size Distribution (gm)						Normal Stress kN/m^2
Av	Max		<180µm	180-355 µm	355-710 µm	710 µm-1 mm	1-1.4 mm	1.4-1.7 mm	>1.7 mm	
37.3	40.7	1 (100 gm)	0.7	0.6	1.3	0.7	0.9	4.2	91.8	41.4
37.3	45.2		0.7	0.6	1.2	0.7	1.0	5.8	90.4	
31.6	38.4	2 (100 gm)	1.4	1.2	2.2	1.0	1.3	4.8	88.2	41.4
30.5	36.2		1.1	0.8	1.6	0.8	1.1	7.2	87.8	
30.5	38.4	5 (100 gm)	2.7	2.2	2.6	1.1	1.7	6.3	83.2	41.4
29.4	36.2		2.8	2.1	2.7	1.1	1.8	6.7	82.8	
31.6	40.7	10 (100 gm)	5.0	2.8	2.8	1.1	2.2	7.2	78.9	41.4
28.2	38.4		4.5	3.3	2.8	1.2	2.4	8.9	76.6	
28.2	36.2	25 (100 gm)	7.1	8.3	3.6	1.7	3.9	10.0	65.2	41.4
28.2	36.2		6.0	9.4	3.7	1.7	4.1	8.5	65.9	

TABLE 3.1.1 Molecular Sieve Material - Variation of Shear Strain

Normal Stress - 41.4 kN/m^2
Sample Thickness - 12.0 mm
Cell Speed - 5 rpm
Sieve Shaker - 5 mins.

Torque (Nm)		No. of Revs (Initial Weight)	Particle Size Distribution (gm)							Normal Stress kN/m²
Av	Max		<180µm	180-355 µm	355-710 µm	710 µm-1 mm	1-1.4 mm	1.4-1.7 mm	>1.7 mm	
31.6	38.4	2 (100 gm)	1.4	1.2	2.2	1.0	1.3	4.8	88.2	41.4
30.5	6.2		1.1	0.8	1.6	0.8	1.1	7.2	87.8	
39.5	45.2	2 (100 gm)	2.6	2.2	3.1	1.2	1.6	3.3	86.4	82.8
39.5	47.5		2.8	2.3	3.4	1.3	1.7	3.7	84.8	
52.0	56.5	2 (100 gm)	4.9	5.0	4.6	1.5	2.2	5.2	76.6	124.0
52.0	56.5		5.4	5.4	4.6	1.5	2.0	5.0	76.3	
61.0	67.8	2 (100 gm)	7.4	5.5	5.1	1.6	2.5	5.5	72.4	166.0
70.1	76.8		5.4	8.0	5.1	1.5	2.1	5.2	73.5	
79.1	85.9	2 (100 gm)	10.0	7.9	5.5	1.7	2.3	4.8	67.8	207.0
79.1	83.6		10.4	7.9	5.4	1.5	2.2	4.6	68.6	
92.7	101.7	2 (100 gm)	11.8	10.1	5.7	1.5	2.2	4.9	64.4	248.0
91.5	99.4		11.3	9.8	5.4	1.4	2.1	3.7	67.1	

TABLE 3.1.2 Molecular Sieve Material - Variation of Normal Stress
Cell Speed - 5 rpm
Sample Thickness - 12.0 mm
Shear Strain - 36.9 per revolution
Sieve Shaker - 5 mins

Torque (Nm)		Number of Revs (Initial Weight)	Particle Size Distribution (gm)						Cell Speed (rpm)
Av	Max		<180µm	180-355 µm	355-710 µm	710 µm-1 mm	1-1.4 mm	1.4-1.7 mm	>1.7 mm	
30.5	40.7	2 (100 gm)	1.2	1.0	1.9	0.9	1.2	2.7	92.8	1.25
28.2	45.2		1.2	1.0	1.9	0.9	1.2	3.0	92.5	
32.8	45.2	2 (100 gm)	1.3	1.0	2.0	0.9	1.2	3.4	91.2	2.5
32.8	45.2		1.2	0.9	1.8	0.8	1.1	3.1	92.6	
31.6	38.4	2 (100 gm)	1.4	1.2	2.2	1.0	1.3	4.8	88.2	5.0
30.5	36.2		1.1	0.8	1.6	0.8	1.1	7.2	87.8	
30.5	33.9	2 (100 gm)	1.1	0.9	1.7	0.7	1.0	2.6	93.1	10.0
33.9	40.7		0.9	0.7	1.4	0.6	0.8	2.4	95.3	
33.9	38.4	2 (100 gm)	0.7	0.6	1.2	0.5	0.8	3.5	93.3	15.0
33.9	38.4		0.8	0.6	1.2	0.5	0.7	3.6	93.3	

TABLE 3.1.3 Molecular Sieve Material - Variation of Strain Rate

Normal Stress - 41.4 kN/m²
Sample Thickness - 12.0 mm
Shear Strain - 36.9 per revolution
Sieve Shaker - 5 mins.

355 - 710 μm	standard deviation 0.214
180 - 355 μm	standard deviation 0.746
<180 μm	standard deviation 0.632
>1.7 mm	standard deviation 0.840
1.4 - 1.7 mm	standard deviation 0.774
1.0 - 1.4 mm	standard deviation 0.10
710 μm - 1.0 mm	standard deviation 0.077
355 - 710 μm	standard deviation 0.221
180 - 355 μm	standard deviation 0.145
<180 μm	standard deviation 0.122

The above results show that there were no significant differences between duplicate runs, confirming that the cell behaved in a consistent manner.

3.2 Effect of Cell Revolutions or Shear Strain

100 gm of sample material of sieve-cut between 1.7 - 2.0 mm was attrited under operating conditions such that only the number of cell revolutions was varied. For convenience, the cell speed was normally set at 5 rpm. This meant that, under standard experimental procedure where material was attrited for up to twenty-five revolutions of the cell, samples were ground for up to five minutes. This corresponded to a mean shear strain of 36.9 per revolution and strain rate of 3.1 sec^{-1}. The attrited product was separated, again using the standard nest of sieves previously specified, on the sieve shaker and the new particle size distribution analysed.

Results are tabulated in Table 3.1.1 and the corresponding graph given in Figure 3.2.1. The graph shows the weight of material in each sieve-cut after attrition for different numbers of revolutions of the cell. The new particle size distribution is bi-modal with the 1.7 mm material grinding down to exhibit a characteristic minimum around the 850 μm size before rising again to a peak at 250 μm with increasing shear strain. Thus, increasing attrition times (shear strain) are seen to produce a monotonic increase in the amount of fines.

3.3 Effect of Normal Stress

100 gm of material of sieve-cut between 1.7 - 2.0 mm was again used, and the normal stress was varied where all other process variables were held constant. The results are shown in Table 3.1.2 and the graphical representation given in Figure 3.3.1.

The weight of material in each sieve-cut is shown for each normal stress used. The graph shows the characteristic minimum at 850 μm as seen before. The amounts of fines produced increased sharply with increasing normal stress in all the finer sieve-cuts, so that there was no intermediate maximum in this case. Although the coarse end of the distribution appears unordered, the fines seem to increase linearly with increasing normal stress. The results were again systematic at the finer end of the distribution.

3.4 Effect of Cell Speed

100 gm of sample of sieve-cut between 1.7 - 2.0 mm was again used and the cell speed varied whilst all other process variables were

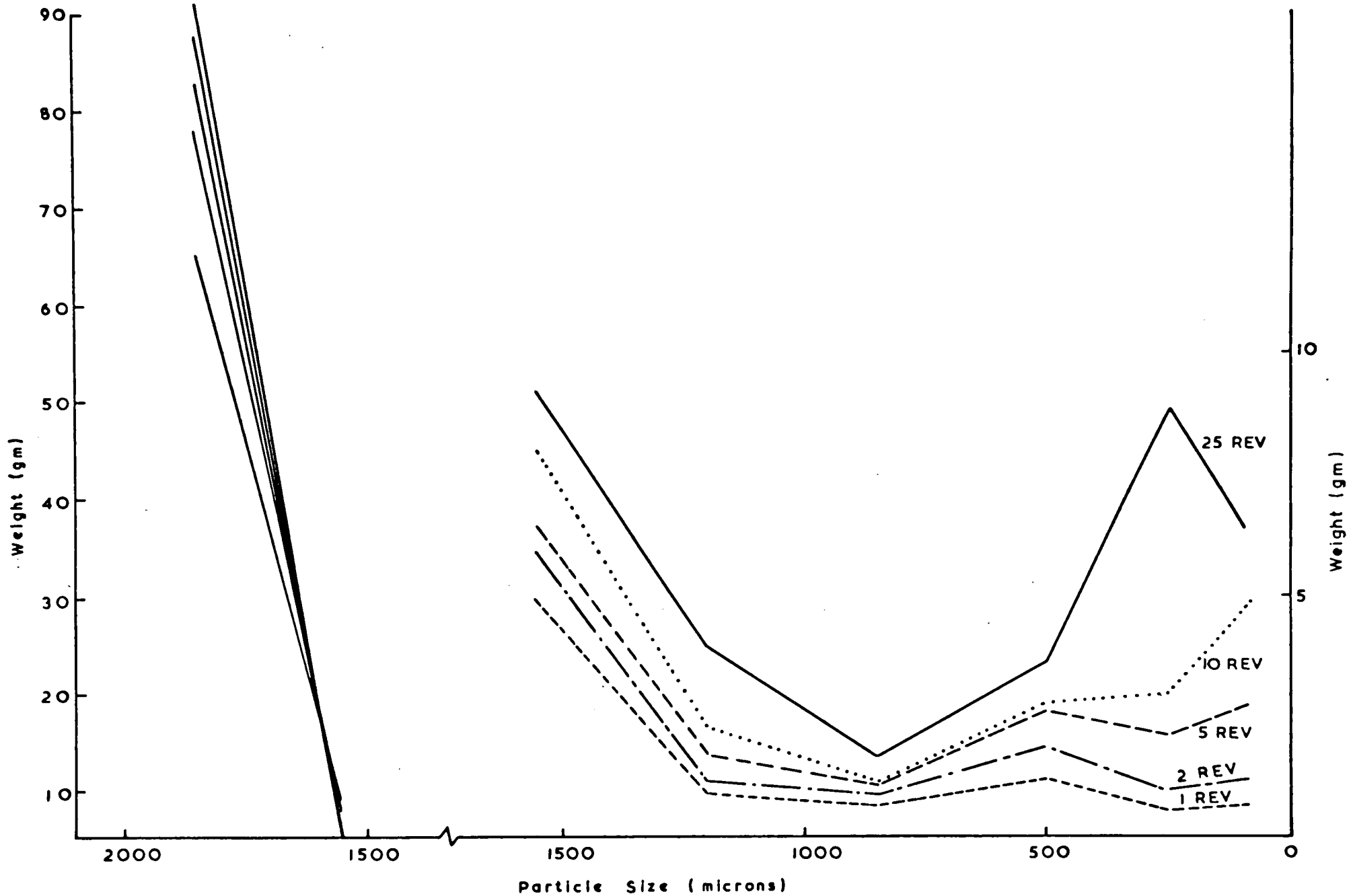


Fig. 3.2.1. Particle Size Distribution of Molecular Sieve beads (1·7-2·0mm) Effect of Strain on Attrition

Normal stress — 41·4 kN/m^2 Sample thickness — 12·0 mm

Shear stress — 36·9 per revolution Cell speed — 5 r.p.m.

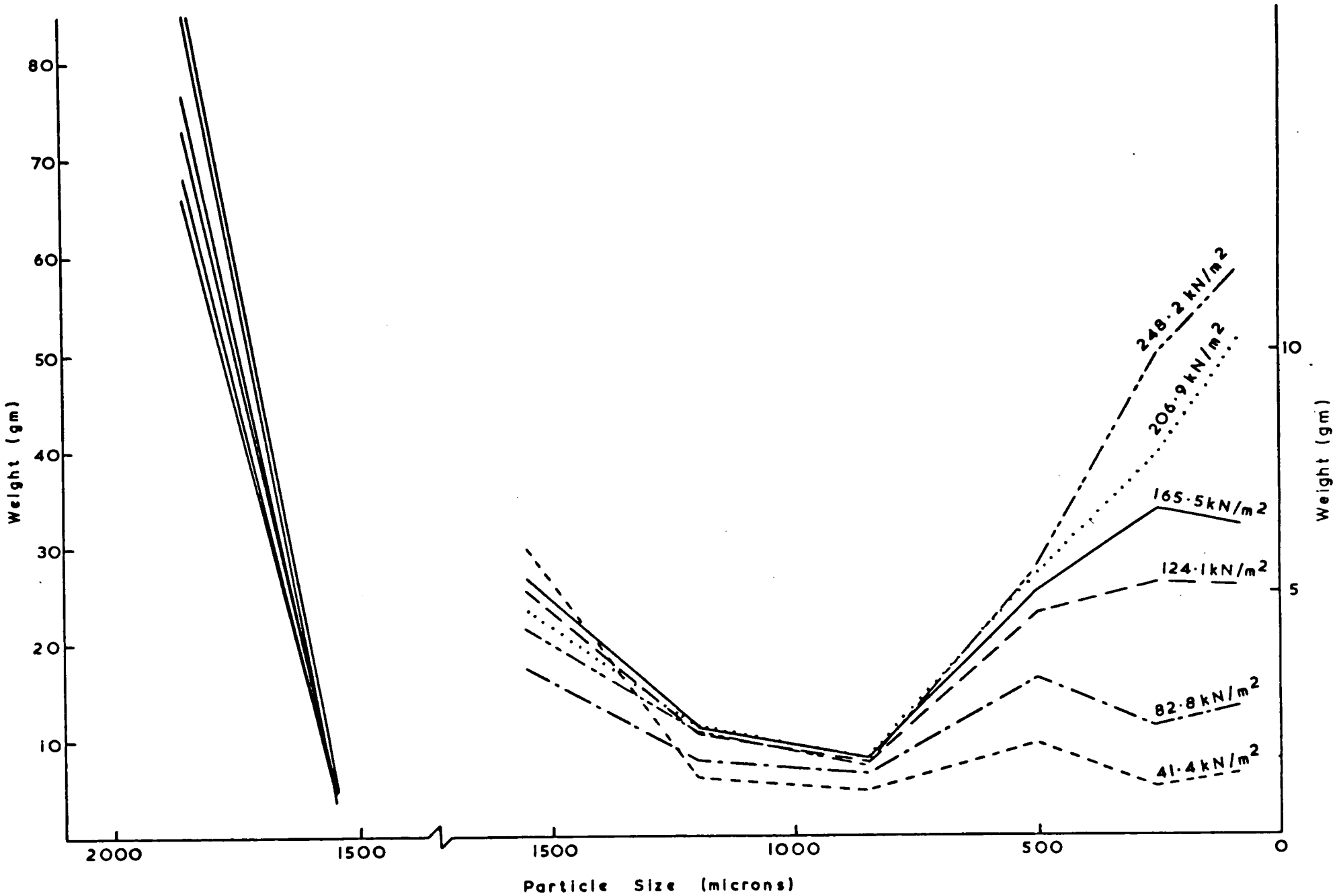


Fig. 3.3.1 Particle Size Distribution of Molecular Sieve beads (1·7–2·0mm).
Effect of Normal Stress on Attrition

No. of revolutions — 2 Shear strain — 36·9 per revolution
Sample thickness — 12·0mm Cell speed — 5 r.p.m.

held constant. Results are given in Table 3.1.3 and Figure 3.4.1.

Results show that particles attrite in a similar manner when the cell speed is varied, although less fines are seen to be produced at the two fastest speeds.

A partial F-test was again used where the variation between groups (ie. between different cell speeds) was analysed, and the figures given below:

>1.7 mm	standard deviation 3.39
1.4 - 1.7 mm	standard deviation 1.96
1.0 - 1.4 mm	standard deviation 0.289
710 μm - 1.0 mm	standard deviation 0.252
355 - 710 μm	standard deviaiton 0.443
180 - 355 μm	standard deviation 0.243
<180 μm	standard deviation 0.306

As seen the variation is small and it is inferred that cell speed did not affect the rate of particle attrition.

3.5 Effect of Sample Thickness

The standard experimental procedure was repeated using different sample weights where the normal stress and cell speed were held constant. Results are shown in Table 3.5.1 and Figure 3.5.1. Since experimental conditions remained unaltered, the energy input per unit mass into the cell to effect attrition should have remained constant.

If, however, the powder behaved in a uniform manner in the cell, the energy input for attrition per unit mass of powder should result in

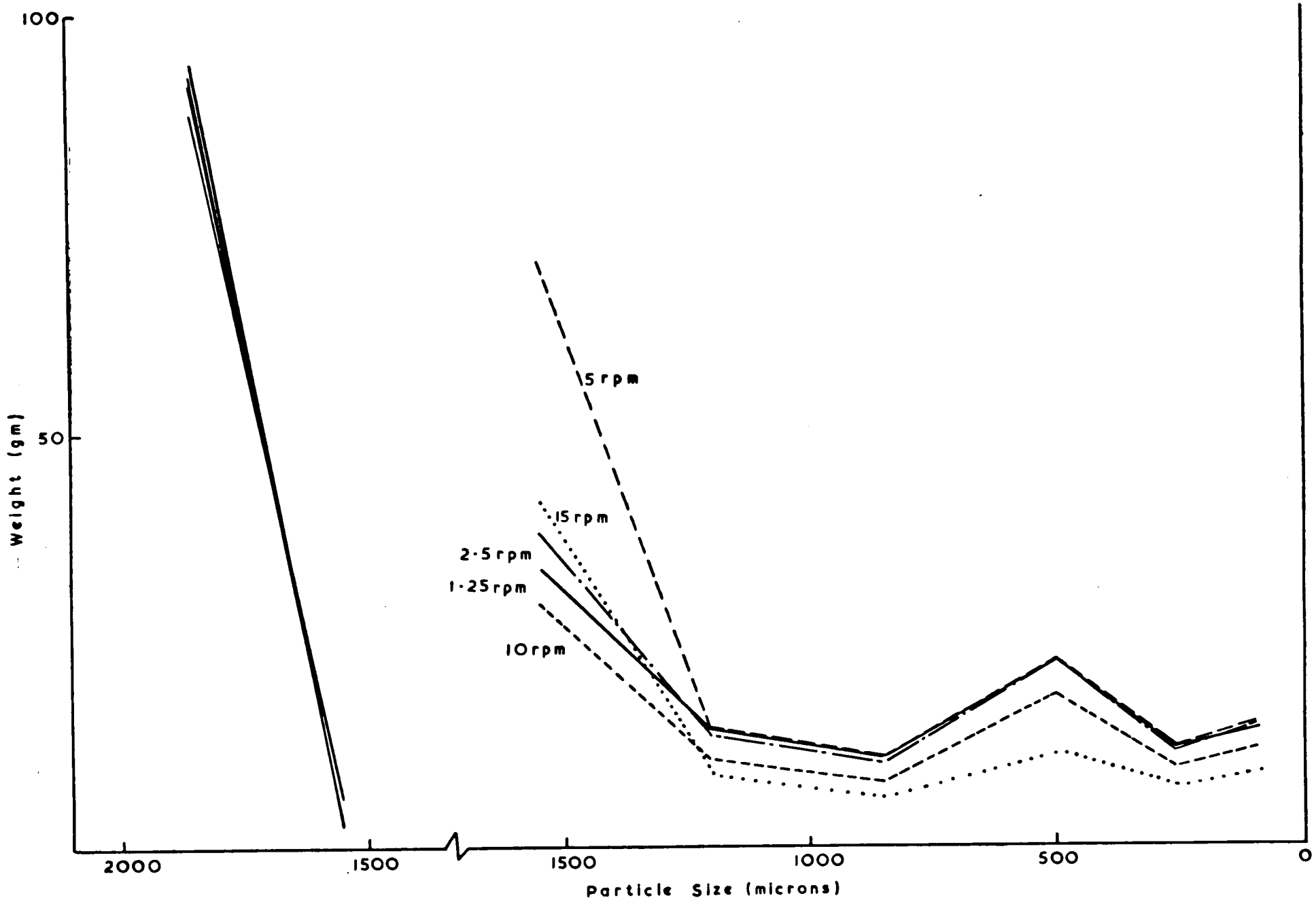


Fig. 3.4.1. Molecular Sieve beads (1·7 – 2·0mm)
Effect of Cell Speed on Attrition

Normal stress – 41·4 kN/m^2 Sample thickness – 12·0mm

Shear strain – 36·9 per revolution Number of revolutions – 2

Torque (Nm)	
Av	Max
28.2	36.2
28.2	33.9
30.5	38.4
29.4	36.2
35.0	42.9
35.0	47.5

Sample Weight (gm)	Particle Size Distribution (gm)							Number of Revs
	<180µm	180-355 µm	355-710 µm	710 µm-1 mm	1-1.4 mm	1.4-1.7 mm	>1.7 mm	
50	5.0	2.2	1.7	0.8	1.6	5.0	34.1	5
	5.1	2.3	1.7	0.9	1.6	4.6	34.2	
100	2.7	2.2	2.6	1.1	1.7	6.3	83.2	5
	2.8	2.1	2.7	1.1	1.8	6.7	82.8	
150	1.1	1.0	1.7	0.6	1.0	5.2	139.6	5
	0.9	0.8	1.4	0.5	0.9	6.5	139.6	

TABLE 3.5.1 Molecular Sieve Material - Variation of Sample Thickness

Normal Stress - 41.4 kN/m^2
Sample Thickness - 6 mm, 12 mm, 18 mm
Shear Strain - 73.8, 36.9, 24.6 per revolution
Sieve Shaker - 5 mins.
Cell Speed - 5 rpm

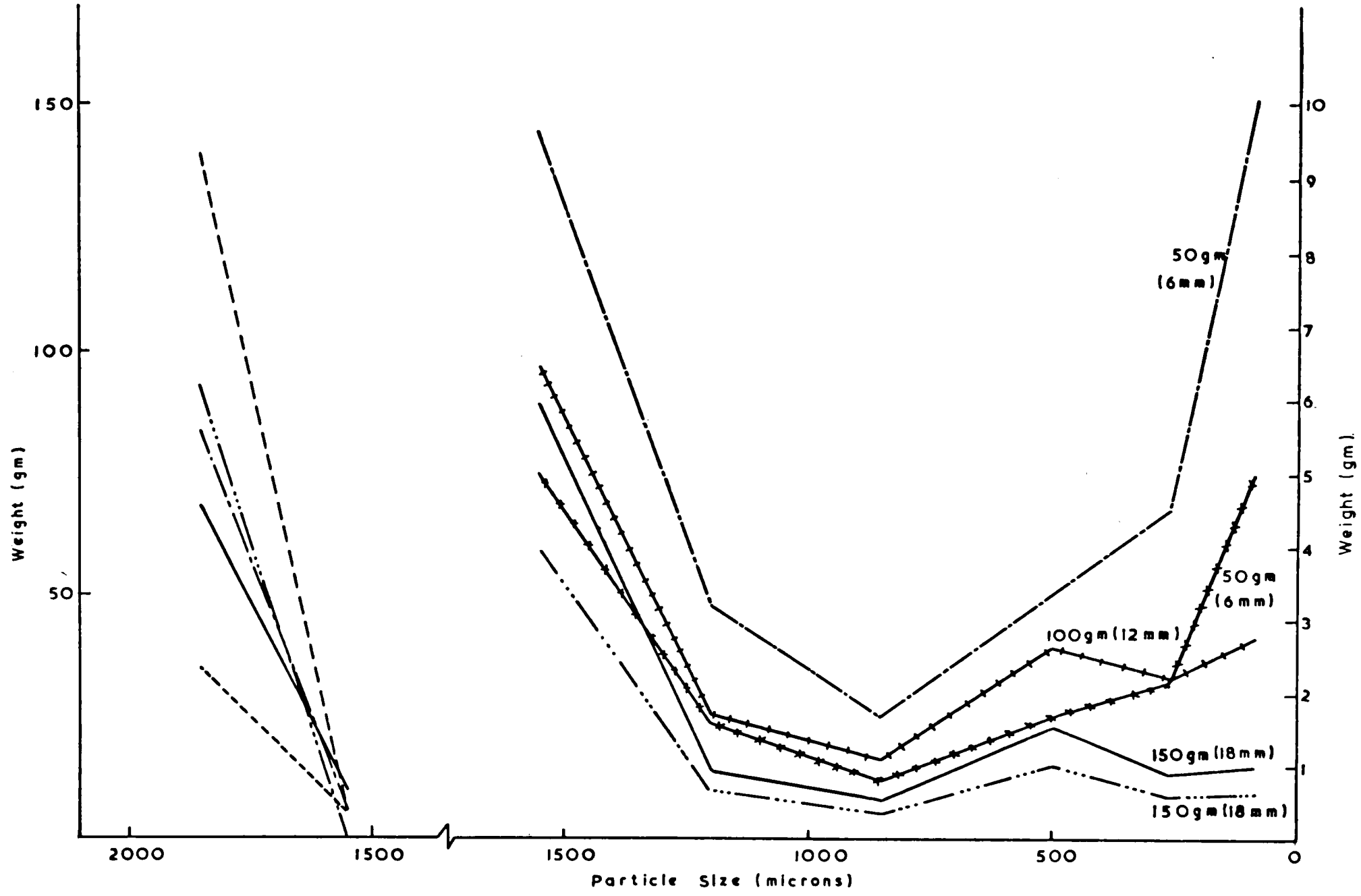


Fig. 3.5.1. Molecular Sieve material (1·7 – 2·0mm). Effect of Sample Thickness on Attrition
Solid Lines – Wt. Distribution. Broken Lines – Wt. Percentage Distribution.

Normal stress – 41·4 kN/m^2 Cell speed – 5 rpm

Sample thickness – 6mm, 12mm, 18mm Shear strain – 36·9 per revolution

No. of revolutions – 5

consistent particle size distributions for the same initial material, provided an appropriate quantity of material exists in the cell for true particle to particle grinding to take place. A series of experiments were then carried out where the particles were subjected to the same shear strain in every case. Sample weights and shear strains were varied in a fixed ratio to achieve this purpose.

Ratios of 10:1 and 50:1 of sample weight to the number of cell revolutions were selected on the basis of the practicable extremes that could be used for a number of sample thicknesses. If the ratios were too large, the sample weight could then have exceeded the failure zone depth. Too small a ratio would have resulted in a very thin particle layer in the cell where crushing, rather than true particle to particle grinding, would have been the controlling mechanism.

The results of the constant shear strain experiments are shown in Figures 3.5.2 and 3.5.3. These results do not show any particular trend except to show that the same minimum is obtained at 850 μm.

However, when the experimental data are plotted as a ratio of weight from each sieve-cut divided by the total weight of sample, ie the percentage weight in each sieve fraction, a much greater uniformity of results is produced, especially at the coarser end of the distribution (Figures 3.5.4, 3.5.5). This uniformity or normalisation of the data also extended to the fine end of the distribution, although in the 50:1 case there was little improvement; thus, at the longer strain, excellent consistency is observed. Some scatter of results is apparent in the 1.4 - 1.7 mm range, the largest but one sieve-cut, which suggests some cell start-up effect.

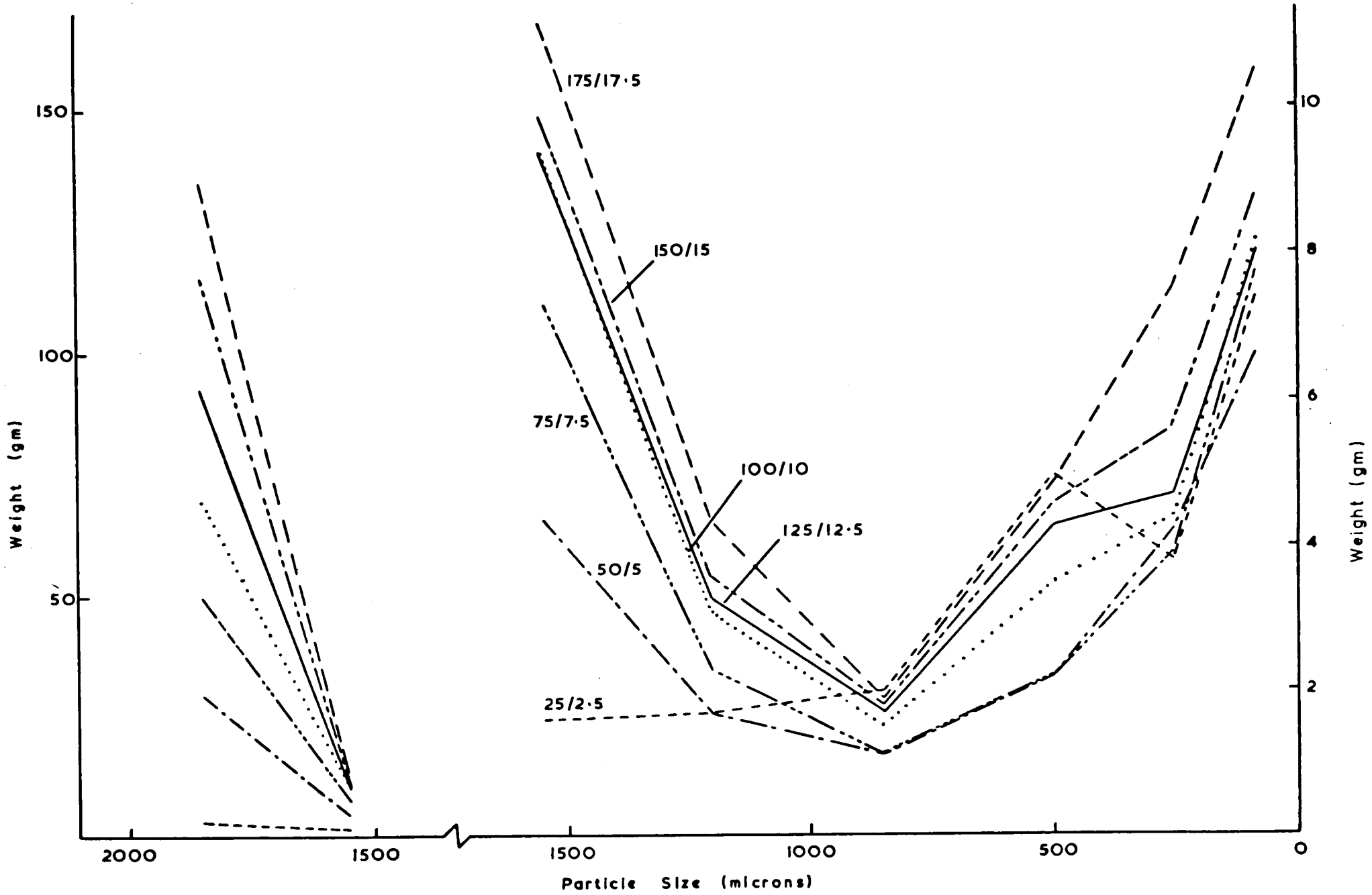


Fig. 3.5.2 Particle Size Distribution of Molecular Sieve material (1·7-2·0mm). Effect of constant sample wt/cell rev. ratio (10/1) on Attrition (wt)

Normal stress – 41·4 kN/m^2 Shear strain — Variable

Sample thickness — 3,6,9,12,15,18,21mm Cell speed — 5r.p.m.

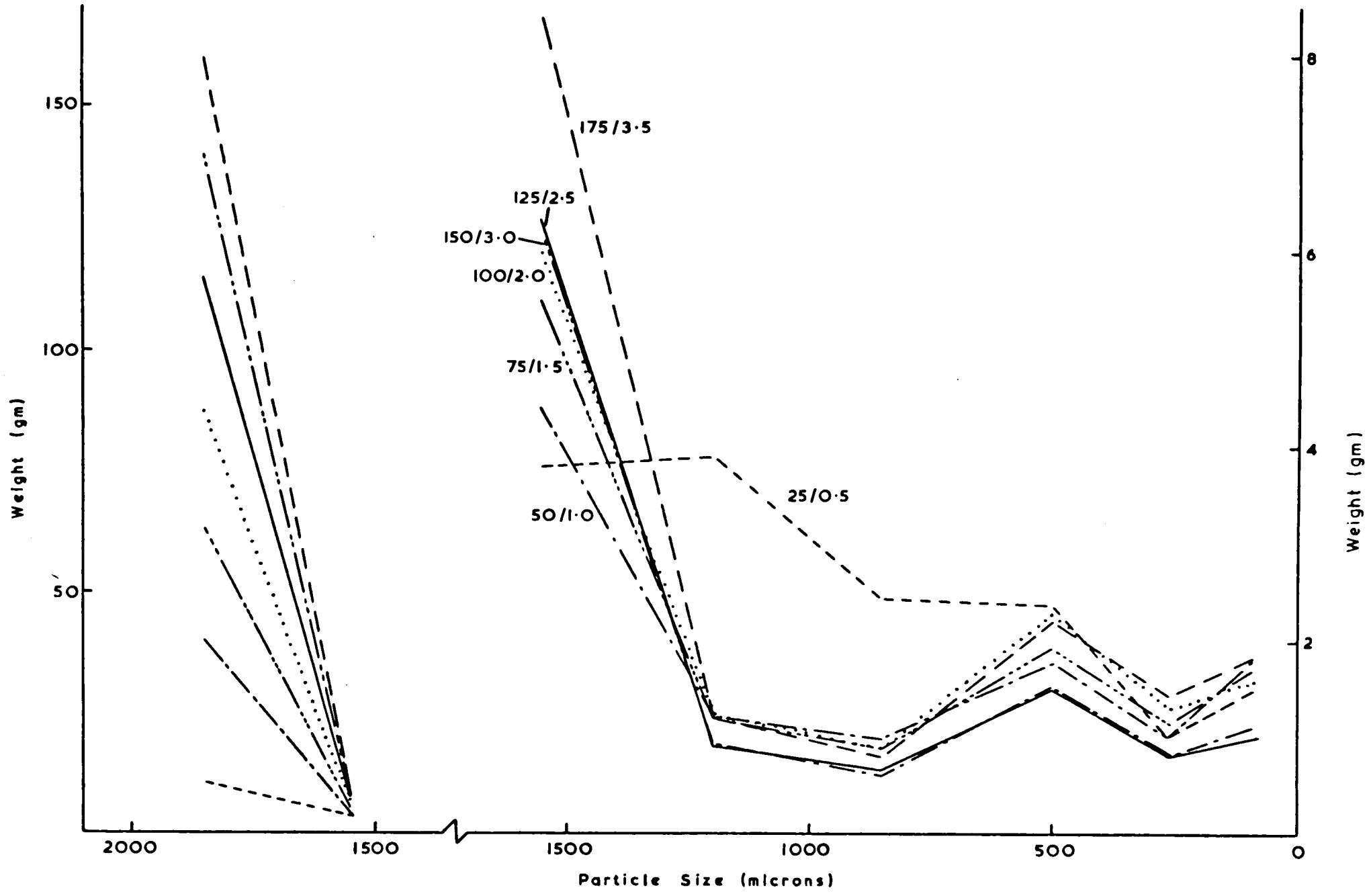


Fig. 3.5.3 Particle Size Distribution of Molecular Sieve material (1·7 – 2·0mm). Effect of constant sample wt/cell rev. ratio (50/1) on Attrition (wt)

Normal stress – 41·4kN/m^2 Sample thickness – 3,6,9,12,15,18,21mm
Cell speed – 5r.p.m.

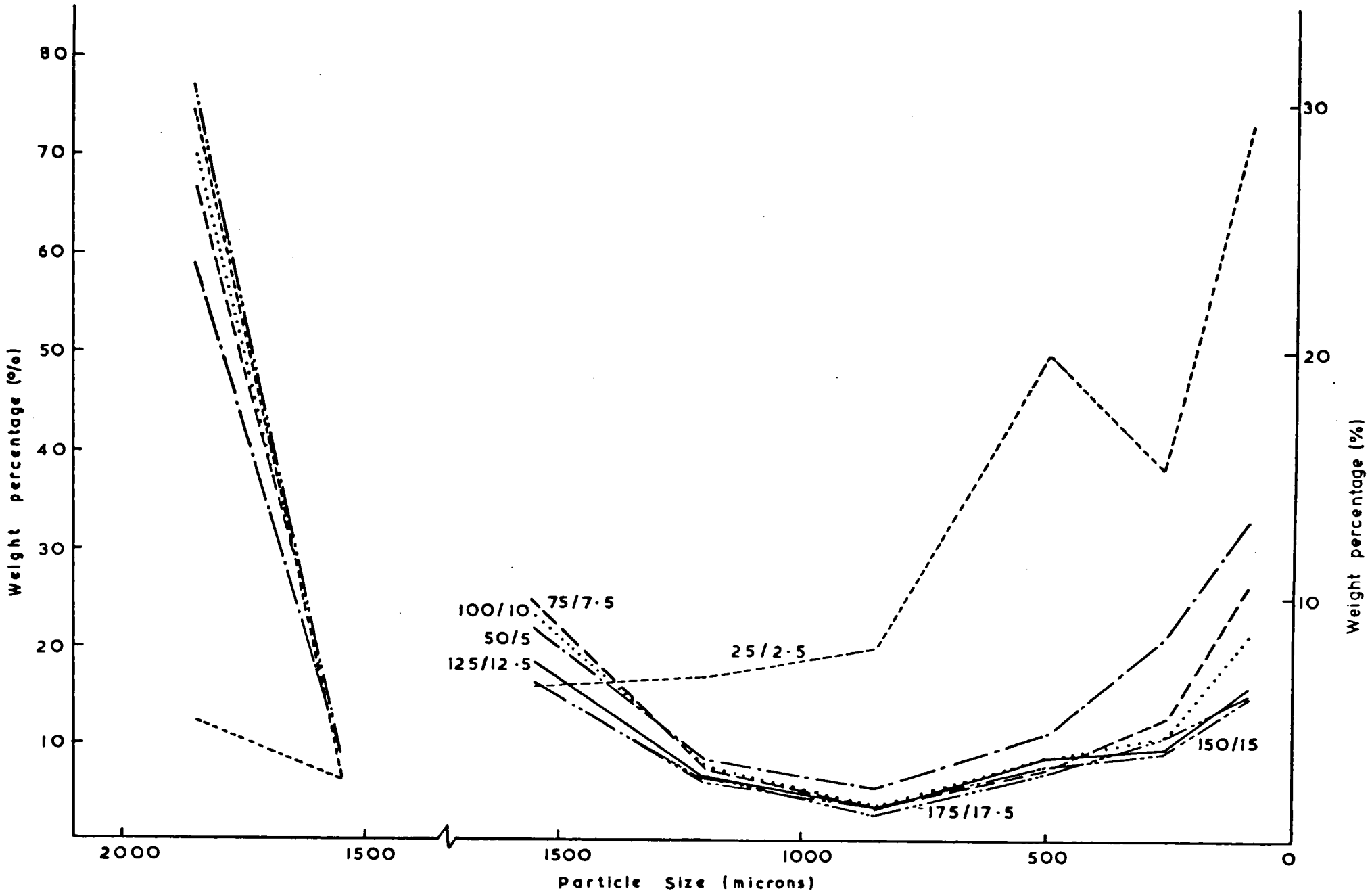


Fig. 3.5.4. Particle Size Distribution of Molecular Sieve material (1·7 – 2·0mm)
Effect of constant sample wt/cell rev. ratio (10/1) on Attrition (wt %)

Normal stress – 41·4 kN/m^2 Sample thickness – 3.6.9.12.15.18.21 mm

Cell speed – 5 r.p.m.

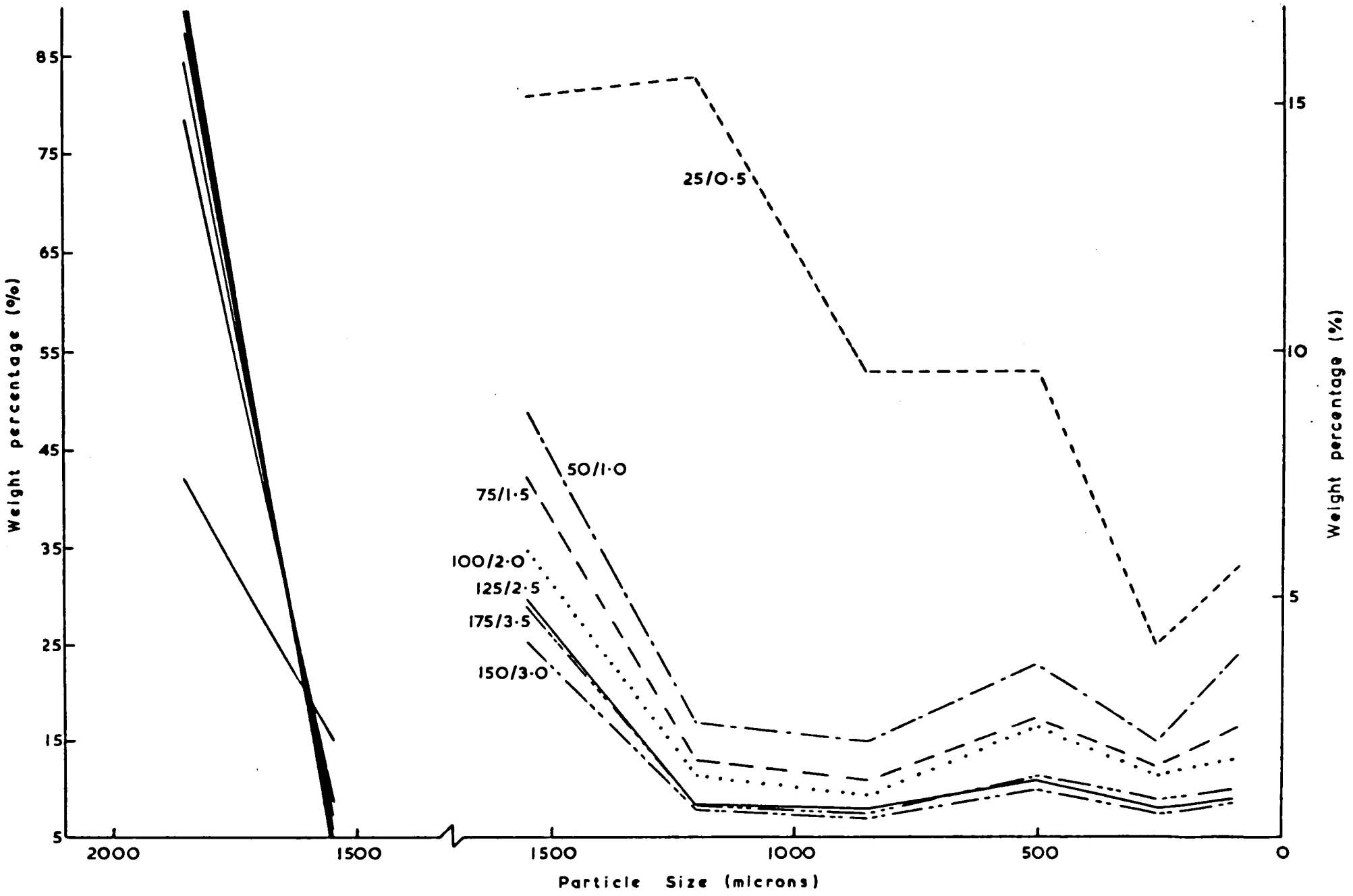


Fig. 3.5.5 Particle Size Distribution of Molecular Sieve material (1·7-2·0mm). Effect of constant sample wt/cell rev. ratio (50/1) on Attrition (wt %)

Normal stress — 41·4 kN/m² Sample thickness — 3,6,9,12,15,18,21 mm
Cell speed — 5 r.p.m.

The smallest weight of sample used (25 gm) in the experiments showed the greatest deviation from the normalised behaviour in both cases. This was due to the presence of a mono-layer of material in the cell, and the resulting attrition during cell operation was deduced to be due more to the crushing of gripped particles rather than to true particle to particle grinding.

The effect of the normalisation procedure showed that samples subjected to a given shear strain produced similar particle size distributions, showing that the powder sample was truly in the failure zone and that attrition effected by the cell was due to true particle to particle grinding for this material.

3.6 Influence of Sample History

In order to determine whether previous history of sample material had any effect on the attrition process, previously ground material was attrited to examine any difference in behaviour.

Samples of 100 gm each of sieve-cut between 1.7 - 2.0 mm was attrited under fixed experimental conditions for one revolution of the cell and the new particle size distribution determined, using sieves, in the normal manner. Results are shown in Table 3.6.1.

The top fraction, i.e. size greater than 1.7 mm, was isolated from each run (Runs A) and mixed together so that a sample of 100 gm was made up of attrited material of diameter between 1.7 - 2.0 mm. This sample was then attrited under the same experimental conditions to obtain the new particle size distribution (Run B).

Torque (Nm) Av	Torque (Nm) Max	Run Type	Particle Size Distribution (gm) <180 µm	180-355 µm	355-710 µm	710 µm-1 mm	1-1.4 mm	1.4-1.7 mm	>1.7 mm	Number of Revs
37.3	40.7	A	0.55	0.5	1.13	0.57	0.75	6.25	90.69	1
87.3	45.2	A	0.55	0.5	1.16	0.55	0.75	6.4	90.5	
37.3	45.2	B	0.61	0.5	1.15	0.55	0.72	6.3	90.53	
31.6	38.4	A	1.1	0.92	1.64	0.79	1.1	7.0	87.7	2
30.5	36.2	A	1.0	0.89	1.63	0.8	1.14	7.3	87.2	
30.5	36.2	B	1.0	0.9	1.6	0.8	1.1	7.1	87.5	
30.5	38.4	A	2.6	2.2	2.68	1.18	1.74	6.33	83.31	5
29.4	38.4	A	2.61	2.21	2.63	1.13	1.7	6.37	83.34	
30.5	36.2	B	2.54	2.22	2.72	1.11	1.82	6.34	83.23	

TABLE 3.6.1 Molecular Sieve Material - Attrition of Coarse end Attrited Product

Normal Stress - 41.4 kN/m^2
Sample Thickness - 12.0 mm
Shear Strain - 36.9 per revolution
Sieve Shaker - 5 mins.
Cell Speed - 5 rpm

A - Attrition of fresh material
B - Attrition of attrited material

A similar procedure was carried out for two and five revolutions of the cell and the results are also included in Table 3.6.1.

Examination of data shows clearly that no significant difference is observed between Runs A and Run B carried out under the same process conditions. A partial F-test, similar to that described in Section 3.1.1, was again carried out on each column of the table and the standard deviation of each group of duplicate runs was determined. These are as follows:

> 1.7 mm	standard deviation 0.16
1.4 - 1.7 mm	standard deviation 0.099
1.0 - 1.4 mm	standard deviation 0.039
710 μm - 1.0 mm	standard deviation 0.022
355 - 710 μm	standard deviation 0.03
180 - 355 μm	standard deviation 0.011
< 180 μm	standard deviation 0.045

Results show that very little difference is seen between the different runs carried out under the same process conditions, indicating that there was no difference between runs of fresh and previously attrited material. Hence, for this material, sample history had little effect on attrition.

3.7 Segregation of Particles

When experiments were carried out using high normal stresses or shear strains, some segregation of attrited material was seen to occur when the cell was emptied for analysis. Fines were seen to have moved to the bottom of the annulus. In order to investigate the effect of segregation on attrition, several experiments with different

sample weights were carried out with the cell operated in the normal vertical position and then repeated with continous inversion, the cell being inverted at the end of every revolution. In each case, the cell was revolved ten times; the results presented in Table 3.7.1.

Again, examination of the data clearly shows that the particle size distributions obtained by operating the cell with and without inversion produced similar values. A partial F-test was also carried out, as explained previously, and the results shown below.

> 1.7 mm	standard deviation 0.592
1.4 - 1.7 mm	standard deviation 0.41
1.0 - 1.4 mm	standard deviation 0.071
710 μm - 1.0 mm	standard deviation 0.029
355 - 710 μm	standard deviation 0.058
180 - 355 μm	standard deviation 0.208
< 180 μm	standard deviation 0.141

Results show very little difference between the two modes of operation. Hence, for this particular material, it was concluded that segregation did not affect the attrition process in the cell under normal operating conditions.

3.8 Results According to Gwyn

Results of the weight of attrited material as a function of shear strain (as opposed to time t) were plotted on a log-log plot in the same manner as Gwyn (1969), and a straight line was obtained as seen in Figure 3.8.1.

Torque (Nm)	
Av	Max
28.2	38.4
31.6	40.7
31.6	40.7
28.2	38.4
28.2	38.4
28.2	38.4

Sample Weight (gm)	Particle Size Distribution (gm)							Number of Revs
	<180µm	180-355 µm	355-710 µm	710 µm-1 mm	1-1.4 mm	1.4-1.7 mm	>1.7 mm	
50	7.7	2.9	2.9	0.9	2.1	6.4	27.1	10
	7.5	3.0	2.8	1.0	2.0	5.8	27.9	
100	5.0	2.8	2.8	1.1	2.2	7.2	78.9	10
	4.8	3.1	2.8	1.3	2.3	8.0	77.8	
150	2.3	1.7	2.3	0.8	1.1	12.8	129.0	10
	2.1	1.3	2.2	0.8	1.2	12.9	129.5	

TABLE 3.7.1 Molecular Sieve Material - Attrition with Cell Inversion

Normal Stress - 41.4 kN/m^2
Sample Thickness - 6 mm, 12 mm, 18 mm
Shear Strain - 73.8, 36.9, 24.6 per revolution
Sieve Shaker - 5 mins.
Cell Speed - 5 rpm

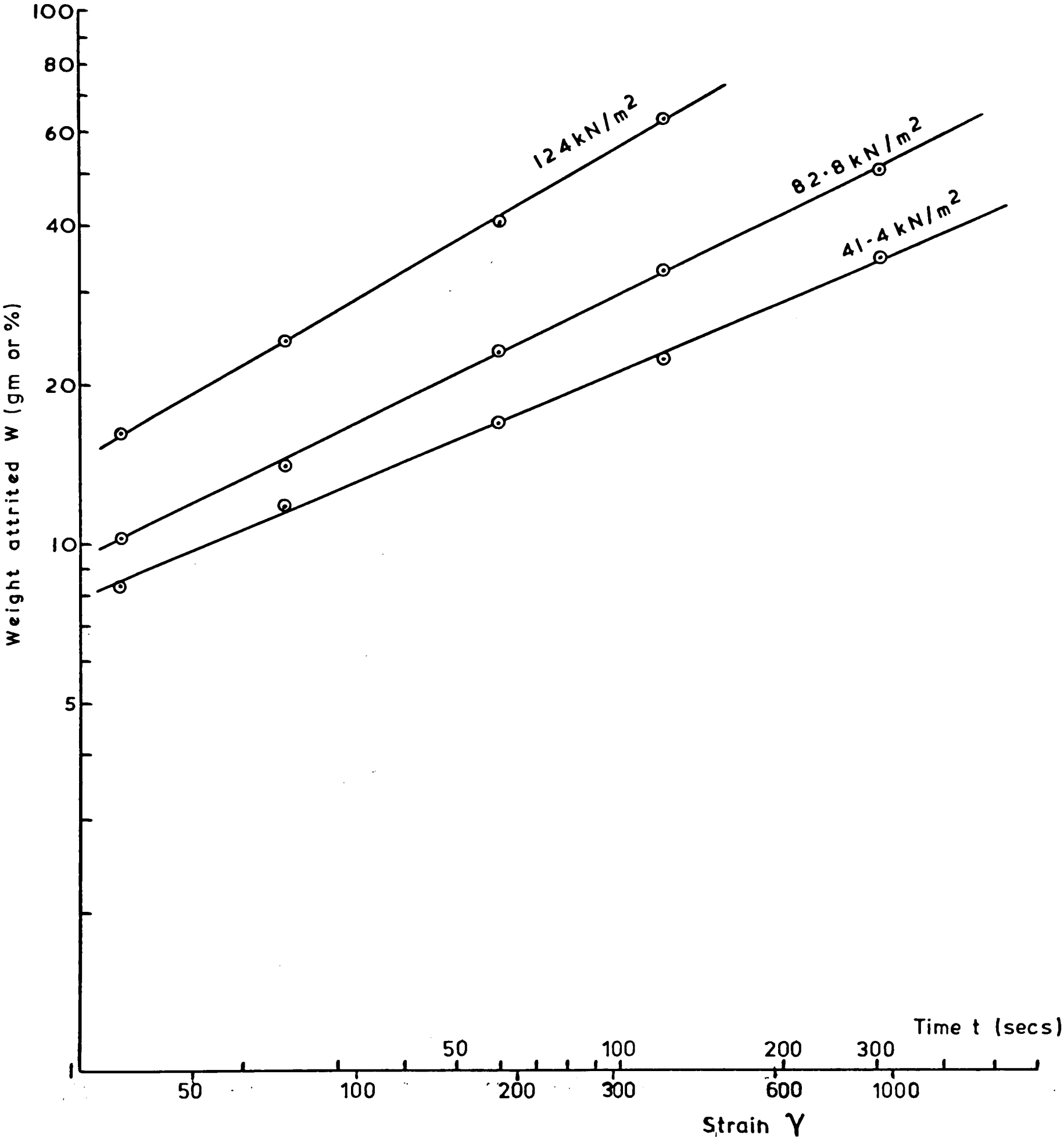


Fig. 3.8.1 Molecular Sieve material (Gwyn Plot)

Sample weight — 100gm

Sample thickness — 12mm

Shear strain — 36·9 per revolution

Cell speed — 5 r.p.m.

Effect of Shear Strain on Attrition at different Normal Stresses

Regression analysis was carried out on the data and the line fitted an equation of the form

$$\log W = 0.43 \log \gamma + 0.25$$

where W is the weight attrited (i.e. weight fraction passing through the top sieve) and γ shear strain.

The effect of normal stress on attrition was also investigated by carrying out experimental runs at higher stresses. Figure 3.8.1 also shows the results of runs at 82.8 kN/m² and 124 kN/m².

Regression analysis was carried out as before to fit the data points and the following equations were obtained.

At 82.8 kN/m²,

$$\log W = 0.51 \log \gamma + 0.21$$

At 124 kN/m²,

$$\log W = 0.60 \log \gamma + 0.27$$

A full summary of the analysis is given in Table 3.8.1. The basis for these expressions is considered in more detail in Chapter 6.

3.9 Mechanism of Attrition

100 gm of material was attrited at 82.8 kN/m² normal stress at a shear strain of 36.9 per revolution for 25 revolutions of the cell. The sample was then analysed using the appropriate nest of sieves. Photographs were taken of the material in each sieve-cut and are shown in Figures 3.9.1a to 3.9.1f.

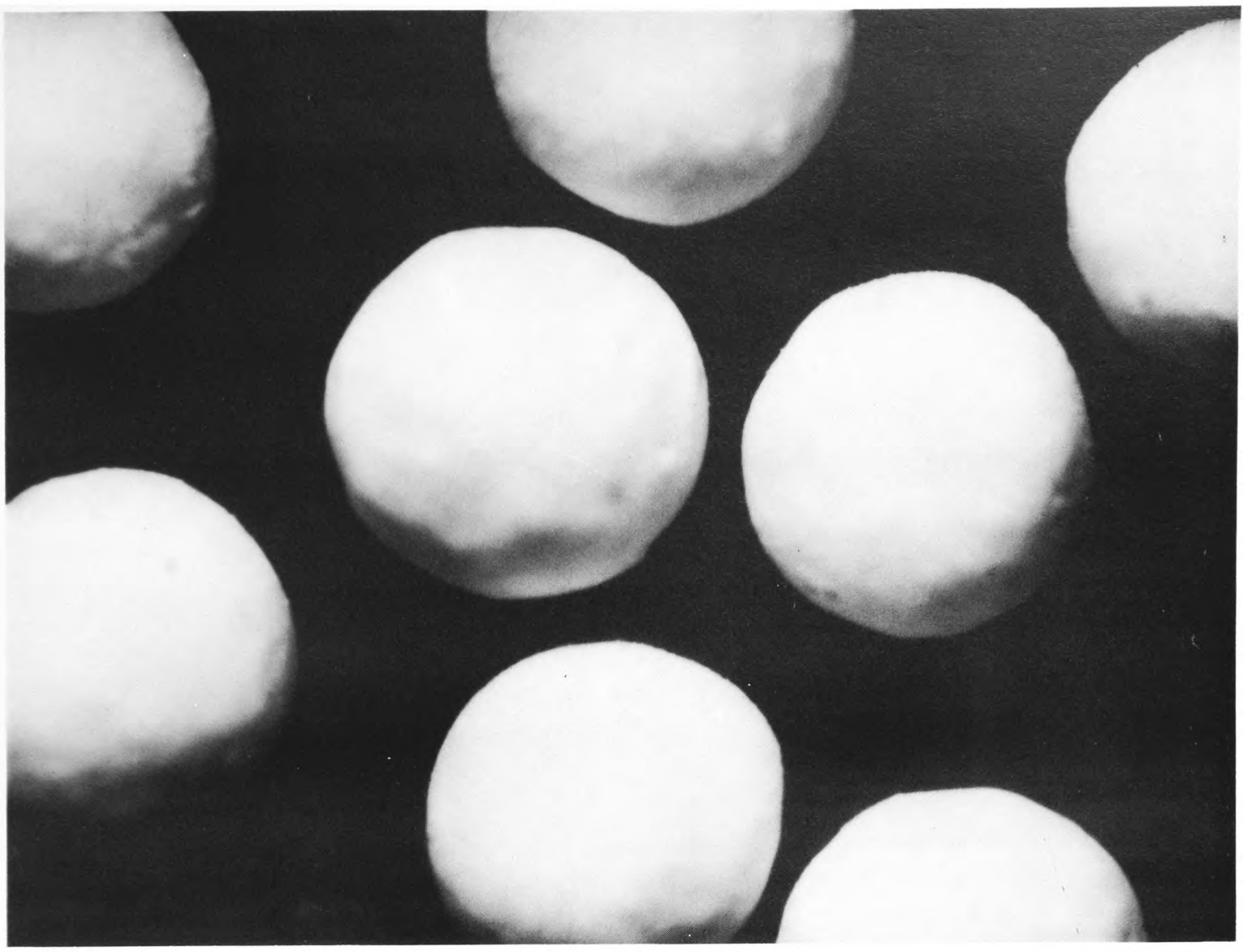
Figures 3.9.1b and 3.9.1c show that these sieve fractions contain both large fragmented particles and others for which several surface layers have been removed together in the form of shells or partial shells. This indicates that the main mechanisms of initial attrition

Normal Stress kN/m^2	Slope	Intercept	Correlation Coefficient %	F-Value	Standard Error of Gradient	Standard Error of Intercept
41.4	0.25	0.46	99.88	1238.4	0.01	0.01
82.8	0.21	0.46	99.97	5380.3	0.007	0.005
124.0	0.27	0.56	99.95	2179.8	0.01	0.01

Table 3.8.1 Molecular Sieve - Summary of Regression Analysis on Gwyn Plots

Fig 3.9.1 Molecular sieve beads attrited at 82.8 kN/m^2 normal stress for 25 revolutions. Relevant sieve cuts shown against each photograph

(a)
1.7-2.0 mm



1 mm

(b)
1.4-1.7 mm



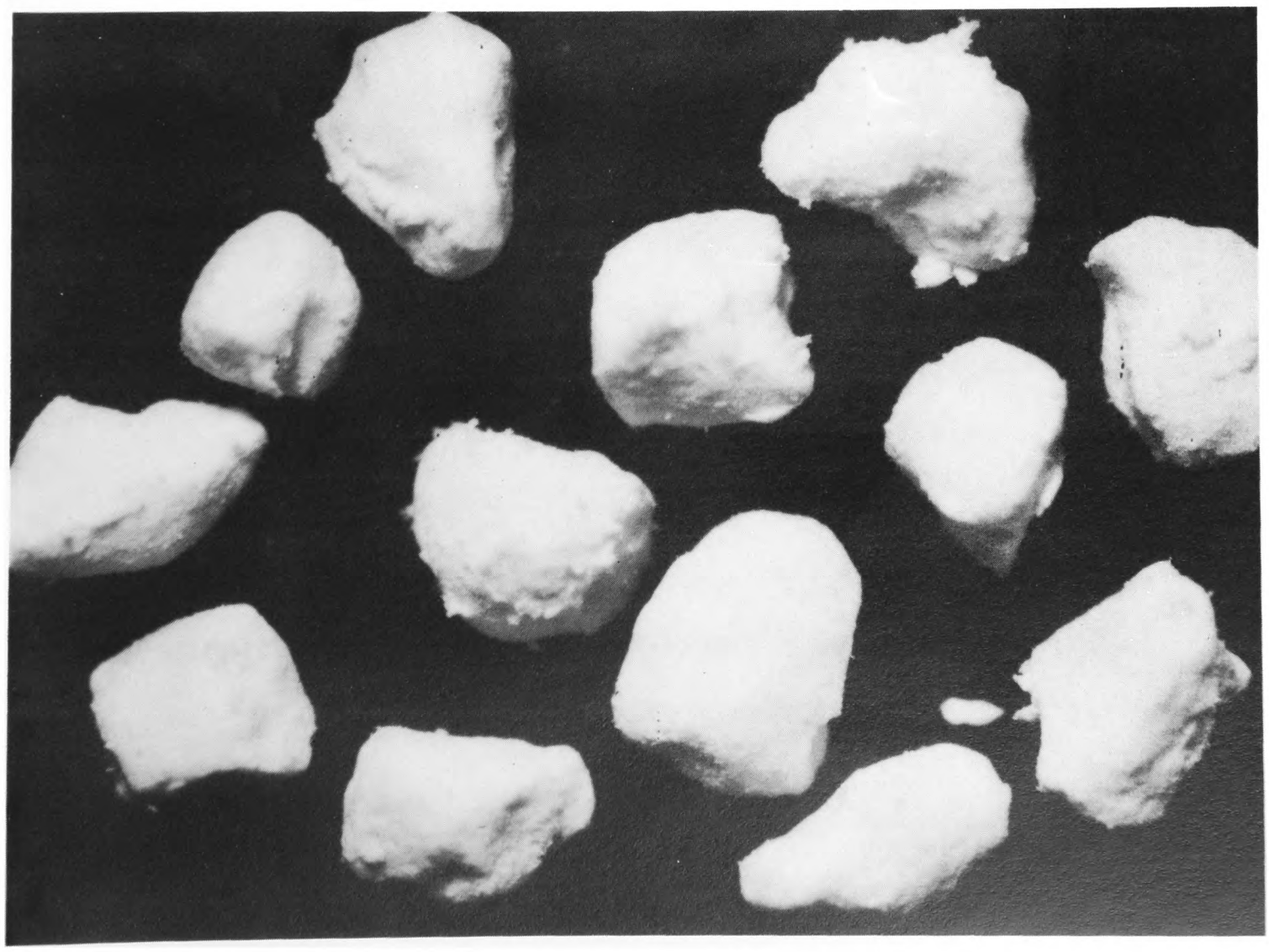
1 mm

(c)
.0-1.4 mm



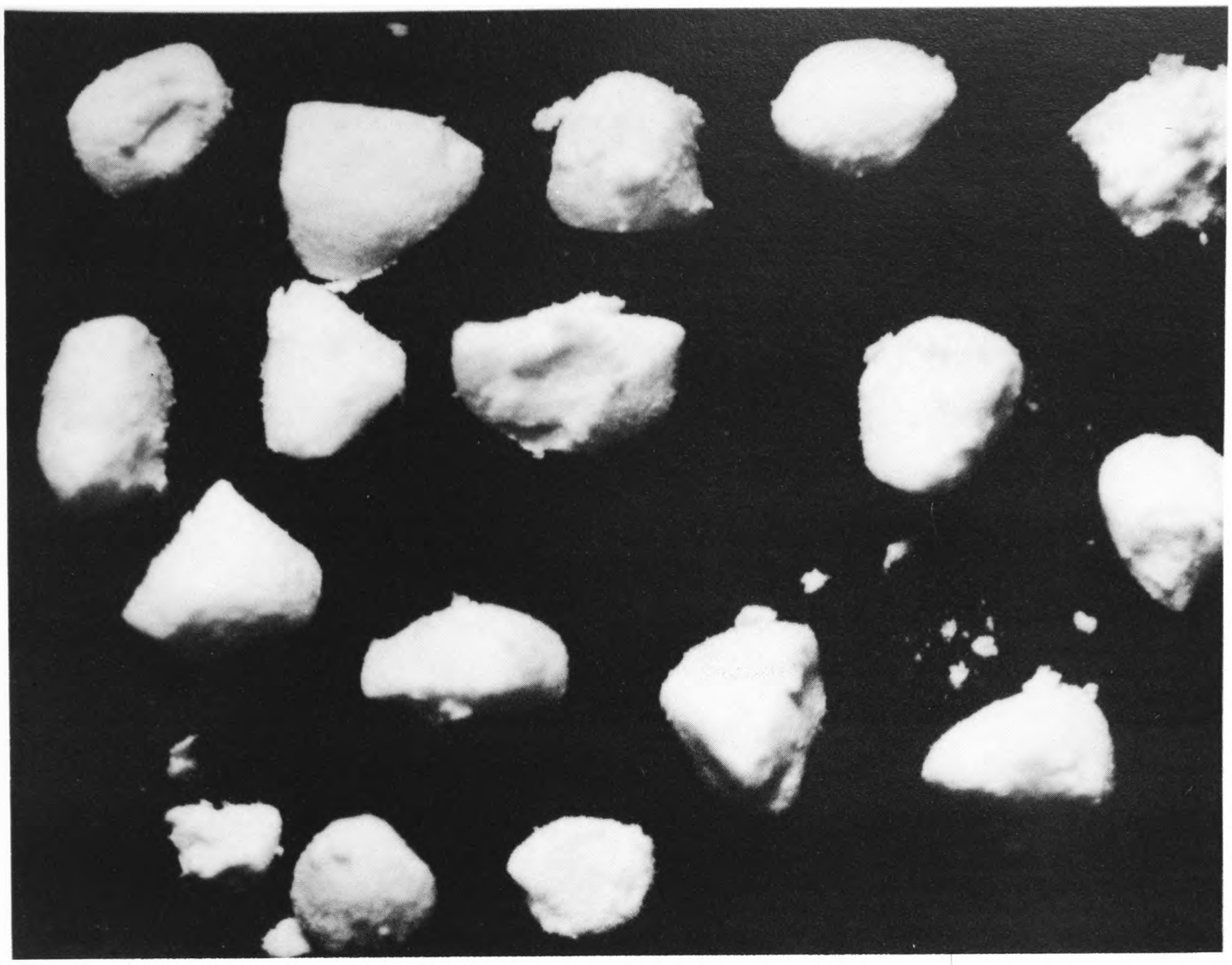
1 mm

d)
m-1.0 mm



1 mm

(e)
355–710 µm



1 mm

(f)
80–355 µm



1 mm

are the shattering of particles with some shelling also taking place. Figures 3.9.1d to 3.9.1f show only fragmented particles and dust, indicating that further attrition takes place mainly by surface grinding. The weaker shells are seen to grind down into fine particles. The smallest sieve fractions, which are not shown, contained only very fine dust particles. Thus, molecular sieve beads were seen to attrite initially by shattering and then by surface grinding.

CHAPTER FOUR

SODIUM CHLORIDE

4.0 Introduction

Three grades of sodium chloride were used, each of which differed in the method of manufacture.

4.0.1 Granular Salt

Granular salt was manufactured by the evaporation of brine using Oslo fluid bed classifying crystallisers. The material is spherical in shape and of bulk density 1140 kg/m^3. Experimental runs were carried out using particles of initial diameter between 1.7 and 2.0 mm. The ground product was then analysed using a nest of sieves of the following sizes: 1.7 mm, 1.4 mm, 1.0 mm, 710 µm, 355 µm, 180 µm, 90 µm, 45 µm.

Most of the experiments were carried out using materials which were not all spherical. The manufacturing process contained a centrifuging stage which damaged some of the particles and the product contained some hemispheres and other debris which could not be removed by sieving. The non-uniform initial shape was thought to introduce new variables in analysing particle attrition and cell performance and, as a result, a quantity of salt was also obtained before the centrifuge stage in the manufacturing process. This material was wholly spherical and is referred to as granular salt (ex. crystalliser) and the previous material as granular salt (ex. centrifuge).

4.0.2 Pure Dried Vacuum Salt (PDV Salt)

Pure dried vacuum salt is also manufactured by the evaporation of brine but this is carried out in conventional forced circulation crystallisers. The salt is separated from the magma by centrifuging, and then dried. PDV salt is cubic in shape with a bulk density of 1260 kg/m^3. Two different sizes of material were used:

(a) most of the experiments were conducted using material of initial size between 500-600 μm, and the following nest of sieves were used in the size analysis of product: 500 μm, 355 μm, 180 μm, 90 μm, 45 μm,

(b) some experiments were also carried out with material of starting size between 250-355 μm, and the following sieves were used in analysing product: 250 μm, 180 μm, 90 μm, 45 μm.

4.0.3 Laboratory Salt (Lab Salt)

Laboratory salt is produced by the evaporation of a solution of PDV salt in a mixed suspension mixed product removal (MSMPR) crystalliser. The long residence time and stirrer speed and shape gave a product that was spherical above 300 μm and cubic below that size. The size range used in experimental runs was between 355-500 μm and hence was spherical in shape with a bulk density of 1140 kg/m^3. Lab salt was available in very limited quantities and so it was only possible to carry out a restricted experimental programme on this material. The following sieves were used in the analysis of product: 355 μm, 180 μm, 90 μm, 45 μm.

4.1 Granular Sodium Chloride

Reproducibility of results was first analysed for granular salt under constant experimental conditions. If the attrition cell behaved in a constant manner, then a fixed quantity of material of a specified sieve-cut under the same experimental conditions would produce a similar particle size distribution of ground product. Results presented in the following sections show that similar distributions are obtained when experiments are carried out under the same process conditions.

The first aspect of cell behaviour to be investigated was the attrition of granular salt when subjected to increasing shear strain. This was achieved by attriting fixed quantities of salt for a varying number of revolutions of the cell where other process conditions remained unaltered. 100 gm of salt (ex. centrifuge) of initial diameter between 1.7-2.0 mm at a normal stress of 41.4 kN/m^2 was used in all experiments. The cell speed was conveniently set at 5 rpm and the salt was attrited up to a maximum of 25 revolutions of the cell which corresponded to a mean shear strain of 44.3 per revolution and strain rate of 3.69 sec^{-1}. The attrited product was separated using the nest of sieves on the sieve shaker and the new particle size distribution analysed. Results are given in Table 4.1.1 and the corresponding graph in Figure 4.1.1. The graph shows the weight of material in each sieve-cut with increasing shear strain. Note that the distribution becomes bi-modal as shear strain increases, with material in the 1.0-1.4 mm sieve-cut being dominant at the highest strain applied. The amount of fines at the

Torque (Nm)	
Av	Max
28.2	31.6
26.0	27.1
28.2	31.6
28.2	31.6
28.2	31.6
29.4	33.9
29.4	36.2
31.6	36.2
29.4	36.2
30.5	36.2
29.4	36.2

Number of Revs (Initial Weight)	Particle Size Distribution (gm)							Normal Stress kN/m²
	<180 μm	180-355 μm	355-710 μm	710 μm-1 mm	1-1.4 mm	1.4-1.7 mm	>1.7 mm	
1 (100 gm)	0.2	0.2	0.9	2.1	4.2	12.8	79.4	41.4
	0.2	0.1	0.4	0.9	2.8	19.3	76.3	
	0.1	0.1	0.5	1.3	3.1	12.0	82.6	
2 (100 gm)	0.2	0.3	1.1	2.6	5.4	13.0	77.1	41.4
	0.1	0.2	0.9	2.1	5.0	12.1	79.3	
5 (100 gm)	0.3	0.5	2.1	4.8	9.0	14.4	68.6	41.4
	0.3	0.5	2.0	4.6	9.1	13.3	69.8	
10 (100 gm)	1.2	0.9	3.2	7.4	13.6	15.7	57.5	41.4
	0.8	0.7	3.1	7.1	13.5	15.7	58.8	
25 (100 gm)	0.8	1.2	5.2	12.3	21.1	14.7	44.2	41.4
	0.7	1.1	5.5	12.3	19.5	20.4	40.0	

TABLE 4.1.1 Granular Sodium Chloride (ex. centrifuge) - Variation of Shear Strain

Normal Stress - 41.4 kN/m²
Sample Thickness - 10.0 mm
Cell Speed - 5 rpm
Sieve Shaker - 5 mins.

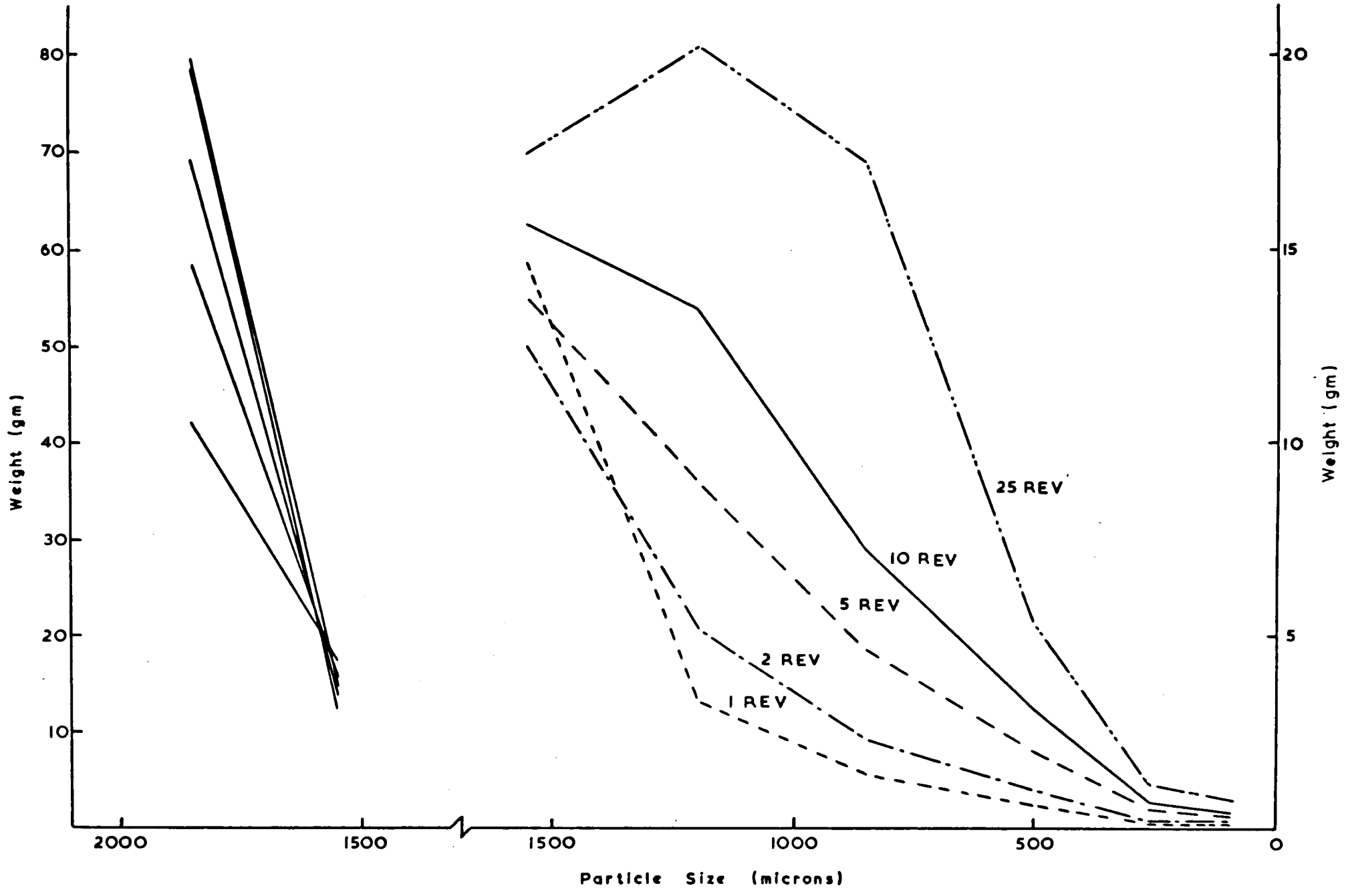


Fig. 4.1.1 Particle Size Distribution of Granular Sodium Chloride (1·7—2·0mm) (ex. centrifuge) Effect of Strain on Attrition

Granular NaCl — Mean size 1·85mm
Sample weight — 100gm
Shear strain — 44·3 per revolution
Cell speed — 5r.p.m.
Sample thickness — 10·0 mm
Normal stress — 41·4 kN/m^2

lower end of the distribution is also seen to increase with shear strain, but this is very gradual.

The effect of attrition of salt (ex. crystalliser) with increasing shear strain was also analysed. 100 gm of material of initial size between 1.7-2.0 mm diameter was again used which yielded a mean shear strain of 44.3 per revolution and strain rate of 3.69 sec^{-1}. This material was ground for a maximum of 60 revolutions of the cell and the attrited product analysed in the usual manner. Results are tabulated in Table 4.1.2 and Figure 4.1.2. The graph shows similar behaviour to that of salt (ex. centrifuge) up to twenty-five revolutions of the cell. The distribution is seen to become bi-modal with increasing shear strain with material in the 1.0-1.4 mm becoming dominant. However, as shear strain is increased (up to sixty revolutions of the cell), the dominant sieve-cut is seen to shift to the 710 μm - 1.0 mm size range. Again, the amount of fines shows a gradual increase with increasing strain.

The effect of increasing normal stress on salt (ex centrifuge) is shown in Table 4.1.3 and Figure 4.1.3. 100 gm of salt of initial size between 1.7-2.0 mm diameter was attrited at various normal stresses where all other process conditions were held constant. The graph shows that an increase in normal stress produces an increase in fines thereby creating a minimum at the 260 μm particle size. The results are systematic with stress throughout the distribution.

Torque (Nm)		Number of Revs (Initial Weight)	Particle Size Distribution (gm)							Normal Stress kN/m²
Av	Max		<180 μm	180-355 μm	355-710 μm	710 μm-1 mm	1-1.4 mm	1.4-1.7 mm	>1.7 mm	
28.2	33.9	1 (100 gm)	0.1	0.1	0.5	0.9	2.0	13.4	82.9	41.4
39.5	45.2	2 (100 gm)	0.3	0.4	1.3	2.4	4.6	15.3	75.4	41.4
50.8	56.5	5 (100 gm)	1.3	1.4	3.2	6.2	7.9	13.6	65.0	41.4
39.5	45.2	10 (100 gm)	1.1	1.3	5.8	12.5	13.7	12.7	52.4	41.4
39.5	45.2	25 (100 gm)	1.2	2.0	9.3	20.0	24.4	11.9	30.4	41.4
39.5	45.2	35 (100 gm)	1.4	2.3	11.3	24.6	26.8	11.0	21.7	41.4
39.5	45.2	50 (100 gm)	1.2	2.5	13.8	29.6	27.4	9.0	16.1	41.4
39.5	45.2	60 (100 gm)	1.5	2.9	15.9	32.3	25.4	6.6	14.8	41.4

TABLE 4.1.2 Granular Sodium Chloride (ex.crystalliser) - Variation of Shear Strain

Normal Stress - 41.4 kN/m²
Sample Thickness - 10.0 mm
Cell Speed - 5 rpm
Sieve Shaker - 5 mins.

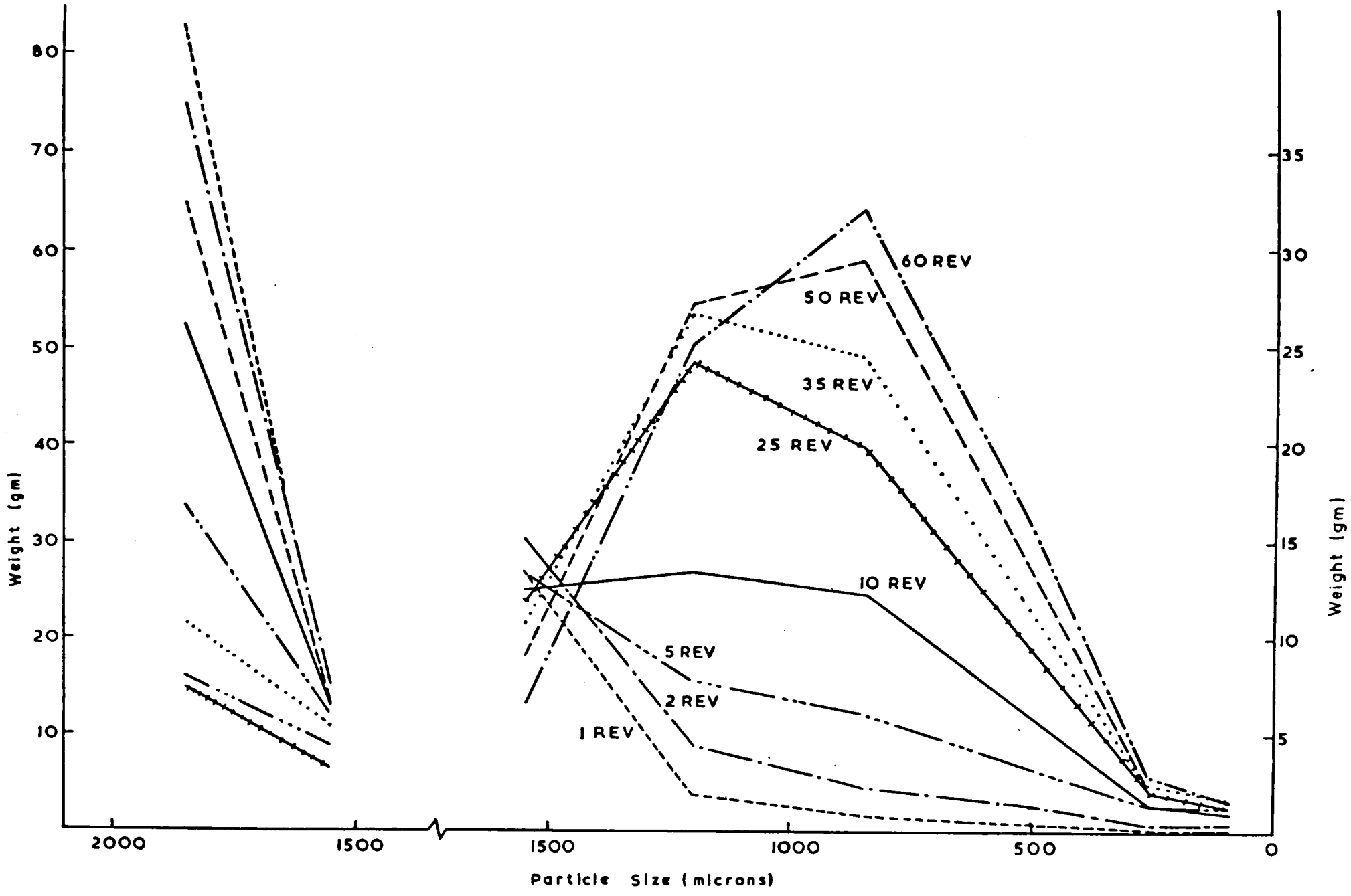


Fig. 4.1.2. Particle Size Distribution of Granular Salt (ex. crystalliser)
Effect of Strain on Attrition

Granular NaCl (ex.crystalliser) – Mean size 1·85 mm
Sample weight – 100 gm
Shear strain – 44·3 per revolution
Cell speed – 5 r.p.m.
Sample thickness – 10·0 mm
Normal stress – 41·4 kN/m^2

Torque (Nm)	
Av	Max
28.2	31.6
26.0	27.1
38.4	42.9
44.1	47.5
50.8	58.8
56.5	63.3
67.8	79.1
67.8	79.1
88.1	94.9
81.4	85.9

Number of Revs (Initial Weight)	Particle Size Distribution (gm)							Normal Stress kN/m²
	<180 μm	180-355 μm	355-710 μm	710 μm-1 mm	1-1.4 mm	1.4-1.7 mm	>1.7 mm	
2 (100 gm)	0.2	0.3	1.1	2.6	5.4	13.0	77.1	41.4
	0.1	0.2	0.9	2.1	5.0	12.1	79.3	
2 (100 gm)	0.9	0.8	3.0	6.1	10.7	15.2	63.0	82.8
	1.0	0.9	3.2	6.4	10.3	15.6	62.3	
2 (100 gm)	1.4	1.1	4.5	8.5	12.2	19.4	52.5	124
	2.2	1.7	5.9	10.2	14.5	12.1	53.1	
2 (100 gm)	3.4	2.1	7.5	11.9	14.6	16.7	43.4	166
	3.2	2.0	7.2	11.7	14.7	16.8	44.1	
2 (100 gm)	4.8	2.8	9.7	14.0	14.7	18.1	35.5	207
	4.6	2.6	9.4	13.7	15.4	18.6	35.4	

TABLE 4.1.3 Granular Sodium Chloride (ex. centrifuge) - Variation of Normal Stress

Shear Strain - 44.3 per revolution
Sample Thickness - 10.0 mm
Cell Speed - 5 rpm
Sieve Shaker - 5 mins.

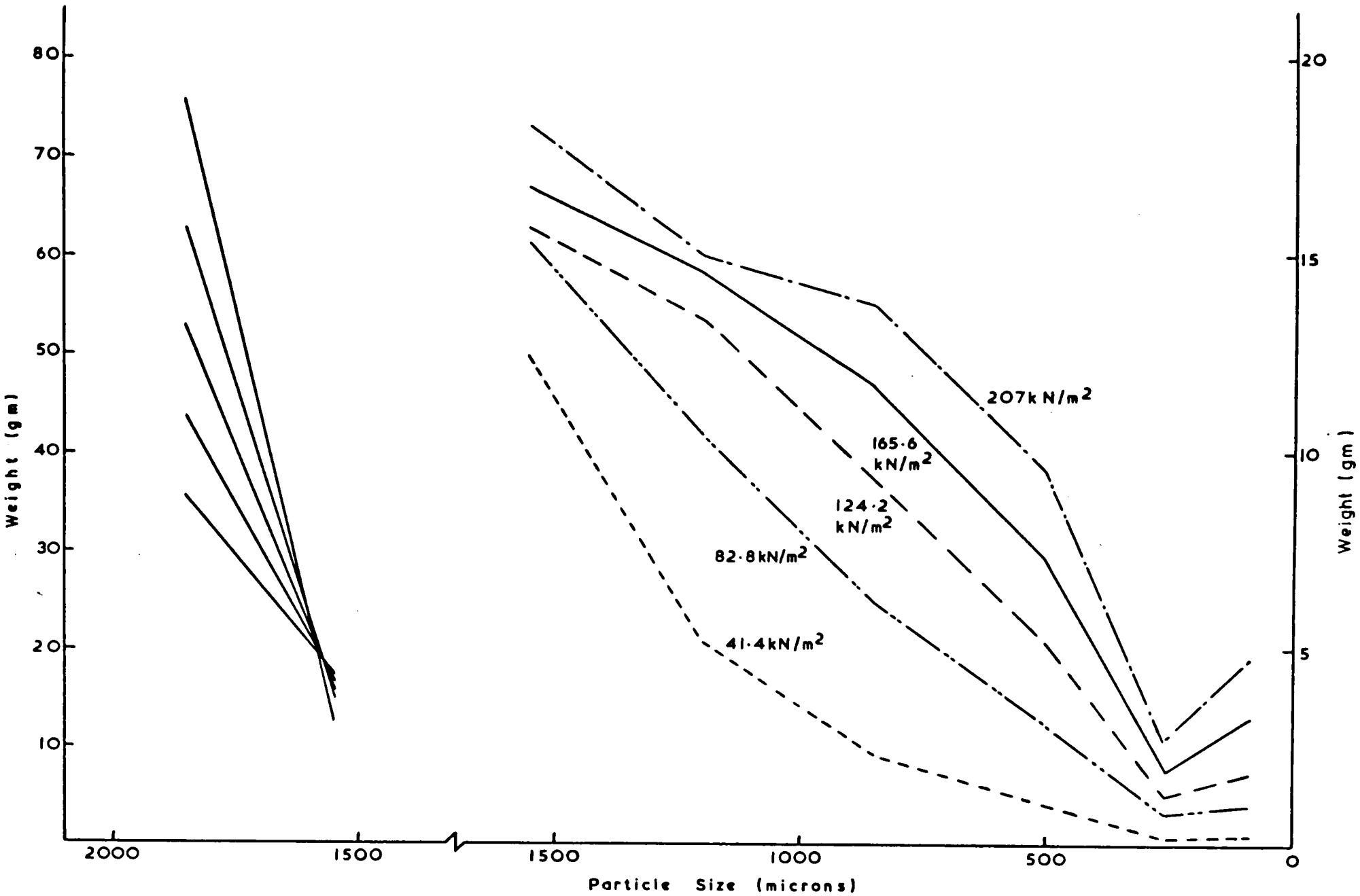


Fig. 4.1.3 Particle Size Distribution of Granular Sodium Chloride (1.7-2.0mm) (ex. centrifuge)—Effect of Normal Stress on Attrition

Granular NaCl — Mean size 1·85mm
Sample weight — 100gm
Shear strain — 44·3 per revolution
Cell speed — 5r.p.m.
Sample thickness — 10·0mm

The standard starting weight of size 1.7-2.0 mm of salt (ex. centrifuge) was used to investigate the effect of cell speed on attrition. Salt was attrited where the speed of the cell was varied, all other process conditions being held constant. Results are given in Table 4.1.4 showing that particles attrite in a similar manner under the same experimental conditions and that it was not possible to distinguish between them. The distribution at 5 rpm did produce a smaller amount of fines, but this is probably due to the age of the sample attrited. Hence, it is seen that cell speed did not influence the rate of attrition of these particles.

The influence of sample weight on attrition rate was investigated. The standard experimental procedure was repeated using different sample weights where the cell speed and normal stress was held constant. Granular salt was then attrited in the cell under fixed energy input per unit mass of material. Constant energy input per unit mass of powder was achieved by varying sample weights and applied shear strains in a fixed ratio.

For experimental purposes, a ratio of 10:1 and 50:1 of sample weight to the number of cell revolutions was selected for practical reasons so that a wide range of sample thicknesses could be investigated. In the case of granular salt where the mean initial diameter was 1.85 mm, the upper limit for sample thickness was governed by the physical dimensions of the cell.

The results of the constant shear strain experiments are shown in Figures 4.1.5 and 4.1.6 for the two different ratios selected. The graphs do not show a clear trend in behaviour although Figure 4.1.6

Torque (Nm)	
Av	Max
27.1	36.2
28.2	40.7
28.2	36.2
28.2	40.7
28.2	31.6
28.2	31.6
29.4	31.6
29.4	31.6
29.4	31.6
29.4	31.6

Number of Revs (Initial Weight)	Particle Size Distribution (gm)							Cell Speed (rpm)
	<180 μm	180-355 μm	355-710 μm	710 μm-1 mm	1-1.4 mm	1.4-1.7 mm	>1.7 mm	
2 (100 gm)	0.6	0.5	1.8	3.7	7.5	18.1	67.7	1.25
	0.6	0.5	1.9	4.1	7.9	17.5	67.4	
2 (100 gm)	0.5	0.5	1.6	3.7	7.5	17.3	68.8	2.5
	0.7	0.5	1.8	3.9	7.1	17.3	68.5	
2 (100 gm)	0.2	0.3	1.1	2.6	5.4	13.0	77.1	5.0
	0.1	0.2	0.9	2.1	5.0	12.1	79.3	
2 (100 gm)	0.7	0.6	2.1	4.5	8.3	19.6	64.1	10.0
	0.7	0.7	2.2	4.5	8.5	17.0	66.4	
2 (100 gm)	0.7	0.7	2.3	4.6	7.9	17.9	65.8	15.0
	0.7	0.7	2.3	4.5	8.1	16.5	67.0	

TABLE 4.1.4 Granular Sodium Chloride (ex.centrifuge) - Variation of Cell Speed

Normal Stress - 41.4 kN/m^2
Sample Thickness - 10.0 mm
Shear Strain - 44.3 per revolution
Sieve Shaker - 5 mins.

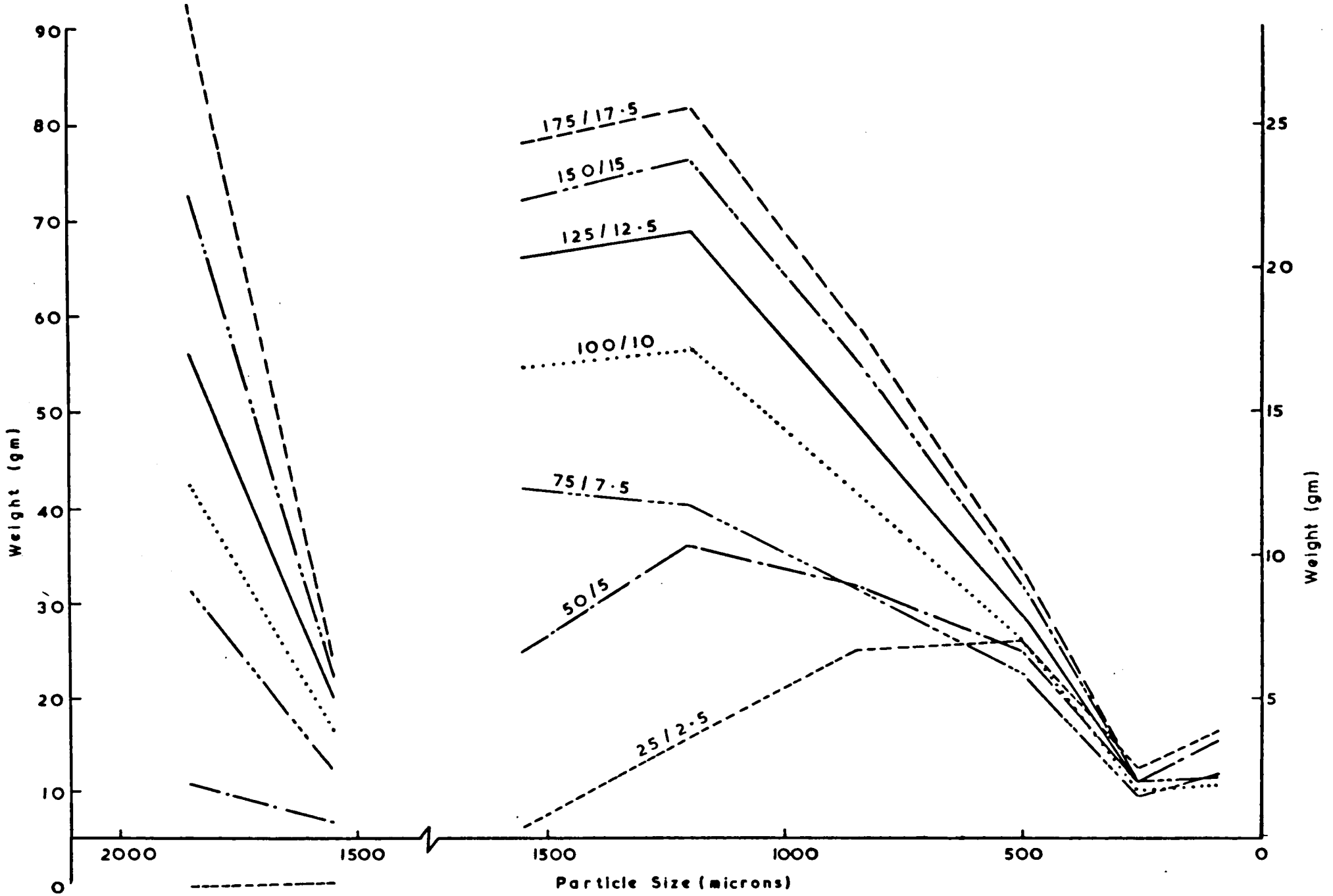


Fig. 4.1.5. Particle Size Distribution of Granular Sodium Chloride (1·7 – 2·0mm) Effect of constant sample wt/cell rev. ratio (10/1) on Attrition (wt)

Normal stress – 41·4 kN/m^2 Sample thickness – 3.6.9.12.15.18.21mm

Cell speed – 5 r.p.m.

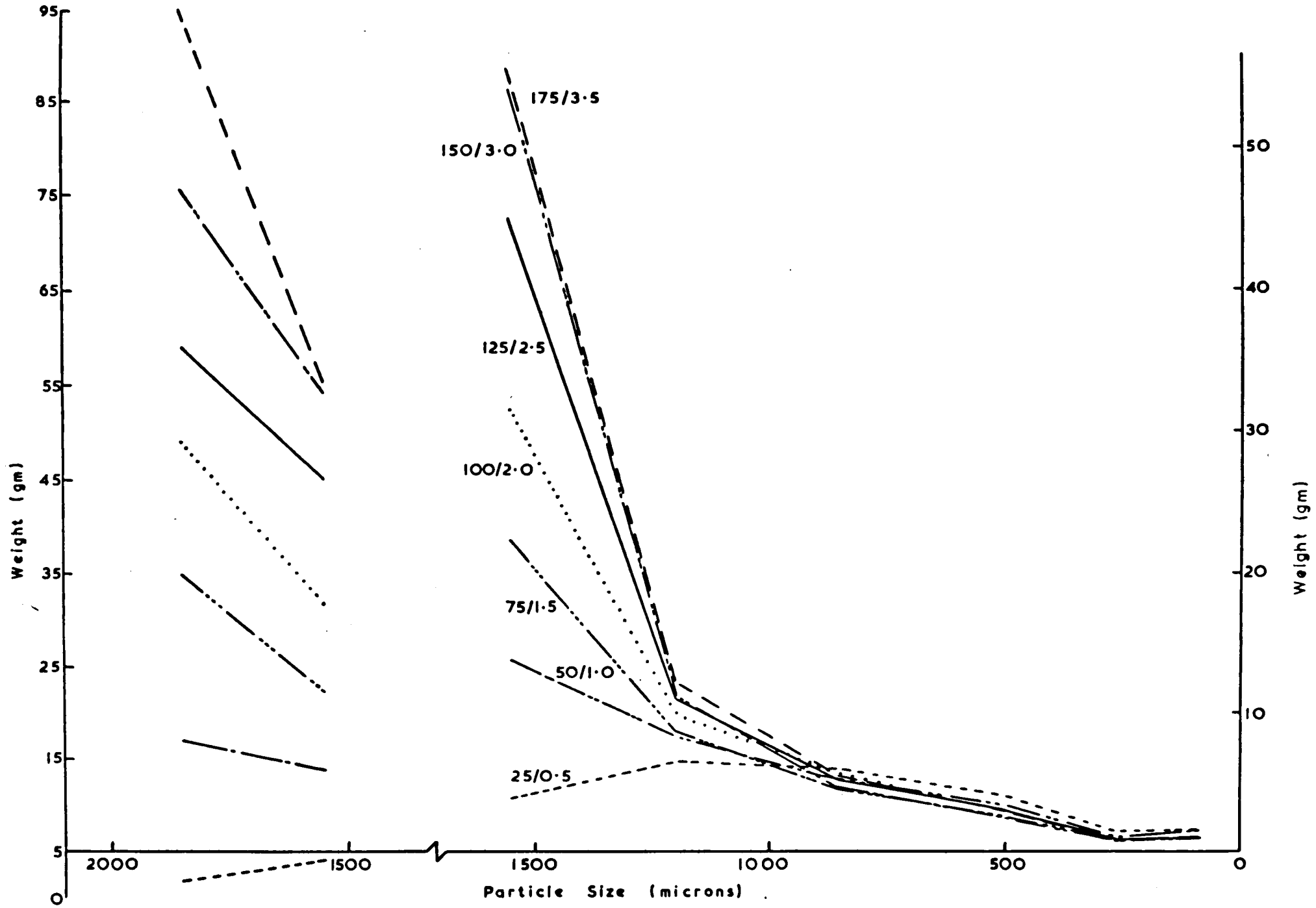


Fig. 4.1.6 Particle Size Distribution of Granular Sodium Chloride (1·7–2·0mm) Effect of constant sample wt/cell rev. ratio (50/1) on Attrition (wt)

Normal stress – 41·4 kN/m^2 Sample thickness – 3, 6, 9, 12, 15, 18, 21 mm

Cell speed – 5 r.p.m.

shows that the behaviour of fines is more ordered than that of the coarse particles. If, however, the graphs are redrawn to show the percentage weight in each sieve fraction, a much more uniform behaviour of particles is seen, especially at the coarser end of the distribution (Figures 4.1.7 and 4.1.8). This normalisation of data also extends to the fines produced except in the 50:1 case where less uniform behaviour of fines at the different sample weights is noted. Some scatter of results is also observed at the 1.4-1.7 mm sieve-cut range.

The smaller weights (25 gm, 50 gm) of samples used showed the greatest deviations from the normalised behaviour in both cases. As for molecular sieve, these weights produced very thin sample layers in the cell and the resulting attrition would have been due more to the crushing of gripped particles rather than to true particle to particle grinding.

Thus, it is inferred that when particle behaviour is normalised by subjecting material to a known shear strain, attrition takes place in an uniform manner indicating that true particle to particle grinding occurs in samples where the failure zone depth is not exceeded or where particle layers are not too thin.

The influence of sample history was analysed by attriting material already subjected to grinding and observing any difference in behaviour. 100 gm of standard experimental material was used to obtain attrited product at one revolution of the cell and the top fraction (i.e. size greater than 1.7 mm) isolated using the nest of sieves. The top fraction of several runs under the same experimental conditions was separated and mixed together so that a new sample of 100 gm of attrited material was obtained. This sample was then

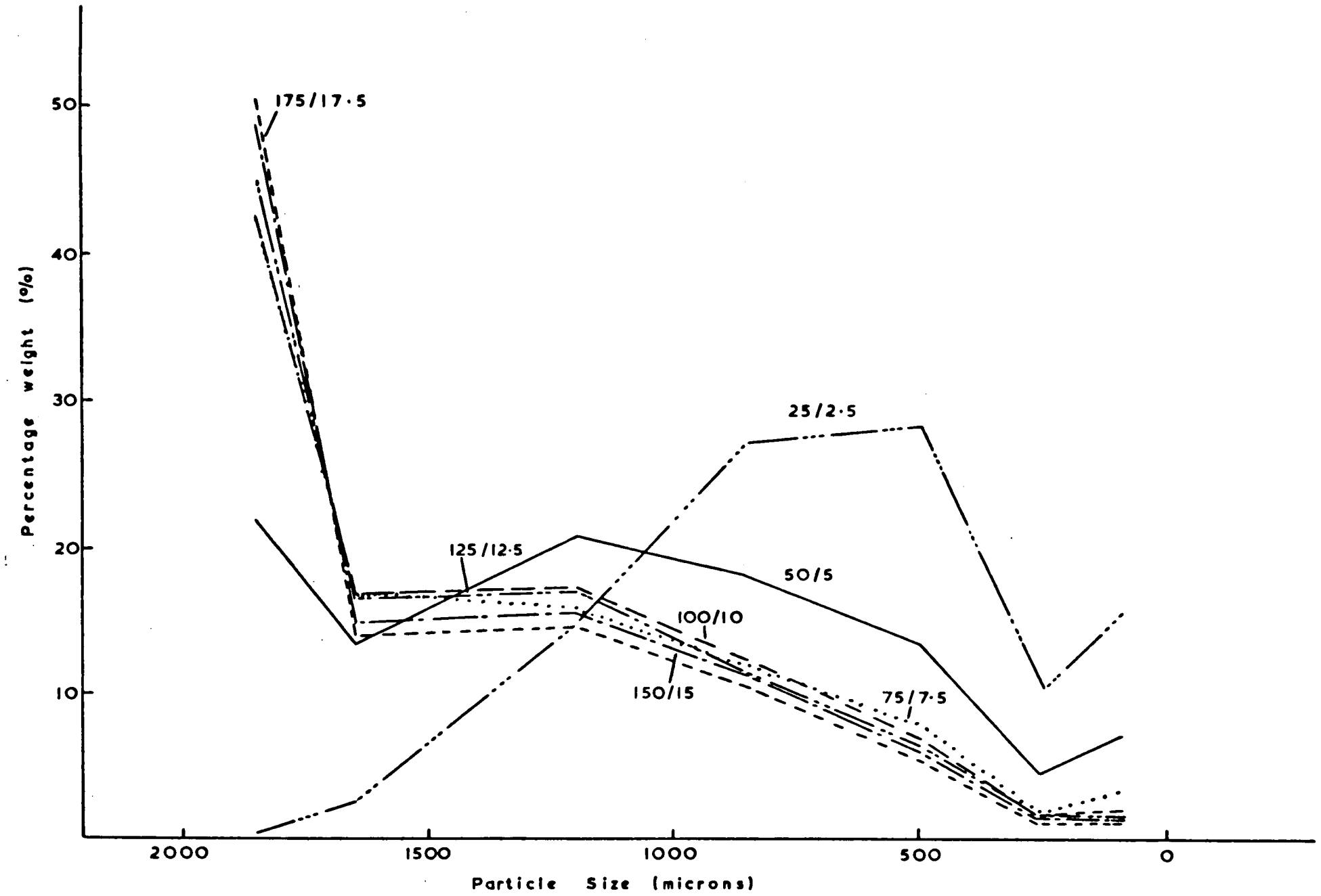


Fig. 4.1.7 Particle Size Distribution of Granular NaCl (1·7 – 2·0 mm)
Effect of constant sample wt/cell rev. ratio (10/1) on Attrition (wt %)

Granular NaCl – Mean size 1·85mm
Sample thickness – 3,6,9,12,15,18,21mm
Sieving – 5 mins
Cell speed – 5 r.p.m.
Normal stress – 41·4 kN/m^2

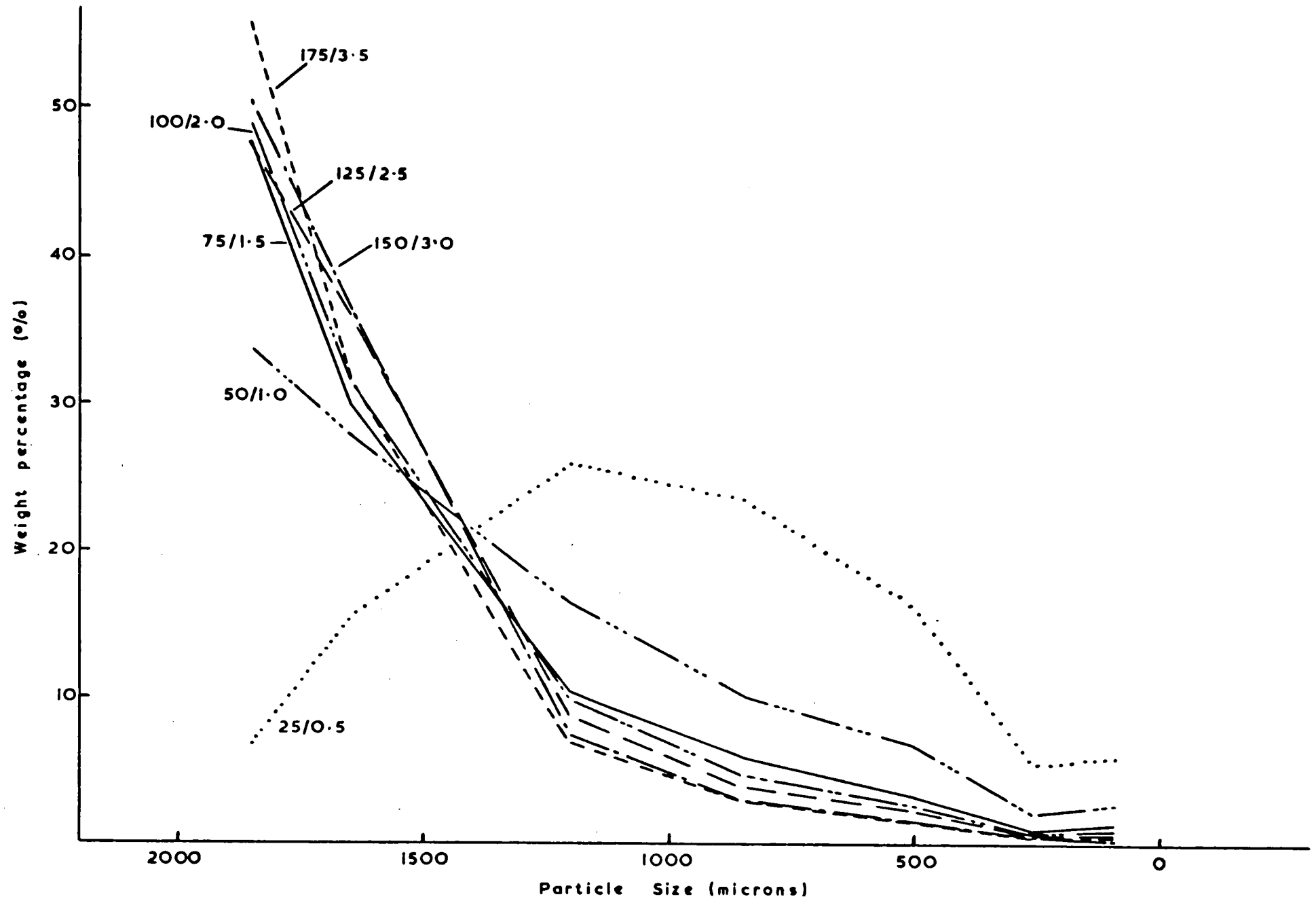


Fig. 4.1.8 Particle Size Distribution of Granular NaCl (1·7 - 2·0mm)
Effect of constant sample wt/cell rev. ratio (50/1) on Attrition (wt %)

Granular Sodium Chloride — Mean size 1·85mm
Sample thickness — 3,6,9,12,15,18,21 mm
Sieving — 5mins
Cell speed — 5 r.p.m.
Normal stress — 41·4kN/m^2

attrited under the same experimental conditions to obtain the new particle size distribution. Table 4.1.9 shows the results of the runs carried out indicating that no significant difference in attrition behaviour was recorded between the various runs.

A similar procedure was also carried out at five and twenty-five revolutions of the cell. These results also show no significant difference in behaviour indicating that, for this material, sample history has little effect on attrition.

Some segregation of attrited product was seen to occur when granular salt was subjected to high strains or normal stresses during the grinding process. When the cell was emptied of ground product, it was observed that the smaller particles had moved to the bottom of the annulus. In order to determine whether segregation had any effect on the attrition process, experiments with different sample weights were carried out under standard operating conditions where material was attrited for five revolutions of the cell with and without inversion, the cell being inverted at the end of each revolution. Results are tabulated in Table 4.1.10 for the different sample weights chosen. The first run at each sample weight was carried out with the cell in the standard upright mode and inversions carried out during the second run. The results show that the two distributions at each weight do not differ significantly, and it was concluded that attrition was not affected by the segregation of fines under normal experimental conditions.

The weight of attrited material was plotted as a function of time on a log-log plot in the same manner as Gwyn (1969). Granular salt was attrited for upto twenty-five revolutions of the cell at a normal stress of 41.4 kN/m^2. A straight line fit was obtained as

Torque (Nm)		Number of Revs (Initial Weight)	Particle Size Distribution (gm)						Run Type
Av	Max		<180 µm	180-355 µm	355-710 µm	710 µm-1 mm	1-1.4 mm	1.4-1.7 mm	>1.7 mm	
28.2	31.6	1 (100 gm)	0.2	0.2	0.6	1.5	3.6	11.9	82.0	A
26.0	27.1		0.1	0.2	0.4	1.5	3.4	12.2	82.1	
28.2	31.6		0.2	0.2	0.4	1.3	3.3	11.5	83.0	B
29.4	33.9	5 (100 gm)	0.3	0.5	2.0	4.7	9.0	13.5	69.9	A
29.4	36.2		0.3	0.5	2.1	4.8	9.1	13.8	69.3	
29.4	33.9		0.3	0.5	2.1	4.6	9.1	14.0	69.3	B
30.5	36.2	25 (100 gm)	0.8	1.2	5.3	12.1	20.9	16.5	43.2	A
29.4	36.2		0.8	1.1	5.4	12.4	19.8	18.1	42.4	
30.5	36.2		0.7	1.2	5.4	12.3	20.2	18.4	41.8	B

TABLE 4.1.9 Granular Sodium Chloride (ex.centrifuge) - Attrition of Coarse end Attrited Product

Normal Stress - 41.4 kN/m²
Sample Thickness - 10.0 mm
Shear Strain - 44.3 per revolution
Sieve Shaker - 5 mins.

A - Fresh material attrited
B - Attrited material attrited

Torque (Nm)	
Av	Max
29.4	33.9
29.4	33.9
29.4	33.9
29.4	33.9
29.4	33.9
29.4	33.9

Sample Weight	Particle Size Distribution (gm)							Mode of Operation
	<180 µm	180-355 µm	355-710 µm	710 µm-1 mm	1-1.4 mm	1.4-1.7 mm	>1.7 mm	
50 gm	2.3	1.5	5.0	8.1	10.8	6.6	15.4	N
	2.4	1.9	5.5	8.3	10.9	6.7	14.3	I
100 gm	0.5	0.5	2.2	4.4	8.2	13.3	70.7	N
	0.6	0.6	2.4	4.5	8.4	13.0	70.5	I
150 gm	0.4	0.4	1.8	3.8	9.3	19.0	115.3	N
	0.4	0.4	1.9	3.8	9.1	19.0	115.2	I

TABLE 4.1.10 Granular Sodium Chloride (ex.centrifuge) - Effect of Segregation

Sample Thickness - 5, 10, 15 mm
Number of Revolutions - 5
Normal Stress - 41.4 kN/m^2
Shear Strain - 88.6, 44.3, 29.5 per revolution
Sieve Shaker - 5 mins.

N - Normal operation of cell
I - Cell inverted at the end of each revolution

seen in Figure 4.1.11. Regression analysis was carried out on the data and the line fitted an equation of the form

$$\log W = 0.40 \log \gamma + 0.56$$

where W is the weight attrited and γ the shear strain.

A Gwyn plot was also carried out on granular salt (ex. crystalliser). Over the linear section, we get a straight line of the form

$$\log W = 0.44 \log \gamma + 0.52$$

Results are shown in Figure 4.1.12 and a summary of the statistical analysis for both cases is given in Table 4.1.13.

It is interesting to note that the gradients and intercepts of both lines are almost identical, indicating that attrition behaviour of granular salt (ex. centrifuge) and granular salt (ex. crystalliser) are similar, despite the fact that the starting size fraction of the latter contained a quantity of damaged spherical material. It would seem that the centrifuging stage did not cause any "hidden" damage to the salt crystals and that the small quantity of part-spherical material was not sufficient to alter the general attrition behaviour of granular salt.

Salt (ex. crystalliser) was also attrited to a maximum of sixty revolutions of the cell and the results plotted according to Gwyn (Figure 4.1.12). It is seen that after twenty five revolutions of the cell (corresponding to a strain of 1100), linear attrition behaviour is lost and the line curves off asymptotically.

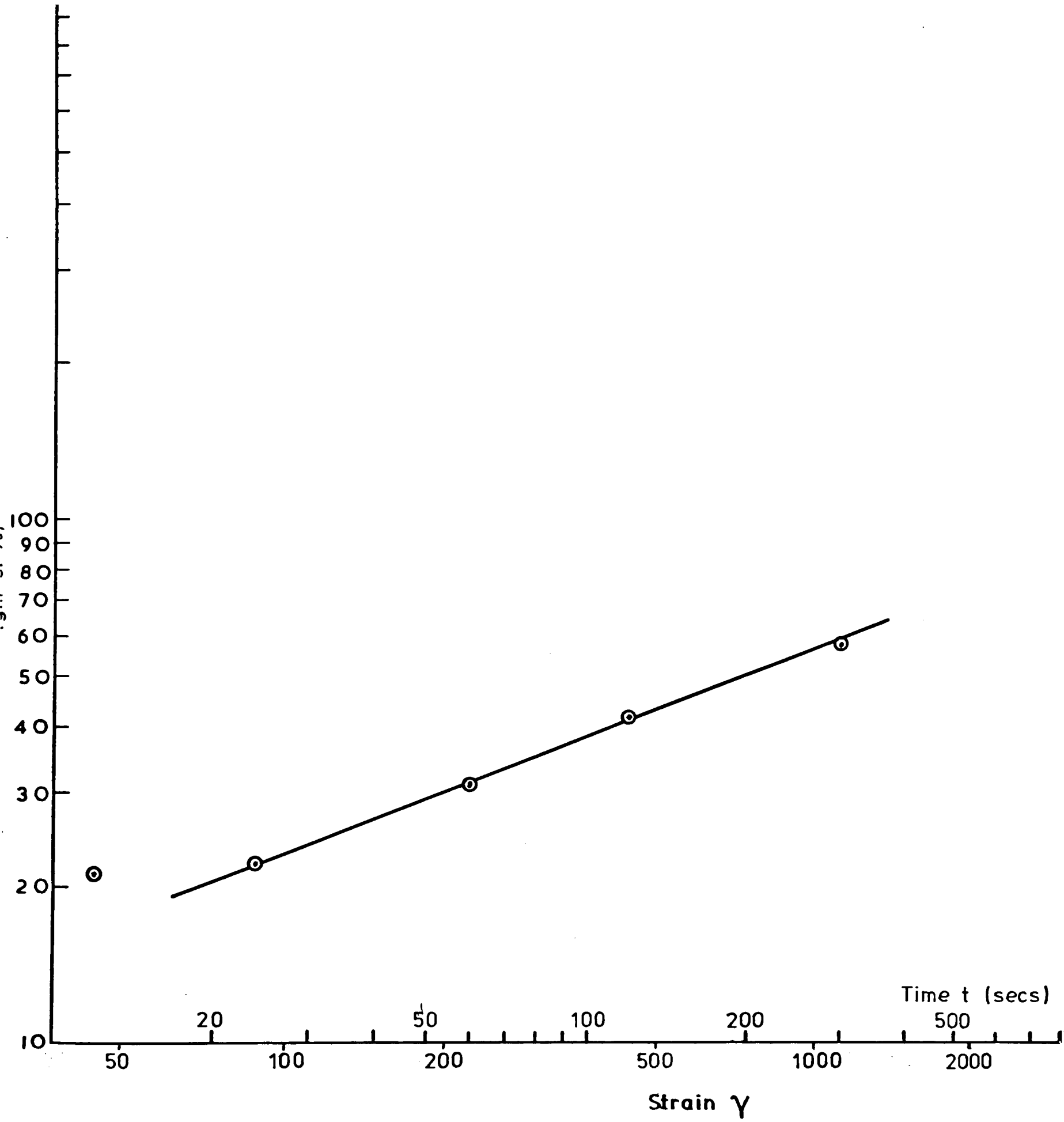


Fig. 4.1.11. Granular Salt (ex-centrifuge) — Gwyn Plot

Effect of Strain on Attrition

Cell speed – 5 r.p.m.
Sample weight – 100 gm
Sample thickness – 10·0mm
Shear strain – 44·3 per revolution
Normal stress – 41·4 kN/m^2

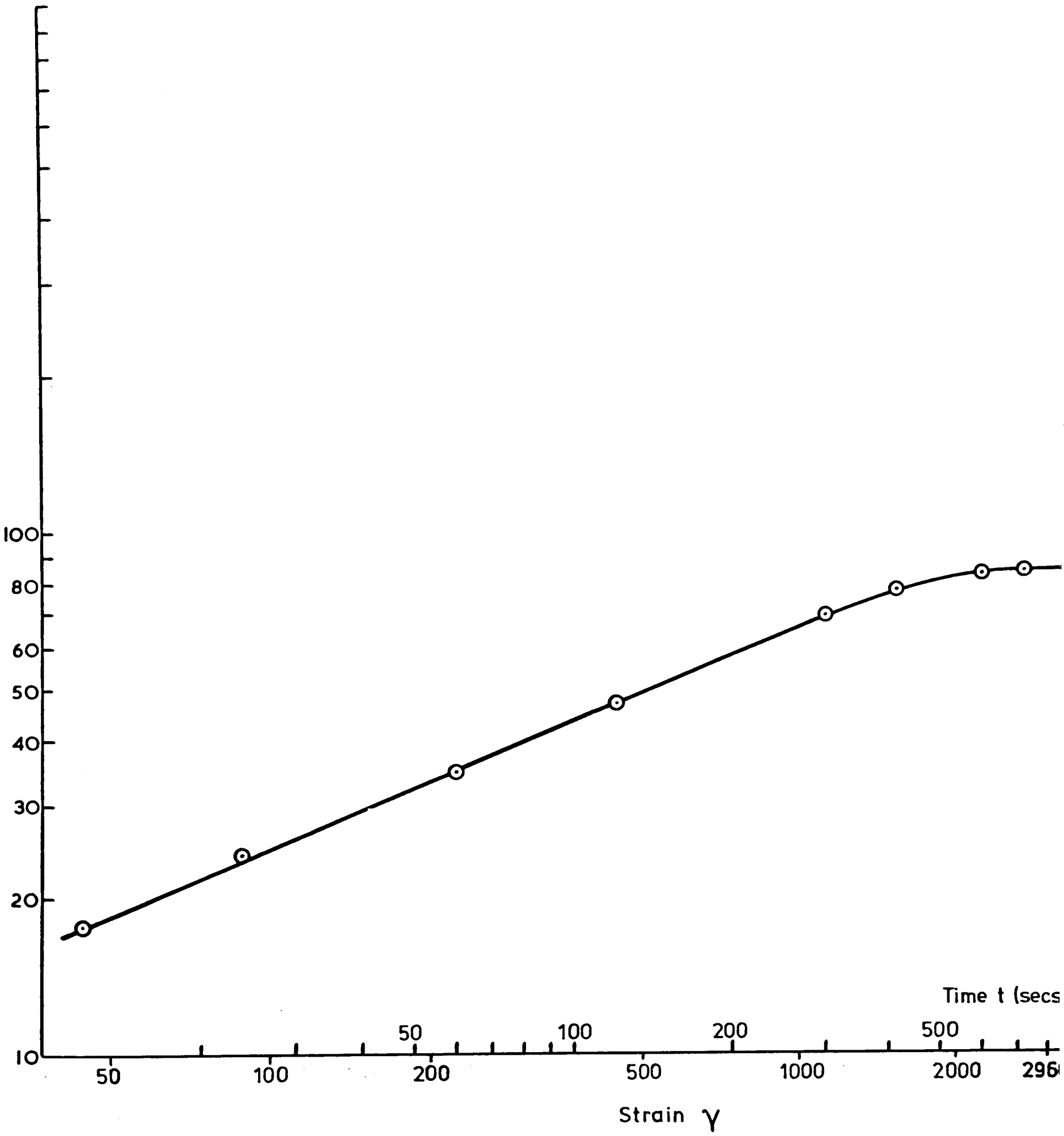


Fig. 4.1.12 Granular Salt (ex. crystalliser)—Gwyn Plot

Effect of Strain on Attrition

Cell speed - 5 r.p.m.

Sample weight - 100gm

Sample thickness - 10mm

Shear strain - 44·3 per revolution

Normal stress - 41·4 kN/m^2

Material	Gradient	Standard Error of Gradient	Intercept	Standard Error of Intercept	Correlation Coefficient %	F-Value
Granular Sodium Chloride (ex.centrifuge)	0.40	0.007	0.56	0.01	99.93	3046
Granular Sodium Chloride (ex.crystalliser)	0.44	0.006	0.52	0.01	99.97	5316

TABLE 4.1.13 Granular Sodium Chloride - Summary of Regression Analysis on Gwyn Plots

4.2 Pure Dried Vacuum Salt (PDV Salt)

Two different sieve-cuts of PDV salt were used in the experimental runs. The bulk of the experiments were conducted using the larger size fraction (500-600 μm) but some runs were also carried out using salt of initial size between 250-355 μm.

Attrition data were again checked for reproducibility under constant process conditions. Tables of results, presented subsequently under the various experimental conditions, show that runs carried out under the same conditions produced attrition products with similar size distributions.

The effect of increasing shear strain on PDV salt was analysed. 100 gm of salt of sieve-cut between 500-600 μm size was attrited for up to twenty-five revolutions of the cell under fixed conditions and the new particle size distribution determined by using the standard nest of sieves previously specified. The particles were subjected to an average shear strain of 49.2 per revolution which corresponds to a strain rate of 4.1 sec^{-1} at 5 rpm. Further experiments were also carried out to investigate attrition at very large strains (up to 300 revolutions of the cell) and all results are given in Table 4.2.1 and the corresponding graph in Figure 4.2.1. It is seen that as shear strain is increased, initially material is being attrited sufficiently to pass through the top sieve, thus producing a maximum in the particle size distribution at the next sieve (425 μm). As particles are ground for very long times, this maximum is seen to shift to the next sieve size (260 μm). The amount of fine material also becomes significant at high strains.

When the smaller fraction of PDV salt (250-355 μm) is attrited, a different distribution to the one seen previously is obtained. A

Torque (Nm)	
Av	Max
39.5	45.2
39.5	45.2
39.5	45.2
39.5	45.2
39.5	45.2
39.5	45.2
39.5	45.2
39.5	45.2
39.5	45.2
39.5	45.2

Number of Revs (Initial Weight)	Particle Size Distribution (gm)						Normal Stress kN/m²
	<45µm	45-90 µm	90-180 µm	180-355 µm	355-500 µm	>500 µm	
1 (100 gm)	0.2	0.3	0.5	1.9	39.6	57.2	41.4
	0.2	0.3	0.6	1.8	39.0	57.9	
2 (100 gm)	0.2	0.3	3.5	1.9	41.5	55.4	41.4
	0.2	0.3	0.4	2.0	41.9	55.0	
5 (100 gm)	0.3	0.5	0.8	2.9	43.9	51 4	41.4
	0.3	0.4	0.9	3.0	43.7	51.3	
10 (100 gm)	0.3	0.4	0.6	3.6	46.3	48 5	41.4
	0.3	0.5	0.7	3.4	46.7	48.1	
25 (100 gm)	0.4	0.6	1.0	4.8	48.1	44.7	41.4
	0.4	0.7	1.1	5.0	48.7	43.7	

TABLE 4.2.1

(Cont.)

TABLE 4.2.1 - CONTINUED

Torque (Nm)		Number of Revs (Initial Weight)	Particle Size Distribution (gm)						Normal Stress kN/m^2
Av	Max		<45 µm	45-90 µm	90-180 µm	180-355 µm	355-500 µm	>500 µm	
39.5	45.2	50 (100 gm)	0.4	0.5	1.1	7.6	50.2	40.0	41.4
39.5	45.2	100 (100 gm)	0.8	1.1	2.0	17.9	47.4	30.4	41.4
39.5	45.2	200 (100 gm)	1.4	1.9	4.6	33.4	33.7	24.9	41.4
39.5	45.2	300 (100 gm)	1.9	2.8	7.7	39.2	24.1	24.1	41.4

TABLE 4.2.1 PDV Salt (500-600 µm) - Variation of Shear Strain

Cell Speed - 5 rpm
Sample Thickness - 9.0 mm
Sieve Shaker - 5 mins.

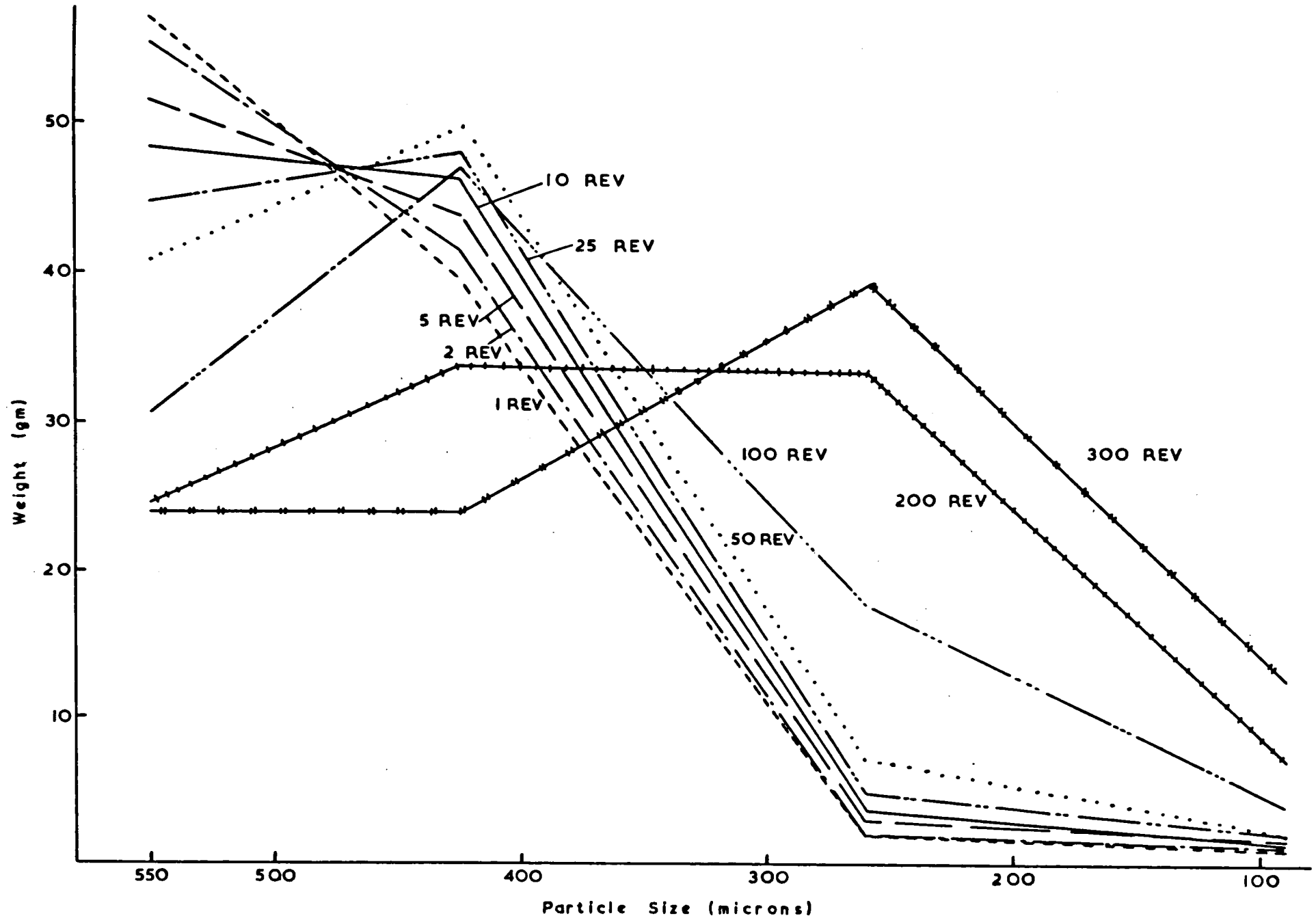


Fig. 4.2.1 Particle Size Distribution of PDV Salt (500 – 600 μm) Effect of Strain on Attrition

PDV Salt — Mean size 550 μm
Sample weight — 100 gm
Sample thickness — 9·0 mm
Cell speed — 5 r.p.m.
Normal stress — 41·4 kN/m²
Shear strain — 49·2 per revolution

more ordered distribution of ground product is seen as shown in Figure 4.2.2 and Table 4.2.2. Attrited product at the coarse end of the distribution is seen to increase monotonically with increasing shear strain, but the rate of increase of fine material was not significant.

PDV salt was also subjected to varying normal stresses in the cell. 100 gm of salt of initial size between 500-600 μm was attrited under fixed process conditions where only the normal stress was varied. The new particle size distribution was obtained by using the specified nest of sieves and is shown in Table 4.2.3 and Figure 4.2.3. It is seen that, as stress is increased, a maximum of attrited material is also found around 425 μm. It is also interesting to see that doubling the stress from 41.4 kN/m² to 82.8 kN/m² made hardly any difference to the amount of attrited product produced, the reason for this being unknown.

Particle behaviour with varying sample thicknesses was investigated next, where different weights of sample were attrited such that the ratio of sample weight to number of cell revolutions remained constant. Ratios of 10:1 and 50:1 were again chosen and the results of these experiments for both cases are given in Figures 4.2.4 and 4.2.5. The fine end of the distribution shows more ordered behaviour at both the ratios selected.

When the graphs were re-plotted as a weight percentage in each sieve-cut (Figs. 4.2.6 and 4.2.7) the distribution is seen to rise to a maximum at the 425 μm size and this does much to reduce the uniformity of behaviour in the smaller sample weights. It is once again seen that the greatest deviations are caused by the smallest weights of sample used, which produce thin layers of material in the cell.

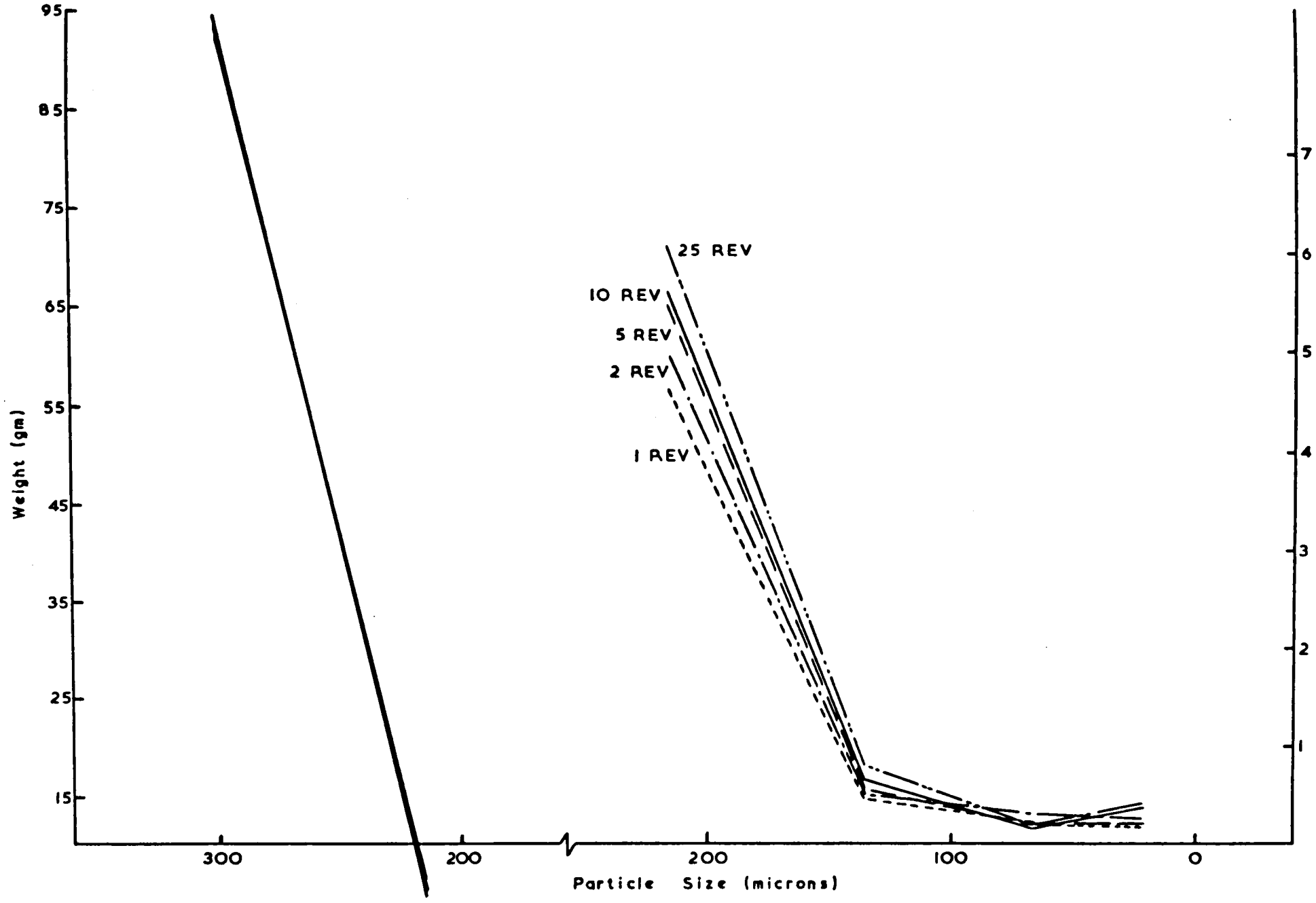


Fig. 4.2.2 Particle Size Distribution of PDV Salt (250–355 μm)
Effect of Strain on Attrition

PDV Salt — Mean size 300μm
Sample weight — 100gm
Normal stress — 41·4 kN/m^2
Cell speed — 5 r.p.m.
Sample thickness — 9·0mm
Shear strain — 49·2 per revolution

Torque (Nm)	
Av	Max
38.4	40.7
38.4	40.7
38.4	40.7
38.4	40.7
38.4	40.7
38.4	40.7
38.4	40.7
38.4	40.7
38.4	40.7
38.4	40.7

Number of Revs (Initial Weight)	Particle Size Distribution (gm)					Normal Stress kN/m²
	<45 µm	45-90 µm	90-180 µm	180-250 µm	>250 µm	
1 (100 gm)	0.2	0.3	0.5	4.7	94.5	41.4
	0.2	0.2	0.6	4.8	94.3	
2 (100 gm)	0.2	0.3	0.5	5.0	94.0	41.4
	0.3	0.3	0.5	5.2	93.7	
5 (100 gm)	0.2	0.2	0.5	5.5	93.4	41.4
	0.2	0.2	0.5	5.6	93.3	
10 (100 gm)	0.4	0.2	0.6	5.6	93.1	41.4
	0.3	0.2	0.6	5.9	92.9	
25 (100 gm)	0.4	0.2	0.8	6.1	92.2	41.4
	0.4	0.2	0.9	6.2	92.1	

TABLE 4.2.2 PDV Salt (250-355 µm) - Variation of Shear Strain

Cell Speed - 5 rpm
Sample Thickness - 9.0 mm
Shear Strain - 49.2 per revolution
Sieve Shaker - 5 mins.

Torque (Nm)		Number of Revs (Initial Weight)	Particle Size Distribution (gm)						Normal Stress kN/m²
Av	Max		<45 µm	45-90 µm	90-180 µm	180-355 µm	355-500 µm	>500 µm	
12.4	13.6	5 (100 gm)	0.1	0.1	0.2	1.1	30.9	67.5	20.7
39.5	45.2	5 (100 gm)	0.3	0.5	0.8	2.9	43.9	51.4	41.4
50.8	56.5	5 (100 gm)	0.4	0.6	0.9	3.6	44.4	49.9	82.8
79.1	90.4	5 (100 gm)	0.8	0.8	1.3	5.7	49.2	42.2	165.0

TABLE 4.2.3 PDV Salt (500-600 µm) - Variation of Normal Stress

Cell Speed - 5 rpm
Sample Thickness - 9.0 mm
Shear Strain - 49.2 per revolution
Sieve Shaker - 5 mins.

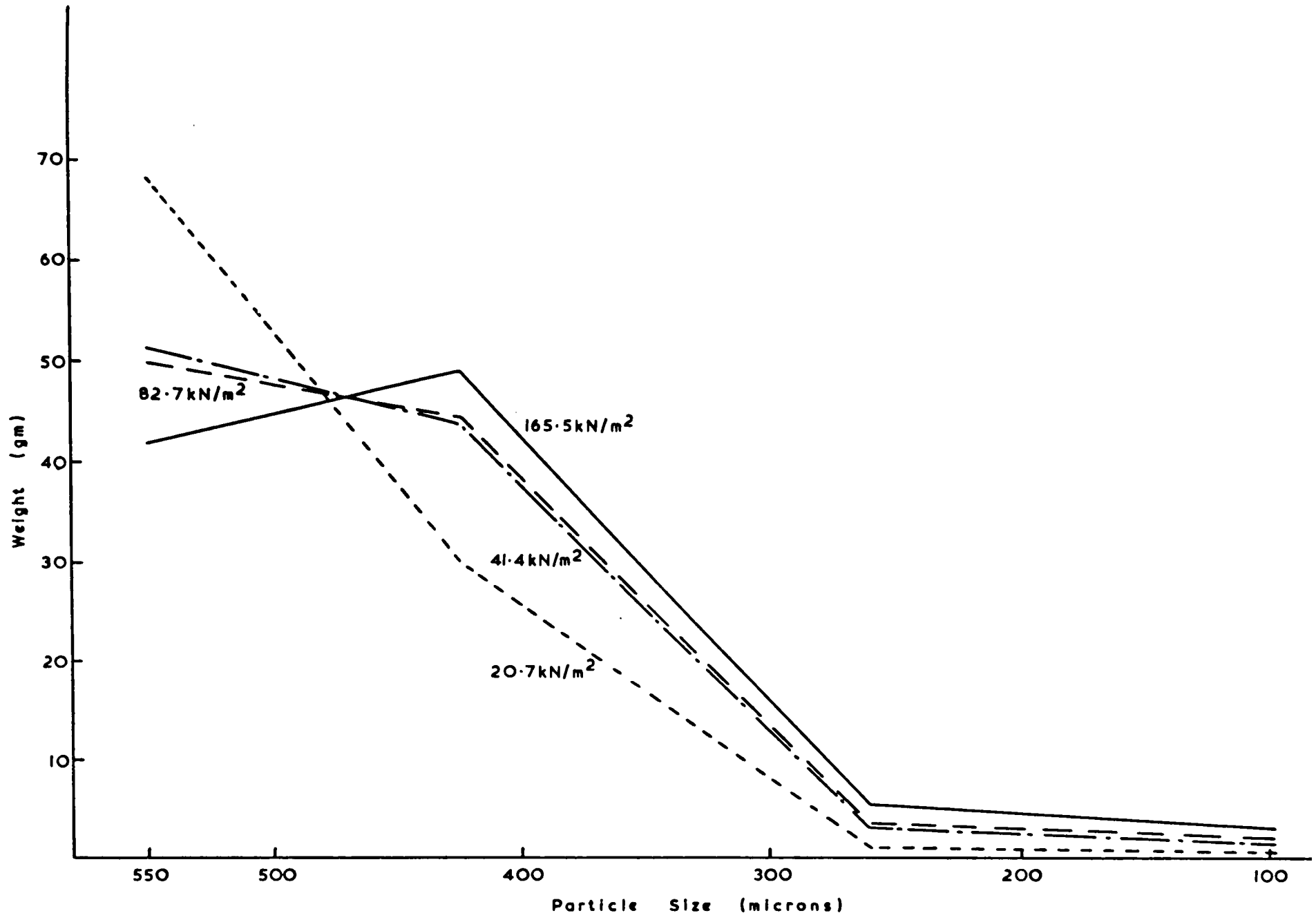


Fig. 4.2.3 Particle Size Distribution of PDV Salt (500–600 μm)
Effect of Normal Stress on Attrition

PDV Salt — Mean size 550μm
Sample weight — 100gm
No. of revolutions — 5
Cell speed — 5 r.p.m.
Sample thickness — 9·0mm
Shear strain — 49·2 per revolution

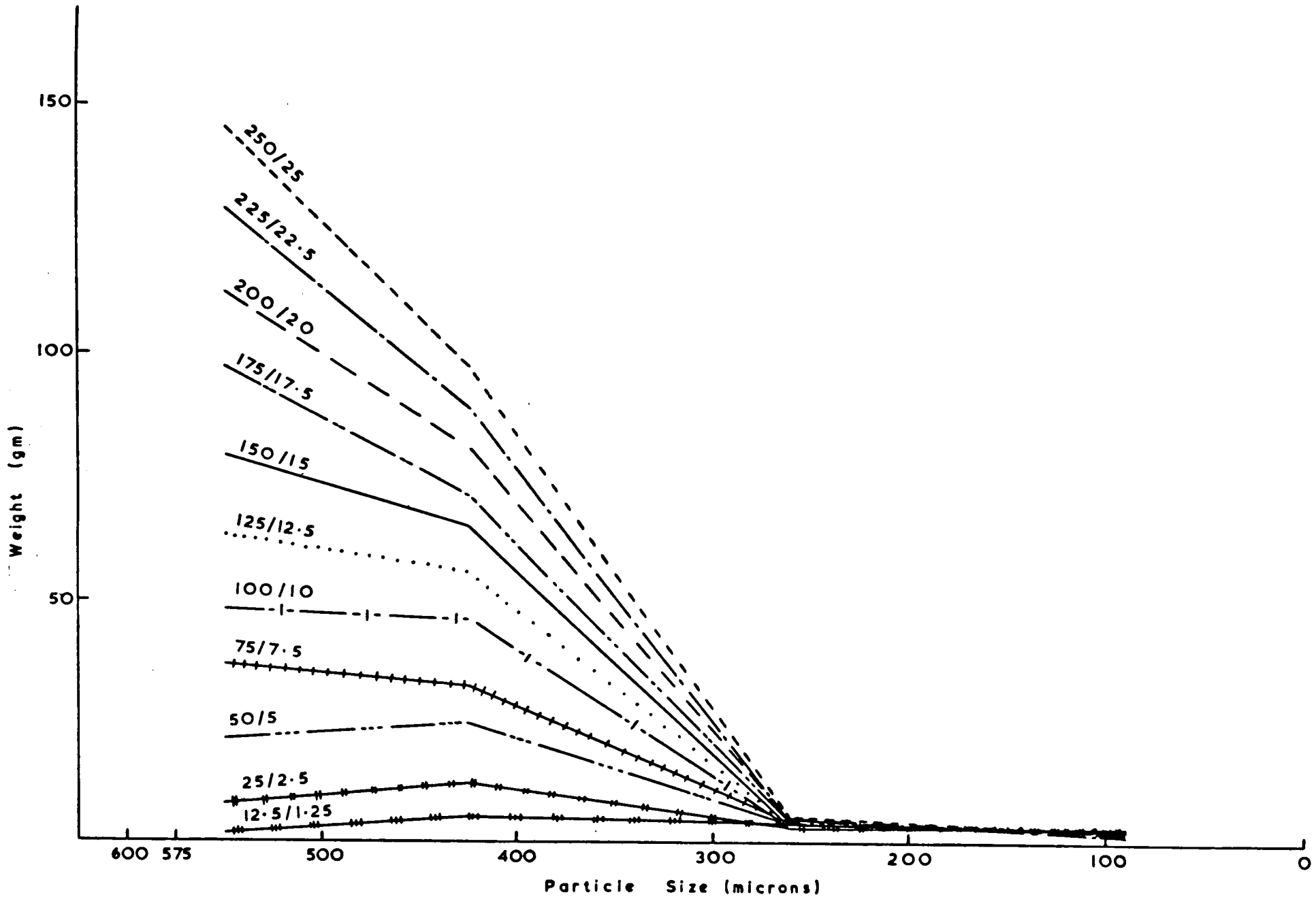


Fig. 4.2.4 Particle Size Distribution of PDV Salt (500 - 600 μm). Effect of constant sample wt/cell rev. ratio (10/1) on Attrition (wt)

PDV Salt — Mean size 550 μm
Normal stress — 41·4 kN/m^2
Cell speed — 5 r.p.m.
Sieving — 5 mins

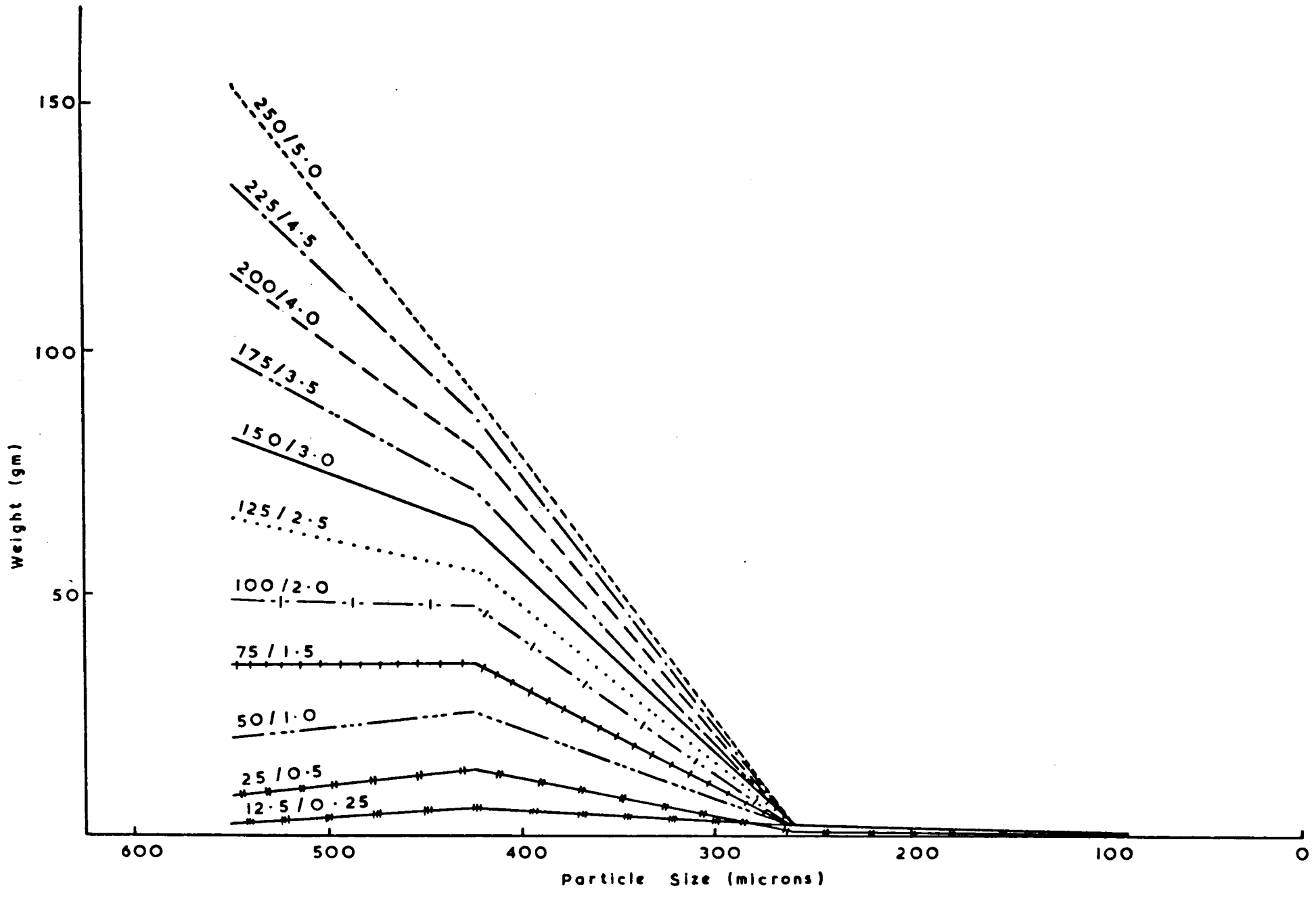


Fig. 4.2.5. Particle Size Distribution of PDV Salt (500 – 600 μm)
Effect of constant sample wt/cell rev. ratio (50/1) on Attrition (wt)

PDV Salt – Mean size 550 μm
Normal stress – 41·4 kN/m^2
Cell speed – 5 r.p.m.
Sieving – 5 mins

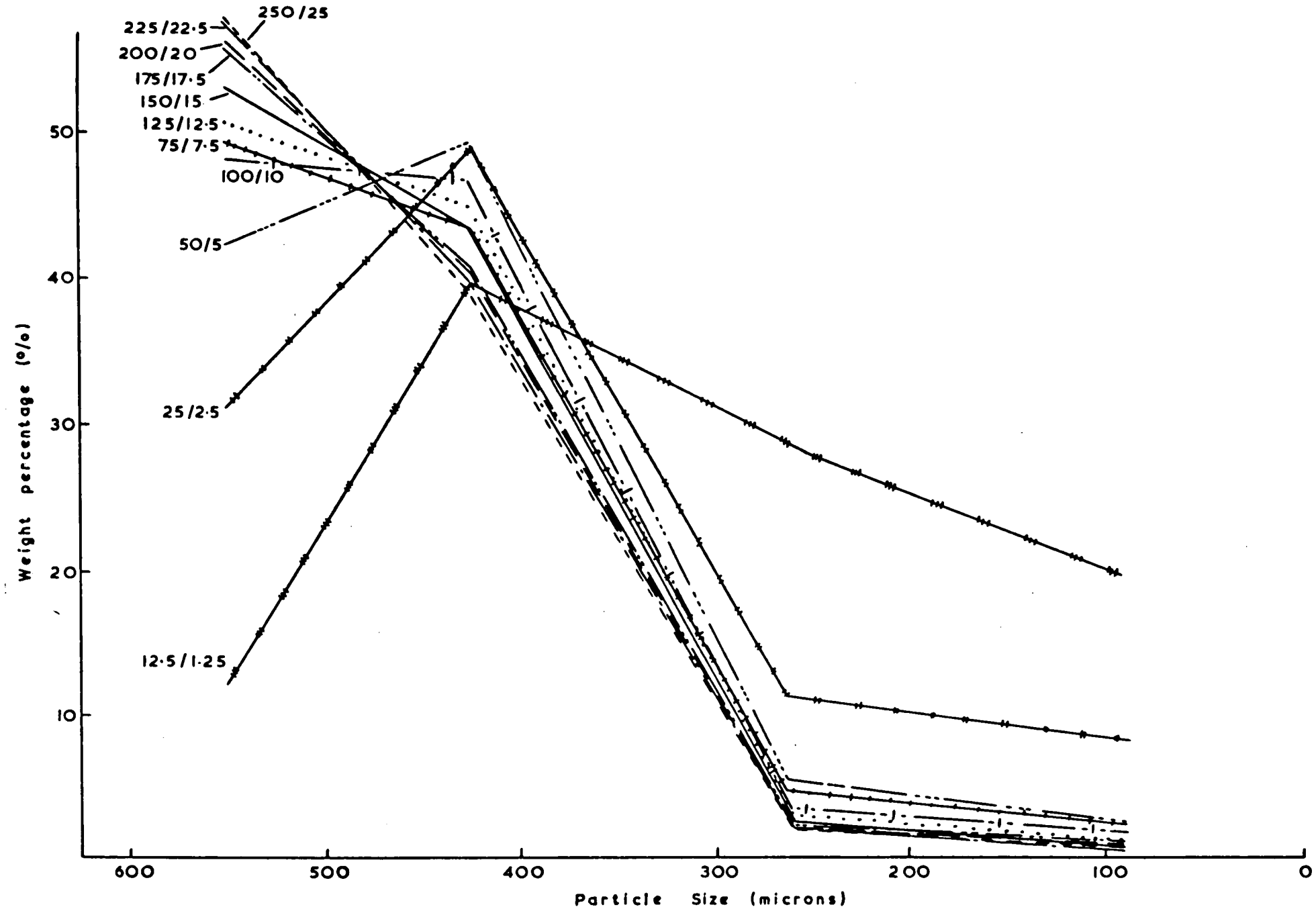


Fig. 4.2.6 Particle Size Distribution of PDV Salt (500 – 600μm)
Effect of constant sample wt/cell rev. ratio (10/1) on Attrition (wt %)

PDV Salt — Mean size 550 μm
Normal stress — 41·4 kN/m²
Cell speed — 5 r.p.m.
Sieving — 5 mins

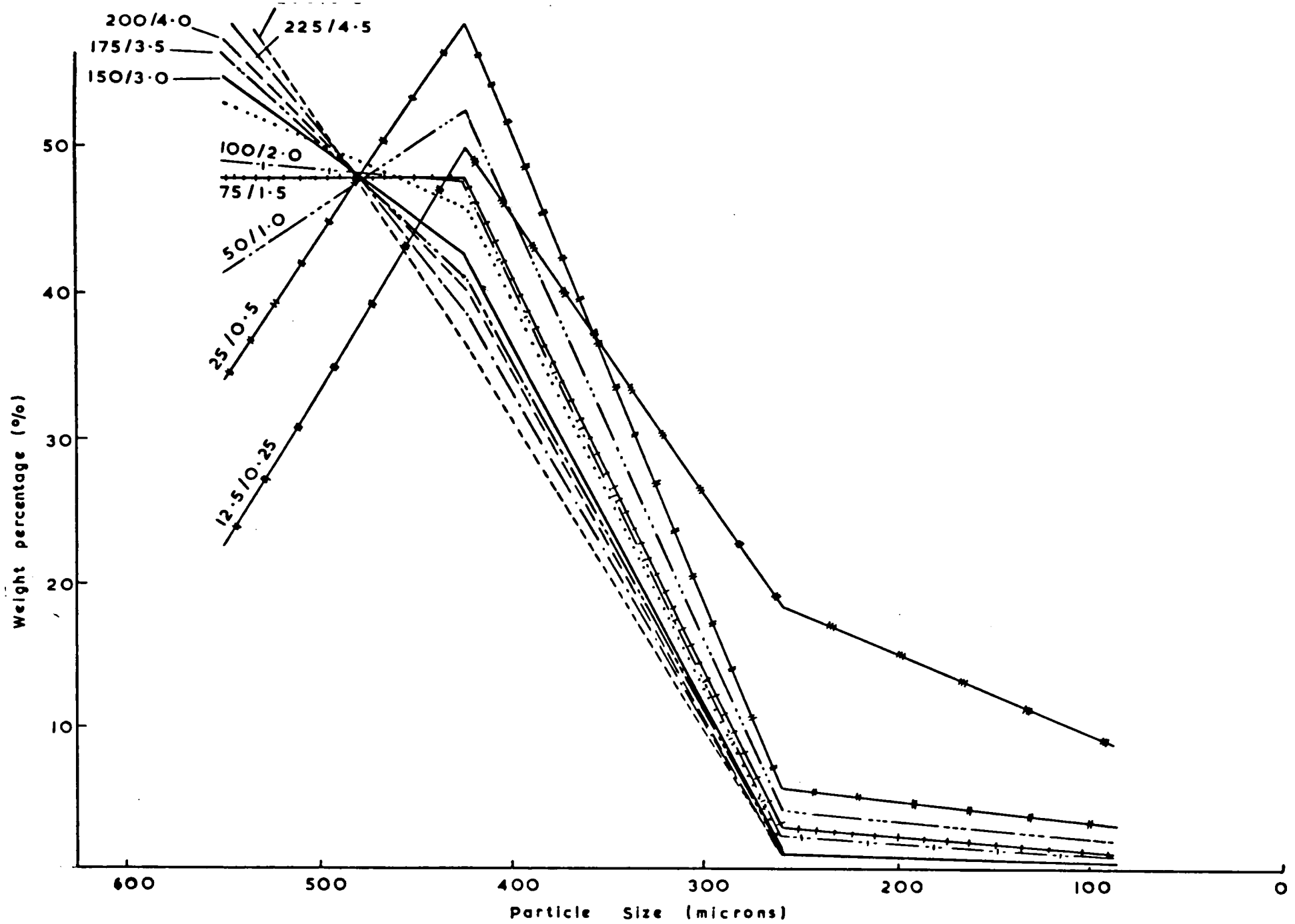


Fig. 4.2.7. Particle Size Distribution of PDV Salt (500 – 600 μm)
Effect of constant sample wt/cell rev. ratio (50/1) on Attrition (wt %)

PDV Salt – Mean size 550 μm

Normal stress – 41·4 kN/m^2

Cell speed – 5 rpm

Sieving – 5 mins

The influence of the segregation of fine material during attrition was also investigated by running the cell in its normal mode of operation for a number of revolutions. The same experiment was then repeated with the cell being inverted at the end of each revolution. This was carried out for ten and twenty-five revolutions of the cell, and the results presented in Table 4.2.8 show that these was no significant difference between runs indicating that segregation did not affect attrition for these particles.

Results obtained when salt was attrited at increasing shear strains were plotted on a log-log plot according to Gwyn (1969). PDV salt (500-600 μm) was attrited for upto a strain of 14760 (300 revolutions of the cell) at a normal stress of 41.4 kN/m^2 and the results are shown in Figures 4.2.9 and 4.2.10. It is seen that linearity is lost after a strain of 2950 (60 revolutionsof the cell). Regression analysis was carried out on the straight line part of the data which fitted an equation of the form

$$\log W = 0.09 \log \gamma + 1.47$$

where W is the weight attrited and γ the strain.

Regression analysis was also carried out on Gwyn plots for PDV salt at various normal stresses and different equations were obtained in each case (Figure 4.2.11).

$\log W = 0.01 \log \gamma + 1.43$ at 1.0 kN/m^2

$\log W = 0.03 \log \gamma + 1.47$ at 20.7 kN/m^2

$\log W = 0.10 \log \gamma + 1.46$ at 82.8 kN/m^2

$\log W = 0.15 \log \gamma + 1.38$ at 165 kN/m^2

Torque (Nm)		Number of Revs (Initial Weight)	Particle Size Distribution (gm)						Mode of Operation
Av	Max		<45 μm	45-90 μm	90-180 μm	180-355 μm	355-500 μm	>500 μm	
39.5	45.2	10 (100 gm)	0.3	0.5	0.9	3.0	43.8	51.4	N
39.5	45.2		0.3	0.4	1.0	2.9	43.9	51.5	I
39.5	45.2	25 (100 gm)	0.4	0.7	1.1	4.9	48.5	44.3	N
39.5	45.2		0.4	0.8	1.0	4.8	48.2	44.7	I

TABLE 4.2.8 PDV Salt (500-600 μm) - Effect of Segregation

Cell Speed - 5 rpm
Sample Thickness - 9.0 mm
Shear Strain - 49.2 per revolution
Normal Stress - 41.4 kN/m_2
Sieve Shaker - 5 mins.

N - Normal operation of cell
I - Cell inverted at the end of each revolution

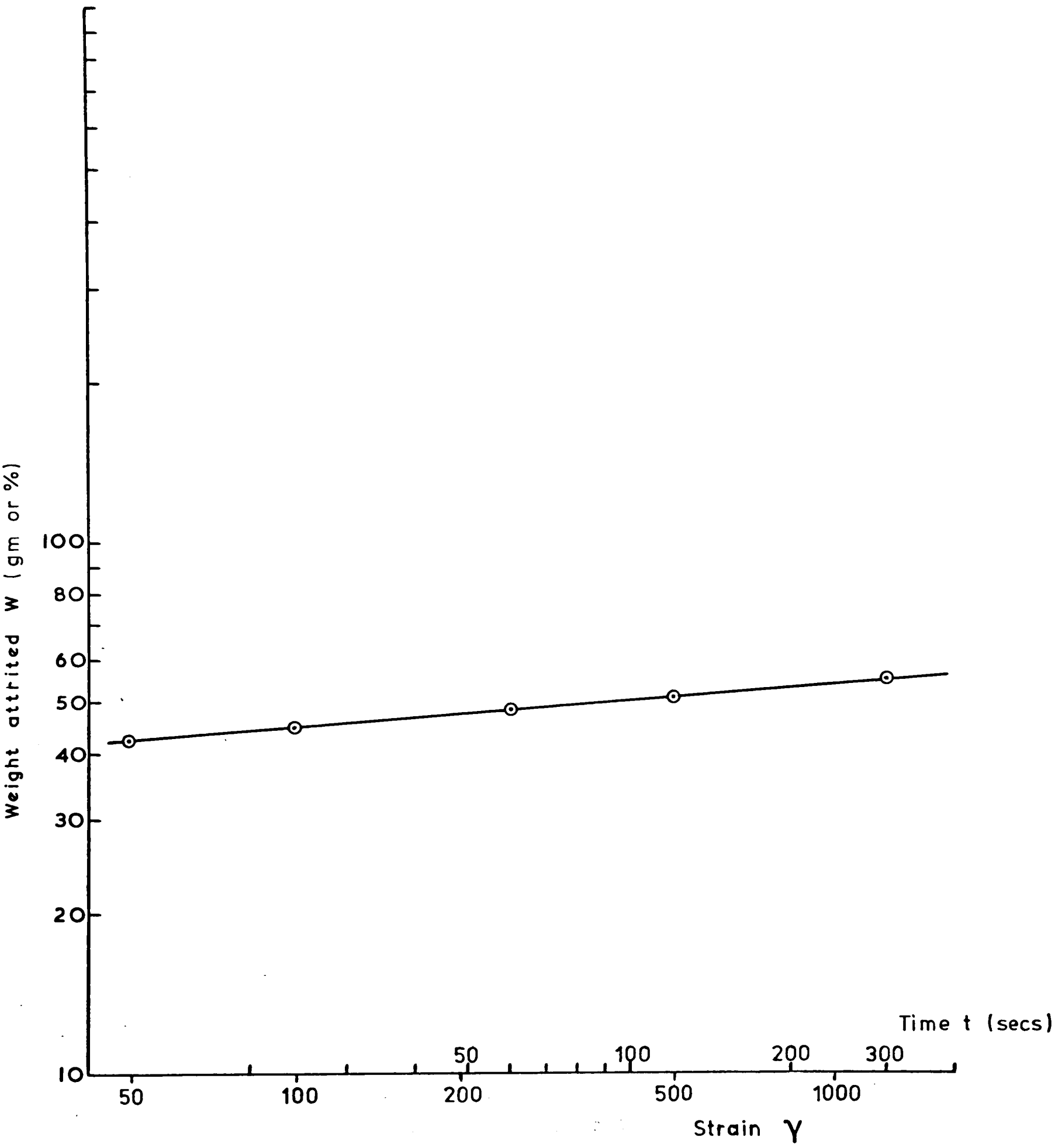


Fig. 4.2.9 PDV Salt (500 - 600 μm) – Gwyn Plot

Effect of Strain on Attrition

Cell speed – 5 r.p.m.

Sample weight – 100gm

Sample thickness – 9·0 mm

Shear strain – 49·2 per revolution

Normal stress – 41·4 kN/m^2

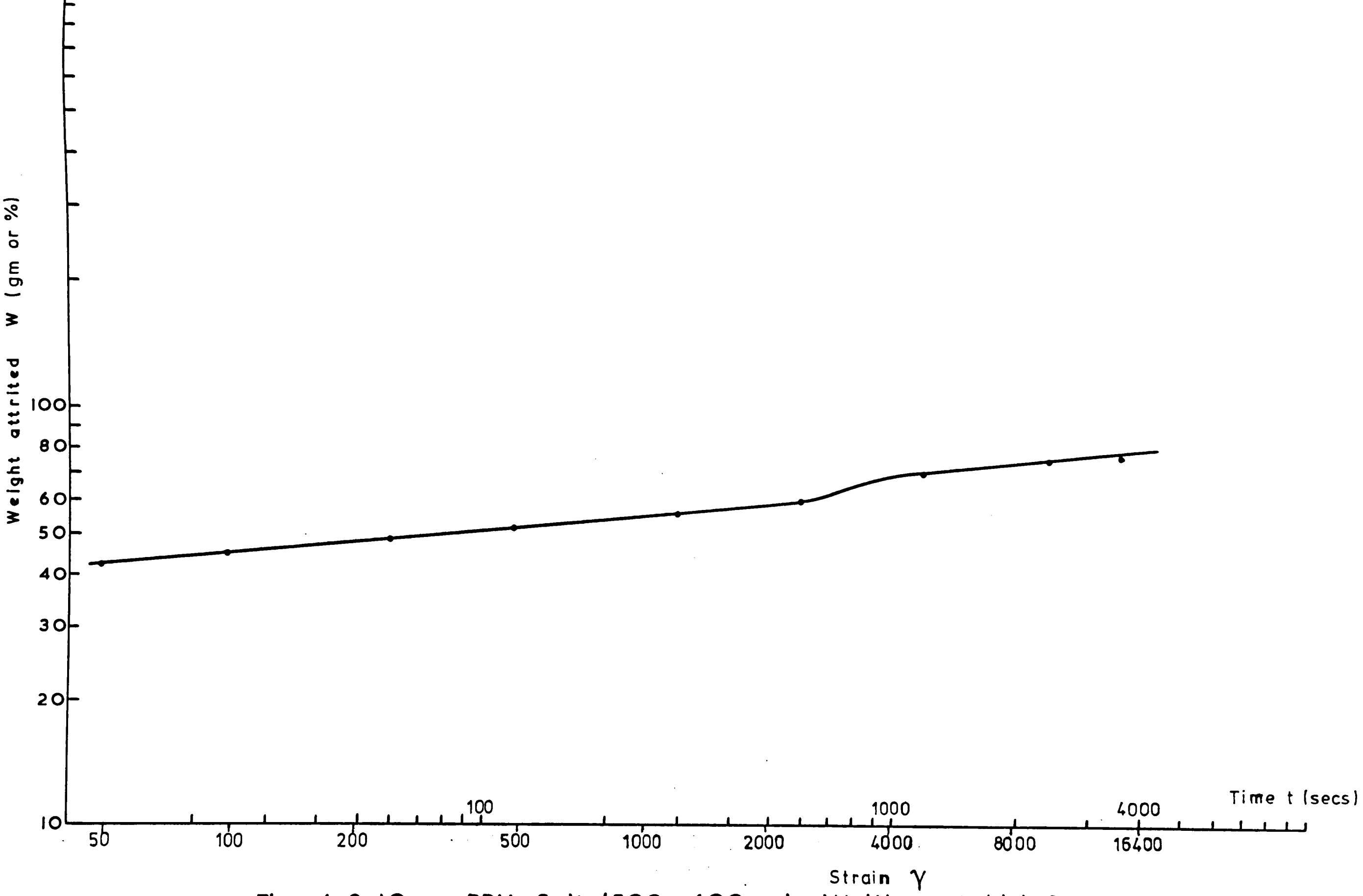


Fig. 4.2.10 PDV Salt (500 - 600 μm) – Attrition at high Strains. Conditions as for Fig. 4.2.9

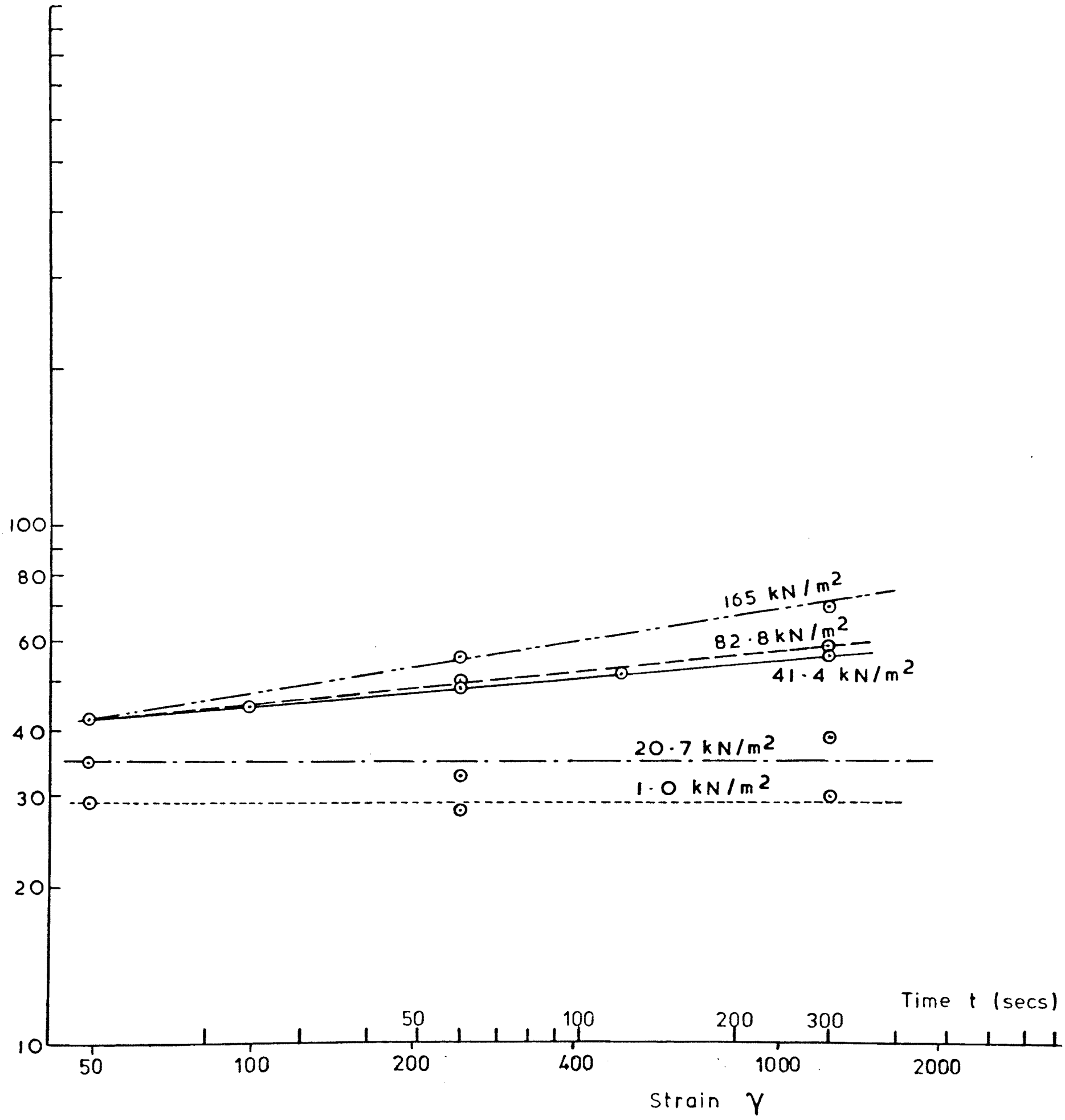


Fig. 4.2.11. PDV Salt (500 - 600 μm) – Gwyn Plot

Effect of Strain on Attrition at different Normal Stresses

Cell speed – 5 r.p.m.

Sample weight – 100 gm

Sample thickness – 9·0 mm

Shear strain – 49·2 per revolution

A full summary of the statistical analysis is shown in Table 4.2.11.

In all cases it was noted that the values of the intercept did not differ greatly, associated with the fact that initial attrition was not very dependent on normal stress. The gradient, however, increased steadily as stress increased. The values for intercept were the highest of all materials tested.

Experiments were carried out at small strains (less than one revolution of the cell) to see how the linear relationship would be affected and also to observe how attrition occurred. Runs were carried out at $\frac{1}{8}$, $\frac{1}{4}$ and $\frac{1}{2}$ revolutions of the cell (Figure 4.2.12); it is seen that the linear behaviour is lost. It was not possible to carry out runs at very small strains as it would not have been possible to measure these values accurately.

The Gwyn plot was also extended to PDV salt of the smaller size fraction (250-355 μm) and results are shown in Figure 4.2.13. A linear relationship was again established and the line fitted the equation

$$\log W = 0.10 \log \gamma + 0.57 \quad \text{at} \quad 41.4 \text{ kN/m}^2$$

The intercept here was very much smaller than that for the larger sized PDV salt under the same conditions, but the gradient was the same as that for the higher stress run (82.8 kN/m^2) using 500-600 μm material.

Material	Normal Stress kN/m^2	Gradient	Standard Error of Gradient	Intercept	Standard Error of Intercept	Correlation Coefficient %	F-Value
PDV Salt (500-600 µm)	1.0	0.01	0.02	1.43	0.004	49.14	0.32
	20.7	0.03	0.05	1.47	0.04	59.01	0.53
	41.4	0.09	0.001	1.47	0.001	99.96	5443
	82.8	0.1	0.004	1.46	0.007	99.9	478
	165.0	0.15	0.02	1.38	0.02	98.94	460
PDV Salt (250-355 µm)	41.4	0.1	0.003	0.57	0.001	99.84	918

TABLE 4.2.11 PDV Salt - Summary of Regression Analysis for Gwyn Plots

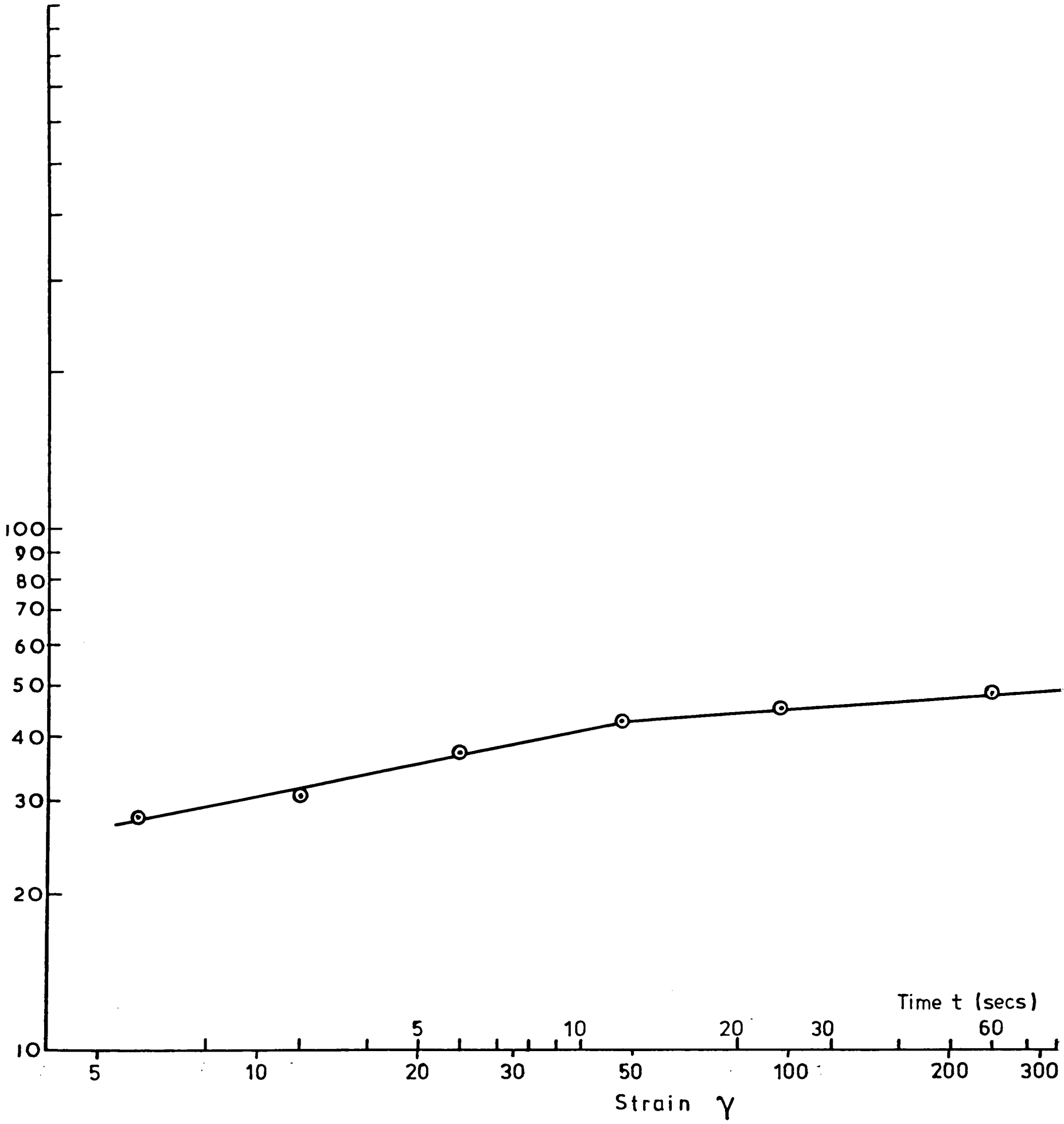


Fig. 4.2.12. PDV Salt (500 – 600 μm)—Gwyn Plot

Effect of small Strain on Attrition

Cell speed – 5 r.p.m.

Sample weight – 100 gm

Sample thickness – 9·0 mm

Shear strain – 49·2 per revolution

Normal stress – 41·4 kN/m^2

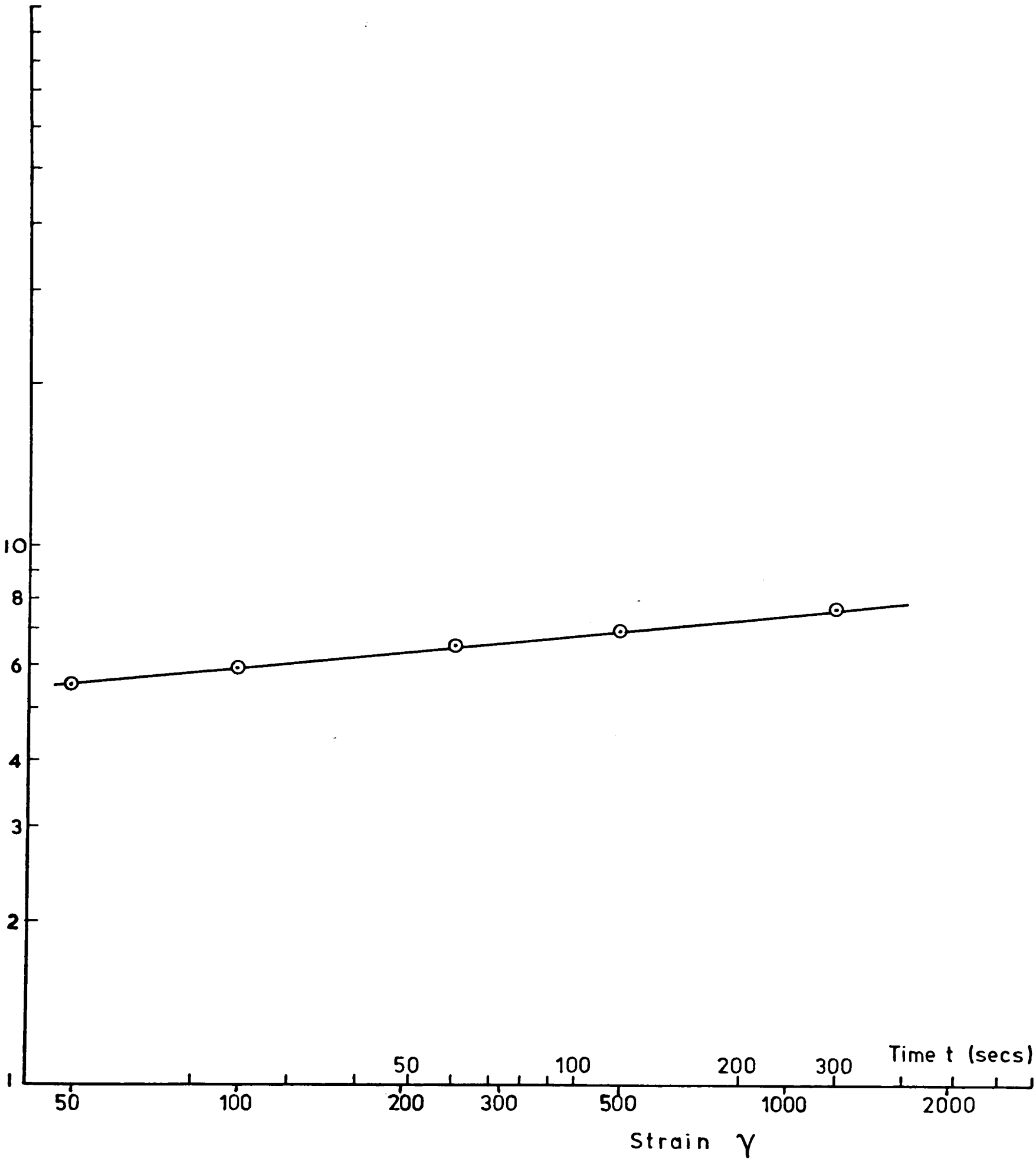


Fig 4. 2.13. PDV Salt (250 – 355 μm)—Gwyn Plot

Effect of Strain on Attrition

Cell speed – 5 r.p.m.

Sample weight – 100gm

Sample thickness – 9·0 mm

Shear strain – 49·2 per revolution

Normal stress – 41·4 kN/m^2

4.3 Laboratory Salt

An abridged experimental programme was carried out as only a limited quantity of this material was available.

The effect of increasing shear strain was measured. 100 gm of material of initial diameter between 355-500 μm was isolated by sieving and subjected to a maximum of twenty-five revolutions in the cell. At a cell speed of 5 rpm, this corresponded to an average shear strain of 44.3 per revolution and strain rate of 3.69 sec^{-1}. The ground product was then analysed by using the standard nest of sieves to obtain the new particle size distribution. Results are given in Table 4.3.1 and Figure 4.3.1.

It is seen that the fines increase monotonically with shear strain; the maximum obtained in the case of granular salt is absent here although both material are spherical in shape.

The results obtained by attriting salt with increasing shear strain was then interpreted according to Gwyn (1969). Regression analysis was carried out and the data (Figure 4.3.2) fitted by an equation of the form

$$\log W = 0.18 \log \gamma + 0.53$$

The correlation coefficient of fit was 99.9% and F-value 1250. The standard error of the gradient was 0.005 and of the intercept 0.003. The gradient and intercept were both lower than that for granular salt indicating that lab salt attrited less readily than the former.

Torque (Nm)	
Av	Max
28.2	33.9
28.2	33.9
28.2	33.9
28.2	33.9
33.9	45.2

Number of Revs (Initial Weight)	Particle Size Distribution (gm)					Normal Stress kN/m^2
	<45µm	45-90 µm	90-180 µm	180-355 µm	>355 µm	
1 (100 gm)	0.1	0.2	0.9	5.4	93.3	41.4
2 (100 gm)	0.1	0.2	0.9	6.4	92.4	41.4
5 (100 gm)	0.1	0.2	1.3	7.0	91.3	41.4
10 (100 gm)	0.2	0.3	1.4	8.0	90.0	41.4
25 (100 gm)	0.2	0.5	1.8	9.2	88.1	41.4

TABLE 4.3.1 Lab Salt - Variation of Shear Strain

Cell Speed - 5 rpm
Sample Thickness - 10.0 mm
Shear Strain - 44.3 per revolution
Sieve Shaker - 5 mins.

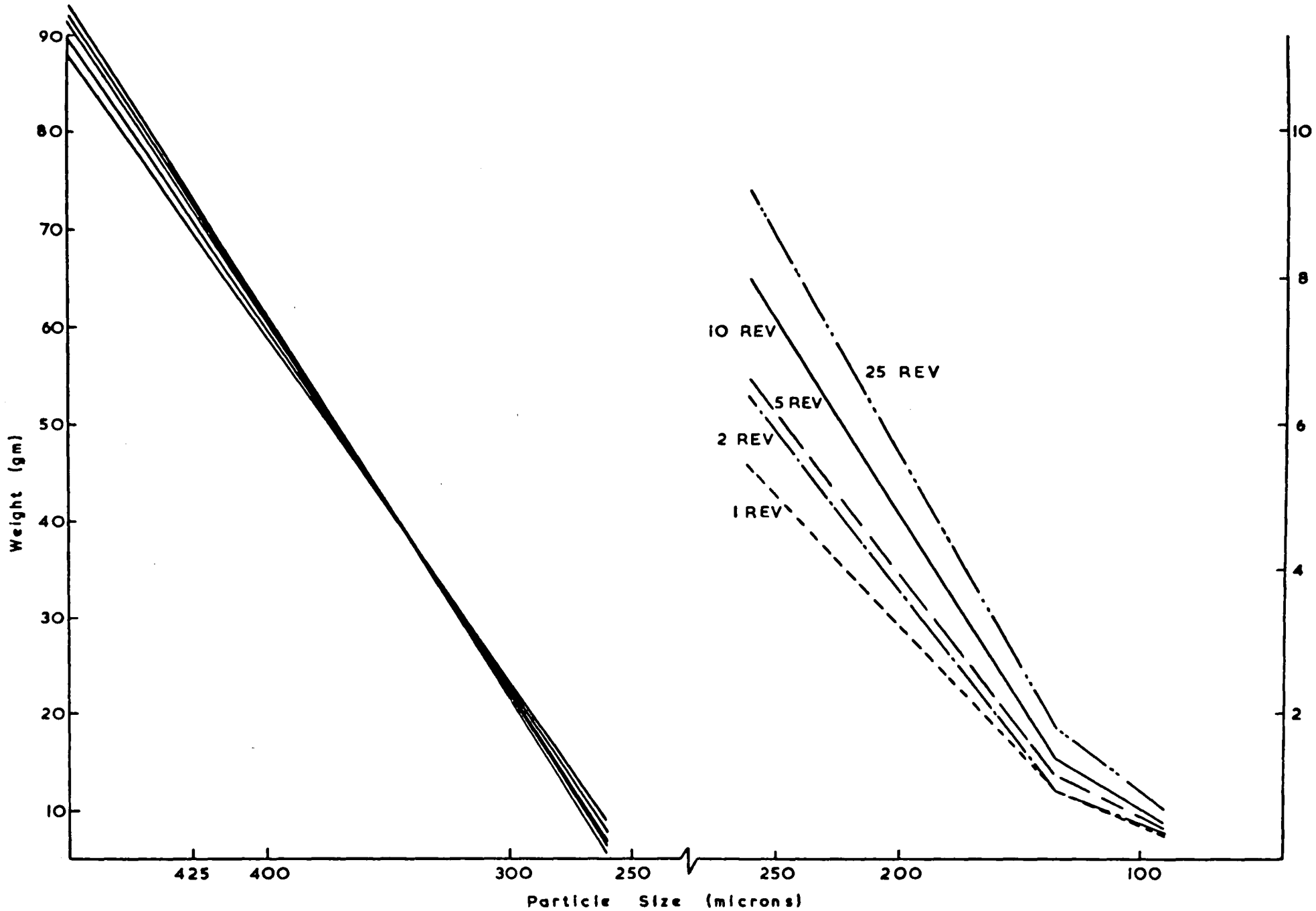


Fig. 4.3.1 Particle Size Distribution of Lab Spherical Salt (355 - 500μm)
Effect of Strain on Attrition

Lab Salt — Mean size 425 μm
Sample weight — 100gm
Normal stress — 41·4kN/m²
Cell speed — 5r.p.m.
Sample thickness — 10·0mm
Shear strain — 44·3 per revolution

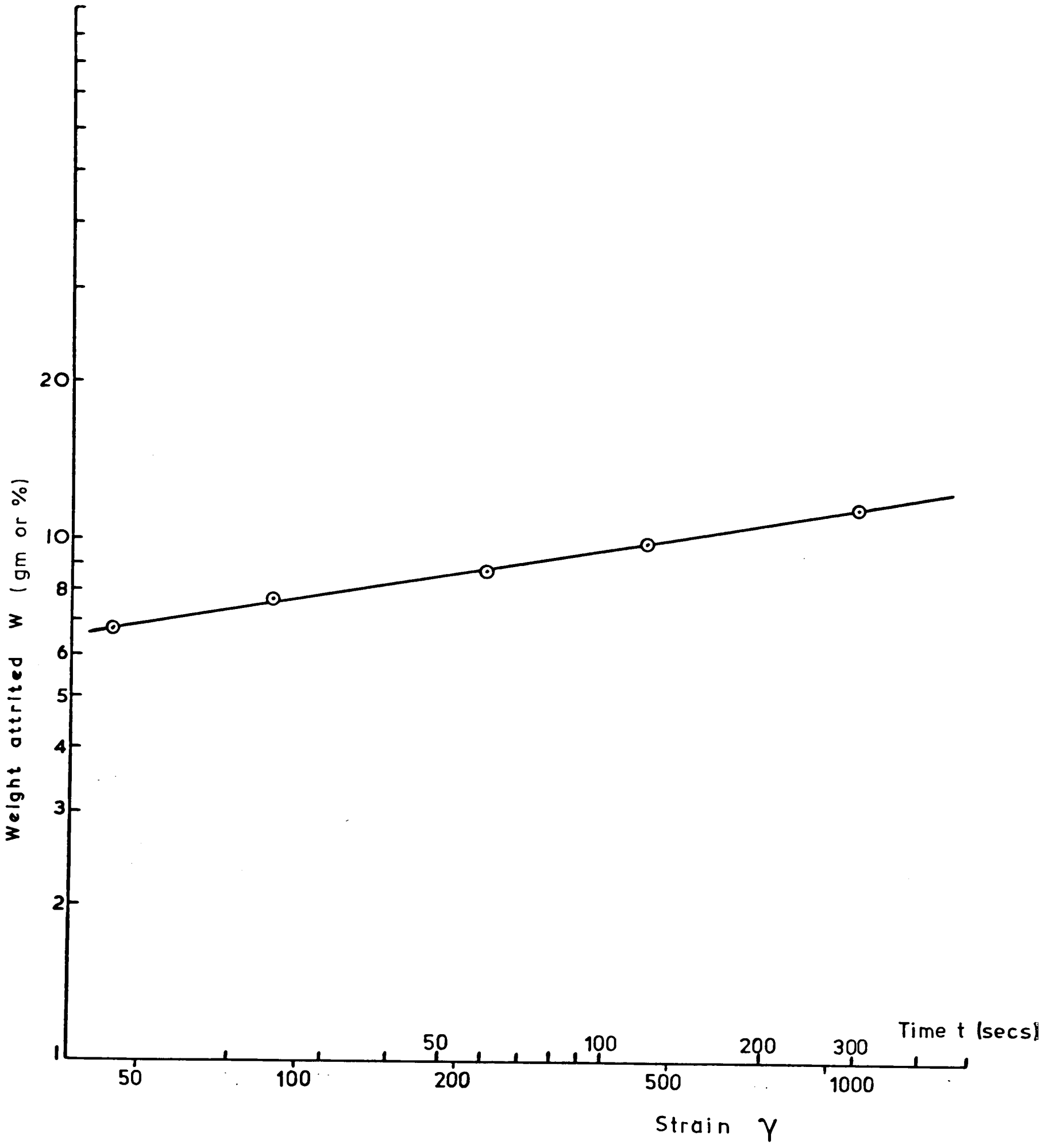


Fig. 4.3.2 Lab Salt (355 - 500 μm) — Gwyn Plot

Effect of Strain on Attrition

Mean size - 425 μm

Sample weight - 100 gm

Sample thickness - 10·0 mm

Shear strain - 44·3 per revolution

Normal stress - 41·4 kN/m^2

Cell speed - 5 r.p.m.

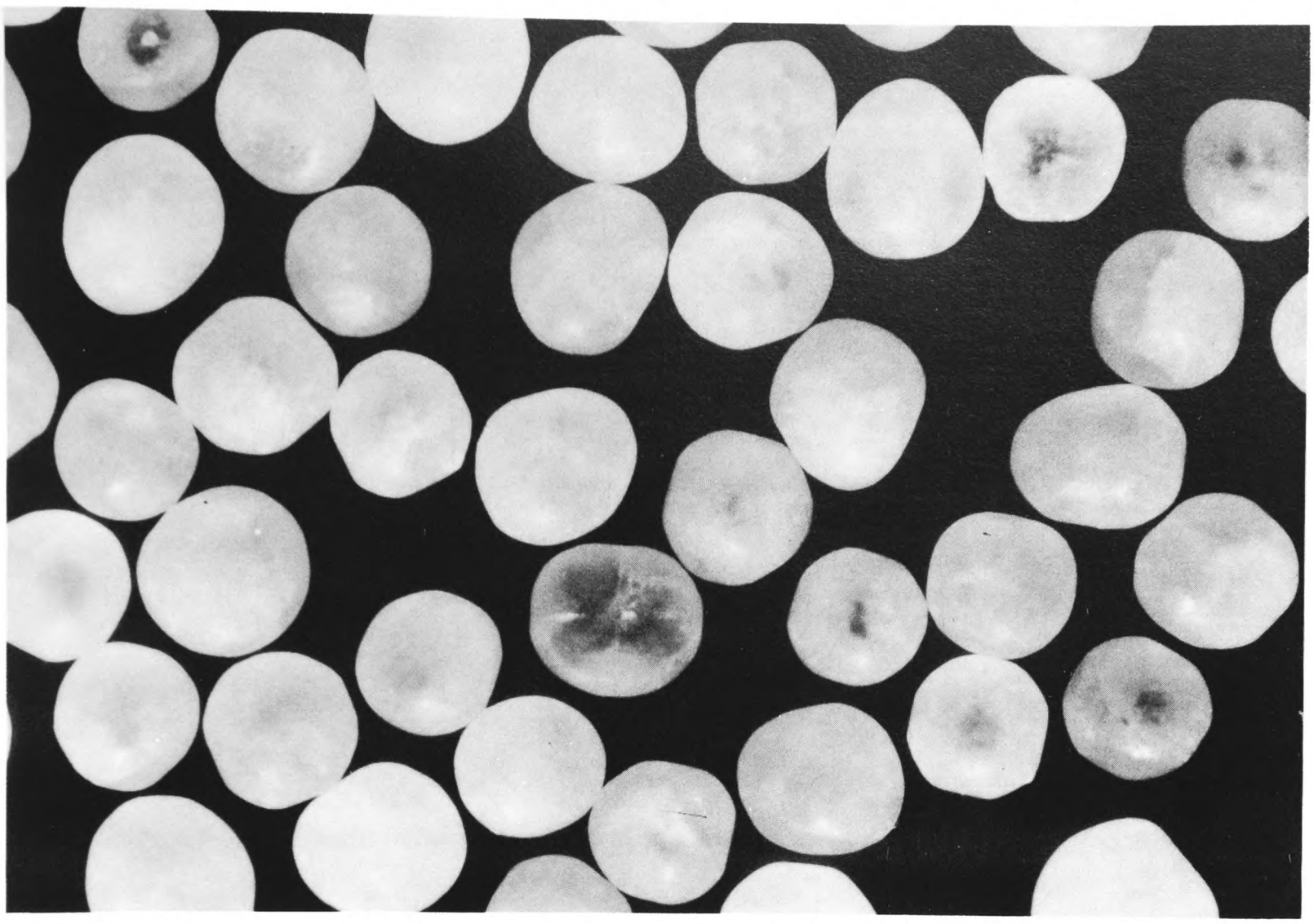
4.4 Mechanisms of Attrition

Photographs of granular salt are presented in Figures 4.4.1a to 4.4.1e and Figures 4.4.2a to 4.4.2e. These show material at a normal stress of 41.4 kN/m^2 ground for one and twenty-five revolutions of the cell. Initial spherical material is seen to shatter into radial fragments as evidenced by the number of half-spheres and radial fragments seen in the larger size fractions. The photographs of the smaller material show that the larger fragments either grind down to dust or shatter further as attrition continues. Photographs of finer size fractions at higher revolutions of the cell show that these jagged fragments have assumed a more rounded shape showing that surface grinding has taken place.

Photographs of attrited PDV salt at one and two hundred revolutions of the cell at a normal stress of 41.4 kN/m^2 (Figures 4.4.3a to 4.4.3d, Figures 4.4.4a to 4.4.4e) show that this material shatters into smaller cubes. As attrition continues, further shattering occurs where more cubic material is created. Prolonged attrition (200 revs) shows that the cubic shape is gradually lost by the rounding of edges and that debris produced during the shattering process grinding to dust.

g. 4.4.1 - Granular sodium chloride attrited at 41.4kN/m^2 normal stress for 1 rev. Relevant sieve-cuts shown against each photograph

(a)
-2.7 mm



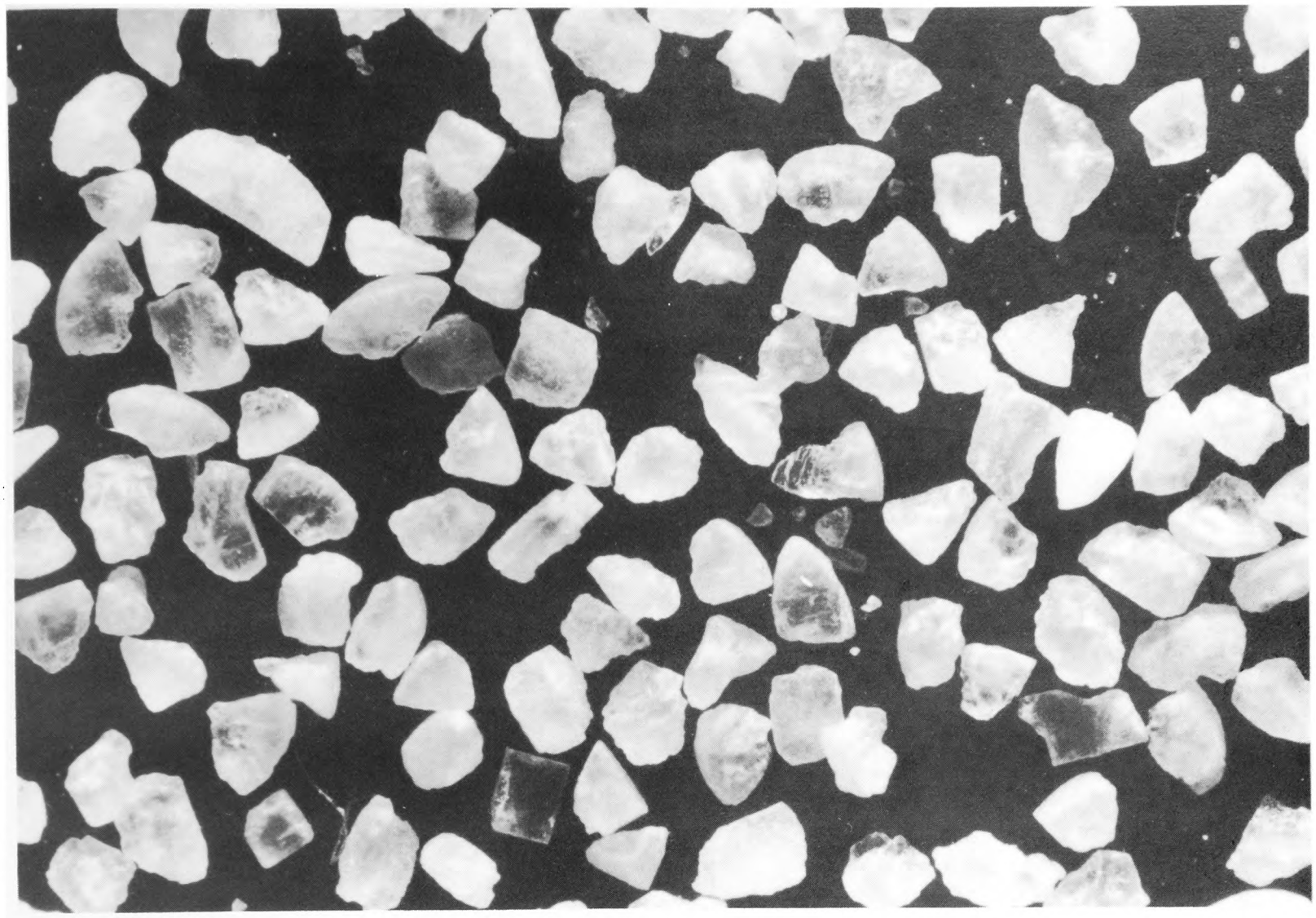
1mm

(b)
1.4 mm



1mm

(c)
500 µ



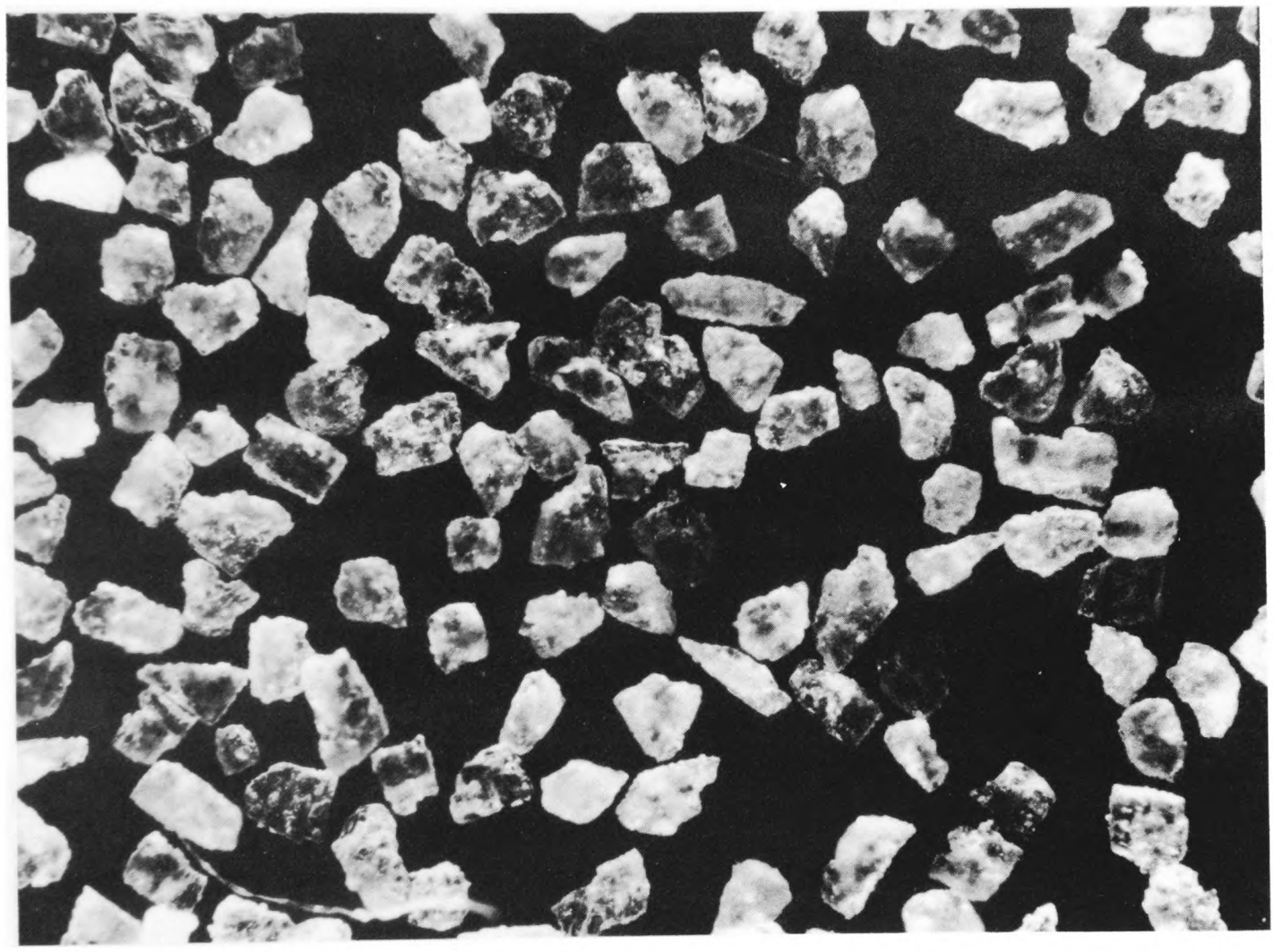
1 mm

)
55 µm



1 mm

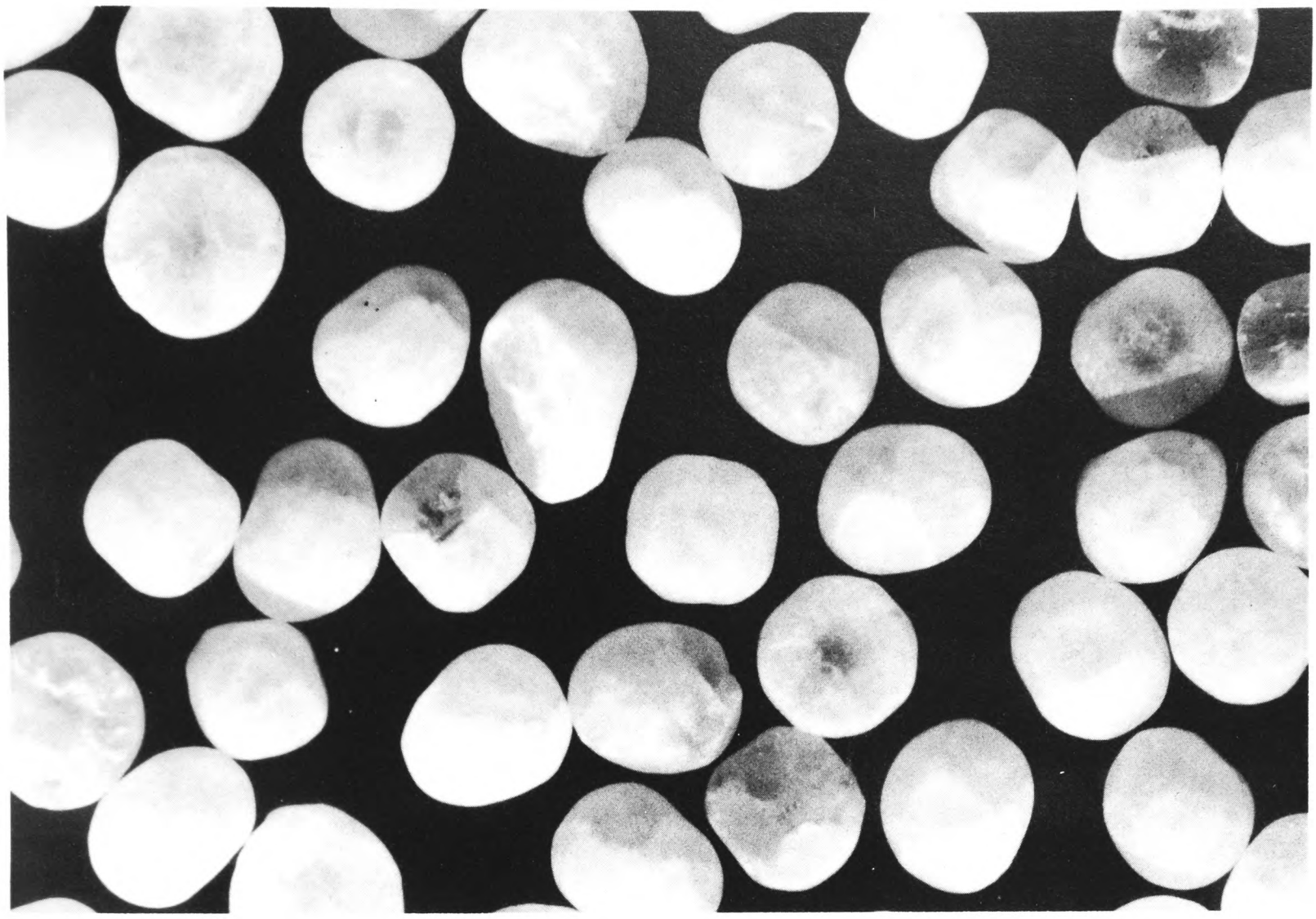
(e)
150-180 μm



1 mm

Fig. 4.4.2 - Granular sodium chloride attrited at 41.4 kN/m^2 normal stress for 25 revs. Relevant sieve-cuts shown against each photograph.

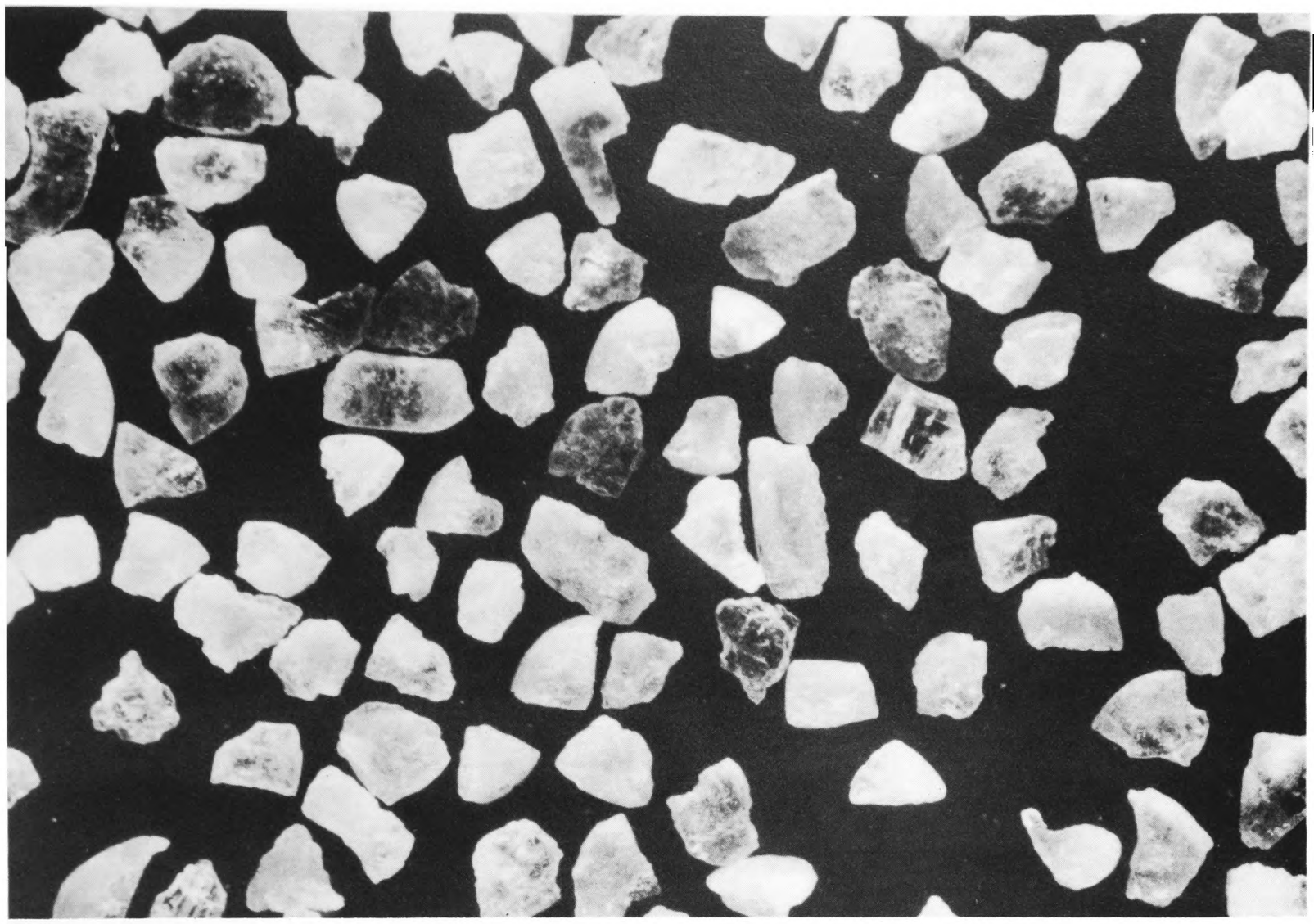
(a)
2.0 mm



)
.4 mm



(c)
5-500 µm



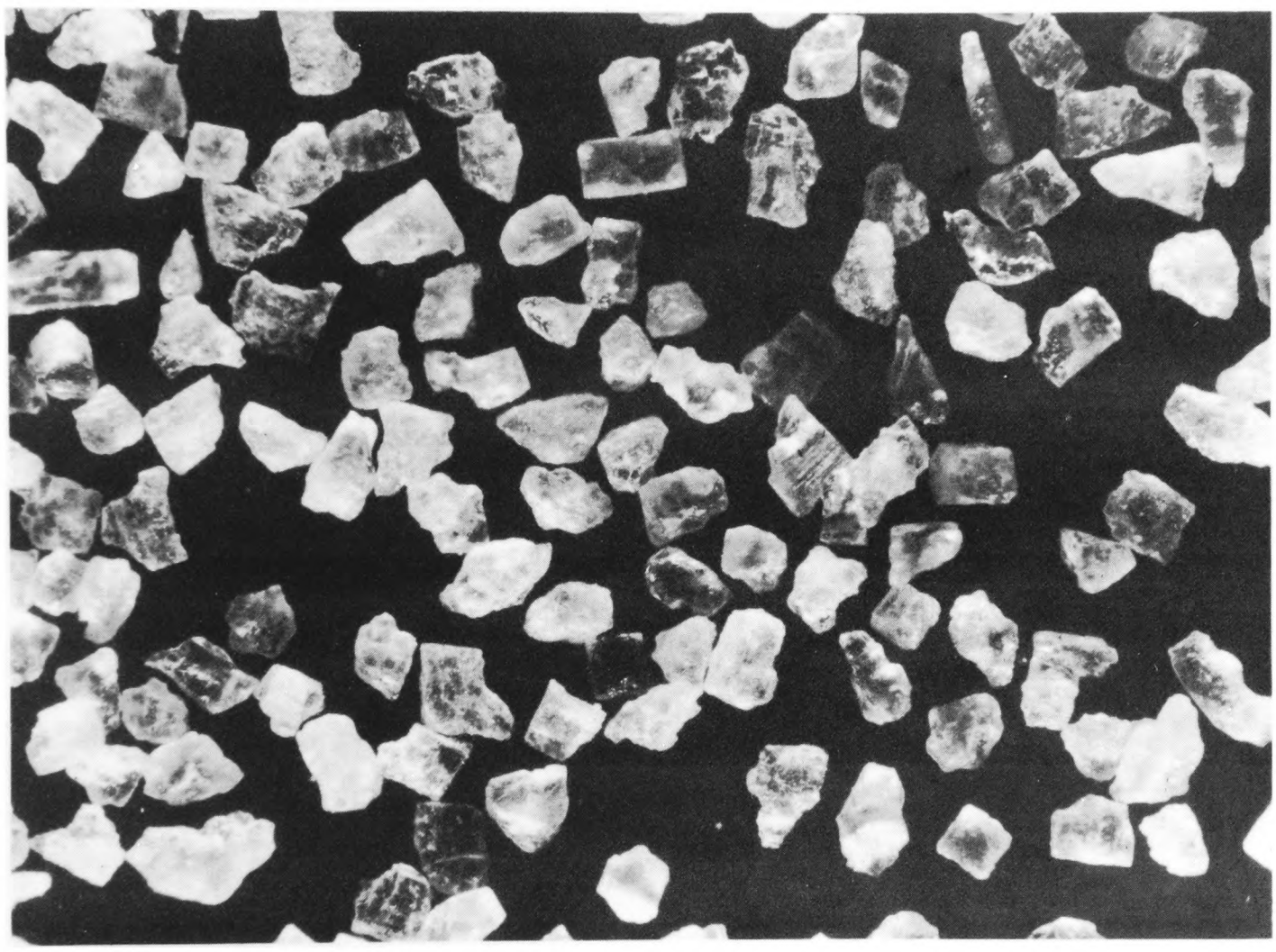
1 mm

(d)
55 µm



1 mm

(e)
150-180 μm



1 mm

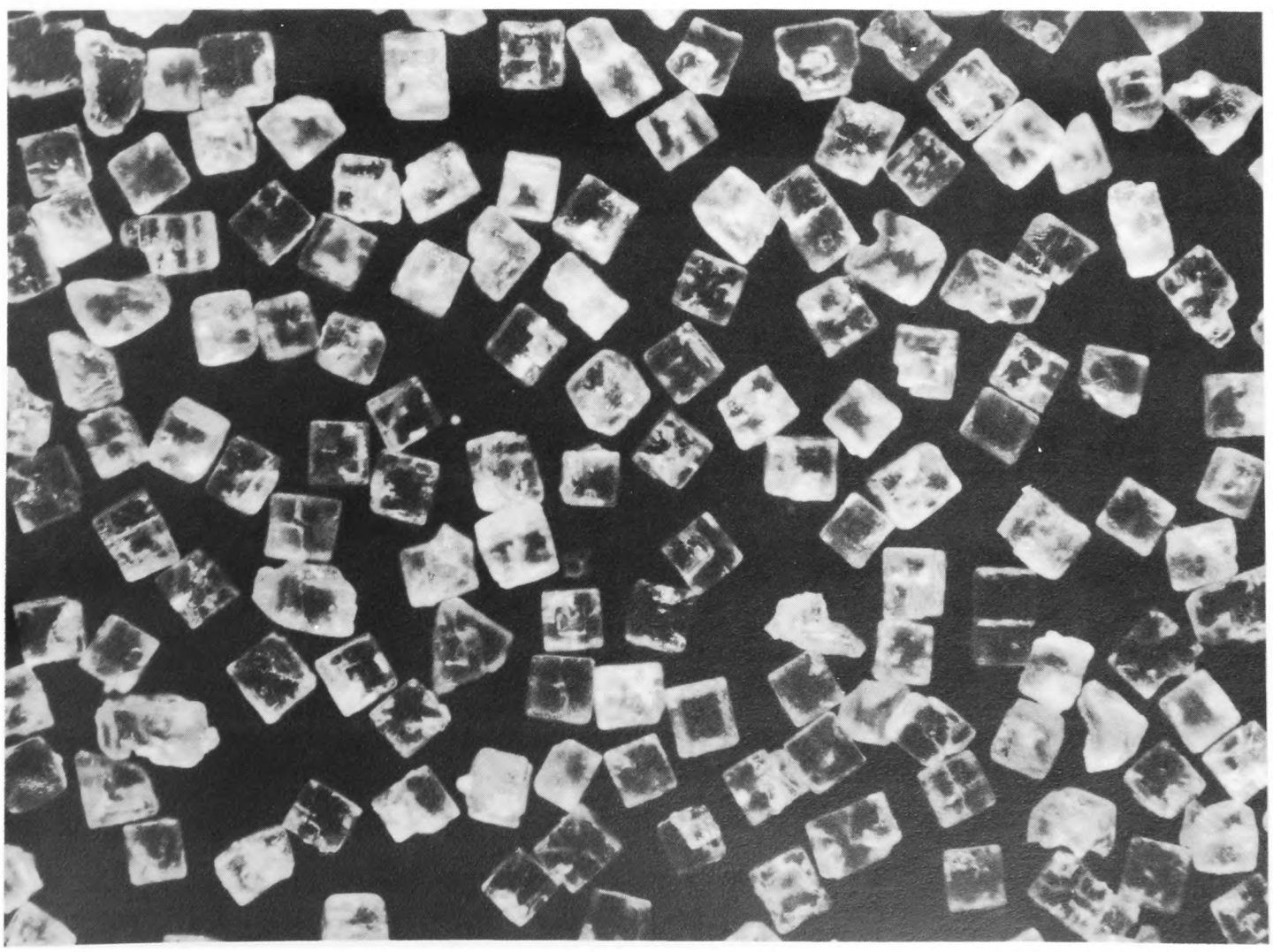
Fig. 4.4.3 - PDV Salt attrited at 41.4 kN/m^2 normal stress for 1 rev. Relevant sieve-cuts shown against each photograph.

(a)
250-300 μm



1 mm

(b)
212-250 μm



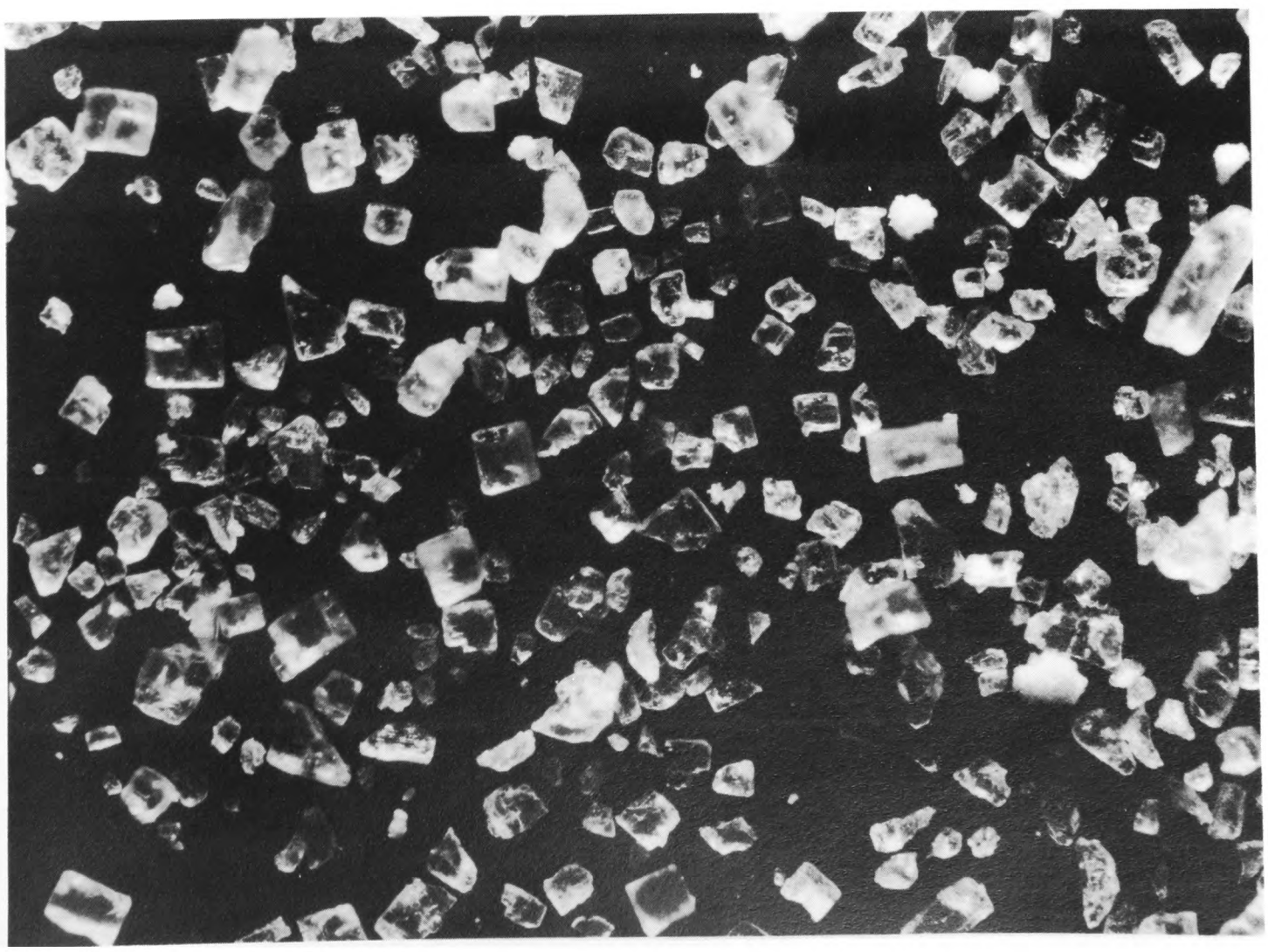
1 mm

(c)
180-212 µm



1 mm

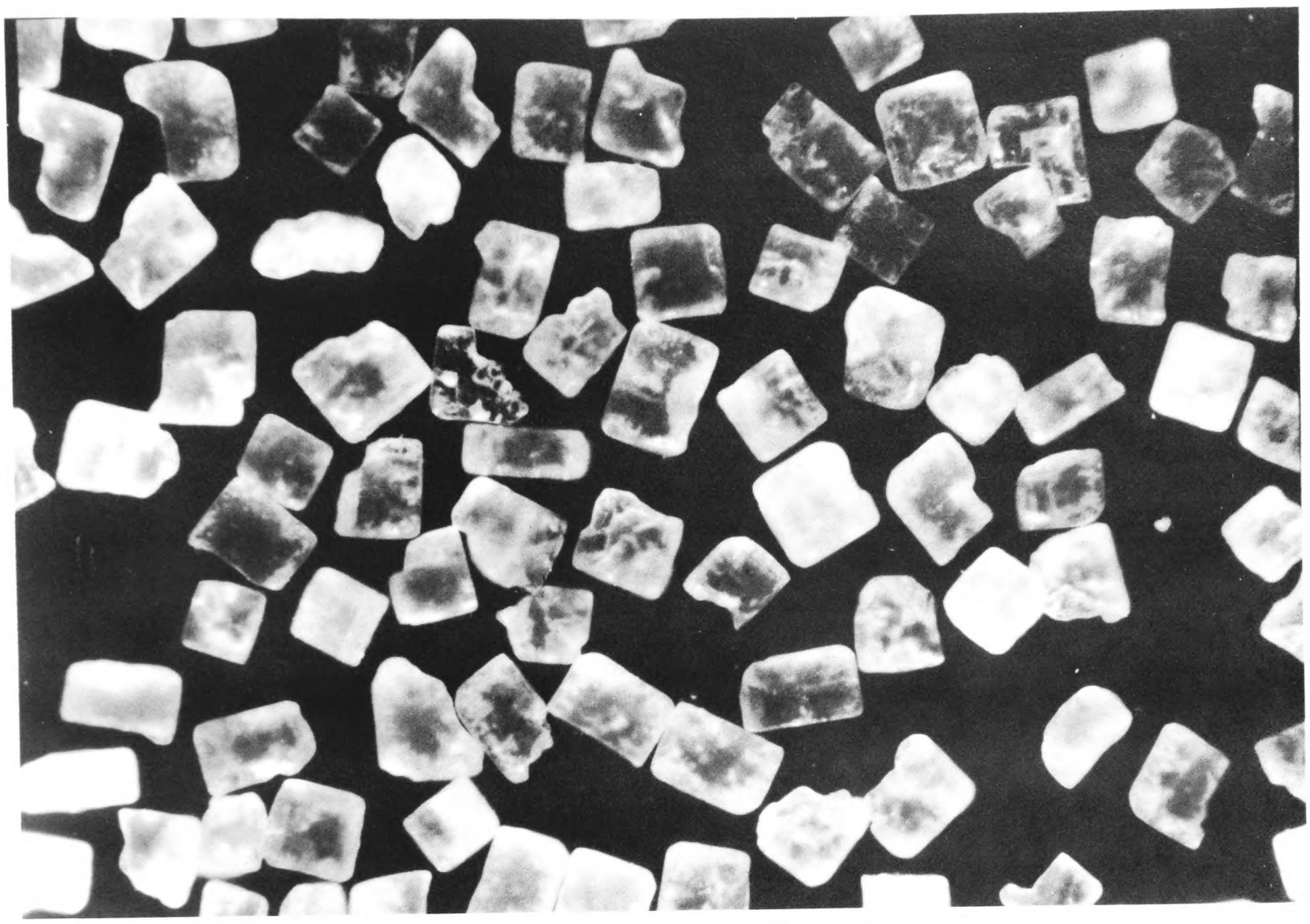
(d)
< 180 µm



1 mm

Fig. 4.4.4 - PDV Salt attrited at 41.4 kN/m^2 normal stress for 200 revs. Relevant sieve-cuts shown against each photograph.

)
55 µm



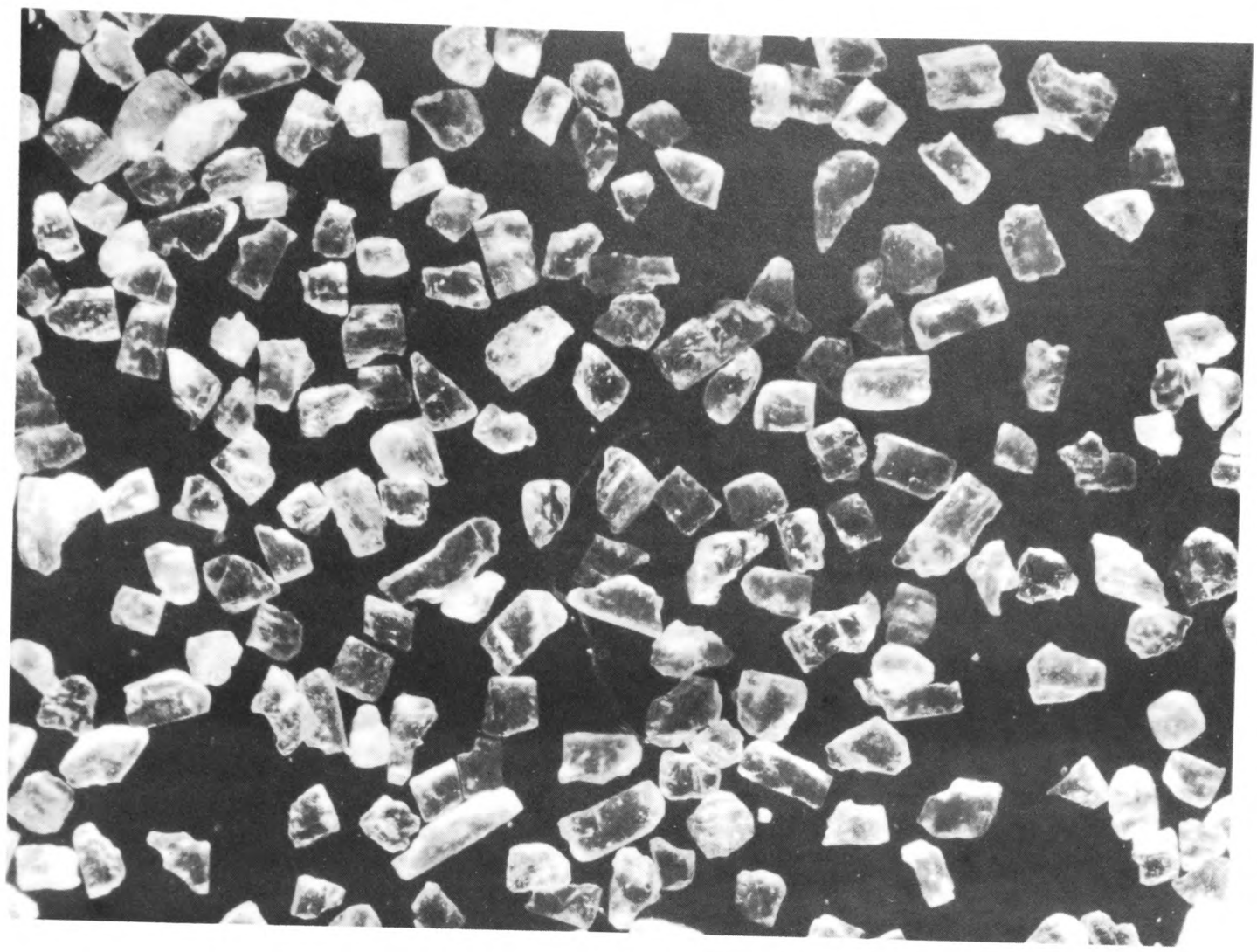
1 mm

(b)
150-180 µm



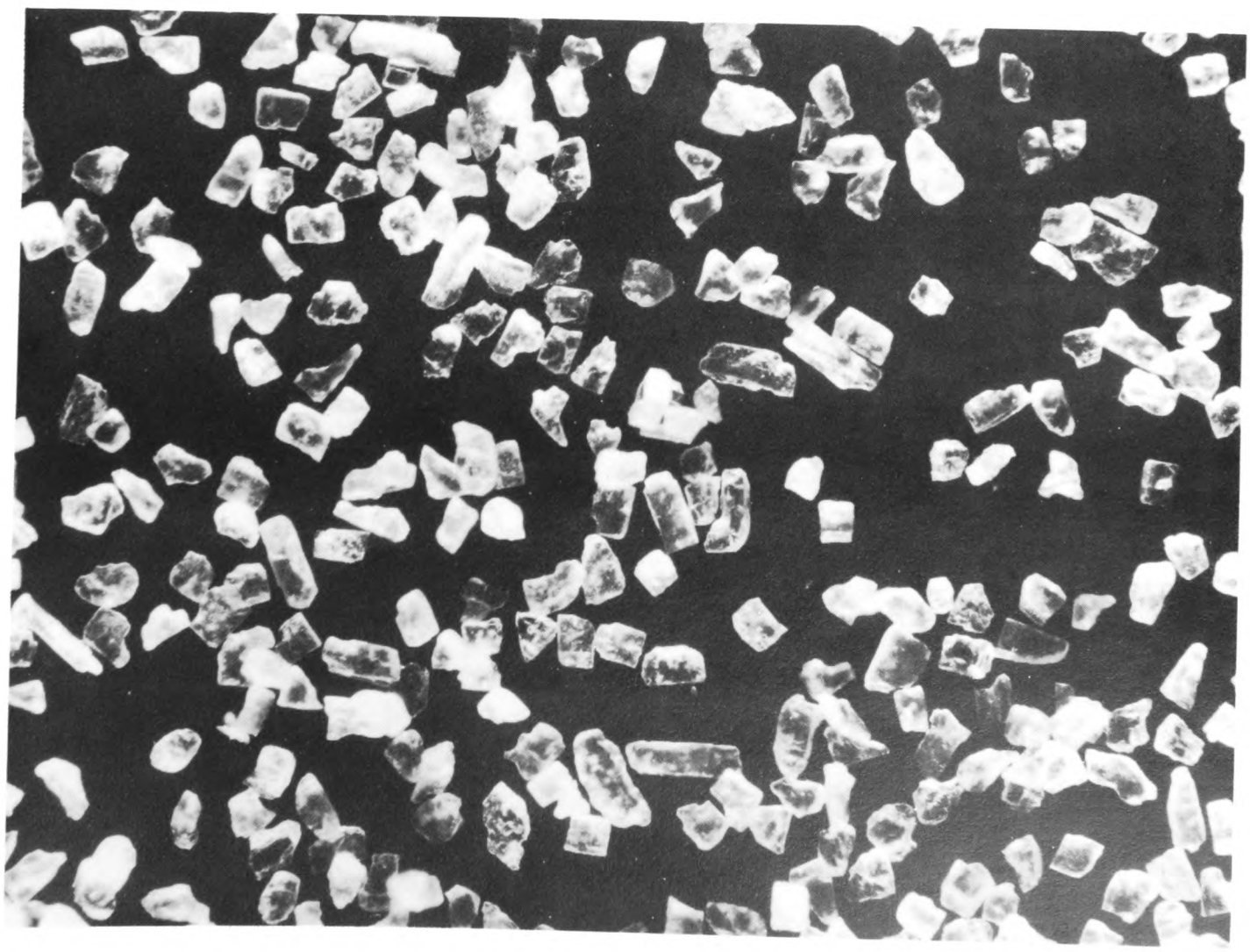
1 mm

(c)
100-150 µm



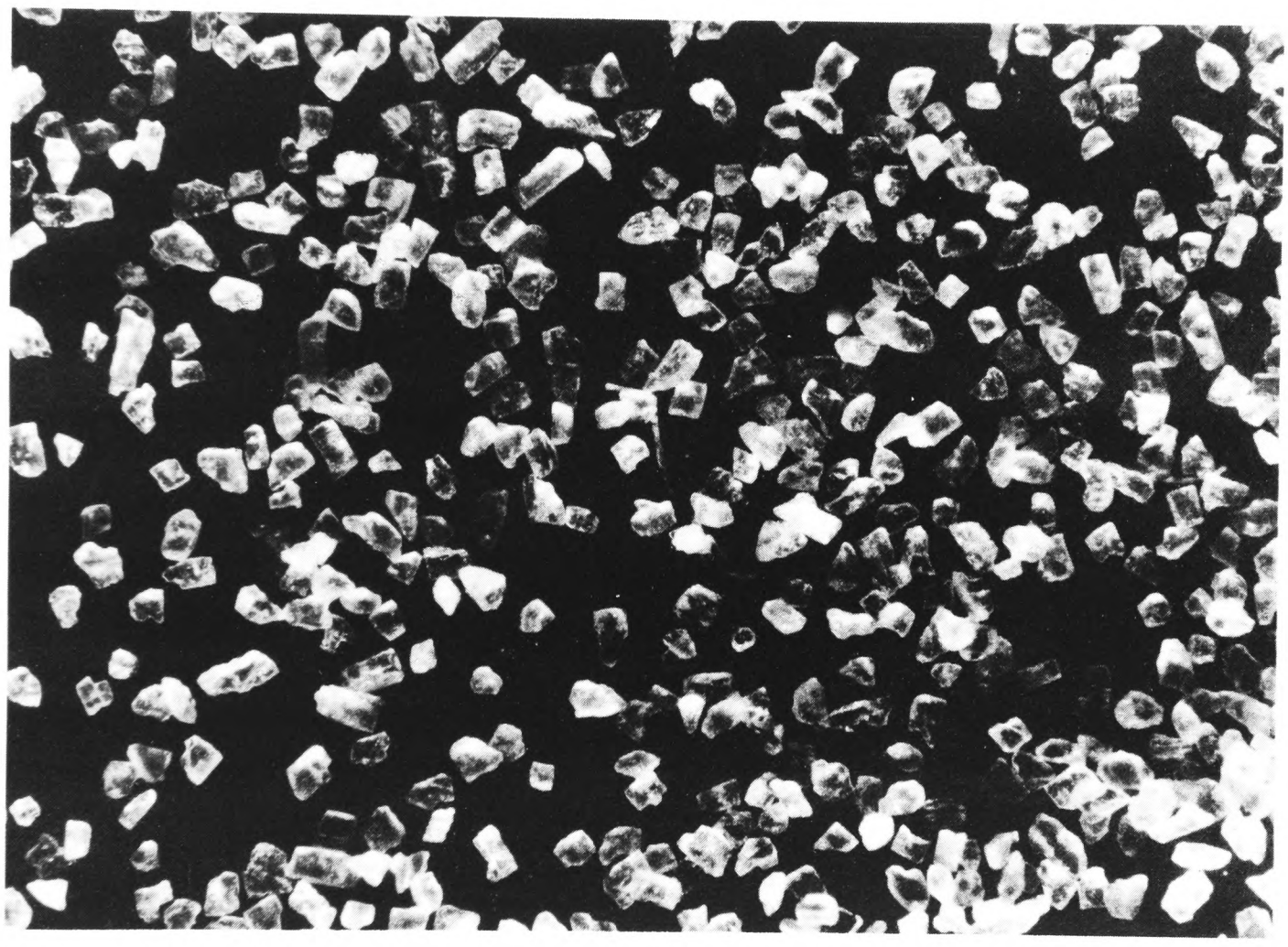
1 mm

(d)
90-100 µm



1 mm

(e)
63-90 µm



1 mm

CHAPTER FIVE

SODIUM CARBONATE (SODA ASH)

5.0 Introduction

Sodium carbonate or soda ash was used in further assessing cell performance. The particular material studied is called heavy ash and it is maunufactured from light ash, another form of sodium carbonate, produced by the ammonia-soda process. The light ash is converted to sodium carbonate monohydrate and then calcined. The product crystals are three times the size of light ash and are much more uniform in shape. The crystals are elongated hexagons and have a bulk density of 1060 kg/m^3. Experimental runs were carried out using particles of initial diameter between 250-355 μm. The ground product was analysed using the sieves: 250 μm, 180 μm, 90 μm, 45 μm. Experiments were carried out to assess the effect of varying cell revolutions, normal stress and sample thickness.

5.1 Experimental Runs

Reproducibility of results was established during the experimental programme. The various tables of results presented later under the different process conditions show that experiments repeated under fixed conditions produce consistent particle size distributions. This indicates that the cell behaves in a systematic manner when soda ash is attrited.

Heavy ash was subjected to varying shear strains and the effect on attrition behaviour analysed. 100 gm of ash of initial size between 250-355 μm was attrited for a maximum of twenty-five revolutions of the

cell where all other process conditions were held constant. For convenience, the cell speed was set at 5 rpm which corresponded to a mean shear strain of 41.4 per revolution and strain rate of 3.5 sec^{-1}. The attrited material was separated, using the standard nest of sieves previously specified, on the sieve shaker and the new particle size distribution determined. Results are given in Table 5.1.1 and the corresponding graph in Fig.5.1.1. A monotonic increase in fine material is observed as shear strain increases, and the amount of fines is seen to increase sharply at the highest strain applied.

100 gm of ash of size between 250-355 μm was used to investigate the effect of normal stress on attrition, all other process conditions being held constant. The results are shown in Table 5.1.2 and in Fig.5.1.2. Increasing normal stress produces an increasing amount of fines, and a sharp increase of fines is noted at the highest stress applied (165 kN/m^2). The results are systematic throughout the distributions at the different stresses.

Tests were also carried out to determine the effect of segregation, if any, on attrition. 100 gm of sample size between 250-355 μm was attrited for two, five and twenty-five revolutions of the cell under standard experimental conditions. The first run in each pair of runs was carried out with the cell is the customary upright position, and the second run was effected with the cell being inverted after each revolution. Results, tabulated in Table 5.1.3, show that the two distributions at each shear strain do not differ significantly and it was concluded that segregation, if it did occur, did not affect the attrition of heavy ash under the experimental conditions tested.

Torque (Nm)	
Av	Max
33.9	36.2
33.9	36.2
33.9	36.2
33.9	36.2
33.9	36.2
33.9	36.2
33.9	36.2
33.9	36.2
38.4	49.7
38.4	49.7

Number of Revs (Initial Weight)	Particle Size Distribution (gm)					Normal Stress kN/m^2
	<45 μm	45-90 μm	90-180 μm	180-250 μm	>250 μm	
1 (100 gm)	0.5	0.6	1.1	18.8	79.0	41.4
	0.5	0.6	1.1	18.6	79.2	
2 (100 gm)	0.7	0.8	1.5	19.0	77.7	41.4
	0.7	0.8	1.4	18.9	77.9	
5 (100 gm)	1.3	1.5	2.4	19.7	74.9	41.4
	1.3	1.5	2.3	19.5	75.2	
10 (100 gm)	1.6	2.3	3.3	19.5	72.8	41.4
	1.6	2.4	3.4	19.2	72.7	
25 (100 gm)	4.5	3.2	4.8	20.0	67.1	41.4
	4.4	3.1	4.9	20.1	67.3	

TABLE 5.1.1 Soda Ash (250 μm - 355 μm) - Variation of Shear Strain

Cell Speed - 5 rpm
Sample Thickness - 10.7 mm
Shear Strain - 41.4 per revolution
Sieve Shaker - 5 mins.

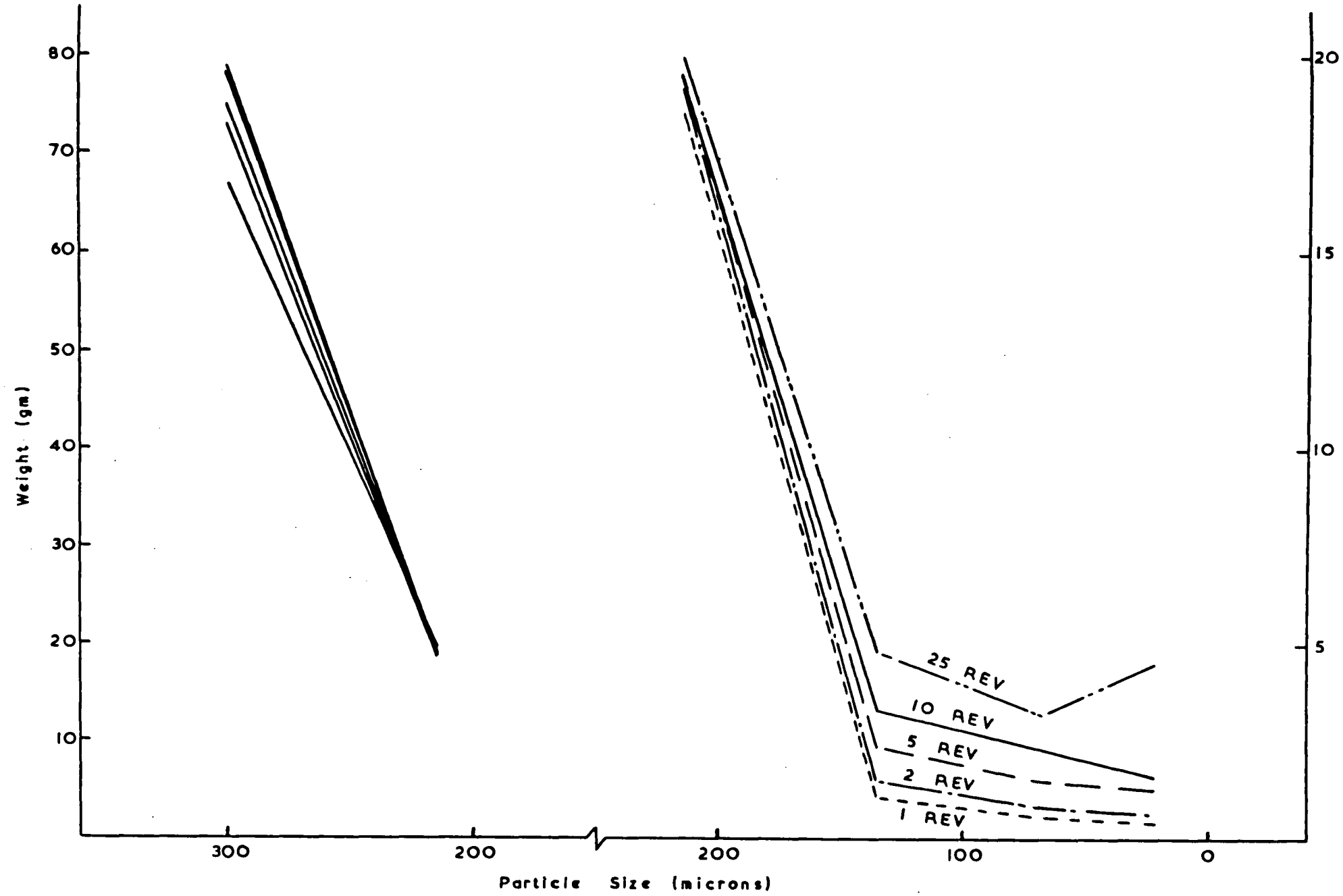


Fig. 5.1.1 Particle Size Distribution of Soda Ash (250–355 μm) Size. Effect of Strain on Attrition

Soda Ash — Mean size 300 μm
Sample weight — 100 gm
Sample thickness — 10·7 mm
Shear strain — 41·4 per revolution
Normal stress — 41·4 kN/m^2

Torque (Nm)		Number of Runs (Initial Weight)	Particle Size Distribution (gm)					Normal Stress kN/m²
Av	Max		<45 μm	45-90 μm	90-180 μm	180-250 μm	>250 μm	
33.9	36.2	1 (100 gm)	0.5	0.6	1.1	18.7	79.1	41.4
38.4	52.0	1 (100 gm)	0.8	0.9	1.4	19.1	77.9	82.8
38.4	40.0	1 (100 gm)	2.2	1.9	1.8	19.3	74.6	165.0

TABLE 5.1.2 Soda Ash (250 μm - 355 μm) - Variation of Normal Stress

Cell Speed - 5 rpm
Sample Thickness - 10.7 mm
Shear Strain - 41.4 per revolution
Sieve Shaker - 5 mins.

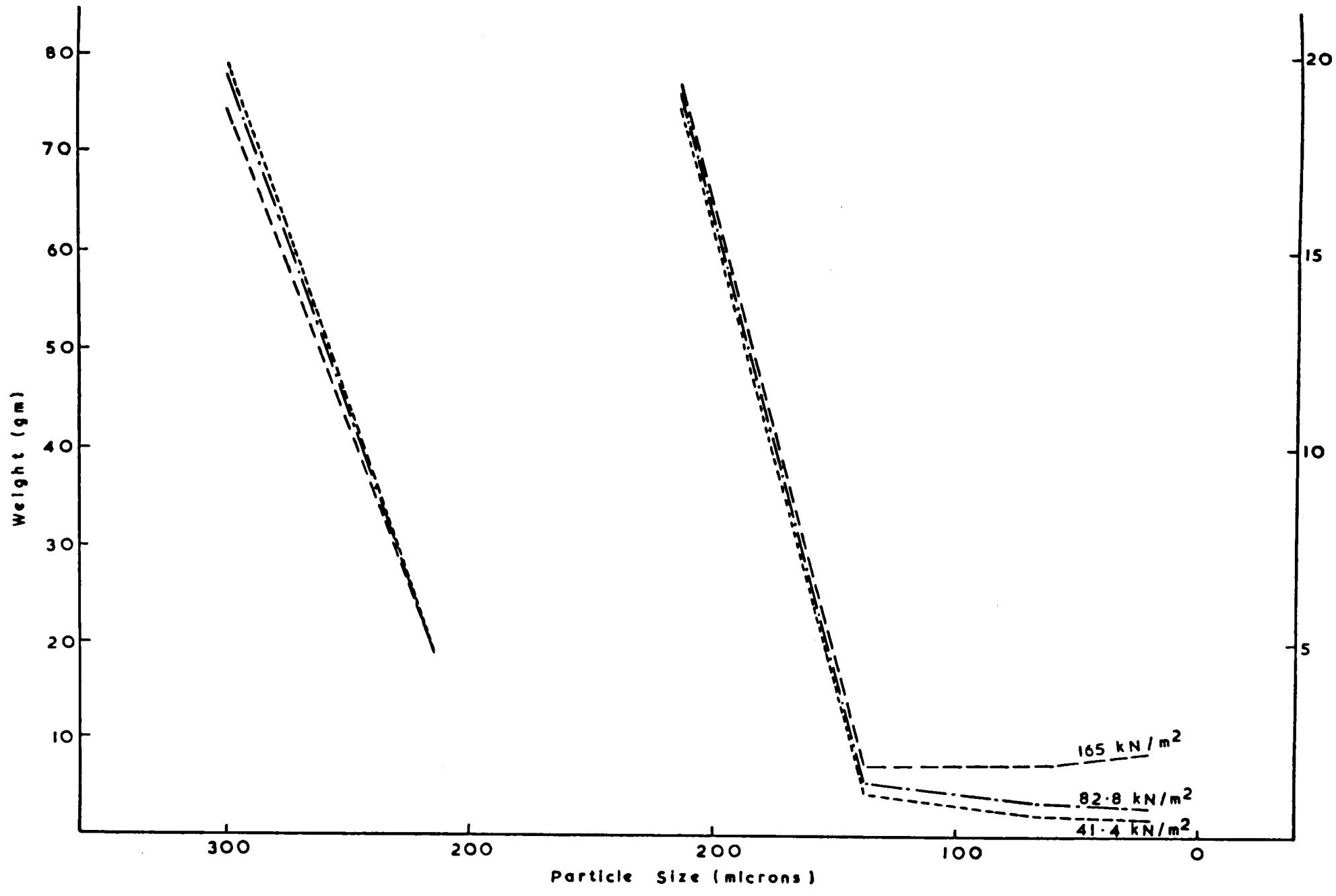


Fig. 5.1.2. Particle Size Distribution of Soda Ash (250–355 μm) Size
Effect of Normal Stess on Attrition

Soda Ash – Mean size 300μm — Sample weight – 100 gm

Sample thickness – 10·7 mm — Shear stress – 41·4 per revolution

No. of revolutions — 1

Torque (Nm)		No. of Runs (Initial Weight)	Particle Size Distribution (gm)					Mode of Operation
Av	Max		<45 μm	45-90 μm	90-180 μm	180-250 μm	>250 μm	
33.9	36.2	2 (100 gm)	0.7	0.8	1.6	18.8	79.0	N
33.9	36.2		0.7	0.8	1.5	18.9	77.8	I
33.9	36.2	5 (100 gm)	1.3	1.5	2.4	19.7	74.9	N
33.9	36.2		1.2	1.5	2.2	19.8	75.0	I
38.4	49.7	25 (100 gm)	4.5	3.2	4.8	20.0	67.1	N
38.4	49.7		4.3	3.0	5.0	20.1	67.3	I

TABLE 5.1.3 Soda Ash (250 μm - 355 μm) Effect of Segregation

Cell Speed - 5 rpm
Normal Stress - 41.4 kN/m²
Sample Thickness - 10.7 mm
Shear Strain - 41.4 per revolution
Sieve Shaker- 5 mins.

N - Normal operation of cell
I - Cell inverted at the end of each revolution

Different weights of sample were subjected to the standard experimental conditions where the ratio of cell speed to sample weight was held constant maintaining the energy input per unit mass of material. A ratio of 10:1 of sample weight to cell revolutions was chosen for experimental purposes and the resultant particle size distributions shown in Fig.5.1.4. The graph shows that fine material behaviour is fairly systematic, but the coarse end exhibits wide scatter. If the same results are re-plotted as a weight percentage in each sieve fraction, then a much more normalised distribution is obtained (Fig. 5.1.5). Normalisation of the fine end of the distribution is not improved greatly but for the coarse end it is much more evident. It is also noted that the three smallest weights exhibit a greater normalisation. The two largest weights show some scatter at the 215 μm sieve cut. This is probably due to the failure zone depth being exceeded by the powder sample, as a 100 gm sample weight corresponds to approximately thirty particle diameters. It is also seen that attrition due to crushing which took place in other materials at the smallest sample weights is not seen here, probably because the small initial size of ash produces an adequate thickness of sample for true particle to particle grinding to take place. Thus, it is seen that for sample thicknesses which lie within the failure zone, true particle to particle grinding takes place as seen by the normalised particle size distributions produced.

5.1.1 Correction of Data

All the previous experiments on soda ash were carried out using initial material of the required sieve-cut (250-355 μm) which was normally isolated by hand-sieving bulk ash. It was noticed that

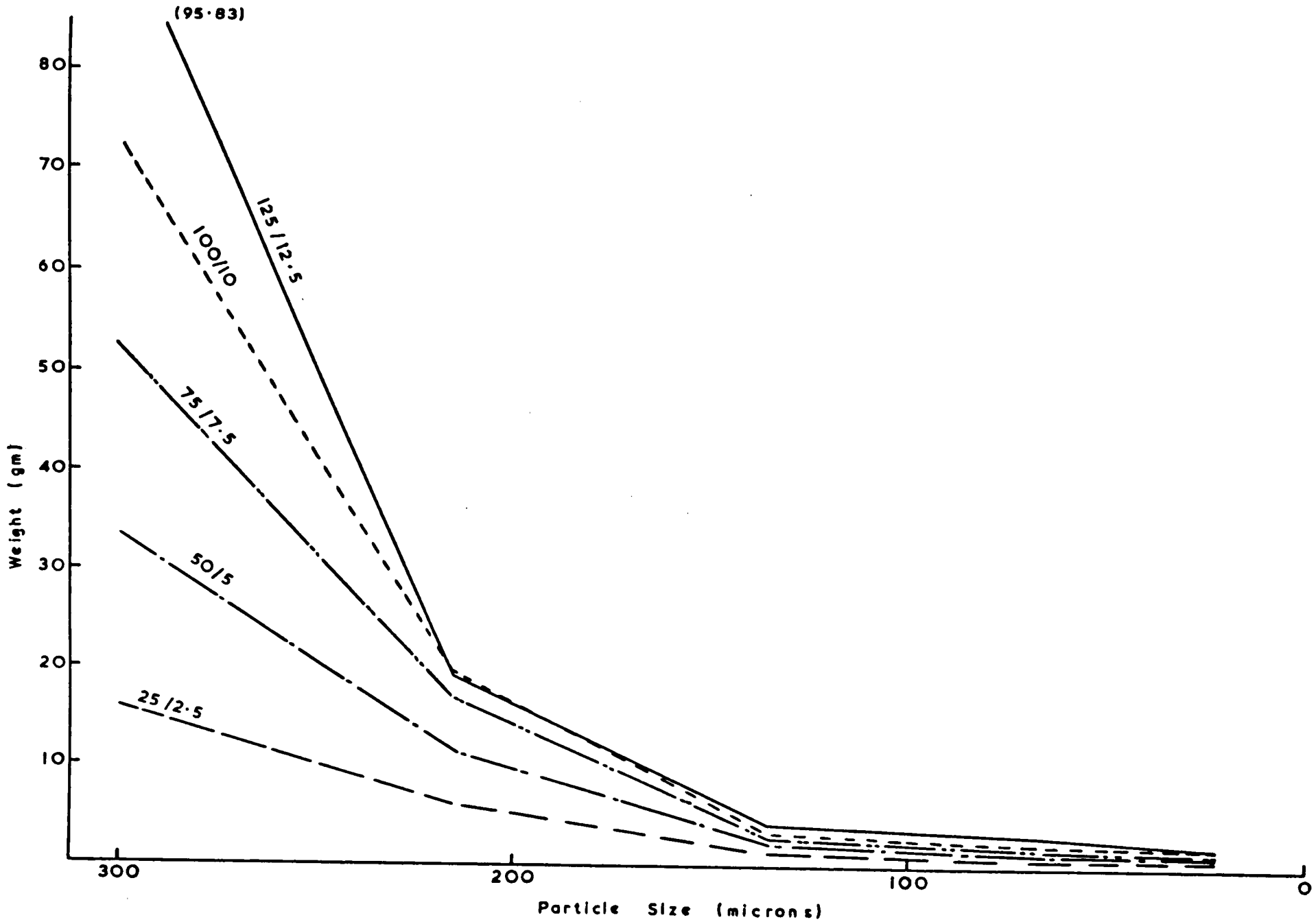


Fig. 5.1.4 Particle Size Distribution of Sodium Carbonate
Effect of constant sample wt/cell rev. ratio (10/1) on Attrition (wt)

Soda Ash — Mean size 300 μm
Pressure — 41 4 kN/m²
Cell speed — 5 r.p.m.
Sieving — 5 mins

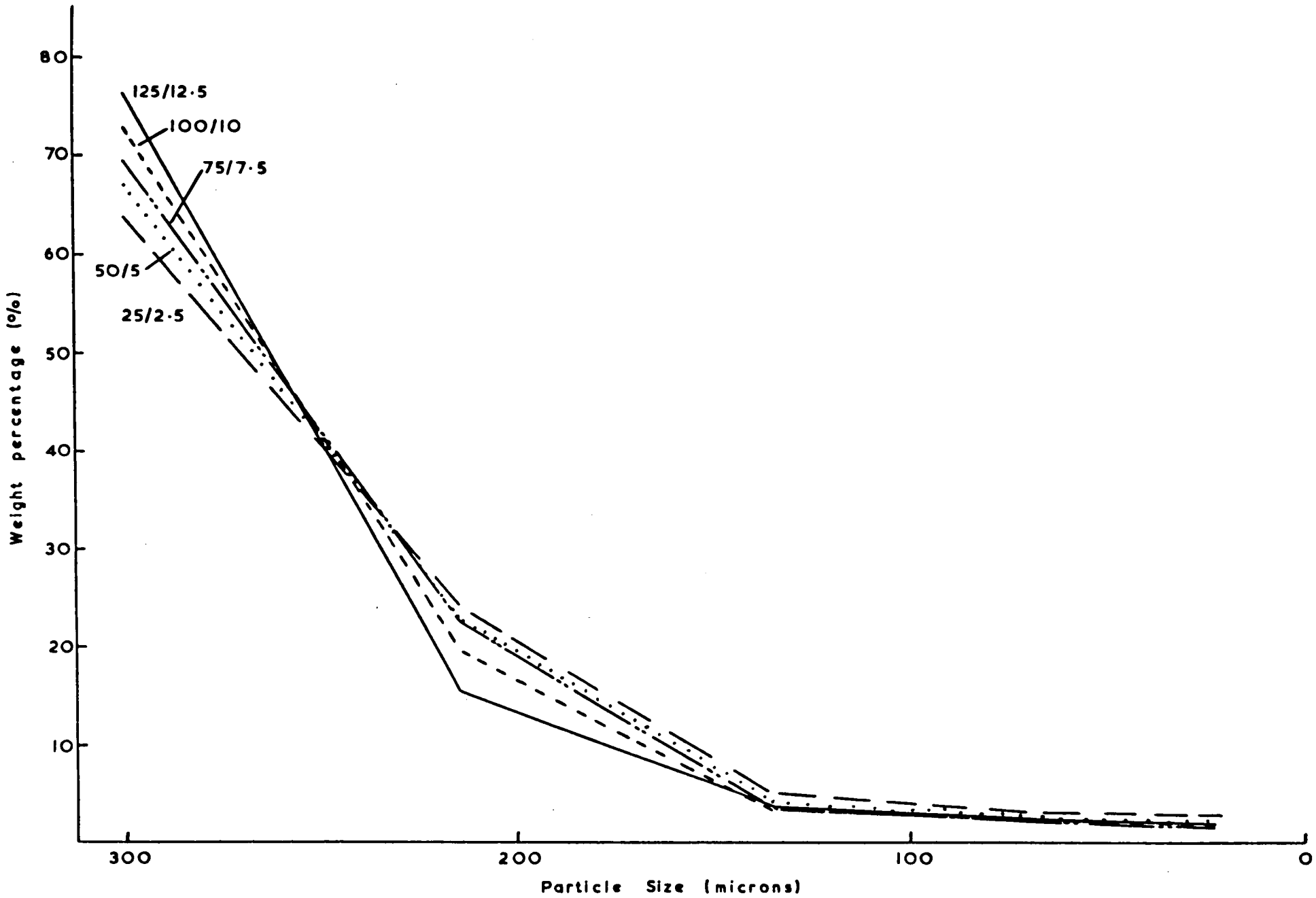


Fig. 5.1.5 Particle Size Distribution of Sodium Carbonate
Effect of constant sample wt/cell rev. ratio (10/1) on Attrition (wt%)

Soda Ash – Mean size 300 μm
Pressure – 41·4kN/m²
Cell speed – 5r.p.m.
Sieving – 5mins

when this material was machine-sieved on the sieve shaker, particles continued to pass through the 250 μm sieve which meant that the initial material contained particles which were smaller than the specified sieve range. This was probably due to the elongated shape of the particles which, when sieved in bulk, may have approached the mesh sideways and not passed through the top sieve. The material passing through was found to be mainly in the 180-250 μm sieve cut. Table 5.1.6 shows the different weights of material passing through the top sieve when 100 gm of hand-sieved ash was machine-sieved on the sieve shaker for 5-3600 seconds. These results were first used to determine the end-point for sieving by plotting them according to Whitby (1958). Fig. 5.1.6 shows that an end-point of approximately 4.5 minutes is obtained. Table 5.1.6 shows that at the standard sieving time of five minutes, 16.5 gm of material passed through the top sieve and it is seen later that these values were used to correct the particle size distributions obtained when hand-sieved ash was attrited.

When 100 gm of bulk ash was mechanically sieved for one hour on the sieve shaker, particles were still observed to pass through the top sieve. However, the percentage passing through the 250 μm sieve after five minutes of machine sieving was less than 0.5% of the charge which was corroboration that the end point had been reached (BS 410, 1976). As a result, it was decided to machine-sieve 100 gm of bulk ash for five minutes on the sieve shaker and to use this as the standard starting material for all future experiments.

100 gm of machine sieved ash was then attrited for up to ten revolutions of the cell under standard experimental conditions.

Time of Sieving (Secs)	Particle Size Distribution (gm)					Sample Weight (gms)
	<45 µm	45-90 µm	90-180 µm	180-250 µm	>250 µm	
5	← 2.5 →				97.5	100
10	← 3.2 →				96.7	100
20	← 5.0 →				94.9	100
40	← 7.3 →				92.7	100
75	← 9.2 →				90.7	100
150	← 12.0 →				88.0	100
300	-	-	0.2	16.3	83.5	100
600	-	-	0.2	17.5	82.5	100
900	-	-	0.2	18.4	81.4	100
1800	-	-	0.2	21.5	78.2	100
3600	-	-	0.3	22.8	76.8	100

TABLE 5.1.6 Soda Ash Hand-Sieved Starting Material sieved on the Sieve Shaker

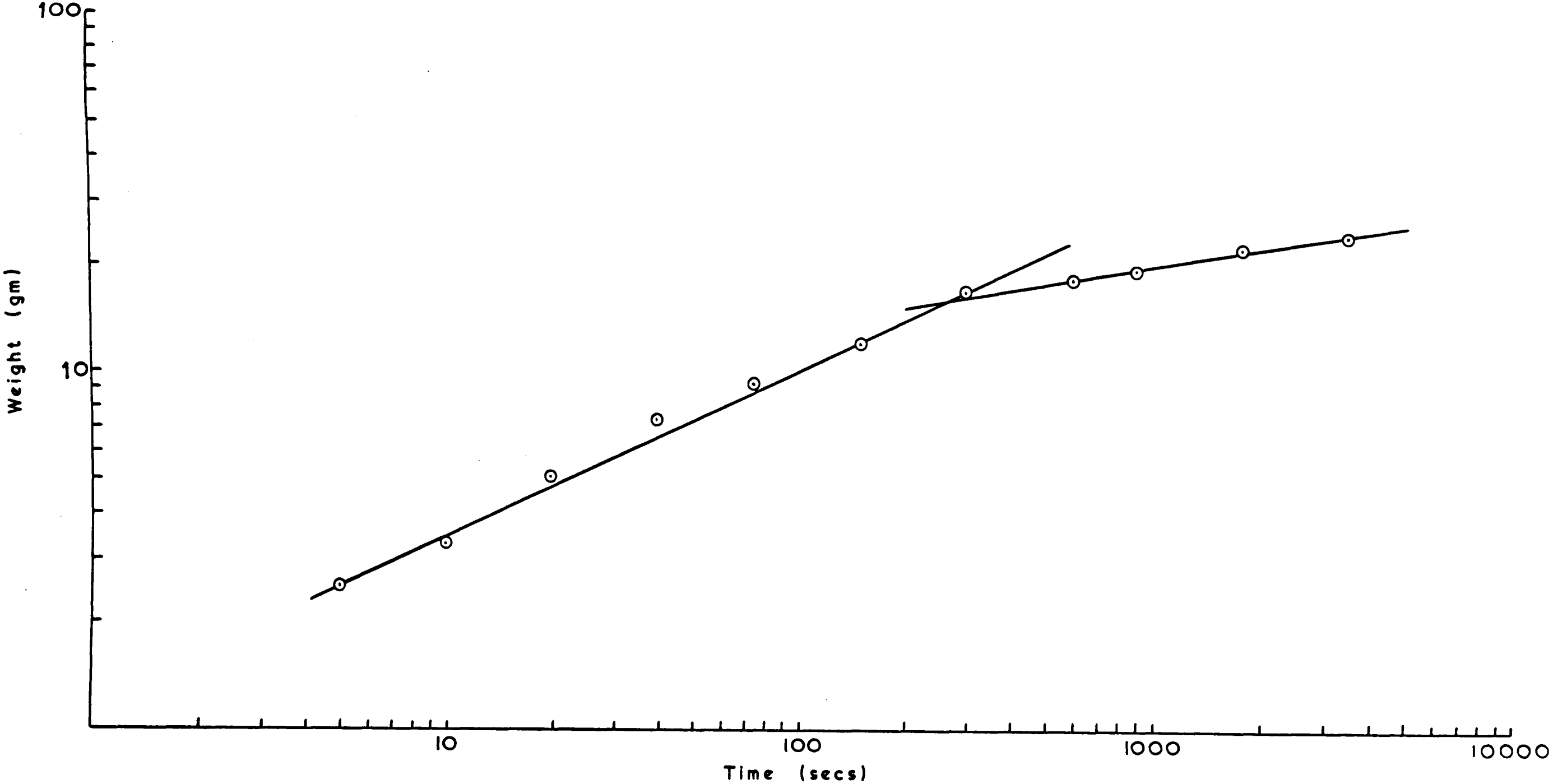


Fig. 5.1.6 Variation of Sieving times — Hand-Sieved material on Sieve Shaker

The attrited material was then sieved for 5-3600 seconds on the sieve shaker and the resultant particle size distributions presented in Table 5.1.7 - 5.1.10. These values were first used to establish the end-point for sieving by plotting them according to Whitby (1958). These results are shown in Figs. 5.1.7 - 5.1.10 and it is seen that a clearly defined end-point is not obtained using this method.

Using the data presented in the above Tables, Gwyn plots were drawn for the following sieving times: 5, 10, 15, 30 and 60 minutes. Regression analysis was then carried out on each Gwyn plot at the different sieving times and the summary of results presented in Table 5.1.11. It can be seen that the values of the gradients (0.26 - 0.33) and intercepts (0.33 - 0.64) vary. For the standard sieving time of five minutes, a gradient of 0.3 and intercept of 0.33 was obtained.

To determine the effect of sample preparation on the attrition of soda ash, data obtained by attriting hand-sieved initial material (Table 5.1.1) was plotted according to Gwyn. Results at various normal stresses are shown in Fig. 5.1.12 and a summary of the regression analysis presented in Table 5.1.12. It is seen that a gradient of 0.14 and intercept of 1.1 is obtained, which is quite different to the values obtained for the machine-sieved case (gradient 0.3, intercept 0.33). The differences exist due to the smaller particles present in the initial sieve-cut of the hand-sieved material passing through the top sieve during sieving, thereby creating a greater amount of fines than actually caused by attrition.

Time of Sieving (Secs)	Particle Size Distribution (gm)					Number of Revs. (Initial Weight)
	<45 μm	45-90 μm	90-180 μm	180-250 μm	>250 μm	
5	← 2.4 →				97.6	1 (100 gm)
10	← 2.5 →				97.4	1 (100 gm)
20	← 3.0 →				96.9	1 (100 gm)
40	← 3.8 →				96.2	1 (100 gm)
75	← 4.4 →				95.5	1 (100 gm)
150	← 5.6 →				94.4	1 (100 gm)
300	0.3	0.5	0.7	5.6	92.9	1 (100 gm)
600	0.3	0.4	0.7	7.1	91.4	1 (100 gm)
900	0.3	0.4	0.7	7.3	91.1	1 (100 gm)
1800	0.3	0.4	0.7	8.7	89.7	1 (100 gm)
3600	0.3	0.4	0.7	9.9	88.4	1 (100 gm)

TABLE 5.1.7 Soda Ash Variation of Sieving Times of Attrited Material after 1 Revolution of the Cell

Time of Sieving (Secs)	Particle Size Distribution (gm)					Number of Revs (Initial Weight)
	<45 µm	45-90 µm	90-180 µm	180-250 µm	>250 µm	
5	← 3.3 →				96.6	2 (100 gm)
10	← 3.5 →				96.4	2 (100 gm)
20	← 4.2 →				95.7	2 (100 gm)
40	← 5.0 →				95.0	2 (100 gm)
75	← 6.5 →				93.5	2 (100 gm)
150	← 7.0 →				93.0	2 (100 gm)
300	0.6	0.7	1.0	5.7	92.0	2 (100 gm)
600	0.6	0.7	1.0	7.2	90.5	2 (100 gm)
900	0.6	0.6	1.0	7.5	90.2	2 (100 gm)
1800	0.5	0.7	1.0	9.0	88.5	2 (100 gm)
3600	0.5	0.6	1.0	11.7	85.9	2 (100 gm)

TABLE 5.1.8 Soda Ash Variation of Sieving Times of Attrited Material after 2 Revolutions of the Cell

Time of Sieving (Secs)	Particle Size Distribution (gm)					Number of Revs. (Initial Weight)
	<45 µm	45-90 µm	90-180 µm	180-250 µm	>250 µm	
5	←	5.4	→		94.6	5 (100 gm)
10	←	6.1	→		93.9	5 (100 gm)
20	←	7.0	→		92.9	5 (100 gm)
40	←	7.6	→		92.4	5 (100 gm)
75	←	8.1	→		91.8	5 (100 gm)
150	←	9.6	→		90.3	5 (100 gm)
300	1.0	1.4	2.1	6.6	88.8	5 (100 gm)
600	1.2	1.3	2.0	7.8	87.5	5 (100 gm)
900	1.1	1.4	2.0	10.7	84.6	5 (100 gm)
1800	1.2	1.3	2.0	11.4	83.9	5 (100 gm)
3600	1.1	1.4	2.0	12.1	83.0	5 (100 gm)

TABLE 5.1.9 Soda Ash Variation of Sieving Times of Attrited Material after 5 Revolutions of the Cell

Time of Sieving (Secs)	Particle Size Distribution (gm)					Number of Revs. (Initial Weight)
	<45 μm	45-90 μm	90-180 μm	180-250 μm	>250 μm	
5	←	7.6	→		92.3	10 (100 gm)
10	←	8.8	→		91.1	10 (100 gm)
20	←	9.7	→		90.2	10 (100 gm)
40	←	10.8	→		89.2	10 (100 gm)
75	←	12.5	→		87.4	10 (100 gm)
150	←	12.8	→		87.2	10 (100 gm)
300	1.8	2.1	3.2	6.7	85.9	10 (100 gm)
600	2.0	2.1	3.1	8.7	83.9	10 (100 gm)
900	1.9	2.2	3.0	10.1	82.3	10 (100 gm)
1800	2.1	2.1	3.0	12.8	79.6	10 (100 gm)
3600	2.1	2.2	2.9	13.8	78.5	10 (100 gm)

TABLE 5.1.10 Soda Ash Variation of Sieving Times of Attrited Material after 10 Revolutions of the Cell

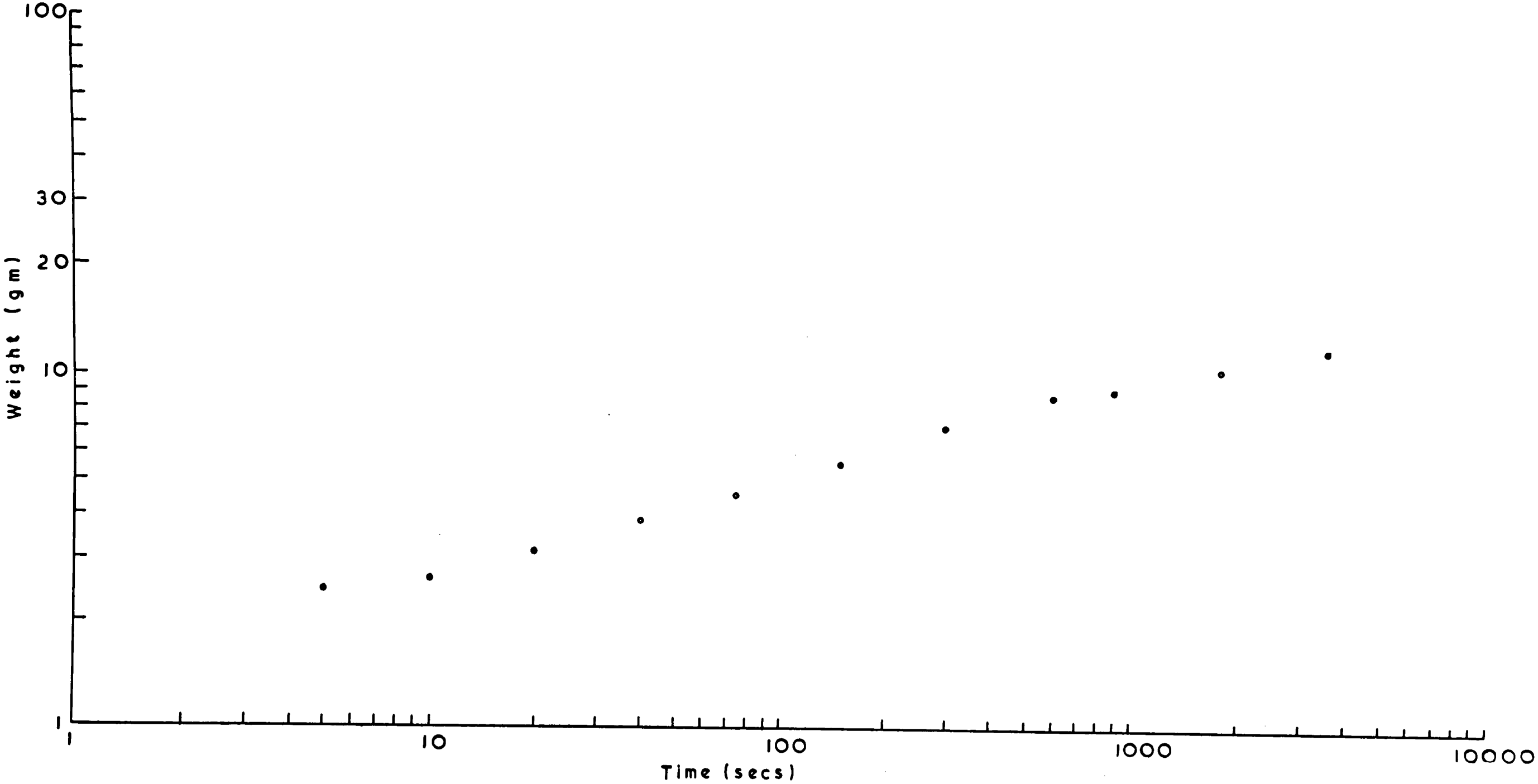


Fig. 5.1.7. Variation of Sieving times – 1 Revolution of Cell

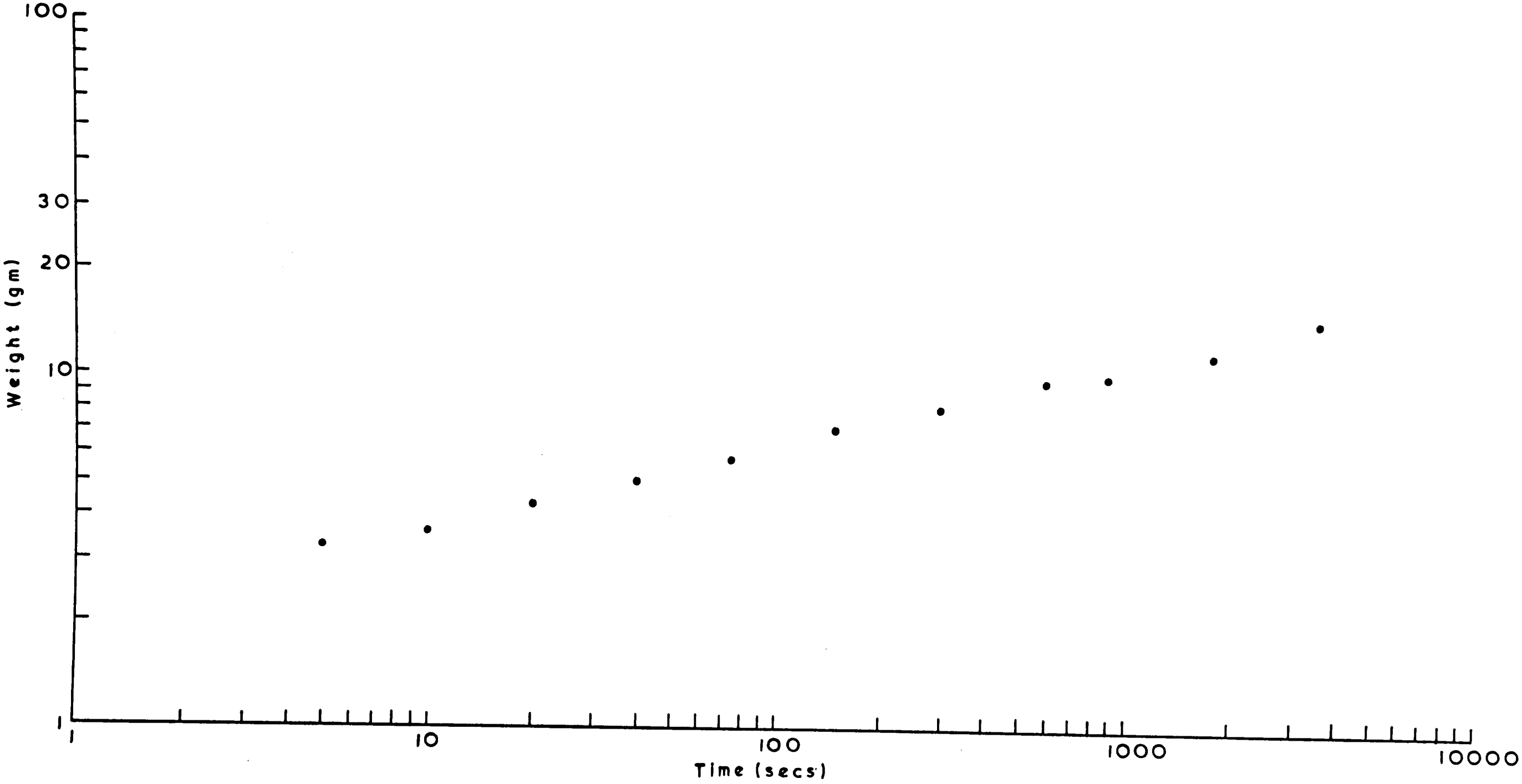


Fig. 5.1.8. Variation of Sieving times – 2 Revolutions of Cell

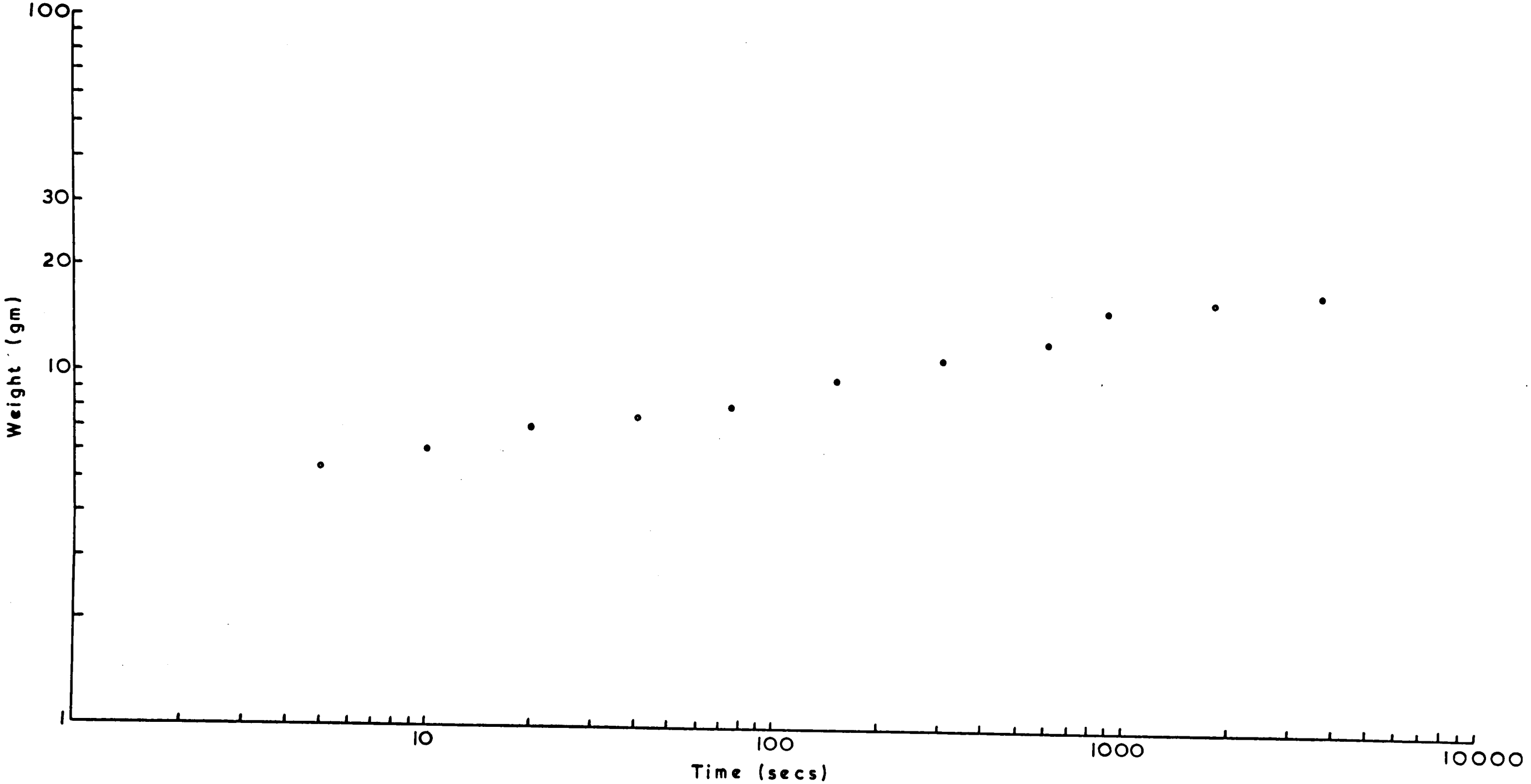


Fig. 5.1.9 Variation of Sieving times — 5 Revolutions of Cell

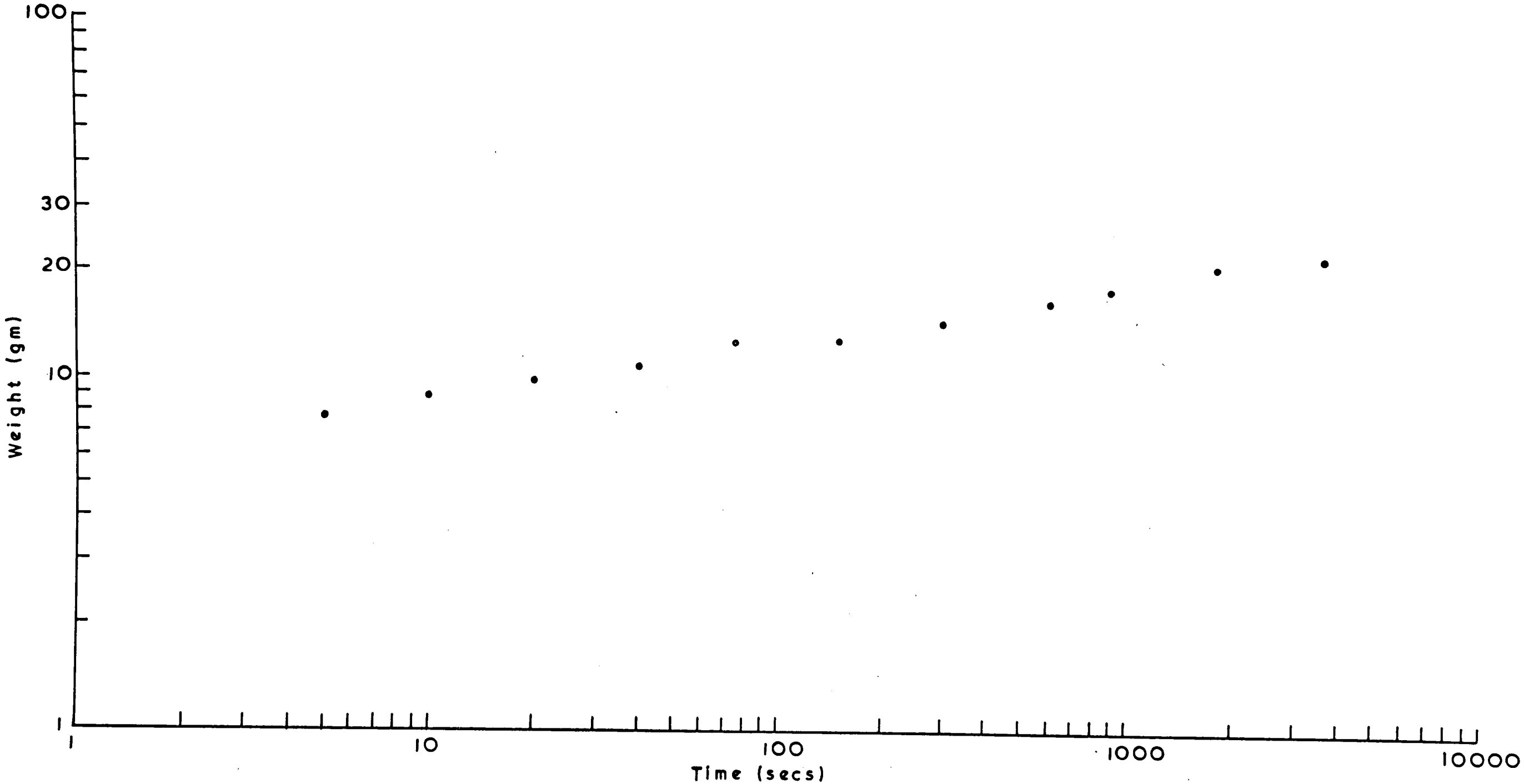


Fig. 5.1.10. Variation of Sieving times – 10 Revolutions of Cell

Sieving Time (Mins)	Gradient	Standard Error of Gradient	Intercept	Standard Error of Intercept	Correlation Coefficient (%)	F Value
5	0.31	0.03	0.33	0.06	99.2	121
10	0.28	0.03	0.47	0.06	98.7	76
15	0.33	0.05	0.40	0.08	97.8	46
30	0.31	0.03	0.50	0.06	99.0	99
60	0.26	0.02	0.64	0.02	99.6	221

BLE 5.1.11 Soda Ash - Summary of Regression Analysis of Gwyn plots for different sieving times.

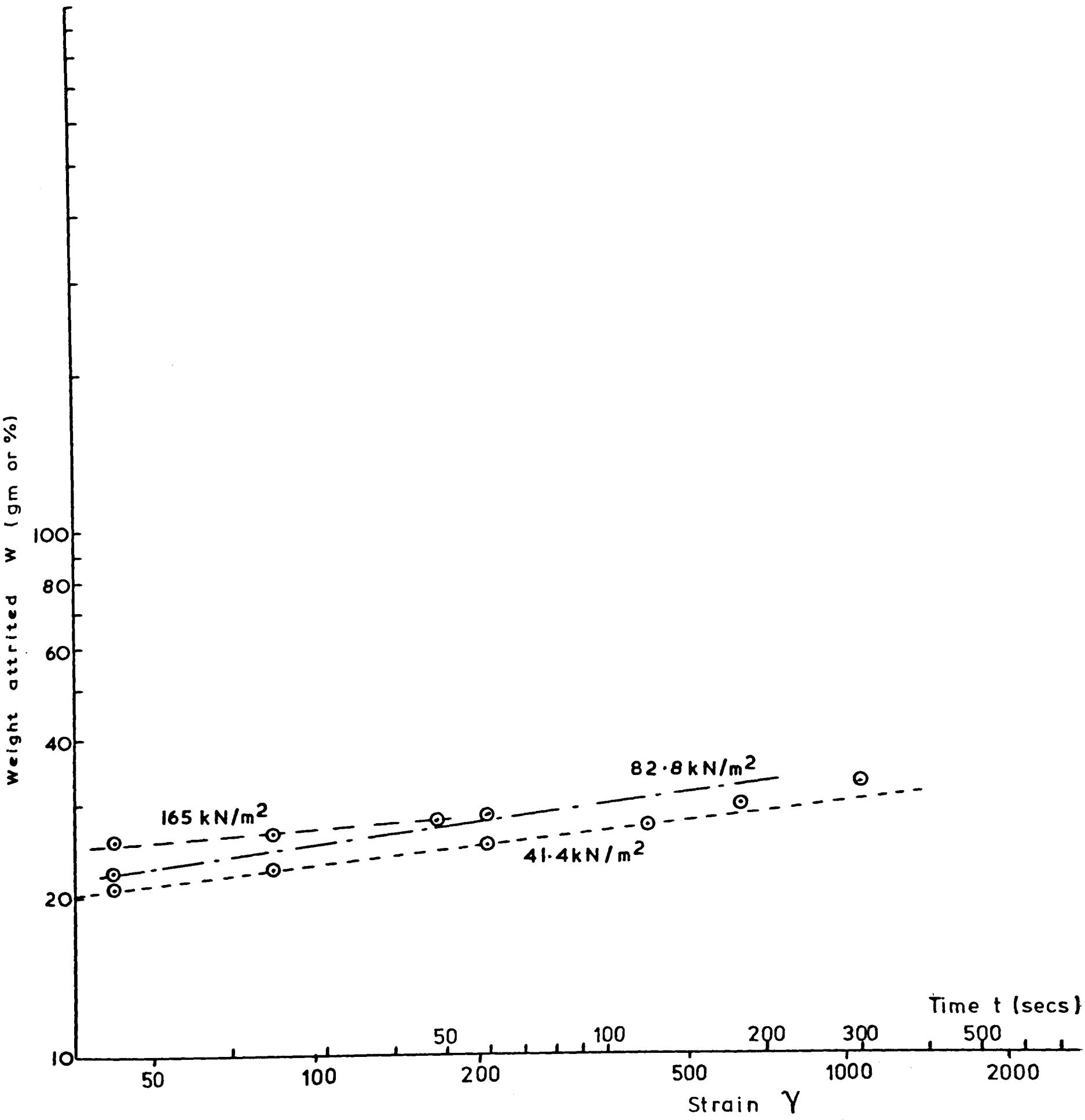


Fig. 5.1.12 **Soda ash (250–355μm) size**—Gwyn Plot

Effect of Strain on Attrition at different Normal Stresses

Cell speed – 5 r.p.m.

Sample weight – 100 gm

Sample thickness – 10·7 mm

Shear strain – 41·4 per revolution

Sieving – 5 mins

Normal Stress kN/m²	Gradient	Standard Error of Gradient	Intercept	Standard Error of Intercept	Correlation Coefficient (%)	F-Value
41.4	0.14	0.01	1.08	0.01	98.7	112
82.8	0.11	0.04	1.18	0.09	94.7	9
165	0.07	0.02	1.29	0.01	97.5	19

ABLE 5.1.12 Soda Ash - Summary of Regression Analysis of Gwyn plots using hand-sieved initial material.

In an effort to reconcile the differing values of gradients and intercepts for the two differently prepared starting materials, correction was made. It was seen earlier that when hand-sieved original material was machine-sieved, 16.5 gm of material passed through the top sieve for a sieving time of five minutes (Table 5.1.6). This figure was used to correct the particle size distribution of the hand-sieved original material on a percentage basis.

Table 5.1.13 shows a summary of the regression analysis carried out on particle size distributions obtained by attriting hand-sieved initial samples which have now been corrected using values given in Table 5.1.6 to correspond to the machine-sieved case for a sieving time of five minutes. Excellent agreement is obtained.

In view of the scatter obtained in the normalisation curve in Fig. 5.1.5 at the larger weights, it was decided to repeat the Gwyn plots at smaller initial weights of sample. 25, 50 and 75 gm of machine-sieved original material were attrited in the usual manner and the results plotted in Fig. 5.1.14. The corresponding regression coefficients are seen in Table 5.1.14 where it is interesting to note that varying sample weights did not greatly affect the gradients, although the intercepts were different.

5.2 Mechanism of Attrition

100 gm of soda ash was attrited at 41.4 kN/m² normal stress at a shear strain of 41.4 per revolution for twenty-five revolutions of the cell. The sample was then analysed using the appropriate nest of sieves. Photographs of the original material and attrited ash in each sieve-cut are shown in Figs. 5.2.1a to 5.2.1c.

Correction Basis (Sieving time-mins)	Gradient	Standard Error of Gradient	Intercept	Standard Error of Intercept	Correlation Coefficient (%)	F-Value
P(5)	0.3	0.01	0.34	0.01	99.9	1306

TABLE 5.1.13 Soda Ash - Summary of Regression Analysis of Gwyn plots for corrected hand-sieved initial material.

P - Percentage basis

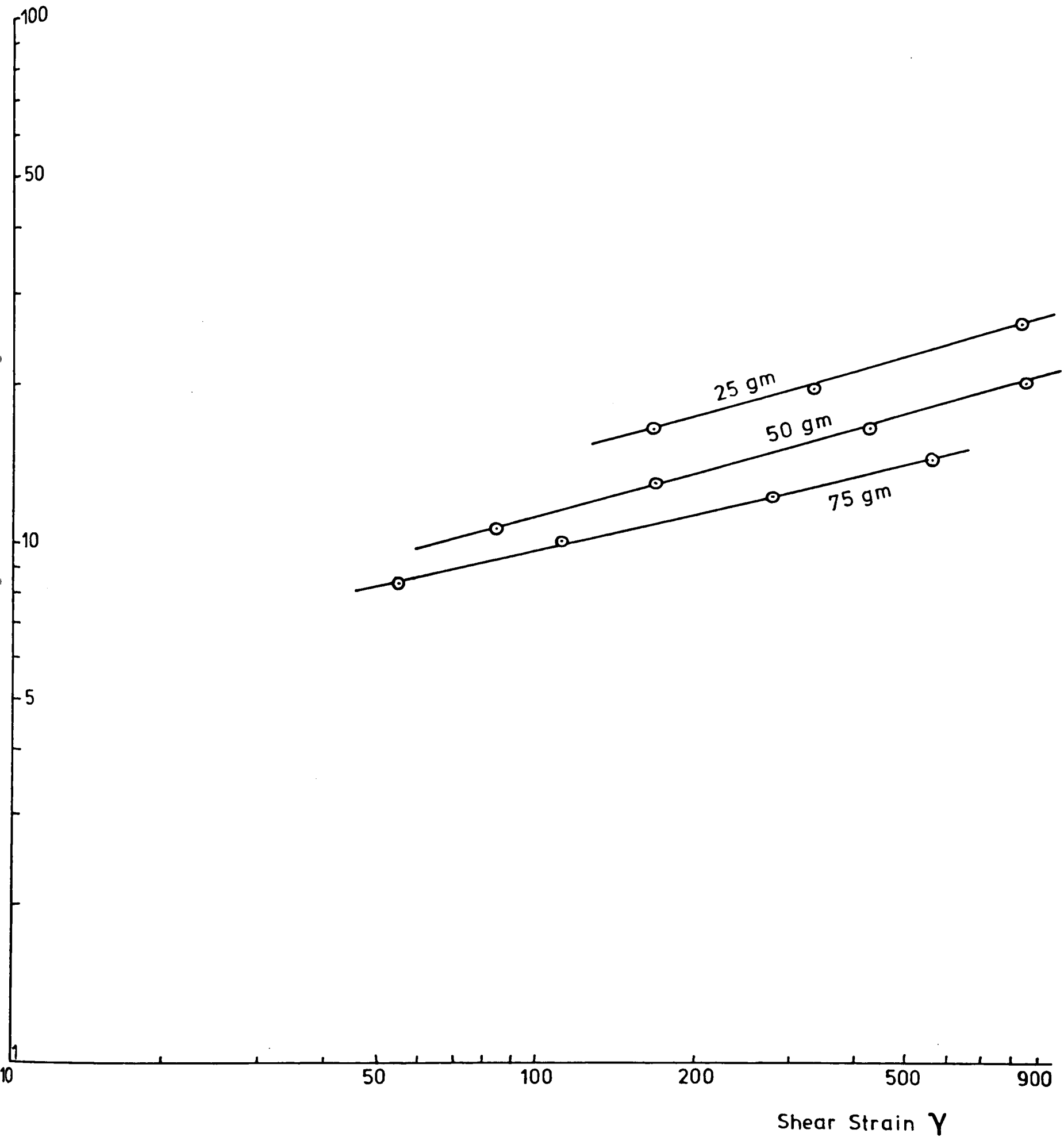


Fig. 5.1.14 Soda Ash (250–355μm) – Machine sieved starting material. Effect of Strain on Attrition at different sample weights.

Cell speed – 5 r.p.m

Normal stress – 41·4 kN m^2

Shear strain – 164, 83·5, 55·4 per revolution

Sample thickness – 2·7, 5·3, 8·0 mm

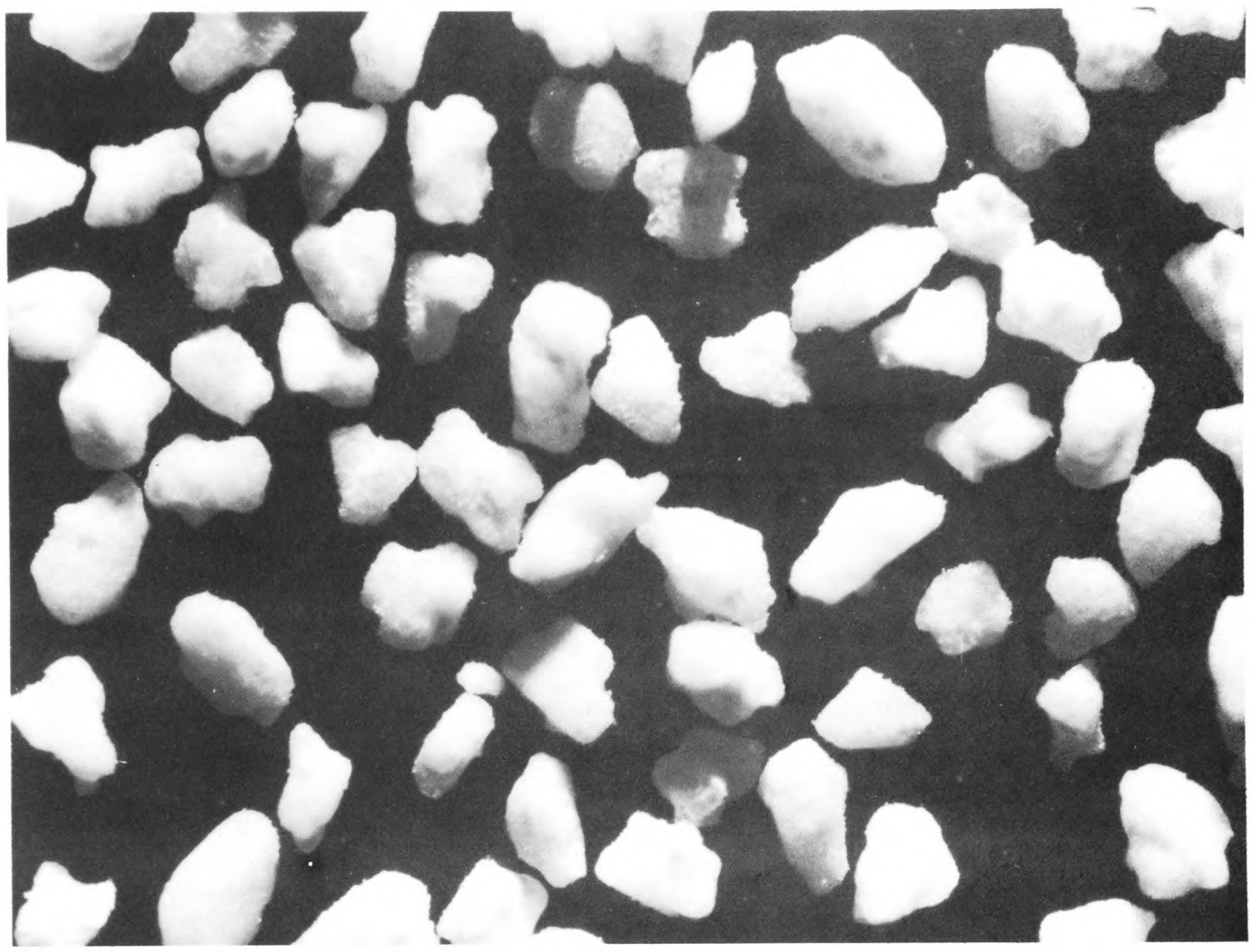
Sieving – 5 mins.

Sample Weight (gm)	Gradient	Standard Error of Gradient	Intercept	Standard Error of Intercept	Correlation Coefficient (%)	F-Value
25	0.28	0.01	0.60	0.007	99.9	587
50	0.27	0.004	0.51	0.002	99.9	4300
75	0.23	0.01	0.53	0.008	99.9	380

TABLE 5.1.14 Soda Ash - Summary of Regression Analysis for Gwyn plots at different sample weights.

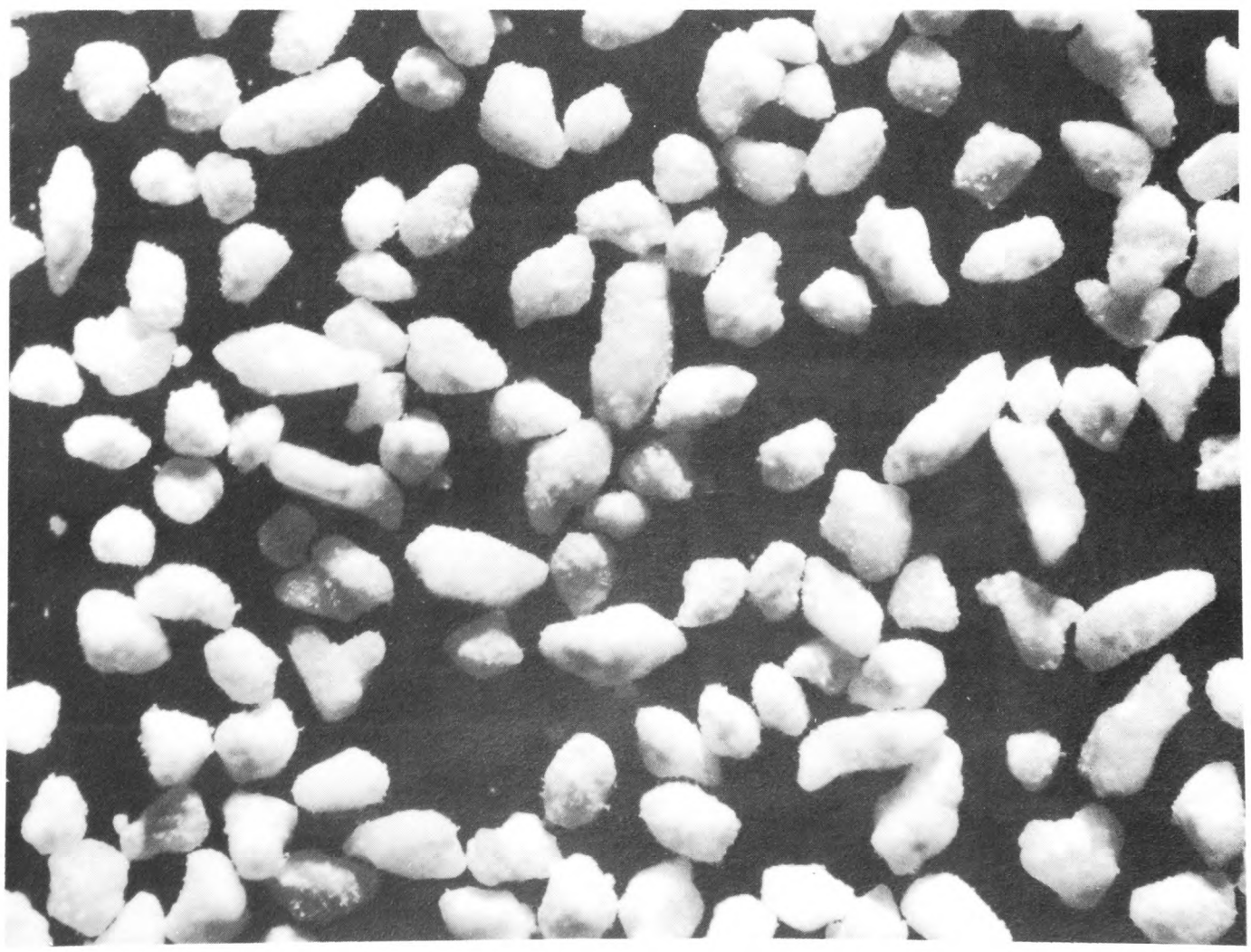
Fig. 5.2.1 Sodium Carbonate attrited at 41.4 kN/m^2 normal stress for 25 revs. Relevant sieve-cuts shown against each photograph.

(a)
250-355 μm



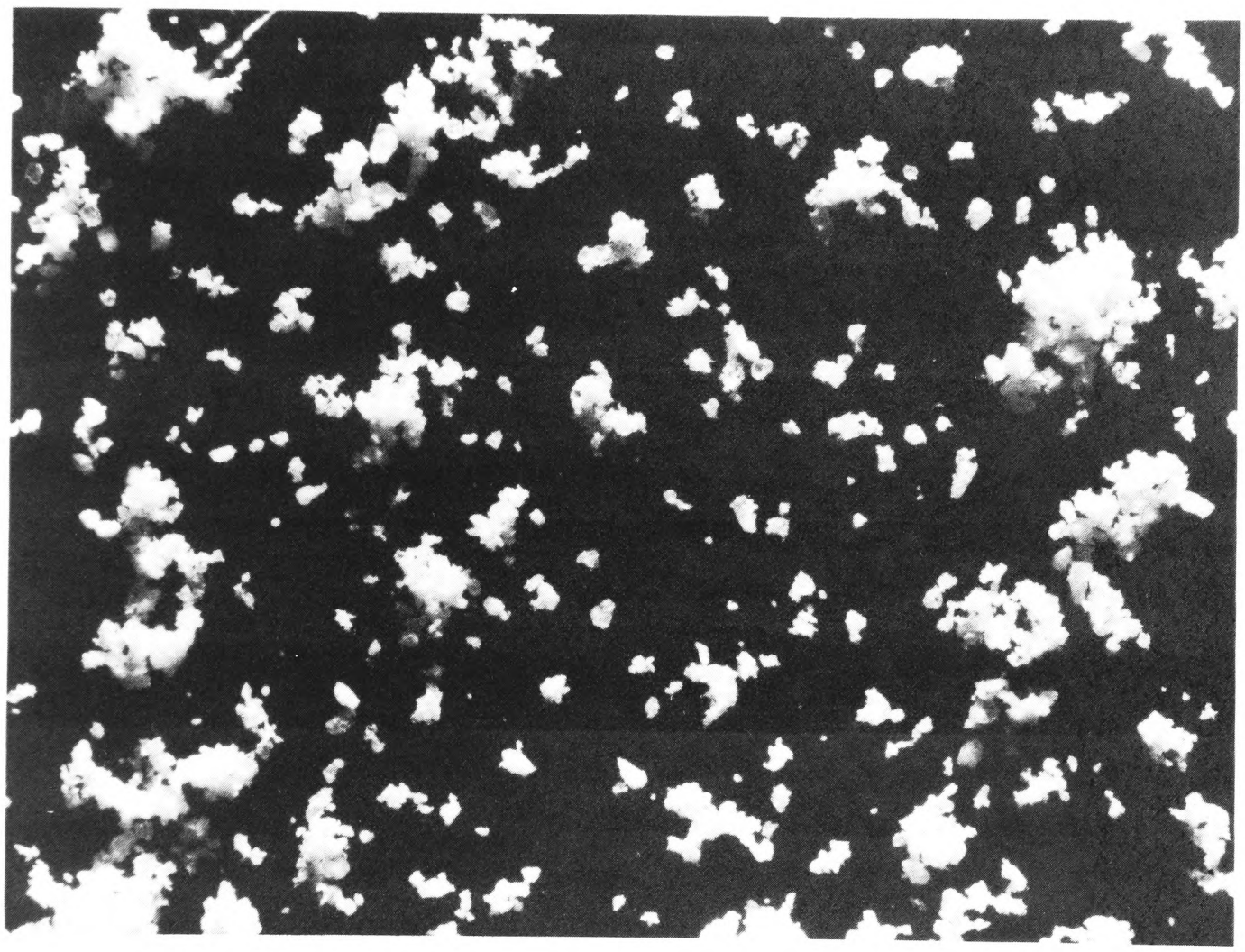
1 mm

(b)
178-250 μm



1 mm

(c)
< 63 µm



1 mm

It is seen that soda ash undergoes attrition by surface grinding. The original hexagonal material retains its basic shape even after prolonged attrition in the cell, but with its sharp edges more rounded after grinding. The fines, when analysed, were not of any particular shape and it was inferred that this material was formed by the surface erosion of parent crystals.

CHAPTER SIX

THEORY AND DISCUSSION

6.1 Summary of Results from Gwyn Plots

Three different materials were used in assessing cell performance. Various grades of some materials were also used, these differing from each other in initial shape and/or size. It was seen that attrition behaviour was very different in each case, as summarised in Table 6.1.1.

When the Gwyn coefficients are analysed, it is seen that m (gradient) varies from 0.1 to 0.6 for the various materials. Photographic evidence of attrited material shows that the increase in m corresponds to an increase of surface grinding during the attrition process. Of the materials tested, those which show surface grinding at low strain exhibit higher values of m (molecular sieve beads, granular sodium chloride), whereas materials showing surface abrasion after very high strain have relatively low values of m (PDV salt).

When the sample size of soda ash is increased from 25gm to 75gm, the value of m remains unchanged, although K_p is seen to decrease. This suggests that the rate of surface grinding of soda ash particles is independent of sample size.

The effect of increasing normal stress is seen in the case of both PDV salt and molecular sieve beads. For both materials, the intercept (K_p) is virtually unchanged whereas the gradient (m) is seen to increase with increasing stress. From this, it is inferred that increasing normal stress increases the surface grinding process for these materials.

As the weight of material ground is given by $K_p \gamma^m$ in the Gwyn formulation, when m is zero the intercept K_p is a measure of the

Material (Sieve-cut)	Stress kN/m	Gradient m	Intercept K_p	Physical Behaviour on Attrition
Soda Ash (250-355 µm) 75 gm sample	41.4	0.23	0.53	General rounding of edges
Soda Ash (250-355 µm) 50 gm sample		0.27	0.51	
Soda Ash (250-355 µm) 25 gm sample		0.28	0.60	
PDV Salt (250-355 µm)	41.4	0.10	0.57	Shattering into smaller cubes, rounding of edges at very high strains
Lab Salt (355-500 µm)	41.4	0.18	0.53	Some shattering, rounding of edges
PDV Salt (500-600 µm)	41.4	0.09	1.47	Shattering into smaller cubes, rounding of edges at very high strains
PDV Salt (500-600 µm)	82.8	0.10	1.46	
PDV Salt (500-600 µm)	165	0.15	1.38	
Granular Salt ex centrifuge (1.7-2.0mm)	41.4	0.40	0.56	Radial shattering, rounding of edges
Molecular Sieve (1.7-2.0mm)	41.4	0.43	0.25	Shelling, shattering, rounding of edges
Molecular Sieve (1.7-2.0mm)	82.8	0.51	0.21	
Molecular Sieve (1.7-2.0mm)	124	0.60	0.27	
Granular Salt ex crystalliser (1.7-2.0mm)	41.4	0.44	0.52	Radial shattering, rounding of edges

Table 6.1.1 Summary of Gwyn Coefficients for all materials tested. 100gm of sample was used unless otherwise indicated.

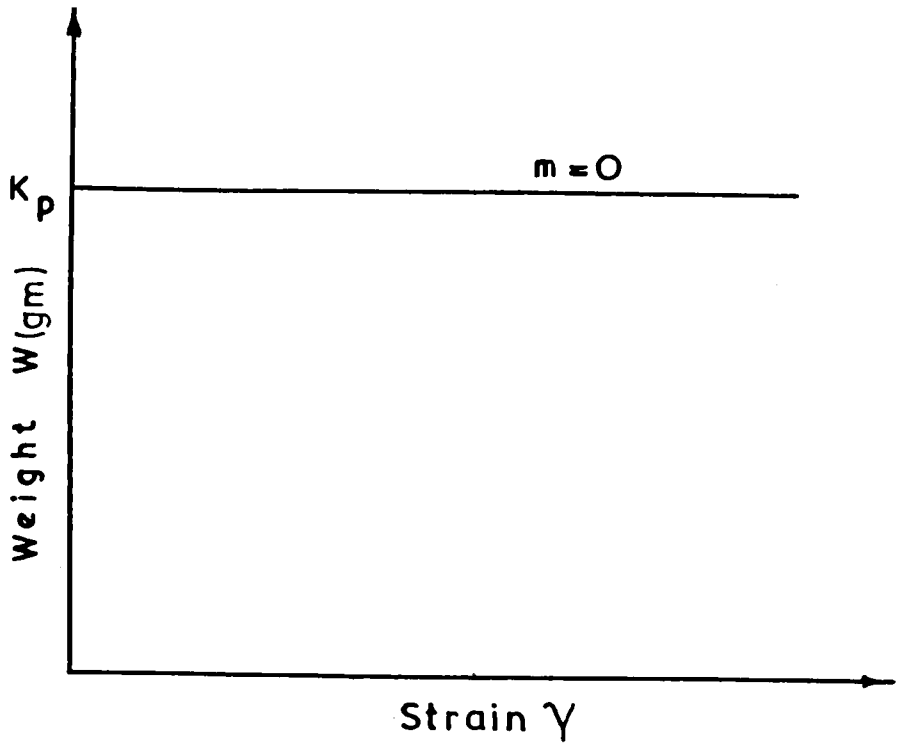
initial attrition of materials (Fig. 6.1.2). Hence, the value of K_p for PDV salt may be taken as a measure of the initial shattering process occurring during attrition. However, as m increases from zero, the dimensions of K_p vary and no significance may be attached to the values of intercept in the Gwyn plots where m is significantly greater than zero.

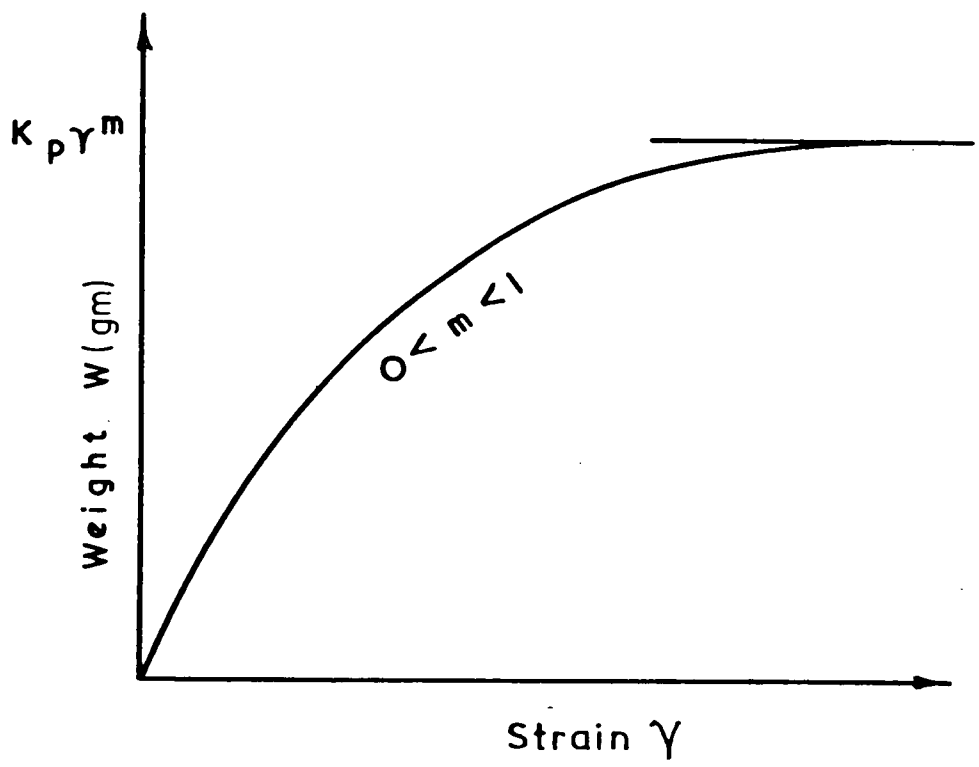
Fig. 6.1.3, following the presentation of Fig. 6.1.2, shows the relationship between m and γ where Gwyn coefficients are used to predict the weight of attrited product at strain γ. It can be seen that the relatively high values of m produce low values of K_p; the converse also happens to be true.

6.1a Effect of Sample Thickness

It is seen that when larger sample weights are used for molecular sieve and granular sodium chloride the normalisation procedure works well, but when the sample weight is small (i.e. when only a two or three particle diameter depth of material is in the cell) departure is observed. When smaller material is attrited (PDV salt), the deviations at small sample weights are not quite as pronounced but still present. Soda ash showed uniform behaviour at all sample weights used, but this is probably because the smallest weight in the cell produced more than a three particle diameter thickness of sample in the cell.

In all cases where true normalisation is observed, it may be concluded that true particle to particle grinding took place and that the results were not machine-sensitive. Thus, the velocity profile of the material would be linear and the rate of strain independent of





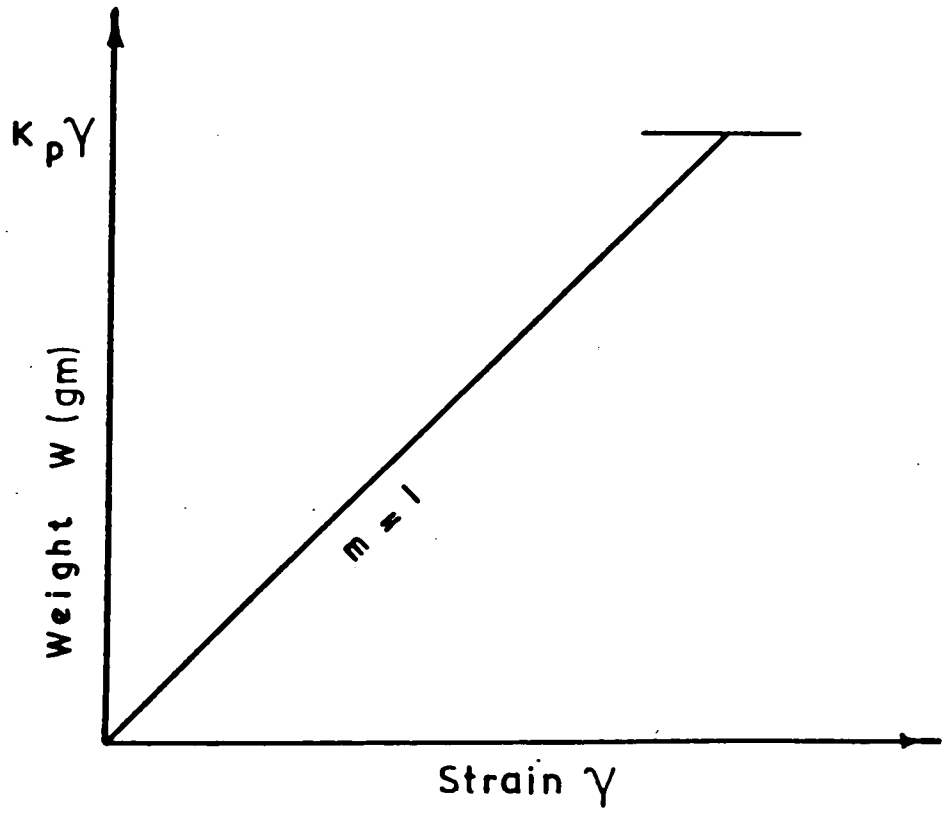


Fig. 6.1.2. Variation of m and K_p in Gwyn eauation

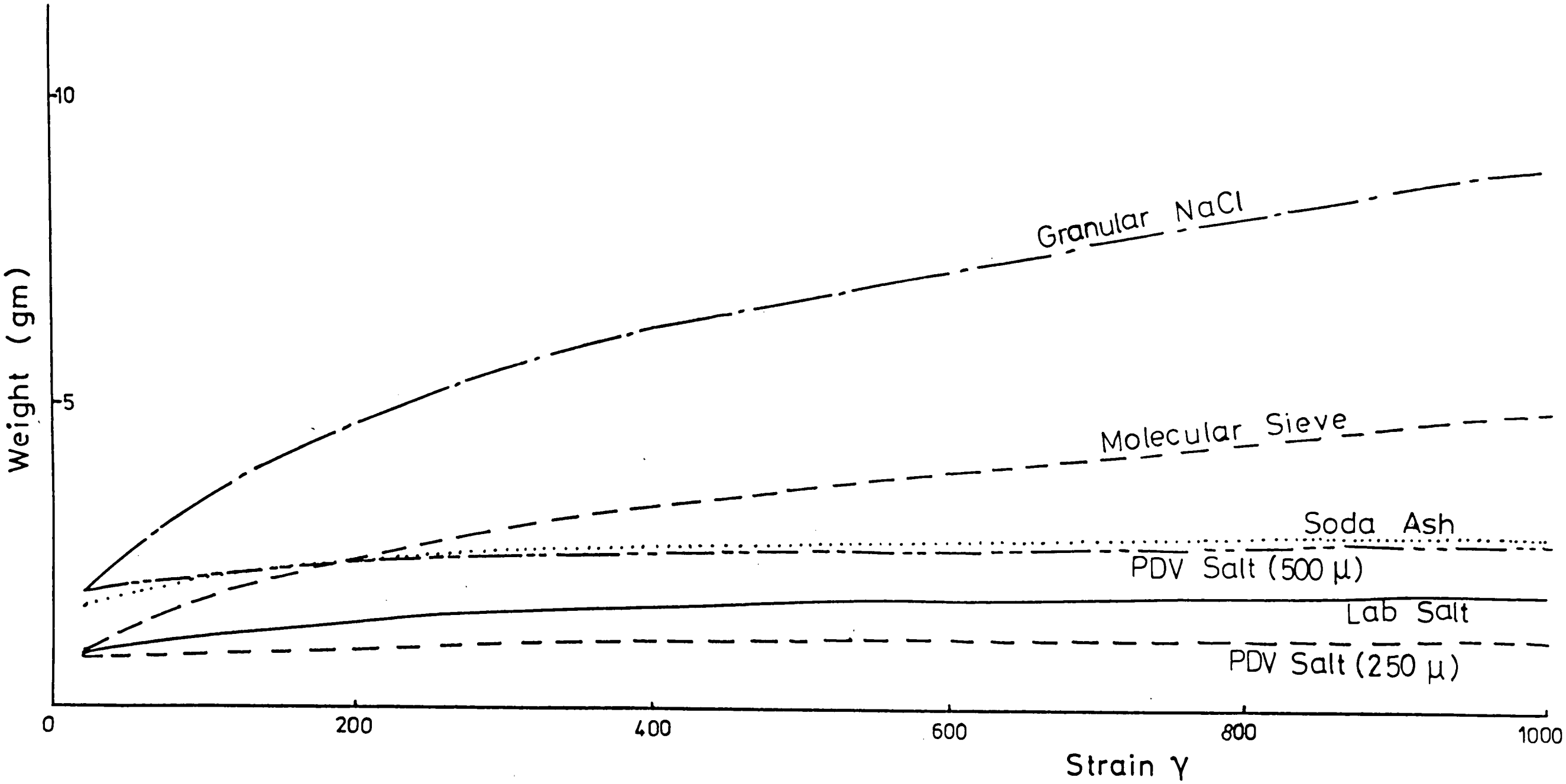


Fig.6.1.3 Predicted attrition weights using Gwyn coefficients

position provided that the sample thickness was greater than about three particle diameters and the failure zone width was not exceeded.

When particles are sheared, voids are formed and filled by particles resulting in a limited amount of vertical movement which is small when compared to the horizontal displacement. Thus, when a sufficient depth of particles is present, powder movements in both directions are possible. For example, a particle moving in the horizontal direction may have to move up and over an obstruction in its path. Stephens (1976) has shown of such movements with his tracer experiments. However, when only two or three particle layers are present in the cell, this vertical movement is severely limited by the close proximity of the gripping rings. Thus, if an obstruction is encountered by a particle as it is being sheared, it is not free to move over the obstruction and is forced to keep moving in the same horizontal direction. This would have to result in some form of catastrophic breakage (i.e. crushing or slicing of the particles) for the cell to continue its shearing motion. Thus, for very thin samples, the general normalised behaviour is not seen.

Although the failure zone depth was not experimentally determined for the smaller samples, it is reasonable to assume that, since the larger particles which were shown to be in the failure zone exhibit normalised behaviour, the smaller particles must also be within the failure zone. Since the cell was designed

to accommodate a failure zone depth of approximately twenty particle diameters, the failure zone depth would only be exceeded if a large quantity of small sized material was used in the cell.

If the sample thickness is more than three particle diameters and less than about twenty, a portion of the linear velocity profile is examined. The success of a normalised presentation is thus a corollary of a linear velocity distribution.

Some notes on cell torque and sample volume changes are presented in Appendix D.

6.2 Theory

One objective in the study of attrition of particulate solids is the development of a mathematical representation of degradation. This could improve the knowledge of the mechanisms by which solids degrade, and also aid the development of processing equipment. As attrition is very complex, an understanding of the degradation mechanisms is made easier by considering each separately.

Here, first attempts to understand the attrition process involved the formulation of simple physical models where the rates of attrition were proportioned to the surface area of the particles and applied shear strain. Attempts were also made to obtain a linear relationship between the weight attrited and the shear strain applied raised to a power, but it was not possible to devise models which described the attrition process satisfactorily.

As seen previously, particle attrition in the present work occurs mainly due to fracture or surface grinding. Even when initial attrition

takes place by fracture, it is seen that subsequent degradation may proceed by surface grinding at high strain. Thus, in practice, a combination of both mechanisms is often present when materials attrite. For theoretical studies, each attrition model has been considered in isolation. The first model deals with the fracture mechanism and the second analyses surface grinding.

6.2.1 Fracture Model (Mass Basis)

In reviewing the theoretical work carried out by early workers, Austin (1971) reports that if the fracture process was analysed statistically, a random probability for breakdown applied to a large number of particles would lead to a first order law:

$$\text{Rate of breakage of size } i = k_i \, w_i \, W$$

This states that the rate of disappearance of particles in a given small size interval due to breakage of this size is proportional to the weight of particles present. The weight of material is $W.w_i$ where W is the total weight and w_i the fractional weight of size i. If the equation is applied to the largest size interval present, then

$$\frac{dw}{dt} = k_a w_a$$

where w_a is the weight of material is the largest size interval.

$$\therefore \; 2.3 \log [w(t)/w(o)] = k_a t$$

Austin verified the first order law by grinding a single size interval in a batch base mill, sampling at various times and plotting log $[w_a(t)/w_a(o)]$ vs t to obtain a linear relationship. Further work, eg using radioactive tracer techniques, has shown that the first order breakage law is valid for all sizes in a mixture of particles. The first order kinetic approach would seem particularly appropriate to those chemicals (PDV Salt) which undergo attrition primarily due to fracture.

Thus, the attrition of particles may be modelled as a first order process, where the rate of breakage is proportional to the weight of unground material M, ie

$$\frac{dM}{d\gamma} \alpha M \qquad (6.2.1.1)$$

where γ denotes shear strain. This equation states that the probability of a particles undergoing fracture (and disappearing completely from the coarsest sieve fraction) is independent of previous strain. Applied in its simplest form, equation (6.2.1.1) gives poor agreement with data since the rate of attrition under initial strain is anomalously high. This high initial attrition rate may be due to:

(a) attached debris being swept away

(b) agglomerates separating along cleavage planes, or

(c) weak particles breaking down easily

Experiments also show that the rate of attrition decreases at high strain (granular salt - Fig.4.1.12). This may mean that certain particles are so hard that they do not attrite, but it might also be due to compaction.

These experimental observations have been used to modify equation (6.2.1.1) to obtain a more realistic representation of the process.

The following nomenclature refers to Fig. 6.2.1.

Let

m_o be the initial weight of sample to be ground

M_o be the weight of unground sample at strain $\delta\gamma$ (where $\delta\gamma \rightarrow 0$)

m_i be the weight of sample ground at strain $\delta\gamma$

m_r be the weight of sample unground at infinite strain, γ_∞

M be the weight of sample unground at any strain, γ

Then

$$\frac{dM}{d\gamma} = -k\,(M - m_r)$$

$$\frac{dM}{(M - m_r)} = -k\,d\gamma$$

Intergrating

$$\ln\,(M - m_r) = -k\gamma + C$$

Since

$M = M_o$ at $\gamma = \delta\gamma$ where $\delta\gamma \rightarrow 0$,

$$\therefore \ln\left[\frac{M - m_r}{M_o - m_r}\right] = -k\gamma$$

But $M_o = m_o - m_i$

$$\therefore \ln\left[\frac{M - m_r}{m_o - m_i - m_r}\right] = -k\gamma$$

A three-parameter model fit was obtained on the computer, by standard regression analysis, using values of M and γ obtained experimentally. Results are shown in Figs. 6.2.2 to 6.2.14. The computer model worked in stages optimising the values of m_r and m_i in turn. A flow diagram is presented in Appendix E.

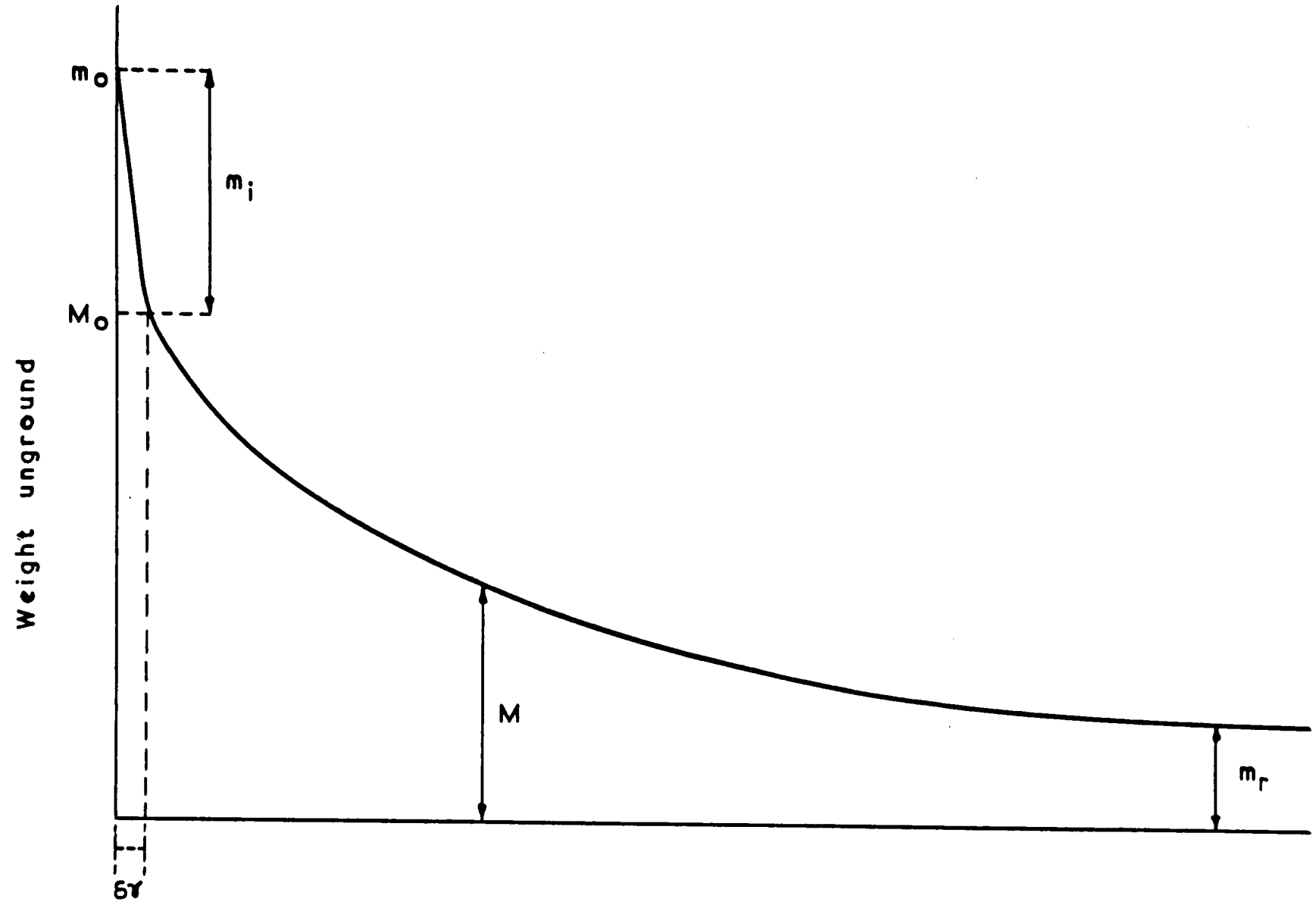


Fig. 6.2.1 Rate of fracture of a particle

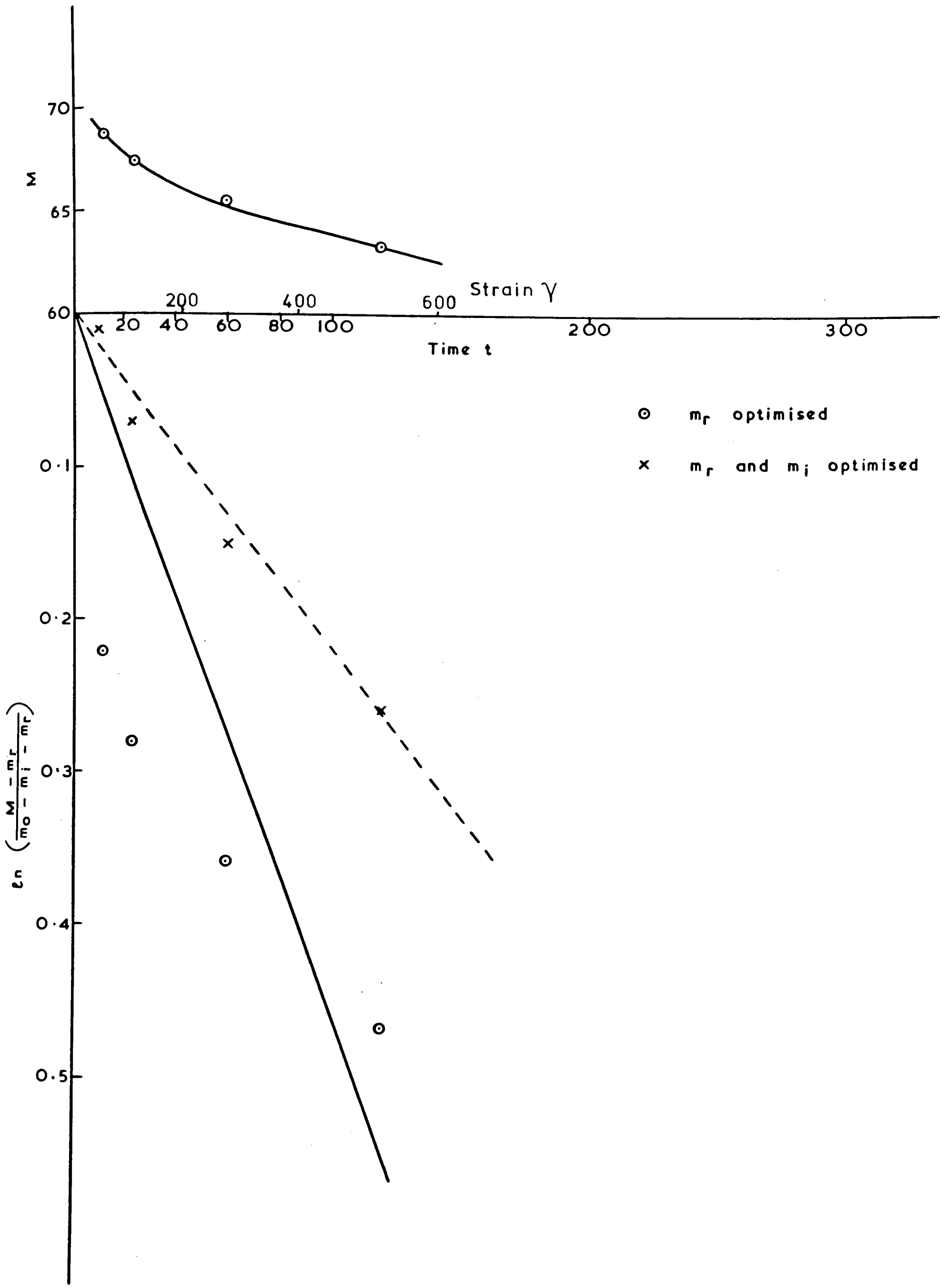


Fig. 6.2.2 Fracture model. Soda Ash (250 – 355μm)
75 gm sample
Stress – 414 kN/m²

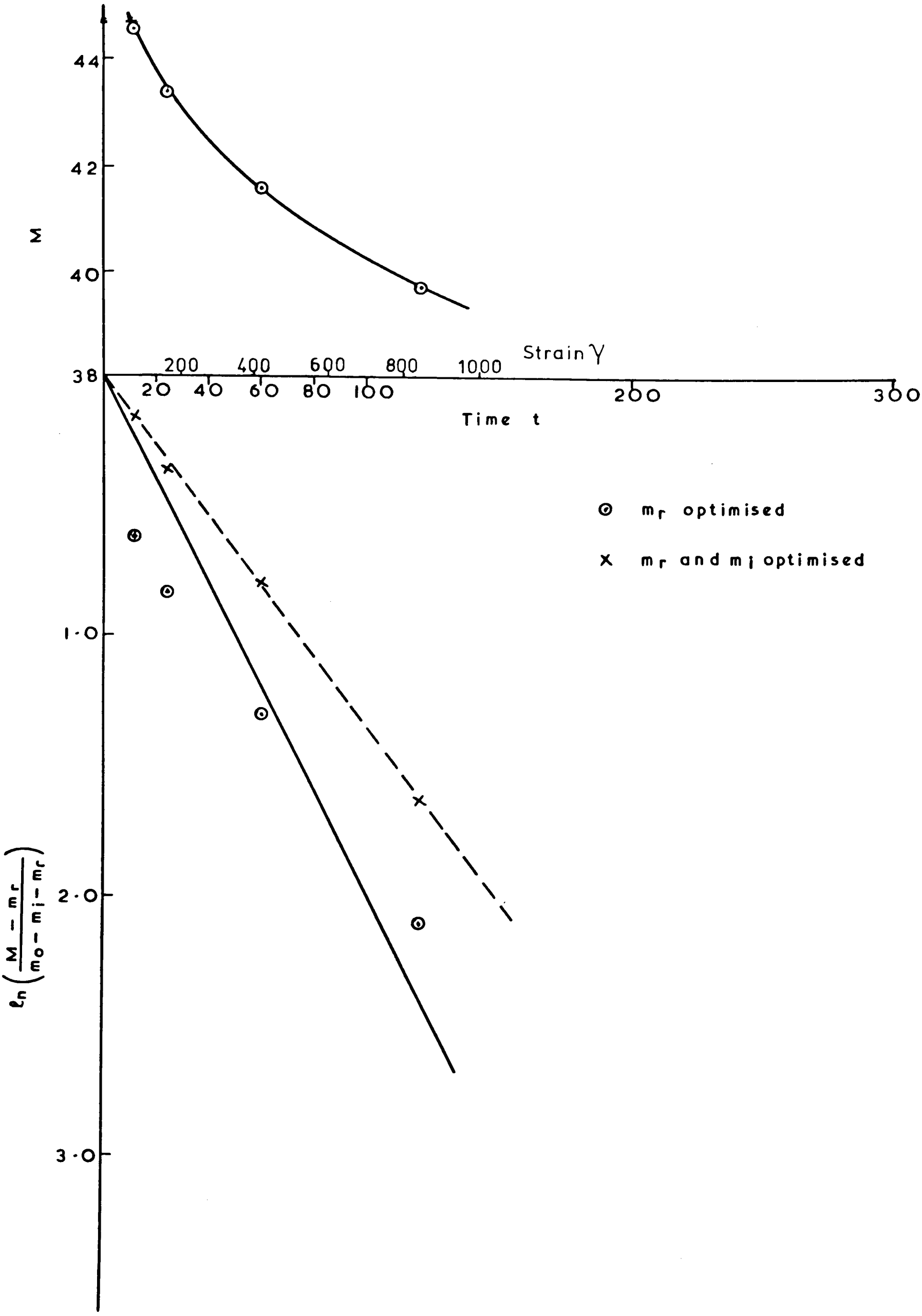


Fig. 6.2.3. Fracture Model. Soda Ash (250-355 μm)
50 gm Sample
Stress-41·4 kN/m²

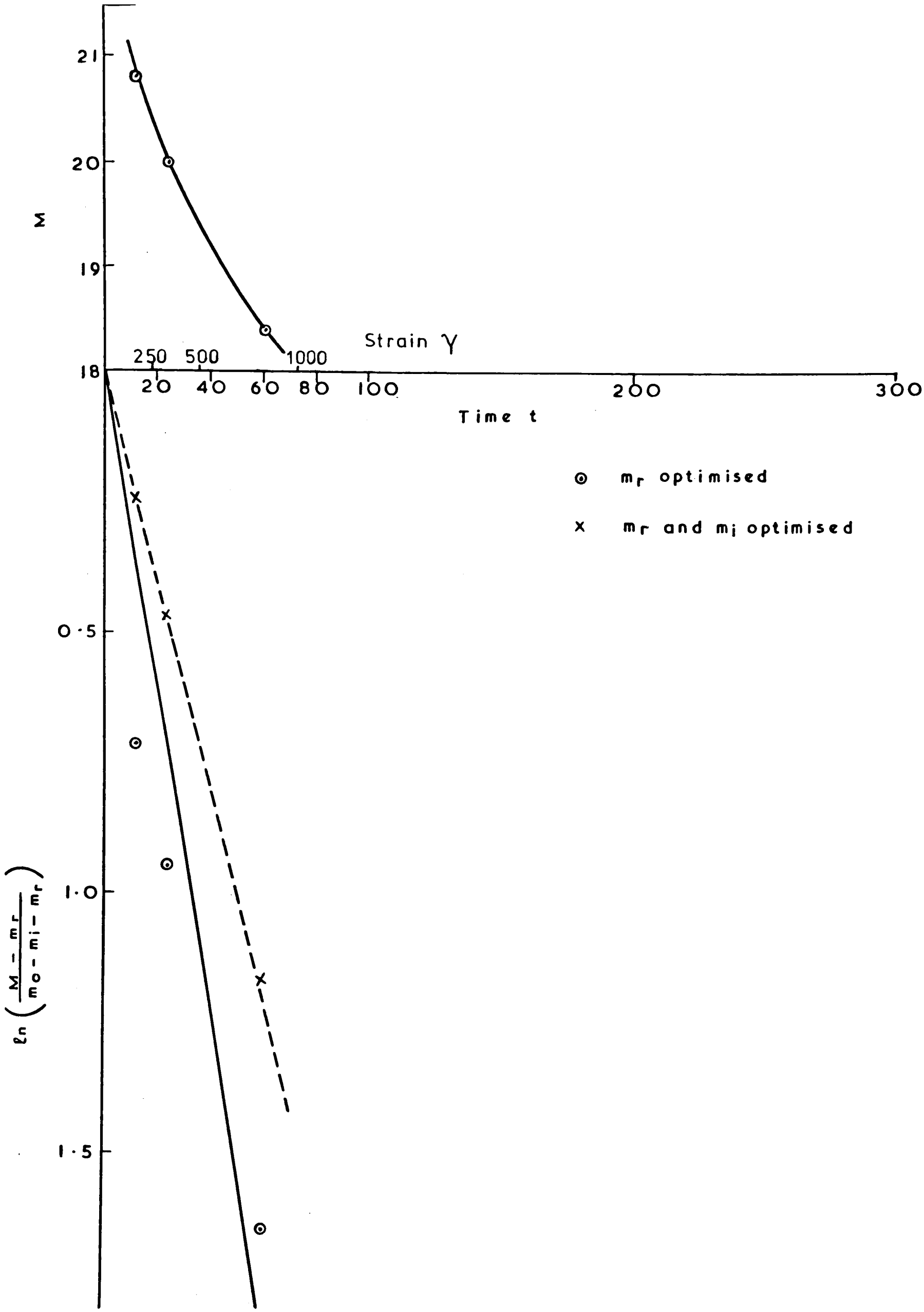


Fig. 6.2.4. Fracture Model. Soda Ash (250 - 355μm) 25 gm Sample

Stress - 41·4 kN/m²

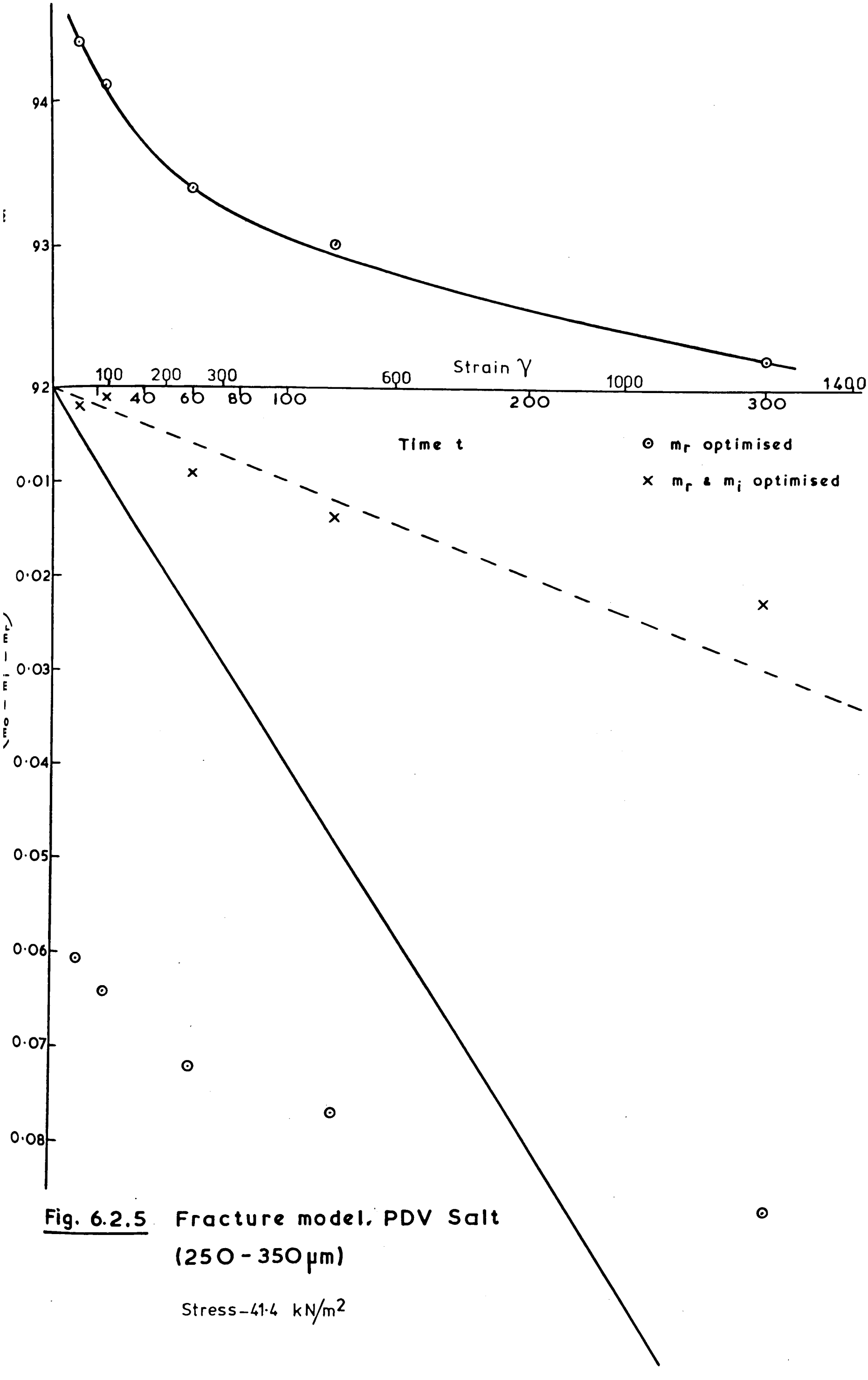


Fig. 6.2.5 Fracture model, PDV Salt (250 - 350 μm)

Stress - 41·4 kN/m²

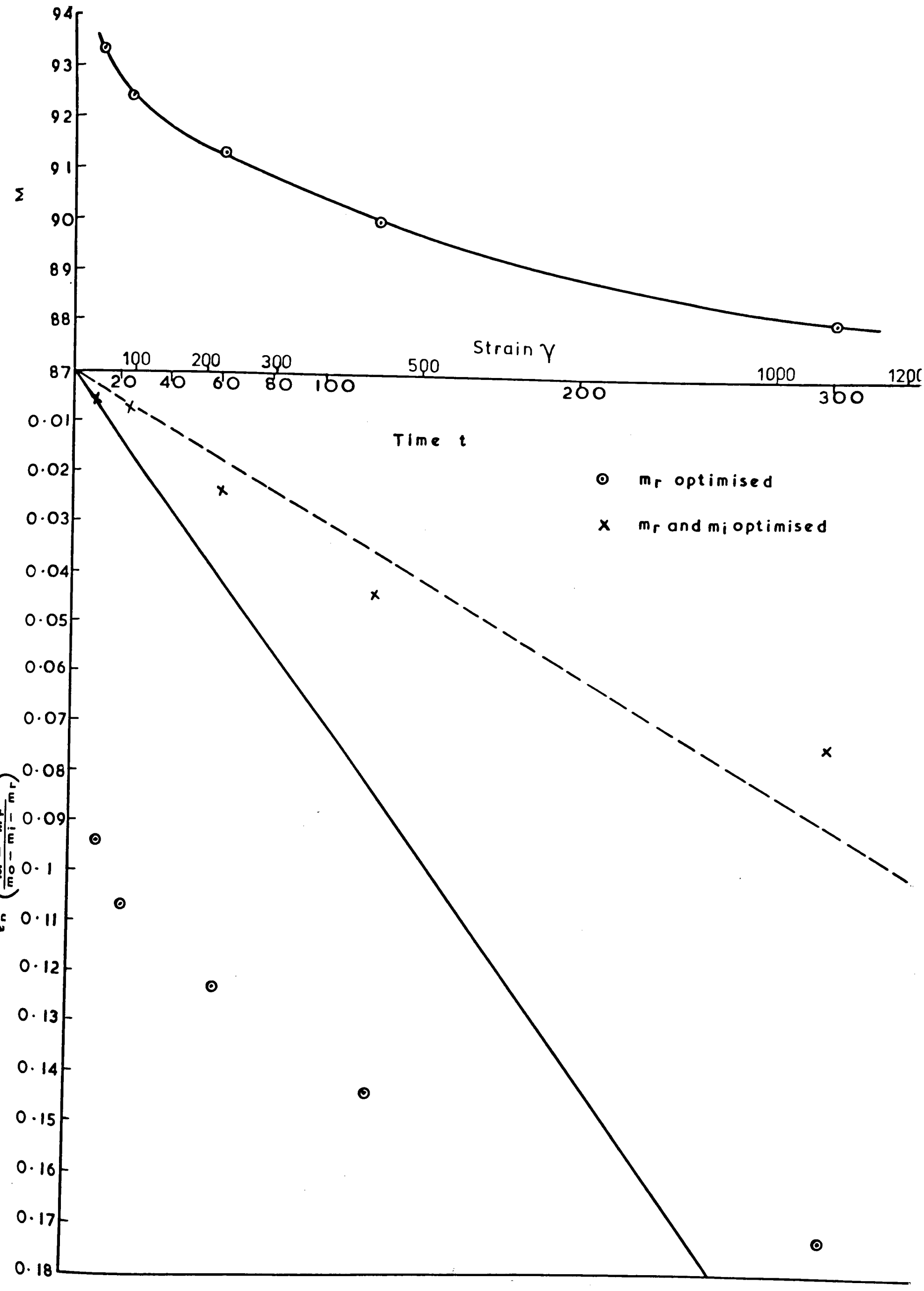


Fig. 6.2.6. Fracture Model.
Lab Salt (355 - 500μm)

Stress – 41·4 kN/m^2

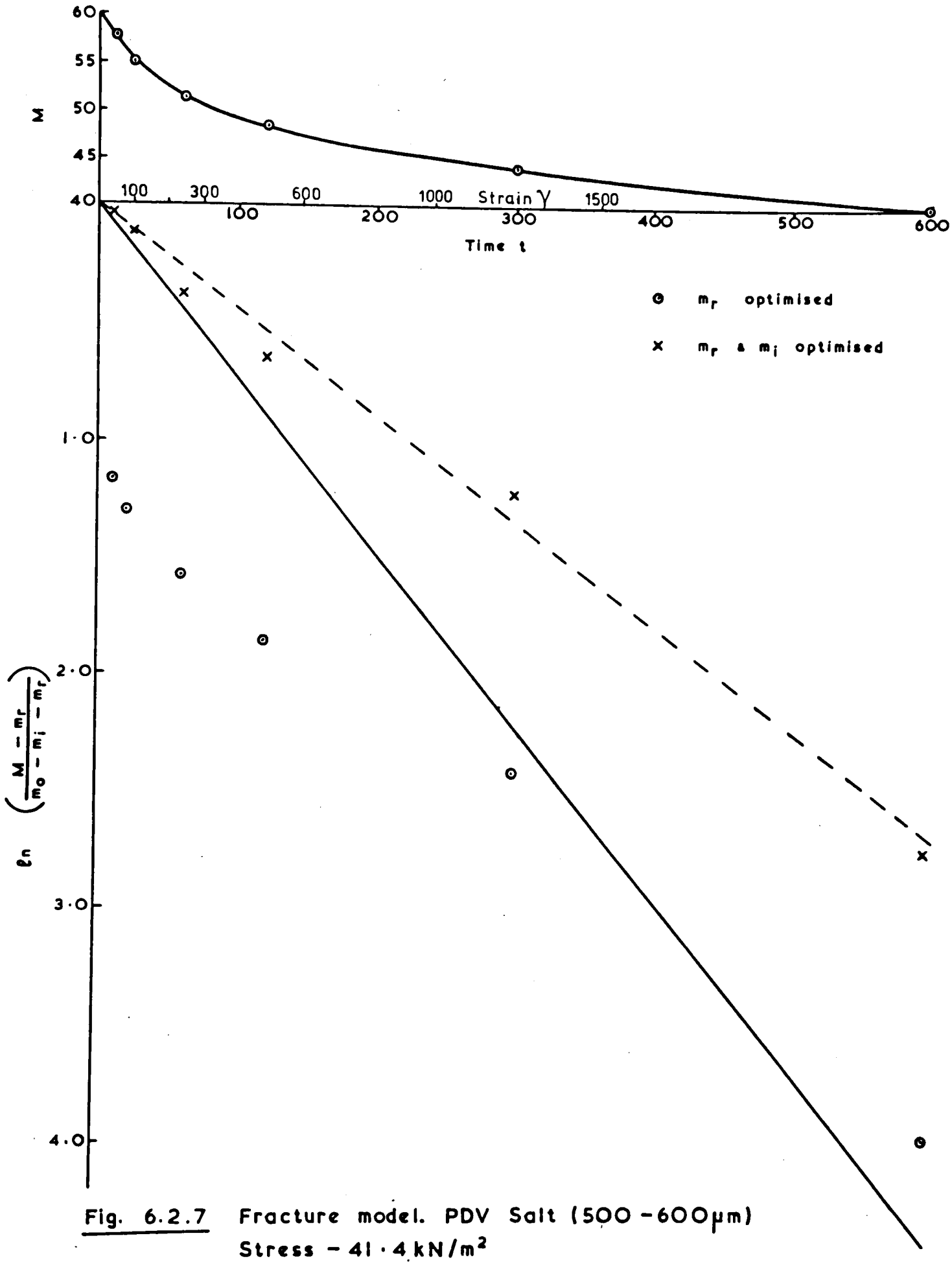


Fig. 6.2.7 Fracture model. PDV Salt (500 - 600μm)
Stress - 41·4 kN/m²

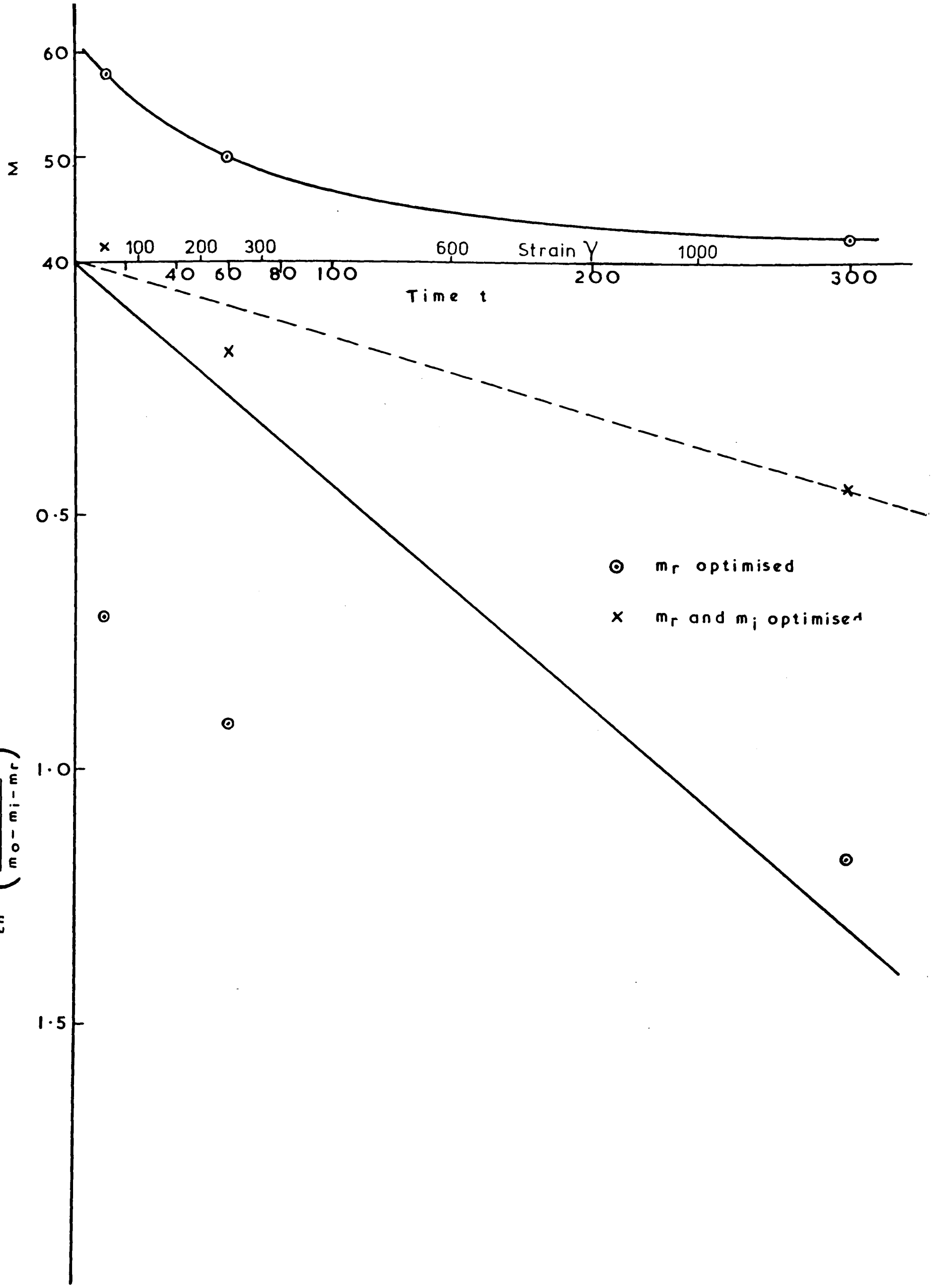


Fig. 6.2.8. Fracture Model · PDV Salt (500 - 600 μm)

Stress - 82 · 8 kN/m²

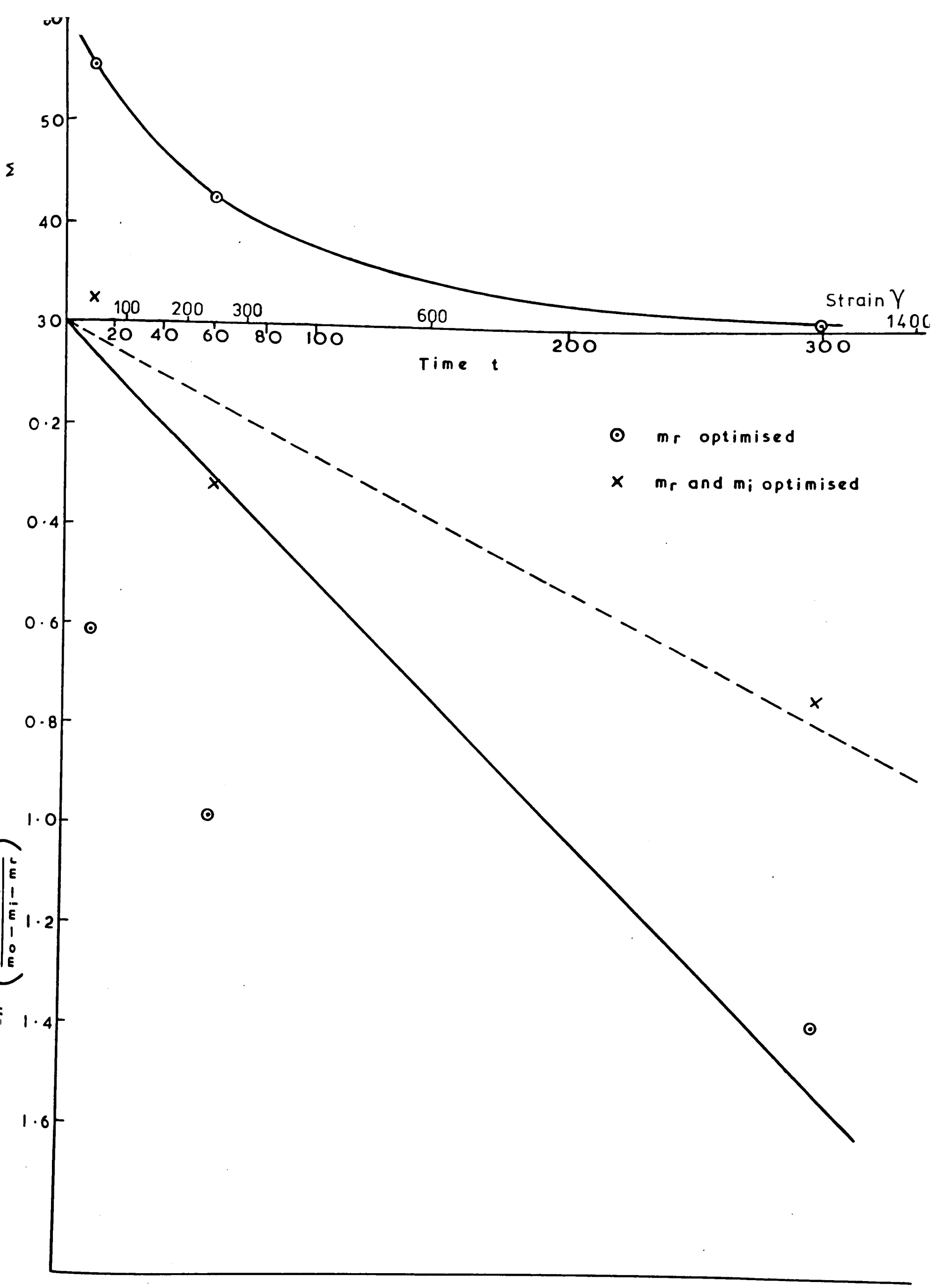


Fig. 6.2.9. Fracture Model. PDV Salt (500-600 μm)

Stress - 165 kN/m²

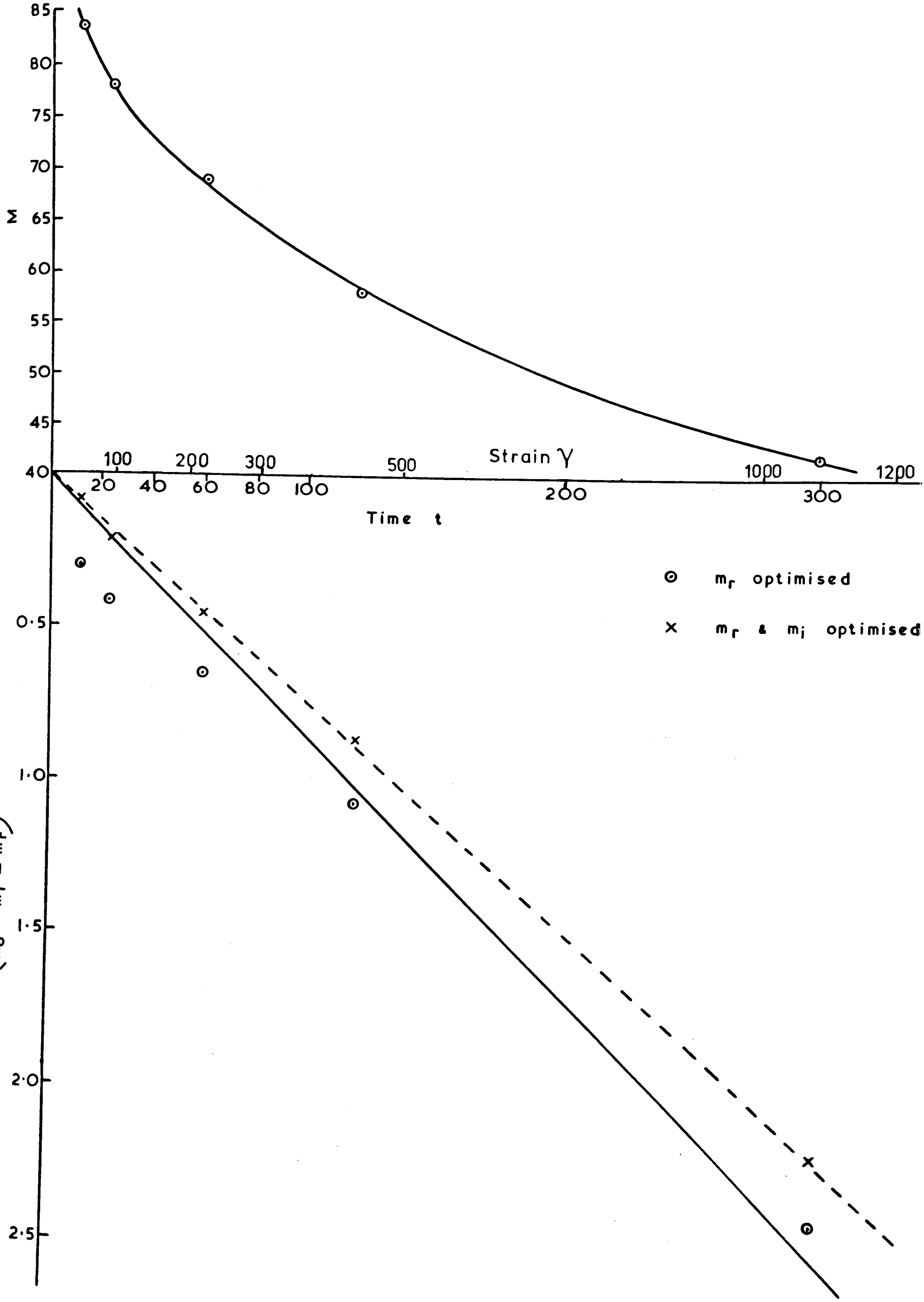


Fig. 6.2.10 Fracture model. Granular Salt (ex. centrifuge) (1·7 - 2·0mm) Stress–41·4 kN/m^2

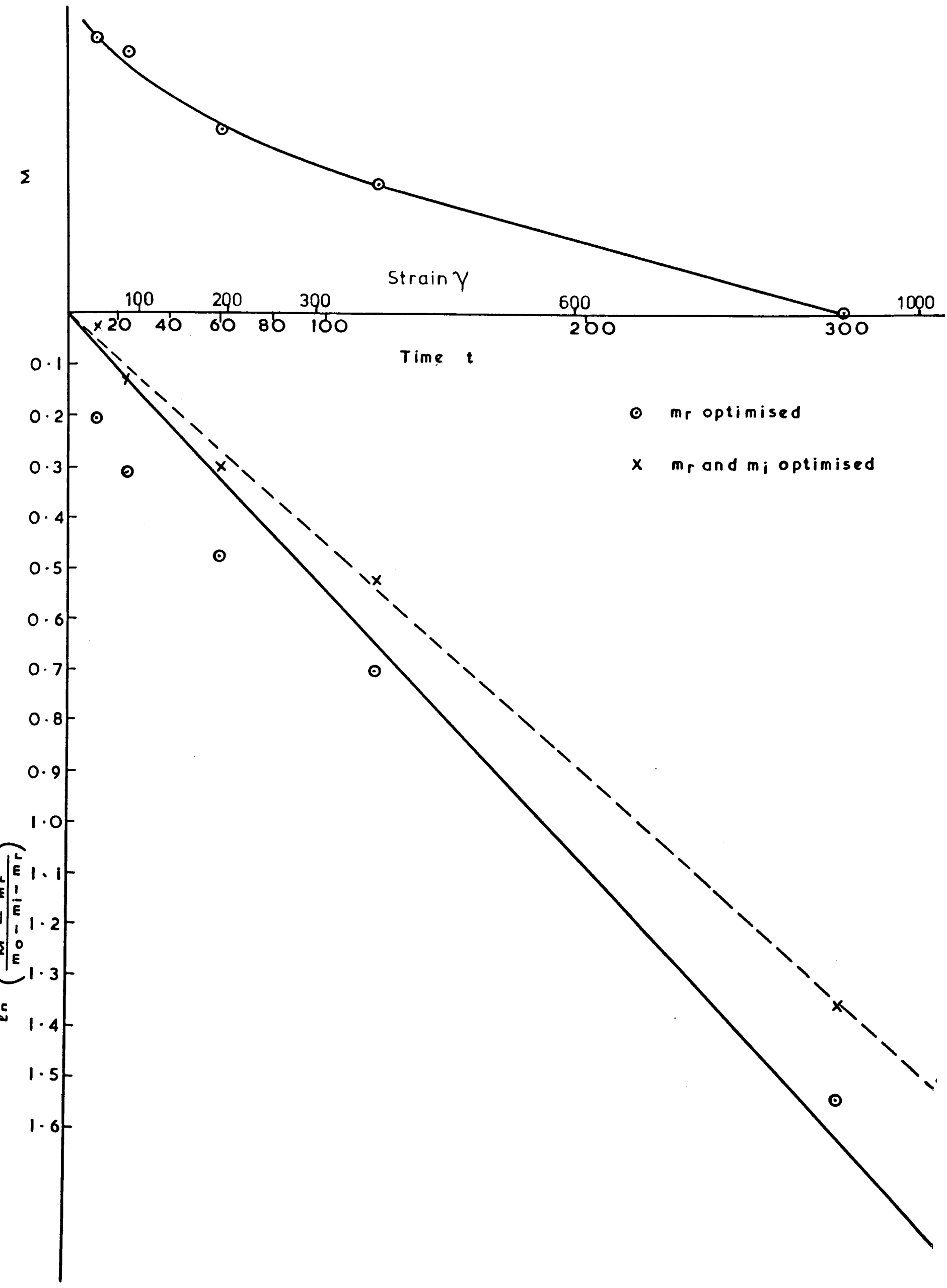


Fig. 6. 2.11. Fracture Model. Molecular Sieve (1·7 – 2·0mm)

Stress = 41·4 kN/m²

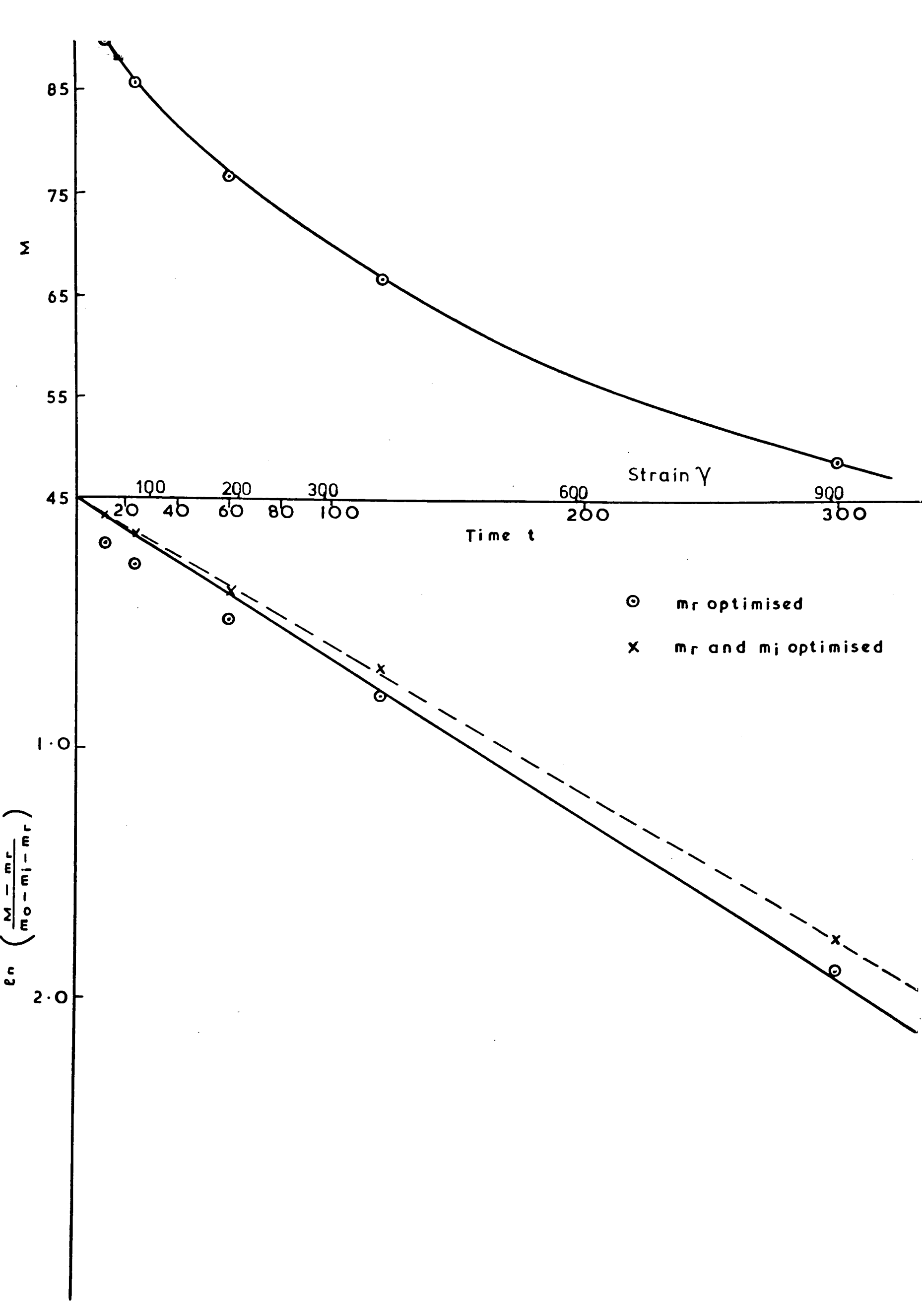


Fig. 6.2.12. Fracture Model-Molecular Sieve Material (1·7 – 2·0 mm)

Stress – 82·8 kN/m²

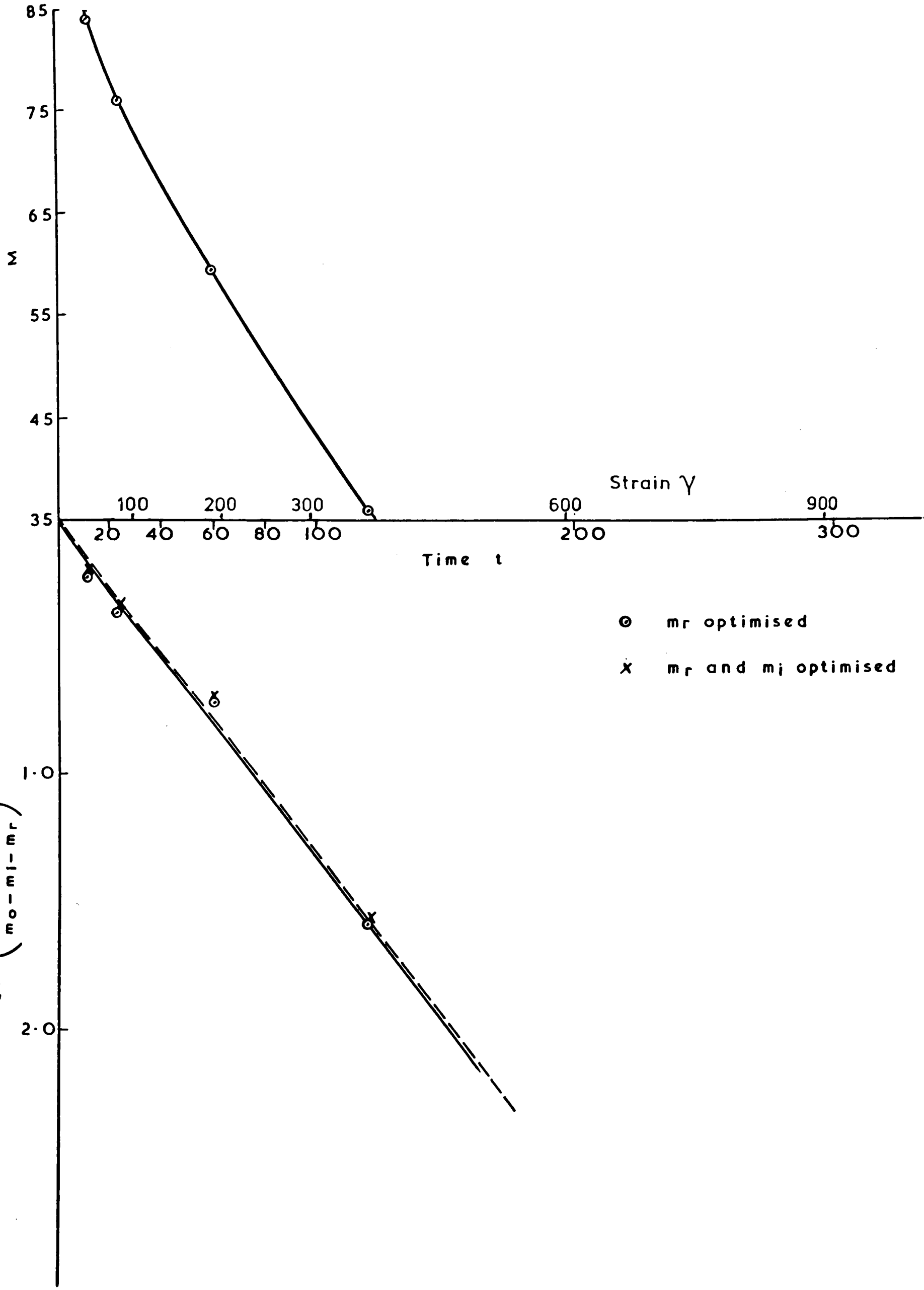


Fig. 6.2.13. Fracture Model. Molecular Sieve material (1·7 – 2·0) mm

Stress – 124 kN/m²

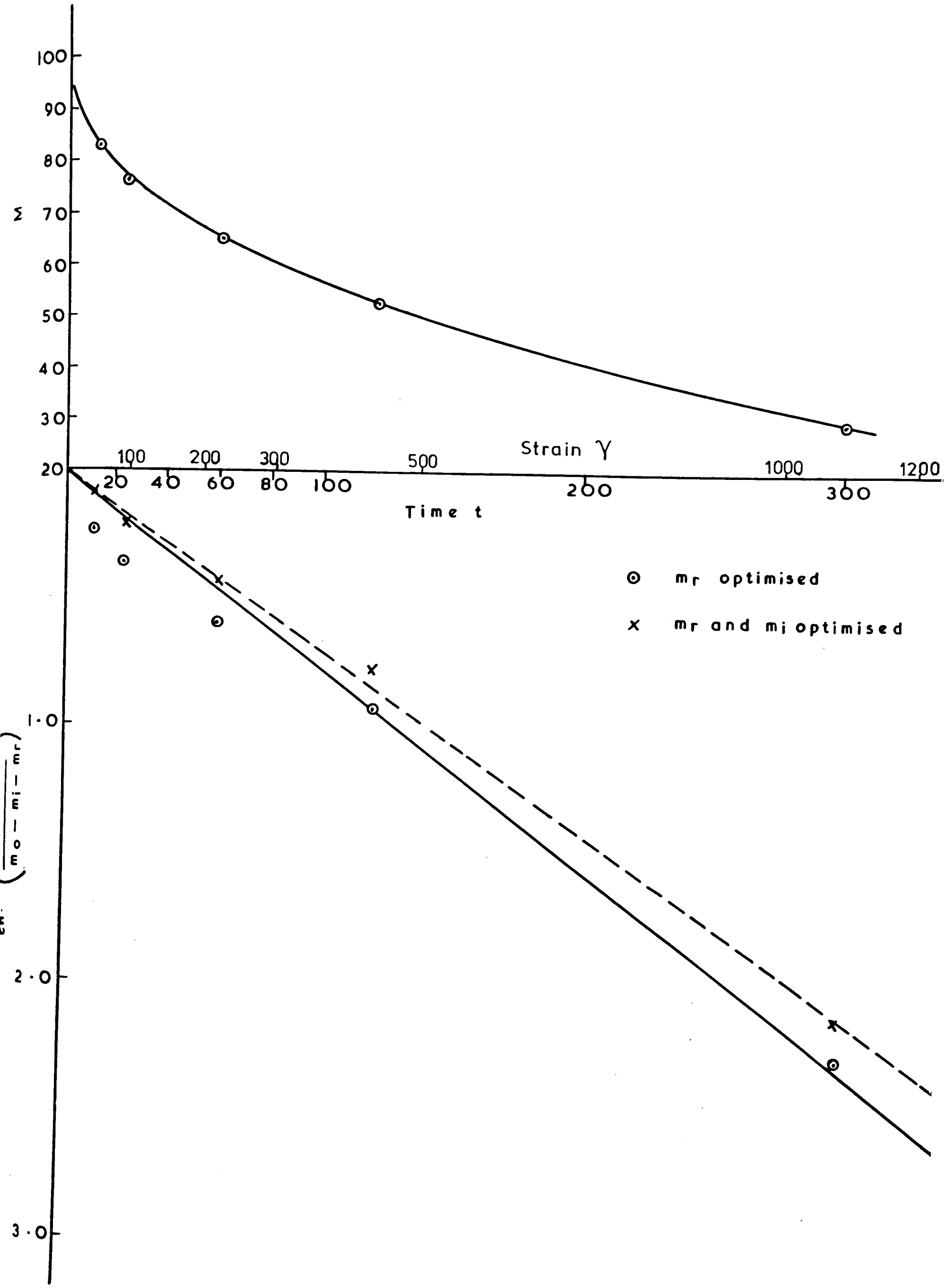


Fig. 6.2.14. Fracture Model. Granular Salt (ex.crystalliser) (1·7 – 2·0 mm)

Stress – 41·4 kN/m²

Table 6.2.1 lists values of m_i, m_r and k for the materials tested. It can be seen that a very much better fit of data is obtained when initial attrition (m_i) is included. The data points, which show curvature when m_i is zero, become more linear with the inclusion of m_i. However, it is seen that for the case of PDV salt and lab salt (Figs. 6.2.5 - 6.2.9) the curvature remains, in spite of some improvement, even after m_i is optimised.

Table 6.2.1 shows that the larger PDV salt is subject to high initial attrition as seen by the large value of m_i. Spherical materials which were prone to shattering (molecular sieve beads, granular sodium chloride) result in lower values of m_i. When these results are compared with the Gwyn coefficients, it can be seen that they are directly comparable, in that a high value of m_i for PDV salt results in a high value of K_p. Hence, K_p is again seen to be associated with initial attrition.

The value of m_i (5.8) for the smaller PDV salt (250 μm) is relatively low for a fracturing material when compared with the 500 μm PDV salt. If the regression coefficients were analysed (Fig. 6.2.1) it was seen that the curve fitting carried out for PDV salt (250 μm) was not as good as that obtained for most of the other materials. On the basis that a good curve fit should be obtained for a fracturing material, the model was not considered suitable to describe attrition of PDV salt (250 μm).

When normal stress is increased, m_i increases for PDV salt and decreases for molecular sieve. This is consistent since PDV salt fractures and molecular sieve attrites by surface grinding.

The value of m_r is seen to decrease for both materials when normal stress is increased. This is consistent with higher amounts of fines

Material (Sieve-cut)		Stress kN/m^2	m_i (gm)	m_r (gm)	k	Correlation Cofficient (%)	F Value
Soda Ash (250-355 µm)	75 gm sample	41.4	6.0	43.4	$0.48x10^{-3}$	99.0	373
	50 gm sample		4.4	38.3	$0.2x10^{-2}$	99.9	5400
	25 gm sample		3.1	16.8	$0.15x10^{-2}$	99.9	33200
PDV Salt (250-355 µm)		41.4	5.8	20.2	$0.24x10^{-4}$	98.3	66.0
Lab Salt (355-500 µm)		41.4	7.1	56.6	$1.4x10^{-4}$	98.2	102
PDV Salt (500-600 µm)		41.4	42.9	38.9	$1.1x10^{-3}$	99.5	937
		82.8	43.4	16.2	$0.37x10^{-3}$	95.6	43.3
		165	46.6	8.10	$0.63x10^{-3}$	94.5	34.7
Granular Salt ex centrifuge (1.7-2.0mm)		41.4	12.0	36.5	$2.0x10^{-3}$	99.9	14600
Molecular Sieve (1.7-2.0mm)		41.4	7.3	55.5	$1.5x10^{-3}$	99.9	3560
		82.8	6.7	39.6	$1.9x10^{-3}$	99.9	11800
		124	2.3	19.8	$0.4x10^{-2}$	99.5	785
Granular Salt ex crystalliser (1.7-2.0mm)		41.4	11.3	21.5	$1.9x10^{-3}$	99.9	3070

Table 6.2.1 Computer Model Solutions for m_i, m_r and k.

being produced at higher stresses. There does not seem to be a clear trend between the values of m_r for material undergoing the two different attrition mechanisms.

The rate constant, k, is generally seen to increase with normal stress. In the case of soda ash, the largest sample size produces a marked reduction in k. Again, there is no clear distinction between material known to fracture and those that surface abrade.

6.2.2a Surface Abrasion Model (Radius Basis)

A model may be developed in which the rate of grinding of material is proportional to its radius, i.e.

$$\frac{dr}{d\gamma} \propto - r^a$$

where r is the radius of the particle at strain γ.

In this formulation, a is assumed to be positive indicating that work-hardening material is being considered. If, however, the material softens as attrition proceeds, then a would be negative indicating that attrition rate increases due to work-softening of the material.

$$\therefore \frac{dr}{d\gamma} = - k_1 r^a$$

$$\frac{dr}{r^a} = - k_1 \, d\gamma$$

Integrating

$$\frac{r^{(1-a)}}{(1-a)} = - k_1 \gamma + C \qquad (a \neq 1)$$

At $\gamma = 0$, $r = r_i$

$$\therefore \frac{r_i^{(1-a)} - r^{(1-a)}}{(1-a)} = k_1 \gamma$$

Let us define r_{il} to be the initial radius of a particle that shrinks to r_1 after strain γ. Thus, r_{il} would be the largest initial radius of the particle that would just pass through the top sieve after having been subjected to strain γ.

Hence

$$\frac{r_{il}^{(1-a)} - r_1^{(1-a)}}{(1-a)} = k_1 \gamma$$

$$r_{il}^{(1-a)} - r_1^{(1-a)} = (1-a)\, k_1 \gamma$$

$$r_{il}^{(1-a)} = r_1^{(1-a)} + (1-a)\, k_1 \gamma$$

As this was difficult to solve, it was decided to follow the same approach but to formulate the rate equation in terms of mass instead of radii.

$$\therefore \quad \frac{dM}{d\gamma} = - k_2 M^A$$

$$\ln \left[- \frac{dM}{d\gamma} \right] = \ln k_2 + A \ln M$$

$\left[- \frac{dM}{d\gamma} \right]$ values were read directly off the experimental curves for the various materials and a graph of $\ln \frac{-dM}{d\gamma}$ vs $\ln M$ plotted to obtain values of A and k_2 using regression analysis.

Table 6.2.15 lists values of the rate constant and exponent for the different materials used. It is seen that the degree of fit obtained was not good, probably because the values of $\left[\frac{dM}{d\gamma}\right]$ were subject to error. The model is thus not a convenient representation of the surface grinding process.

Material (Sieve-cut)	Stress kN/m^2	A	Standard Error of A	k_2	Correlation Coefficient (%)	F Value
Soda Ash (250-355 µm) 75 gm sample	41.4	16.5	4.30	3.3×10^{-31}	93.7	14.4
Soda Ash (250-355 µm) 50 gm sample		14.5	1.80	1.1×10^{-24}	98.5	64.9
Soda Ash (250-355 µm) 25 gm sample		6.03	0.70	1.1×10^{-8}	99.4	75.6
PDV Salt (250-355 µm)	41.4	113	10.0	e^{-516}	98.9	128
Lab Salt (355-500 µm)	41.4	50.9	4.14	e^{-233}	99.0	151.0
PDV Salt (500-600 µm)	41.4	8.99	0.53	1.2×10^{-16}	99.3	286.0
PDV Salt (500-600 µm)	82.8	11.30	4.20	1.9×10^{-20}	93.8	7.3
PDV Salt (500-600 µm)	165	7.10	2.40	1.2×10^{-12}	95.0	8.9
Granular Salt ex centrifuge (1.7-2.0mm)	41.4	2.75	0.27	0.8×10^{-5}	98.6	101
Molecular Sieve (1.7-2.0mm)	41.4	4.16	0.63	0.5×10^{-8}	96.8	44.3
Molecular Sieve (1.7-2.0mm)	82.8	1.96	0.16	1.6×10^{-4}	99.0	141
Molecular Sieve (1.7-2.0mm)	124	0.65	0.30	1.1×10^{-1}	82.4	4.20
Granular Salt ex crystalliser (1.7-2.0mm)	41.4	1.77	0.32	0.7×10^{-3}	95.3	29.9

Table 6.2.15 Computer Solutions for Differential Equation governing Grinding Rate.

6.2.2b Surface Abrasion Model (Radius Change Basis)

A model may also be developed where the rate of grinding is proportional to the reduction in radius of a particle to an arbitrary power, i.e.

$$\frac{dr}{d\gamma} \propto (r_i - r)^{-b}$$

where b >0 for a work-hardening model. Here, r_i denotes the initial radius of a particle and r the radius of the particle at strain γ. The group $(r_i - r)$ is included since it is a measure of the change in shape consequent upon the change in particle radius.

$$\therefore \frac{dr}{d\gamma} = - K (r_i - r)^{-b}$$

$$\int_{r_i}^{r} (r_i - r)^b \, dr = - K \int_{o}^{\gamma} d\gamma$$

and hence

$$\frac{(r_i - r)^{b+1}}{(b+1)} = K\gamma \quad (b \neq -1) \qquad (6.2.2.1)$$

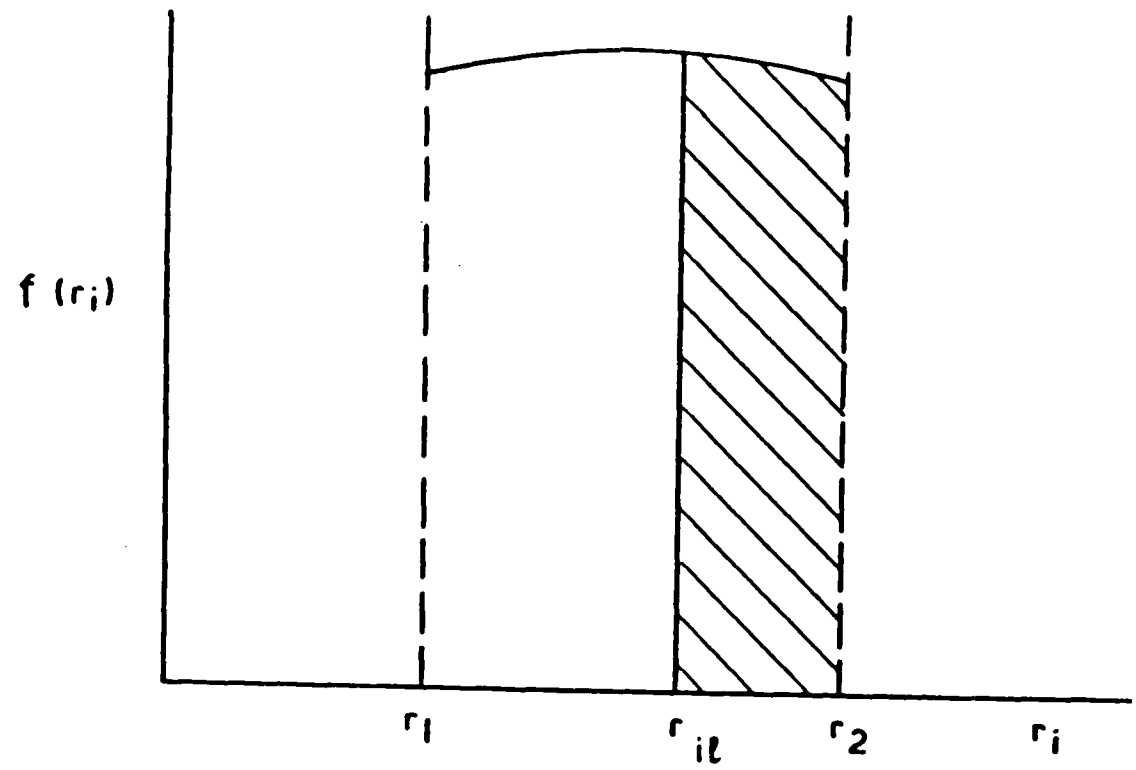
Let the initial weight distribution of sample as a function of its radius (as measured by sieving) be given by $f(r_i)$ and the weight distribution after shear strain γ be given by f(r) (Fig. 6.2.16.). Let the particles in the initial distribution be in the sieve range r_1 to r_2 mm.

Let us define r_{il} to be the initial radius of a particle which shrinks to a value r_1 at strain γ. Applying these conditions to equation (6.2.2.1), we have

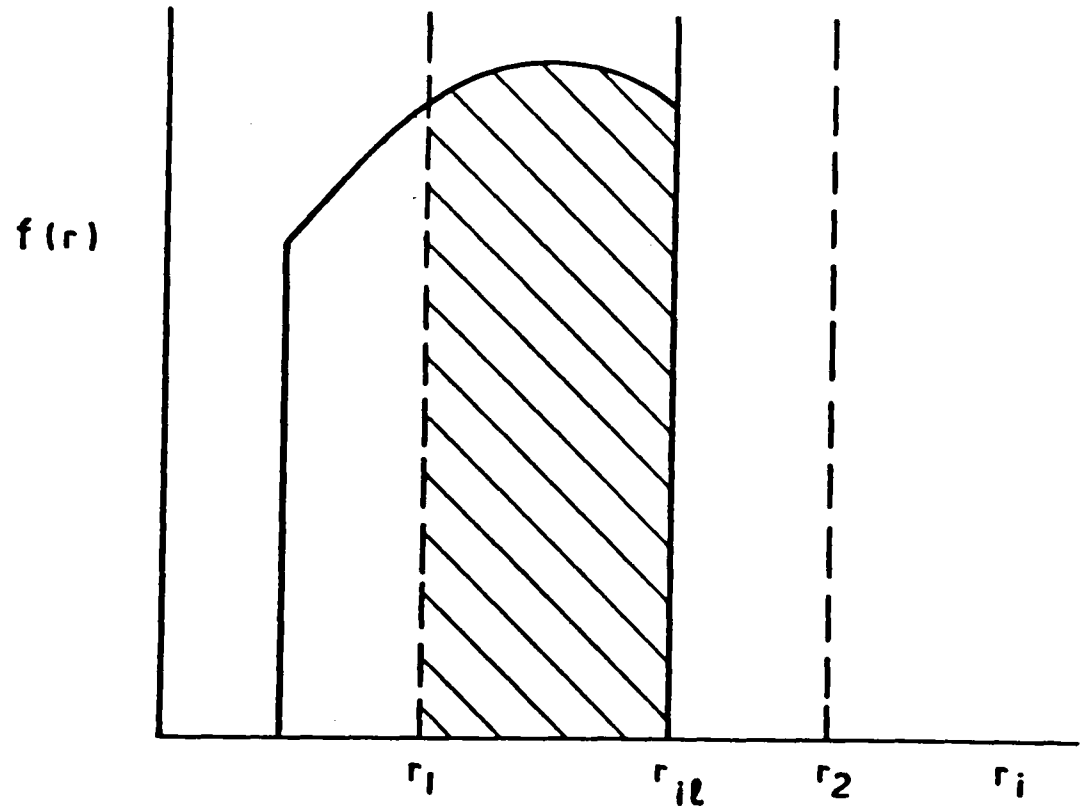
$$\frac{(r_{il} - r_1)^{b+1}}{(b+1)} = K\gamma$$

or

$$(b+1) [\ln (r_{il} - r_1)] = \ln (b+1) + \ln K + \ln \gamma$$



Weight distribution at Strain $\gamma = 0$



Weight distribution at Strain γ

Fig. 6.2.16. Shift of particle size distribution in surface grinding model

$$\therefore \quad \ln (r_{il} - r_1) = \frac{[\ln (b+1) + \ln K]}{(b+1)} + \left(\frac{1}{b+1}\right) \ln \gamma \qquad (6.2.2.2)$$

The weight fraction left on the sieve after grinding for strain γ is

$$\int_{r_{il}}^{r_2} f(r_i)\, dr_i$$

from Fig 6.2.16 assuming that sieving is complete.

Since

$$\int_{r_1}^{r_2} f(r_i)\, dr_i = 1$$

and a uniform initial size distribution is assumed,

$$f(r_i) = \frac{1}{r_2 - r_1}$$

$$\therefore \quad \int_{r_{il}}^{r_2} f(r_i)\, dr_i = \frac{r_2 - r_{il}}{r_2 - r_1}$$

r_{il} is calculated from the experimentally measured weight fraction left on the sieve, it being assumed that this material produced negligible quantities of fines during attrition. Once r_{il} is obtained for a series of experimental runs, a graph of $\ln(r_{il}-r_1)$ vs $\ln \gamma$ may be plotted to obtain values of b and K using regression techniques.

Table 6.2.16 lists values of rate constants and exponents for the different materials used. It can be seen that materials which undergo fracture followed by surface grinding produce the smallest exponents (molecular sieve beads, granular sodium chloride), whilst materials

Material (Sieve-cut)	Stress kN/m^2	b (Index)	K (Rate Constant)	Correlation Coefficient (%)	F Value
Soda Ash (250-355 µm) 75 gm sample	41.4	2.75	$0.15x10^{-11}$	99.8	587
Soda Ash (250-355 µm) 50 gm sample	41.4	2.60	$0.21x10^{-11}$	99.9	4300
Soda Ash (250-355 µm) 25 gm sample	41.4	2.50	$0.18x10^{-11}$	99.9	380
PDV Salt (250-355 µm)	41.4	8.62	$0.35x10^{-29}$	99.8	660
Lab Salt (355-500 µm)	41.4	4.66	$0.36x10^{-16}$	99.9	1130
PDV Salt (500-600 µm)	41.4	10.26	$0.31x10^{-24}$	99.9	5400
PDV Salt (500-600 µm)	82.8	9.12	$0.66x10^{-22}$	99.9	479
PDV Salt (500-600 µm)	165	5.50	$0.18x10^{-16}$	99.0	46.4
Granular Salt ex centrifuge (1.7-2.0mm)	41.4	1.52	$0.63x10^{-6}$	99.9	3050
Molecular Sieve (1.7-2.0mm)	41.4	1.30	$0.57x10^{-6}$	99.9	1200
Molecular Sieve (1.7-2.0mm)	82.8	0.97	$0.47x10^{-5}$	99.9	5200
Molecular Sieve (1.7-2.0mm)	124	0.68	$0.44x10^{-4}$	99.9	2200
Granular Salt ex crystalliser (1.7-2.0mm)	41.4	1.28	$0.21x10^{-5}$	99.9	5300

Table 6.2.16 Computer Solutions for b and K for Surface Grinding Model.

which surface abrade only at high strains produce high values for the index of the rate equation. Materials which partially abrade (soda ash) are seen to lie in between. It is thus possible that the index b is an indication of the dominant mechanism controlling the attrition process for a particular material.

The rate constant is also seen as an indication of the ability for materials to abrade. PDV salt, which after initial attrition requires very high strain for surface abrasion to occur, shows relatively small values of K whereas molecular sieve and granular salt, which attrite relatively quickly, produce larger values of K.

Increasing normal stress shows a marked decrease in the value of b and a correspondingly large increase in K (PDV salt, molecular sieve).

The effect of changing the sample weight is to reduce b slightly but increase K (soda ash).

In the Gwyn formulation,

$$W = K_p \gamma^m$$

$$\therefore \ln W = \ln K_p + m \ln \gamma \qquad (6.2.2.3)$$

Since W is the mass fraction attrited,

$$W = \int_{r_1}^{r_{il}} f(r_i)\, dr_i$$

assuming that the unattrited fraction produces negligible amounts of fine material.

$$\therefore \quad W = \frac{r_{il} - r_1}{r_2 - r_1} \qquad (6.2.2.4)$$

$$\therefore (r_{il} - r_1) = W(r_2 - r_1)$$

If this value for $(r_{il} - r_1)$ is now substituted in equation (6.2.2.2), we get

$$\ln [W(r_2 - r_1)] = \left[\frac{\ln K + \ln (b+1)}{(b+1)}\right] + \left(\frac{1}{b+1}\right) \ln \gamma$$

$$\ln W + \ln (r_2 - r_1) = \left[\frac{\ln K + \ln (b+1)}{(b+1)}\right] + \left(\frac{1}{b+1}\right) \ln \gamma$$

$$\therefore \ln W = \left[\frac{\ln K + \ln (b+1)}{(b+1)}\right] - \ln (r_2 - r_1) + \left(\frac{1}{b+1}\right) \ln \gamma$$

(6.2.2.5)

Comparing equations (6.2.2.3) and (6.2.2.5), we have

$$\ln K_p = \frac{\ln \left[\dfrac{K (b+1)}{(r_2 - r_1)^{b+1}}\right]}{(b+1)}$$

and

$$m = \left(\frac{1}{b+1}\right)$$

If the values of m from the Gwyn formulation are compared with the gradients obtained from equation (6.2.2.5), the values are found to be almost exactly similar. Results of these values from separate formulations are given in Table 6.2.17; the procedures are in essence identical and the Table demonstrates consistency in the calculations.

The values of the intercepts K and K_p will not be the same because equation (6.2.2.5) contains a radius term, seen as a function of the sieving process, which arises when radius terms are converted into a weight function.

Material (Sieve-cut)		Stress kN/m^2	m (GWYN)	m (THEORETICAL)
Soda Ash (250-355 μm)	75 gm sample	41.4	0.267	0.267
	50 gm sample		0.278	0.278
	25 gm sample		0.282	0.282
PDV Salt (250-355 μm)		41.4	0.104	0.104
Lab Salt (355-500 μm)		41.4	0.177	0.177
PDV Salt (500-600 μm)		41.4	0.089	0.089
		82.8	0.099	0.099
		165	0.154	0.154
Granular Salt-ex centrifuge (1.7-2.0mm)		41.4	0.396	0.396
Molecular Sieve (1.7-2.0mm)		41.4	0.435	0.435
		82.8	0.507	0.507
		124	0.595	0.595
Granular Salt-ex crystalliser (1.7-2.0mm)		41.4	0.439	0.439

Table 6.2.17 Comparison of Gwyn Coefficients with Theoretical Values.

Hence, it is seen that the gradient m depends only on the value of b. As normal stress increases b decreases, increasing m (Table 6.2.16) as in the Gwyn plots. The above formulation has shown that the radius reduction model can be reduced to the Gwyn form and that the Gwyn equation has some theoretical basis.

In the model discussed previously, r_{il} was calculated assuming that the initial weight distribution $[f(r_i)]$ is uniform. This is correct around the mode of the distribution. Nonetheless, a more general approach is given below where $[f(r_i)]$ is no longer taken to be uniform.

Let $[f(r_i)]$ be approximated by a linear function

$$f(r_i) = c + d\, r_i$$

$$\therefore \int_{r_1}^{r_2} f(r_i)\, dr_i = \int_{r_1}^{r_2} (c + dr_i)\, dr_i$$

$$= \left[cr_i + \frac{(dr_i)^2}{2} \right]_{r_1}^{r_2}$$

$$= (r_2 - r_1) \left[c + \frac{d}{2} (r_2 + r_1) \right]$$

Since

$$\int_{r_1}^{r_2} f(r_i)\, dr_i = 1$$

we get

$$(r_2 - r_1) \left[c + \frac{d}{2} (r_2 + r_1) \right] = 1 \qquad (6.2.2.6)$$

From the earlier formulation, the amount left on the top sieve after attrition is given by

$$\int_{r_{il}}^{r_2} f(r_i)\, dr_i$$

assuming that this material produced negligible amounts of fine material. Hence, for the non-uniform case

$$\int_{r_{il}}^{r_2} f(r_i)\, dr_i = (r_2 - r_{il}) \left[c + \frac{d}{2} (r_2 + r_{il}) \right]$$

Substituting for c from (6.2.2.6), we get

$$\int_{r_{il}}^{r_2} f(r_i)\, dr_i = (r_2 - r_{il}) \left[\frac{1}{(r_2 - r_1)} - \frac{d}{2} (r_1 + r_2) + \frac{d}{2} (r_2 + r_{il}) \right]$$

$$= \frac{r_2 - r_{il}}{r_2 - r_1} - (r_2 - r_{il}) \left[\frac{d}{2} (r_1 + r_2) - \frac{d}{2} (r_2 + r_{il}) \right]$$

$$= \frac{r_2 - r_{il}}{r_2 - r_1} + \frac{d}{2} (r_2 - r_{il}) (r_{il} - r_1) \qquad (6.2.2.7)$$

The magnitude of the integral depends on the nature of d for a given size of material. If d is positive then the value of r_{il} is closer to r_2, whereas if d is negative then r_{il} is closer to r_1.

Using the cumulative percentage curve for the various bulk materials (Figs. 2.5.1 - 2.5.4), it is possible to estimate the nature of the gradient d of the weight distribution [$f(r_i)$]. In almost all cases, it is seen that the gradient changes direction at the relevant sieve cuts of starting material (i.e. d is zero). Thus, it seems reasonable to assume a constant weight-radius distribution for the present work.

The only exception is PDV salt (500 μm). Here, the gradient is negative which indicates that the value of r_{il} is closer to r_1. Hence, the amount of fines produced initially is high and this may account for the high values of m_i (Table 6.1.1) and a large value for the intercept K_p in the Gwyn formulation.

It is possible to reduce equation (6.2.2.7) to the form of equation (6.2.2.2) and hence compare it directly to the Gwyn formulation.

$$\int_{r_{il}}^{r_2} f(r_i)\, dr_i = 1 - W$$

where W is the weight fraction attrited.

Hence

$$1 - W = \frac{r_2 - r_{il}}{r_2 - r_1} + \frac{d}{2}\left[(r_2 - r_{il})\,(r_{il} - r_1)\right] \quad (6.2.2.7)$$

Let

$$\alpha = r_{il} - r_1$$

$$\beta = r_2 - r_1$$

$$\theta = \frac{d}{2}$$

$$\therefore \beta - \alpha = r_2 - r_{il}$$

For a given sieve-cut of initial material, β and θ are constants.

$$\therefore 1 - W = \left(\frac{\beta - \alpha}{\beta}\right) + \alpha\theta\,(\beta - \alpha) \quad (6.2.2.7)$$

If a quadratic in α is formulated, we get

$$\alpha^2 + \left(\frac{1 - \beta^2\theta}{\beta\theta}\right)\alpha - \frac{W}{\theta} = 0$$

Using the quadratic theory,

$$\alpha = \frac{\left(\frac{\beta^2\theta-1}{\beta\theta}\right) \pm \sqrt{\left(\frac{b^2\theta-1}{\beta\theta}\right)^2 + \frac{4W}{\theta}}}{2}$$

$$= \left(\frac{\beta^2\theta-1}{2\beta\theta}\right) \left[1 \pm \left\{1 + \frac{4W\beta^2\theta^2}{\theta(1-\beta^2\theta)^2}\right\}^{\frac{1}{2}}\right]$$

Expanding the square root term by the binomial theorem and considering the first three terms,

$$\alpha = \left(\frac{\beta^2\theta-1}{2\beta\theta}\right) \left[1 \pm \left\{1 + \frac{2W\beta^2\theta^2}{\theta(1-\beta^2\theta)^2} - \frac{2W^2\beta^4\theta^2}{(1-\beta^2\theta)^4} + \ldots\ldots\right\}\right]$$

The physically acceptable solution is obtained using the negative sign for the expansion, and we get

$$\alpha = \left(\frac{\beta^2\theta-1}{2\beta\theta}\right) \left[\frac{2W^2\beta^4\theta^2}{(1-\beta^2\theta)^4} - \frac{2W\beta^2\theta}{(1-\beta^2\theta)^2} - \ldots\ldots\right]$$

$$= \frac{W\beta}{(1-\beta^2\theta)} - \frac{W^2\beta^3\theta}{(1-\beta^2\theta)^3} - \ldots\ldots \qquad (6.2.2.8)$$

If the weight - radius distribution is uniform, then $\theta \to 0$.

Hence

$$\alpha = W\beta$$

or

$$W = \frac{\alpha}{\beta} = \frac{r_{il} - r_1}{r_2 - r_1}$$

which is the same relationship as seen in equation (6.2.2.4).

In terms of radii, equation (6.2.2.8) becomes

$$(r_{il} - r_1) = \frac{2W\,(r_2 - r_1)}{[2 - (r_2 - r_1)^2 d]} - \frac{4W^2 d\,(r_2 - r_1)^3}{[2 - (r_2 - r_1)^2 d]^3} - \cdots\cdots$$

If only the first term is considered, in logarithmic form

$$\ln (r_{il} - r_1) = \ln W + \ln [2(r_2 - r_1)] - \ln [2 - (r_2 - r_1)^2 d]$$

If this is compared with equation (6.2.2.2), we get

$$\ln W + \ln[2(r_2 - r_1)] - \ln[2-(r_2 - r_1)^2 d] = \left[\frac{\ln(b+1) + \ln K}{(b+1)}\right] + \left(\frac{1}{b+1}\right)\ln \gamma$$

$$\therefore \ln W = \left[\frac{\ln(b+1) + \ln K}{(b+1)}\right] + \ln \left[\frac{2-(r_2 - r_1)^2 d}{2(r_2 - r_1)}\right] + \left(\frac{1}{b+1}\right)\ln \gamma \qquad (6.2.2.9)$$

Comparing equations (6.2.2.3) and (6.2.2.9), we get

$$\ln Kp = \frac{\ln\left\{\dfrac{K(b+1)[2-(r_2 - r_1)^2 d]^{b+1}}{2(r_2 - r_1)^{b+1}}\right\}}{(b+1)}$$

and

$$m = \left(\frac{1}{b+1}\right)$$

Again, if a graph of ln W vs ln γ is plotted, the gradients will be exactly the same as for Gwyn, but the intercepts will be different due to sieving variables.

Hence, it can be seen that the surface grinding model can be reduced to the Gwyn form for materials having both an uniform and non-uniform initial weight distribution. This shows that the Gwyn approach has a theoretical basis and that the value of d, which is the correction factor as applied to a non-uniform initial weight distribution, affects the value of K_p.

Thus, three models have been formulated to develop a theoretical basis for the attrition process. The fracture model was based on first order kinetics which was modified to allow for high initial attrition. The three parameter model was not very suitable for some of the materials tested, probably due to the inherent inaccuracies in the theory. The surface grinding model based on particle radius proved hard to use because grinding data was prone to error. The radius reduction model, though conceived for surface abrasion, was suitable in describing the grinding process for almost all of the test materials. This was a two parameter fit and reduced to the Gwyn formulation in certain circumstances. The balance of evidence in materials tested so far favours the use of the Gwyn formulation.

6.3 Effect of Normal Stress

An increase in normal stress increases the rate of attrition, as more fine material is produced at higher stresses. The effect of increasing normal stress was investigated for molecular sieve and PDV salt where the former attrites mainly by shelling and the latter by shattering. When the Gwyn coefficients are analysed (Fig. 6.1.1), it is seen that increasing the normal stress increases m but K_p remains relatively unchanged. Thus it is concluded that m is a function of normal stress.

Using experimental data for molecular sieve and PDV salt, exhaustive attempts were carried out to obtain relationships on a physical basis. A relationship was tried where the weight attrited was plotted as a function of energy supplied, the product of stress and strain, but a satisfactory relationship was not obtained (Fig. 6.3). Empirical correlations were also attempted where the power of the stress term was varied, but these also failed to produce a good correlation.

The first order kinetics fracture model was also examined (Table 6.2.1). It is seen that as stress increases, the value of m_i increases for PDV salt whilst m_r decreases and k varies in a random manner. For molecular sieve, an increase in normal stress decreases m_i and m_r and k again varies in an uncorrelated manner. Thus, it was not possible to isolate the influence of stress on these variables.

If a graph of m against normal stress (σ) is plotted (Fig. 6.3.1), a linear relationship of the form $m = a\sigma + b$ is obtained by applying linear regression.

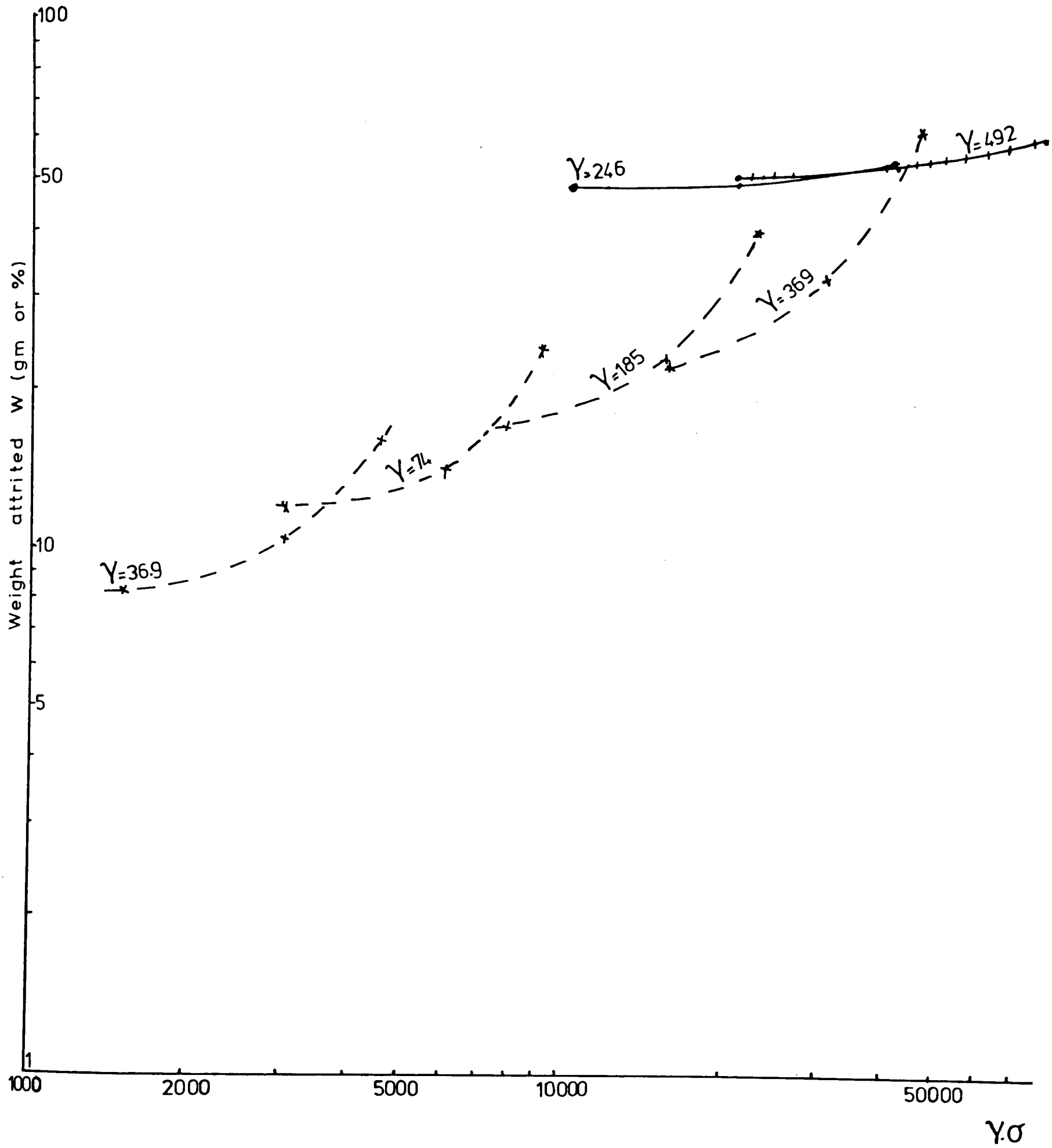


Fig 6.3. Attrition vs energy input (strain γ × stress σ) for Molecular Sieve (broken lines) and PDV Salt (solid lines) at constant strain γ

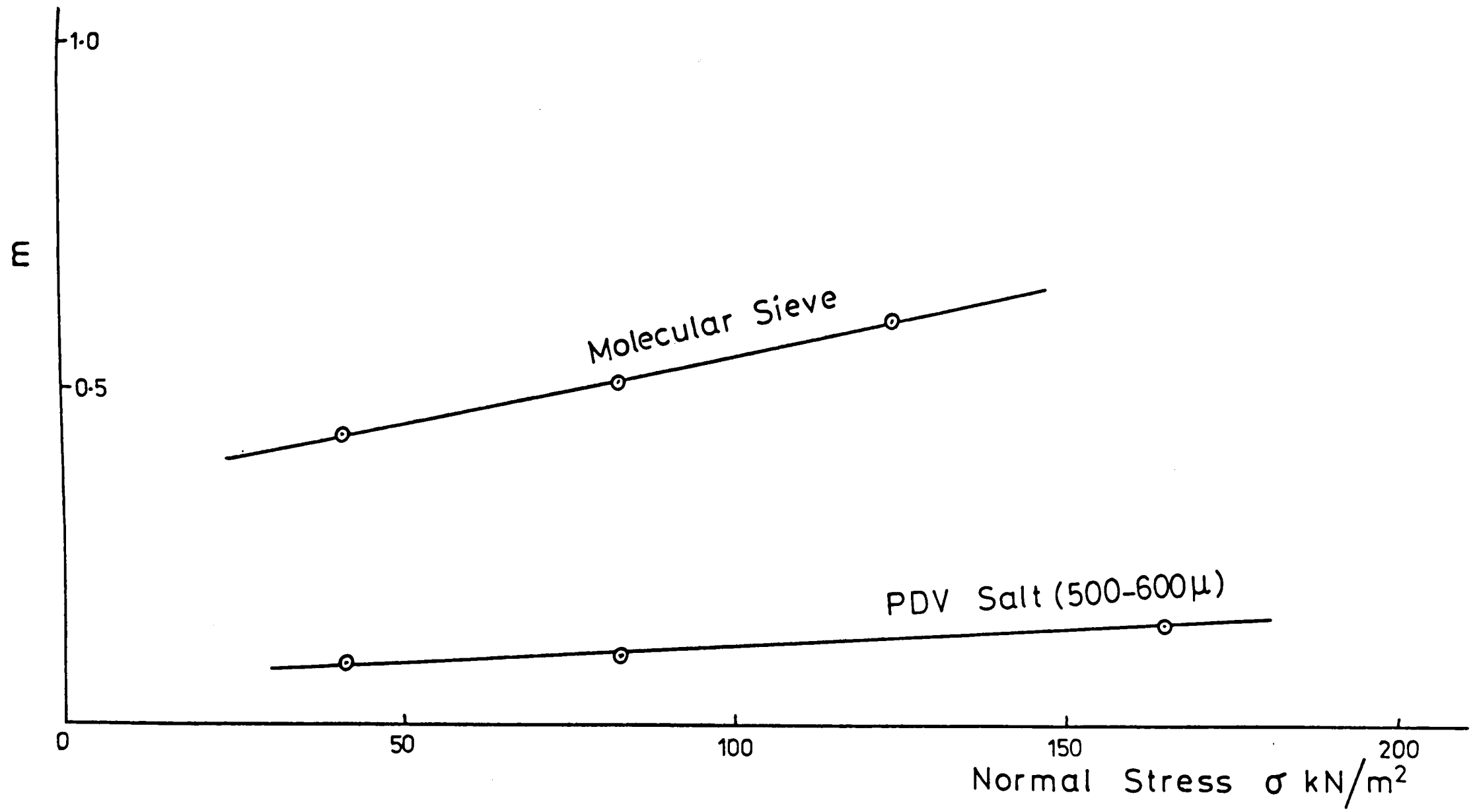


Fig.6.3.1. Variation of Gwyn coefficient m (gradient) with Normal Stress σ

molecular sieve $m = 0.002\,\sigma + 0.343$

PDV salt $m = 0.0005\,\sigma + 0.065$

The Gwyn equation $W = K_p\,\gamma^m$ may be written in logarithmic form as

$$\ln W = \ln K_p + m \ln\gamma$$

Differentiating at constant σ

$$dW/d\gamma = mW/\gamma \qquad (6.3.1)$$

where m is now dependent on the normal stress σ.

When a graph of shear strain vs. normal stress at constant attrited weight (for the same initial starting weight of 100 gm) is plotted, a series of curves were obtained (Fig. 6.3.2 and Fig. 6.3.3) which appeared to converge as the stress increased. The shapes of the curves were such that it was possible to express them empirically as a logarithmic function

$$\gamma = -K_1 \ln\sigma + \text{constant}$$

A plot of $|\gamma|$ vs. $\ln\sigma$ is shown in Fig. 6.3.4 and Fig. 6.3.5 for molecular sieve and PDV salt. The lines are seen to converge to a point which corresponds to a stress denoted by σ_{max}; σ_{max} may be considered to be the limiting stress at which particles attrite rapidly.

$K_1 = f(W)$ and is denoted by $K_1(W)$, the attrited weight function

$$\therefore \quad \gamma = -K_1(W) \ln(\sigma/\sigma_{max}) \qquad (6.3.2)$$

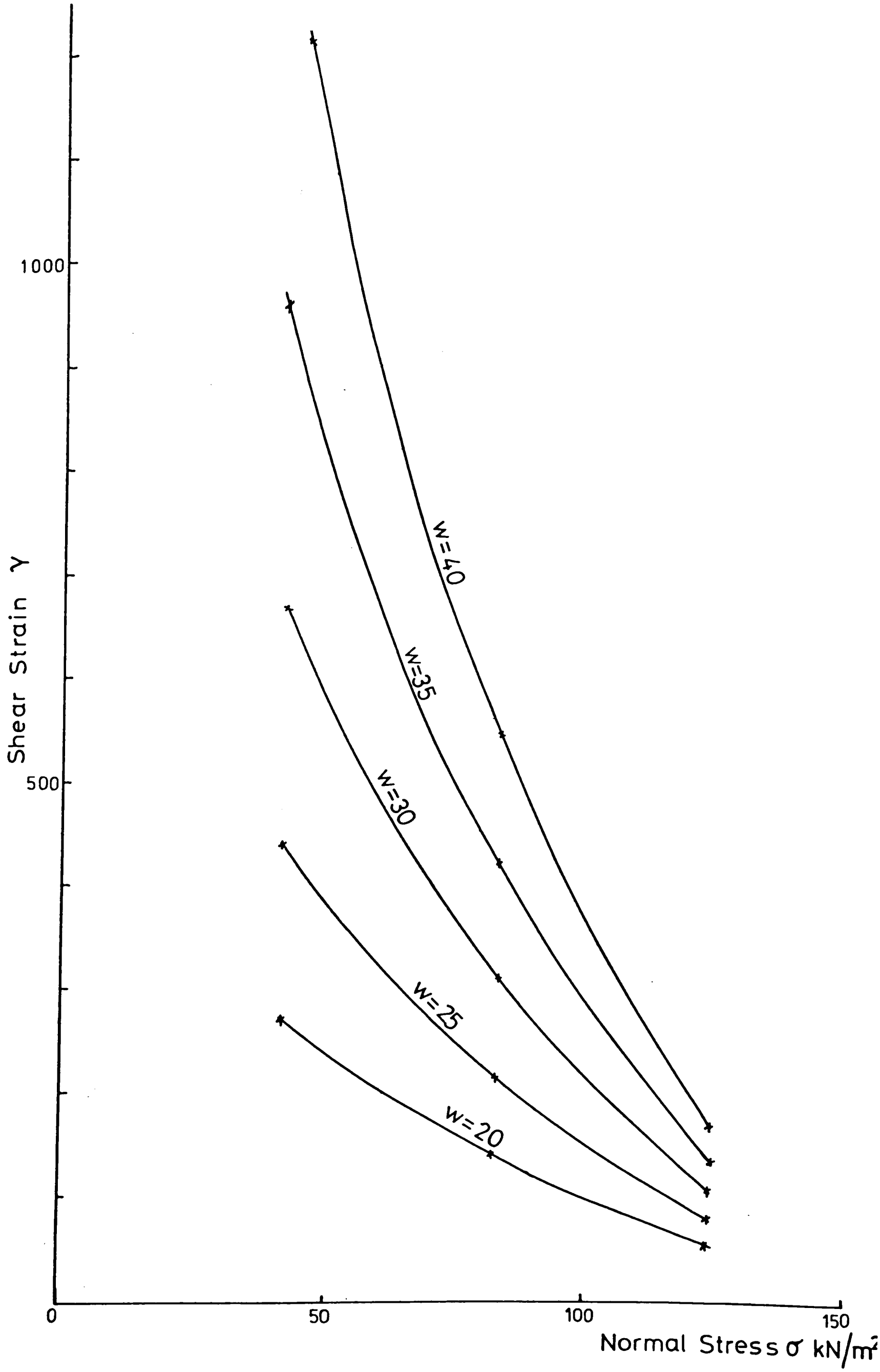


Fig.6.3.2. Variation of Shear Strain γ with Normal Stress σ at constant attrited weight (w) for Molecular Sieve

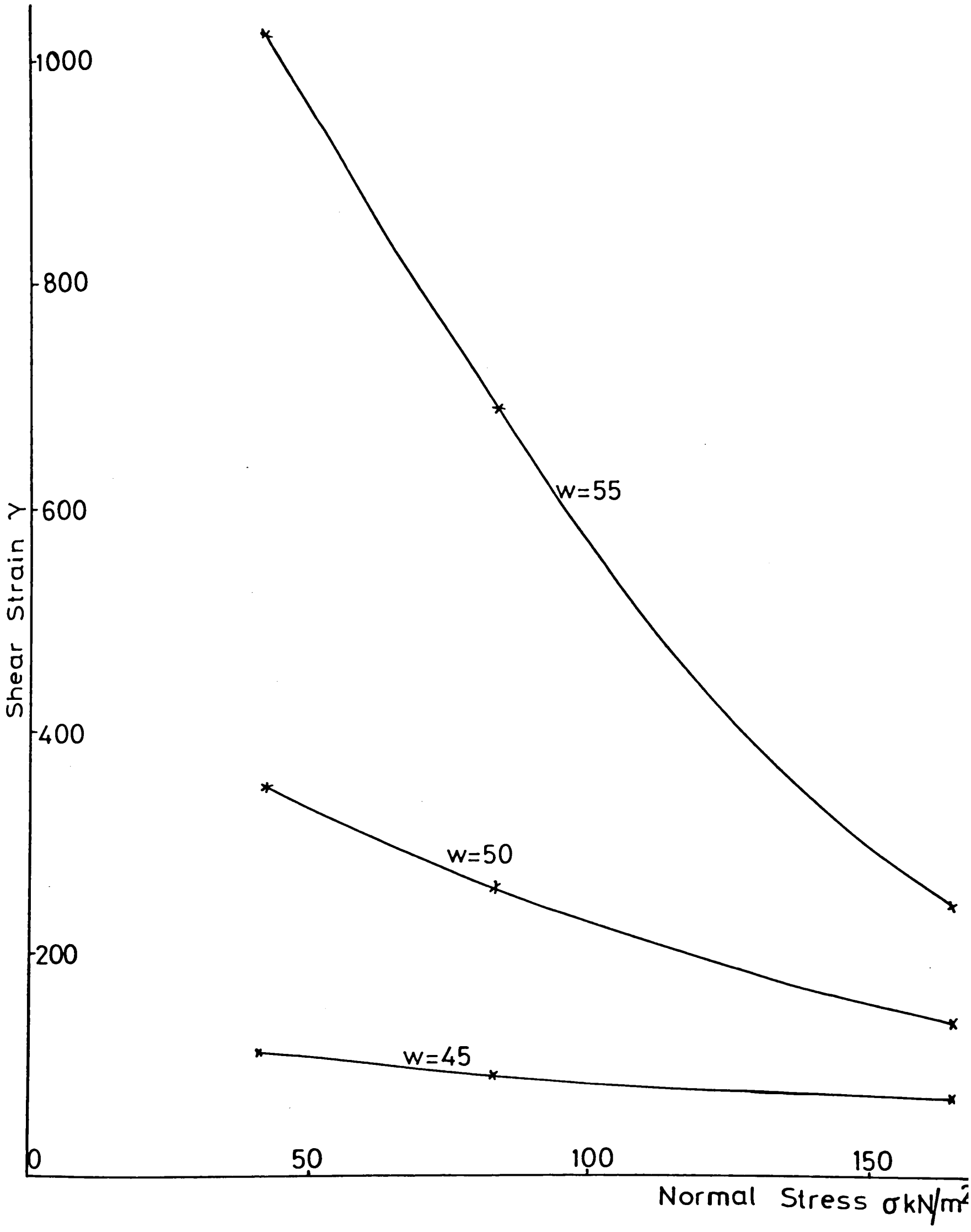


Fig.6.3.3. Variation of Shear Strain with Normal Stress at constant attrited weight (w) for PDV Salt (500–600 μm)

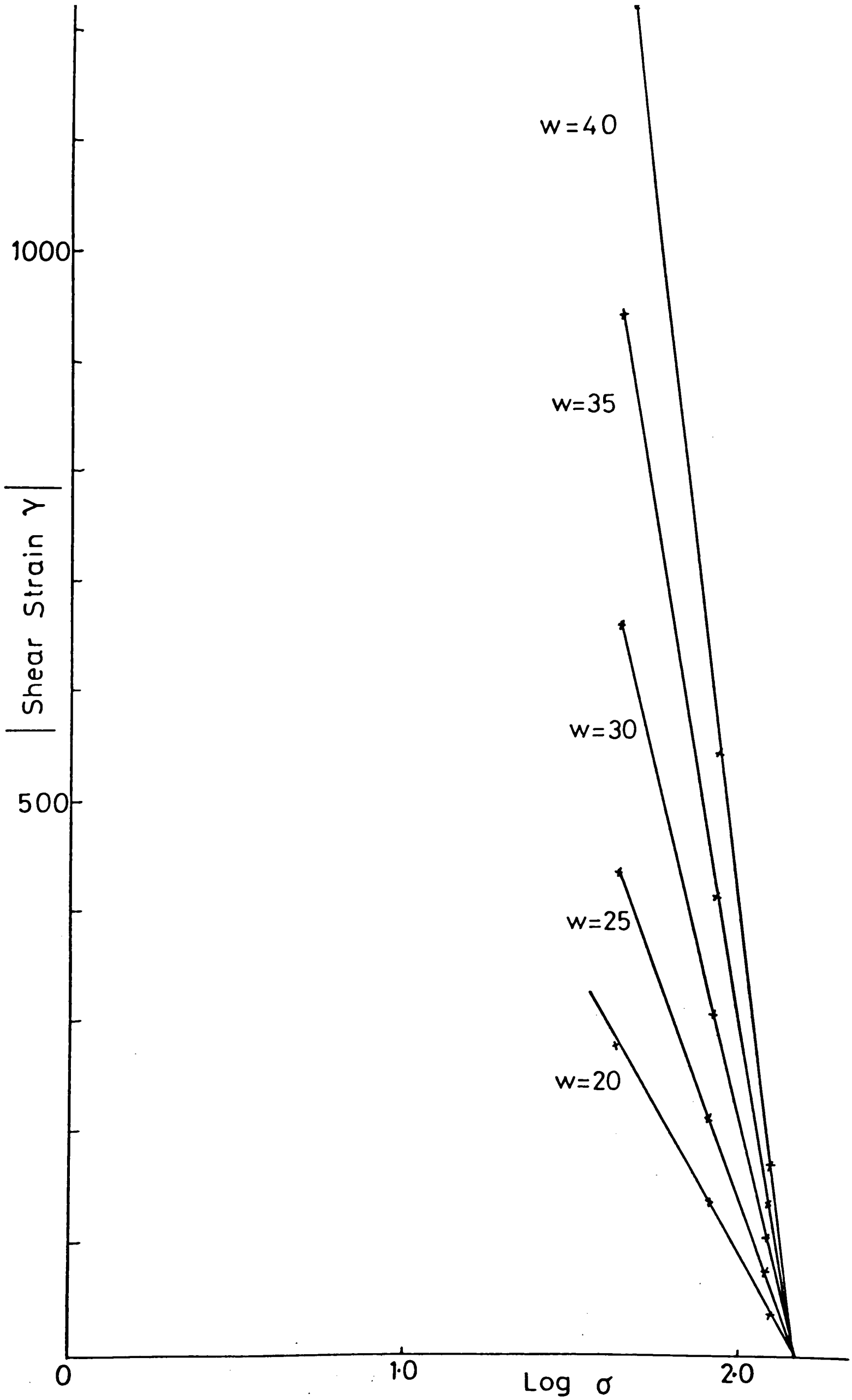


Fig. 6.3.4. Variation of |Shear Strain γ| with Log (Normal Stress σ) at constant attrited weight (w) for Molecular Sieve

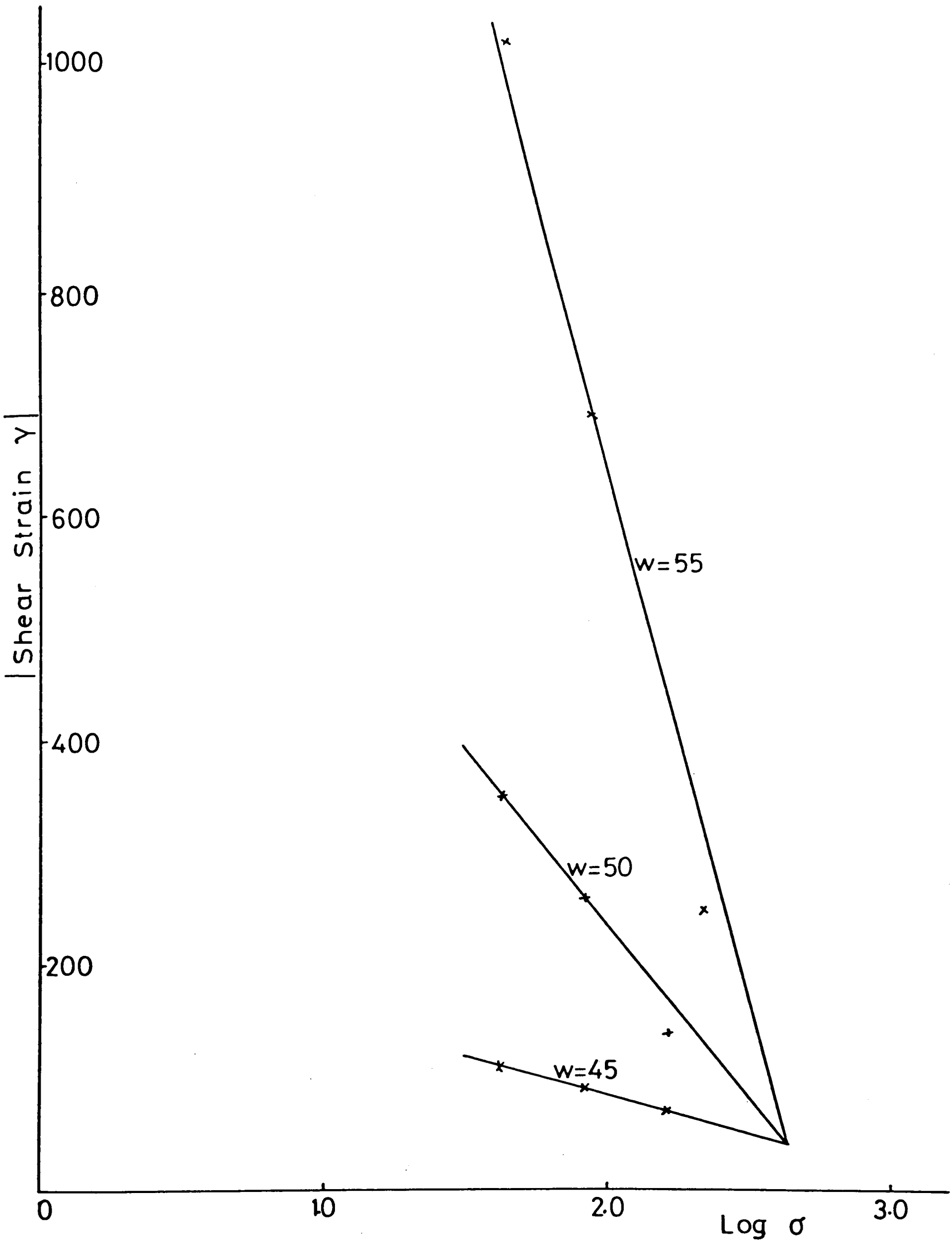


Fig. 6.3.5. Variation of |Shear Strain γ| with Log (Normal Stress σ) at constant attrited weight (w) for PDV Salt (500-600 μm)

For molecular sieve, σ_{max} is seen to lie very close to the normal stress axis, but for PDV salt it is seen to be displaced by an amount of strain γ_o approximately equal to 50. This may be caused by the attrition of PDV salt by bodily fracture and high initial attrition is observed at small strains. Fig. 4.2.12 shows that linear attrition behaviour is lost at a strain of about 50 (corresponding to one revolution of the cell) and thus it is possible that a change in attrition mechanism occurs at this point, possibly a shift from fracture to surface grinding.

For PDV salt equation 6.3.2 has to be modified thus:

$$\gamma - \gamma_o = - K_1(W) \ln (\sigma/\sigma_{max}) \qquad (6.3.3)$$

In the case of molecular sieve γ_o is very small, thus perhaps indicating that there was no sharp change in its attrition behaviour.

If equation 6.3.3 is differentiated with respect to σ

$$\frac{d\gamma}{d\sigma} = - \frac{dK_1(W)}{d\sigma} \ln\left(\frac{\sigma}{\sigma_{max}}\right) - \frac{K_1(W)}{\sigma}$$

$$= \frac{-dK_1(W)}{dW} \cdot \frac{dW}{d\sigma} \cdot \ln\left(\frac{\sigma}{\sigma_{max}}\right) - \frac{K_1(W)}{\sigma}$$

If the realtionship between γ and σ is considered for constant W

$$dW/d\sigma = 0$$

$$\therefore \quad d\gamma/d\sigma = - \frac{K_1(W)}{\sigma} \qquad (6.3.4)$$

Considering the relationship between W and σ for constant γ

$$d\gamma/d\sigma = 0$$

$$\therefore \quad \frac{dK_1(W)}{dW} \cdot \frac{dW}{d\sigma} \cdot \ln\left(\frac{\sigma}{\sigma_{max}}\right) = -\frac{K_1(W)}{\sigma}$$

$$\therefore \quad \frac{dW}{d\sigma} = \frac{-K_1(W)}{\sigma.\ln(\sigma/\sigma_{max})} \cdot \frac{1}{\frac{dK_1(W)}{dW}}$$

$$= \frac{\gamma - \gamma_o}{\sigma} \cdot \frac{1}{\frac{dK_1(W)}{dW}} \qquad (6.3.5)$$

from equation 6.3.3.

Thus it would be possible to relate W to σ if the form of $\left(\frac{dK_1(W)}{dW}\right)$ was known.

A plot of $K_1(W)$ vs. W for molecular sieve and PDV salt is shown in Figure 6.3.6 from which $K_1(W)$ may be expressed as a function of W.

Attempts have been made to correlate the tensile strength of materials (Billam, 1972). The failure load for a single particle crushed between platens depends on the tensile strength of the material and the size and shape of the grain.

In general,

$$\sigma_t \propto P_c/d^2$$

where σ_t is the tensile strength and P_c the failure load for a grain of equivalent sieve diameter d.

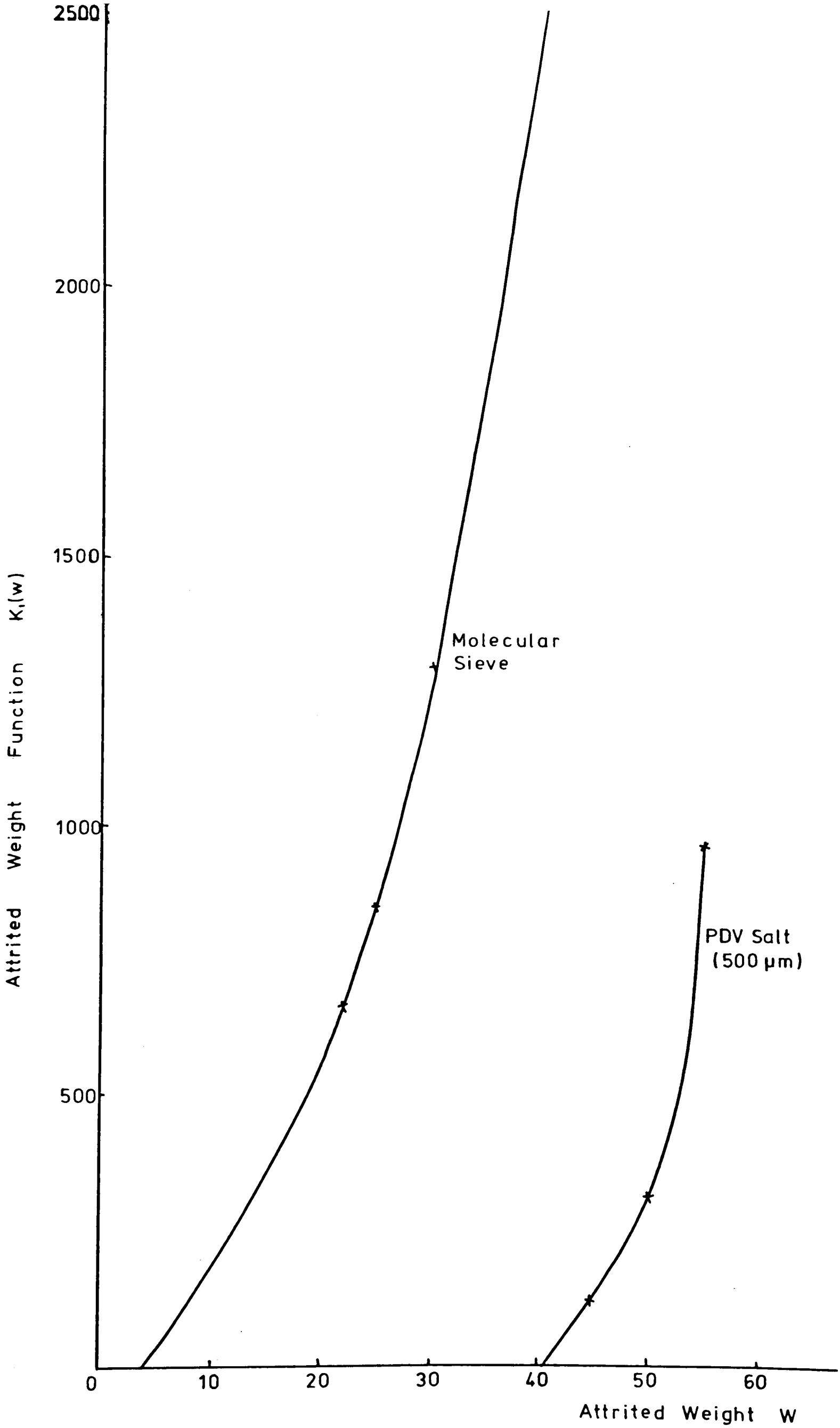


Fig. 6.3.6. Attrited weight function as a function of Attrited weight

Capes (1976) reports the crushing strength of agglomerates between two flat parallel plates. The failure load L is correlated with pellet diameter d by an equation of the form

$$L = kd^n$$

where k is a parameter related to the cohesive forces acting between particles and d^n takes into account the bonded area of the disc over which tensile failure occurs. Since the mode of fracture of a granule is complex and as the contact area will change with load, the values for the breaking load may not be very accurate.

The functional form of Archard and Holm's models state that wear is directly proportional to stress (or load) and strain. However, when the results obtained from the attrition cell are examined it is seen that this is not so. Furthermore, when attempts were made to correlate the attrited weight with the normal stress raised to a power (2/3 or 1) none was found. Since the area of contact is proportional to either $N^{2/3}$ (Hertz) or N (Archard's extended form), this would also indicate that the models of Archard and Holm are not directly applicable to data obtained from the attrition cell.

Considering the equations of Capes (1976) and Griffith (1920) in a simple form, it is seen that they both would require step functions when stress is increased. In the case of Griffith, it is the crack length c which is rate controlling, the presence of which is difficult to predict.

When contact stresses are considered (Molerus 1975, Appendix A),

it is seen that inter-particle forces (load) are directly proportional to the applied stress. The wear theories state that attrition is directly proportional to normal load. Thus, attrition must be directly proportional to the normal stress, but results obtained from the attrition cell show that this is not true for that system. This must mean that the role of normal stress on attrition is far more complicated, and the consideration of the following factors may be directly relevant: particle shape, rotation, crack length, work hardening/softening.

In identifying the effect of normal stress on particle attrition, a simple linear relationship between the Gwyn coefficient (m) and the applied normal stress has been obtained. Kinetic models have been formulated where the attrited weight has been directly related to the normal stress. This model has been linked to the Gwyn equation by parameters which are stress dependent. Applied normal stresses have been related to inter-particle contact forces which have been separated to account for surface wear and fracture. Empirical relationships for the tensile strength of agglomerates have also been considered.

CHAPTER SEVEN

CONCLUSION

The development of the attrition cell has enabled grinding mechanisms to be investigated under controlled experimental conditions where powder behaviour was studied in a simulated failure zone. Cell design and operating techniques were kept as simple as possible and a broad range of experiments has been carried out without any need for modification to the equipment.

In characterising the performance of the cell, reproducibility of results was ascertained. For any material ground in the cell, reproducible particle size distributions were obtained indicating that cell behaviour was consistent. In general, a fixed energy input for attrition per unit mass of material resulted in uniform particle size distributions, establishing systematic particle behaviour. The cell was used to attrite particles of different initial shapes and sizes whilst controlling the basic physical variables such as normal stress and strain rate.

For the different materials tested, increasing normal stress raised the production of fine particles as did shear strain, but strain rate, sample history and the segregation of particles in the cell did not significantly affect attrition rates. For all materials, the relationship between unground weight fractions and grinding time followed the empirical attrition law due to Gwyn.

Particle attrition in the present work occurs mainly due to fracture or surface grinding. Soda ash and lab salt attrite mainly by surface

grinding where edges and corners are gradually lost. PDV salt attrites by bodily fracture whereas molecular sieve and granular salt undergo radial shattering during initial attrition. Prolonged grinding shows that the fractured particles lose edges and sharp corners by surface grinding. Thus, it is seen that both mechanisms are often present when particle diminution occurs.

Simple kinetic models were formulated for a material initially having a narrow size distribution. In all of these, the final result could be presented in terms of the material that is retained on the sieve.

The three models studied employed the following bases:

(i) the rate of loss of the coarsest sieve fraction with strain is proportional to the mass contained in the coarsest sieve fraction.

(ii) the rate of reduction of the radius of a particle with strain is proportional to the radius of the particle raised to some power.

(iii) the rate of reduction of the radius of a particle with strain is proportional to the change of radius from its initial value raised to some power.

On physical grounds, the first model was thought to be more appropriate to a fracture mechanism, the others to a surface grinding process where corners and edges are removed. Modifications had to be carried out to the first order fracture model to allow for initially high attrition rates. The radius reduction model has been shown to reduce to the Gwyn formulation under certain conditions.

The Gwyn coefficient (m) is seen to vary linearly with normal stress. A simple kinetic model was developed which related the normal stress and strain to the attrited weight. A further model related the applied normal stress to fracture and surface wear through inter particle contact forces.

The study of attrition mechanisms in a controlled environment within the failure zone of the attrition cell has enabled complex powder behaviour to be reduced to a level where quantitative models can be established. An awareness of the fundamental mechanisms and the way they may interact provides a foundation for the interpretation of behaviour in complicated practical systems.

A number of areas in attrition can be identified in which further investigations would be useful.

(i) The influence of particle formation method.

(ii) The effect of temperature.

(iii) The significance of moisture and associated water levels in particles, including slurries.

(iv) Investigation of other types of material, eg. plastics.

(v) Understanding the influence of initial particle size distribution.

(vi) Relationship of cell behaviour to equipment performance.

Study of such areas would promote a much fuller understanding of the attrition process.

APPENDIX A

Consider a very small element of material in the annulus of the attrition cell. The stress equations of motion for this element in cylindrical coordinates are

$$\frac{\partial \sigma_{rr}}{\partial r} + \frac{1}{r}\frac{\partial \tau_{\theta r}}{\partial \theta} + \frac{\sigma_{rr} - \sigma_{\theta\theta}}{r} + \frac{\partial \tau_{zr}}{\partial z} + \alpha = R$$

$$\frac{\partial \sigma_{zz}}{\partial z} + \frac{\tau_{rz}}{r} + \frac{\partial \tau_{rz}}{\partial r} + \frac{1}{r}\frac{\partial \tau_{\theta z}}{\partial \theta} + \beta = Z$$

$$\frac{1}{r}\frac{\partial \sigma_{\theta\theta}}{\partial \theta} + \frac{\partial \tau_{r\theta}}{\partial r} + \frac{2\tau_{r\theta}}{r} + \frac{\partial \tau_{z\theta}}{\partial z} + \gamma = \theta$$

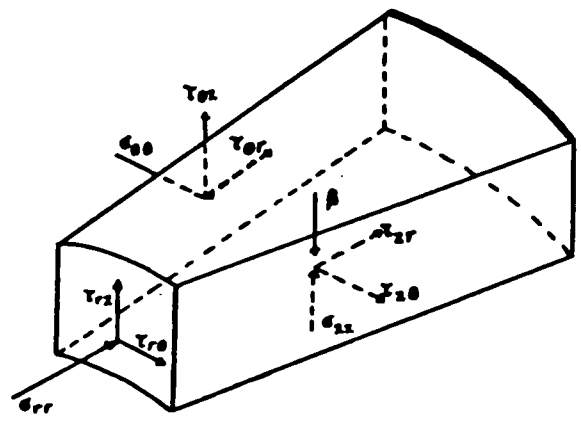
where α, β, γ and R, Z, θ are the components of body and acceleration forces in the r, z, and θ directions. Since the particles in the annulus are not being accelerated and the weight of the element acts only in the z direction, the stress equations at dynamic equilibrium may be obtained (Fig. A.1), thus

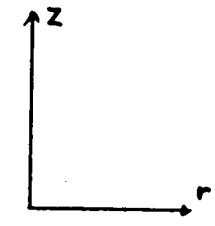
$$\frac{\partial \sigma_{zz}}{\partial z} + \frac{\tau_{rz}}{r} + \frac{\partial \tau_{rz}}{\partial r} + \frac{1}{r}\frac{\partial \tau_{\theta z}}{\partial \theta} = -\beta$$

$$\frac{\partial \sigma_{rr}}{\partial r} + \frac{1}{r}\frac{\partial \tau_{\theta r}}{\partial \theta} + \frac{\sigma_{rr} - \sigma_{\theta\theta}}{r} + \frac{\partial \tau_{zr}}{\partial z} = 0$$

$$\frac{1}{r}\frac{\partial \sigma_{\theta\theta}}{\partial \theta} + \frac{\partial \tau_{r\theta}}{\partial r} + \frac{2\tau_{r\theta}}{r} + \frac{\partial \tau_{z\theta}}{\partial z} = 0$$

In the first equation, since there is no variation of torque or normal stress along the θ plane,





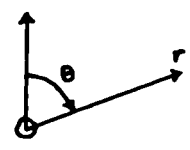


Fig. A.1. The stresses acting on a differential stress element

$$\therefore \frac{\partial \tau_{\theta z}}{\partial \theta} = 0$$

$$\therefore \quad \frac{\partial \sigma_{zz}}{\partial z} + \frac{\tau_{rz}}{r} + \frac{\partial \tau_{rz}}{\partial r} = -\beta$$

$$\frac{\partial \sigma_{zz}}{\partial z} = -\beta - \frac{\tau_{rz}}{r} - \frac{\partial \tau_{rz}}{\partial r}$$

$$= -\beta - \frac{1}{r}\frac{d}{dr}\left(r\tau_{rz}\right)$$

If τ_{rz} is assumed to be negligible (since vertical movement in the annulus is very small compared to horizontal displacement), then

$$\frac{\partial \sigma_{zz}}{\partial z} = -\beta$$

$$\int_{\sigma_n}^{\sigma_{zz}} d\sigma_{zz} = -\beta \int_{0^-}^{z} dz$$

where σ_n—applied normal stress on the element.

$$\therefore \sigma_{zz} - \sigma_n = -\beta z.$$

Since $\sigma_n >>> \beta z$

$$\sigma_{zz} = \sigma_n = \text{constant}.$$

Thus there is no change in the normal stress in the z direction.

Consider the other equations together. Again, since there is no variation of torque or normal stress on the θ plane,

$$\frac{\partial \sigma_{\theta\theta}}{\partial \theta} = \frac{\partial \tau_{\theta r}}{\partial \theta} = 0$$

$$\therefore \quad \frac{\partial \sigma_{rr}}{\partial r} + \frac{\sigma_{rr} - \sigma_{\theta\theta}}{r} + \frac{\partial \tau_{zr}}{\partial z} = 0$$

$$\frac{\partial \tau_{r\theta}}{\partial r} + \frac{2\tau_{r\theta}}{r} + \frac{\partial \tau_{z\theta}}{\partial z} = 0$$

Since there is negligible upward movement, compared to the θ direction, in the r plane,

$$\frac{\partial \tau_{zr}}{\partial z} = 0$$

$$\therefore \quad \frac{\partial \sigma_{rr}}{\partial r} + \frac{\sigma_{rr} - \sigma_{\theta\theta}}{r} = 0$$

$$\frac{\partial \tau_{r\theta}}{\partial r} + \frac{2\tau_{r\theta}}{r} + \frac{\partial \tau_{z\theta}}{\partial z} = 0.$$

It was not possible to simplify these equations any further since the relationship between $\sigma_{\theta\theta}$, σ_{rr} and σ_{zz} is unknown.

Timoshenko (1970) considered the pressure distribution between two spherical bodies in contact. He calculates that the distribution of pressures over the contact surface is represented by the ordinates of a hemisphere constructed on the surface of contact and that the maximum pressure was 1.5 times the average stress on the contact surface. If material properties of the particles were known, it

was possible to compute the area of contact and hence the maximum pressure.

Inter-particle contact may be considered more generally. Consider the transmission of contact forces in a packing of spheres. Geometric isotropy is assumed, i.e. the contact points are equally distributed over the surface of the particles when many are considered (Molerus, 1975).

In a sphere of radius r having a coordination number c, the average number of contacts C per surface element dS is

$$C = \frac{c\,dS}{4\pi r^2}$$

Let σ be the compressive stress (σ_{zz} or σ_n) transmitted through the packing acting on the particles and let this stress act on an arbitrary plane $\overline{gg}$ (Fig. A.2a). Let a sphere cut by the plane $\overline{gg}$ have its centre at a distance λ from the plane (Fig. A.2b). If $\overline{gg}$ cuts n particles, the number of particles at a distance λ and $\lambda + d\lambda$ is

$$n_\lambda = \frac{n}{r}\, d\lambda$$

because of equal probability for any plane of cut in a random packing.

Let F be the resultant of a shear force (due to shear stress τ) and a normal force (due to normal stress σ) acting on a particle making an angle α with the normal to the surface. This force can be resolved normal to the plane $\overline{gg}$ $[F \cos(\phi + \alpha)]$ and along the plane $\overline{gg}$ $[F \sin(\phi + \alpha)]$, where ϕ is the angle the vertical component makes with the normal to the surface.

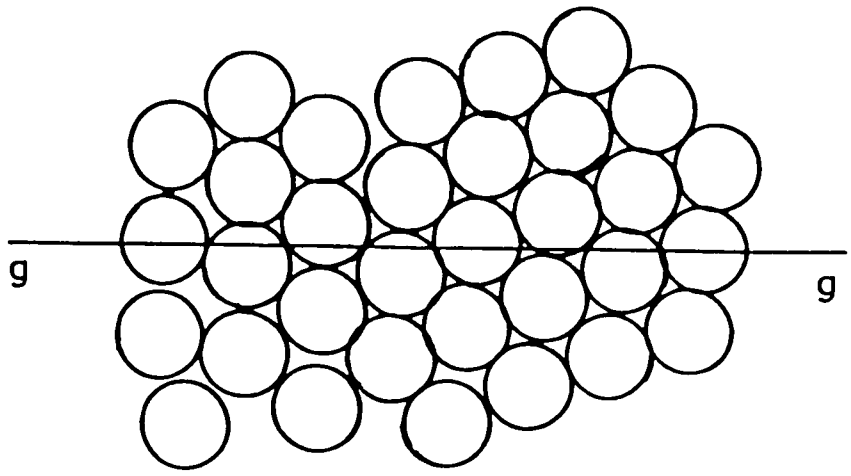


Fig.A.2.a. A plane $\overline{gg}$ in the packing

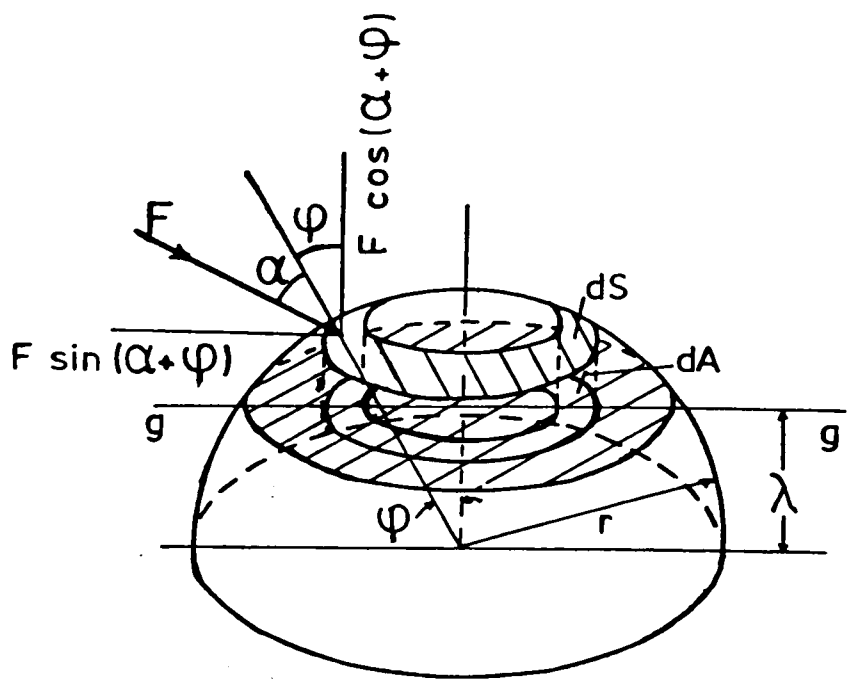


Fig. A.2.b. Force in an inter particle contact

Considering the normal forces first, the total force (dB) transmitted by all the particles between λ and $\lambda + d\lambda$ is

$$dB = \left[\frac{c}{4\pi r^2} \int_S F \cos(\phi + \alpha)\, dS \right] n \frac{d\lambda}{r}$$

If no assumptions are made about the magnitude of the force F, then F is a function of position (λ) and ϕ where

$$\lambda = r \cos\phi$$

The total compressive normal force transmitted on the $\overline{gg}$ plane is

$$B = \frac{cn}{4\pi r^3} \int_o^r d\lambda \int_S F \cos(\phi + \alpha) dS \qquad (A1)$$

The area of a particle cut by the $\overline{gg}$ plane between λ and $\lambda + d\lambda$ is

$$dA_p = \pi(r^2 - \lambda^2)\, n \frac{d\lambda}{r}$$

$\therefore$ Total area of particles cut by $\overline{gg}$ is

$$A_p = \int_o^r \pi(r^2 - \lambda^2)\, n \frac{d\lambda}{r} = \frac{2\pi r^2 n}{3}$$

For a random packing, the volume void fraction (ε) is equal to the void fraction in the plane of the cut, thus

$$A_p = A(1-\varepsilon)$$

where A is the total area of the plane cut by $\overline{gg}$.

Hence, $n = \frac{3A(1-\varepsilon)}{2\pi r^2}$

Insertion of n into the equation for B (equation A1) yields the total compressive normal force transmitted on the plane $\overline{gg}$.

$$\therefore \quad B = \frac{3cA(1-\varepsilon)}{8\pi^2 r^5} \int_o^r d\lambda \int_S F \cos(\phi + \alpha) dS$$

Thus, the relationship between the normal stress (σ) and the contact force (F) on the plane is given by

$$\sigma = B/A$$

$$\text{or} \quad \sigma_{zz} = \frac{3c(1-\varepsilon)}{8\pi^2 r^5} \int_o^r d\lambda \int_S F \cos(\phi + \alpha) dS \qquad \text{(A2)}$$

For forces along the plane $\overline{gg}$ (i.e. shear forces) an identical procedure is followed, except that the total force (dB_1) transmitted is now given by

$$dB_1 = \left[\frac{c}{4\pi r^2} \int_S F \sin(\phi + \alpha) dS\right] n \frac{d\lambda}{r}$$

This gives rise to a shear stress τ where

$$\tau = \frac{3c(1-\varepsilon)}{8\pi^2 r^5} \int_o^r d\lambda \int_S F \sin(\phi + \alpha) dS$$

If the $\overline{gg}$ plane can be constrained to be the shear plane ϕ in the attrition cell, τ and σ may be related on the shear plane by the equation (in the absence of cohesion)

$$\tau = \mu\sigma$$

where μ is the coefficient of the internal angle of friction.

Thus

$$\frac{3c(1-\varepsilon)}{8\pi^2 r^5} \int_0^r d\lambda \int_S F \sin(\phi + \alpha)\, dS = \mu . \frac{3c(1-\varepsilon)}{8\pi^2 r^5} \int_0^r d\lambda \int_S F \cos(\phi + \alpha) dS$$

This gives

$$\mu = \tan \phi_u = \tan(\phi + \alpha)$$

where ϕ_u is the angle of internal friction for the powder.

Hence $\phi_u = \phi + \alpha$

or $|\alpha| = \phi_u - \phi$

i.e. $\alpha = f(\phi)$ since ϕ_u is a constant for a particular material.

The resultant force F can be divided into a tangential force ($F \sin\alpha$) and a normal force ($F \cos\alpha$) at its point of contact. It can be argued that the component ($F \sin\alpha$) gives rise to surface wear and the component ($F \cos\alpha$) gives rise to fracture of the particles. Thus, over the surface of the particle each contact force may be divided in the same way to give components promoting fracture and wear.

When $\alpha = 0$, the resultant force acts normal to the surface and this force may be associated with promoting total fracture of the material.

For this condition, $(\phi_u - \phi) = 0, \pi, 2\pi.....$
giving rise to points of total fracture on a sphere (Fig. A.3a).

When $\alpha = 90^\circ$, the resultant force acts along the surface, and this may be associated with total wear of the material.

For this to occur (Fig. A.3a),

$$\phi_u - \phi = \pi/2, 3\pi/2, 5\pi/2.....$$

It is seen that $\alpha = 0$ occurs at two specific points on the sphere, as when $\alpha = 90^\circ$. Thus it would seem reasonable to assume that there would be two points of pure fracture and two points where total surface wear occurs, at planes 90° to each other.
Particles would then degrade along these points if they did not possess any structural weaknesses.

These two special cases may be thought of as limiting conditions for α. At all other points on the sphere, both fracture and surface wear components would be present and would result in both mechanisms occurring in practice.

From the above, it is also possible to relate the shear plane to the angle of internal friction of the powder in the cell (Fig. A.3b).

If it can be assumed that the resultant force F is constant over the surface of the sphere, the following simplifications may be carried out to the stress equations.

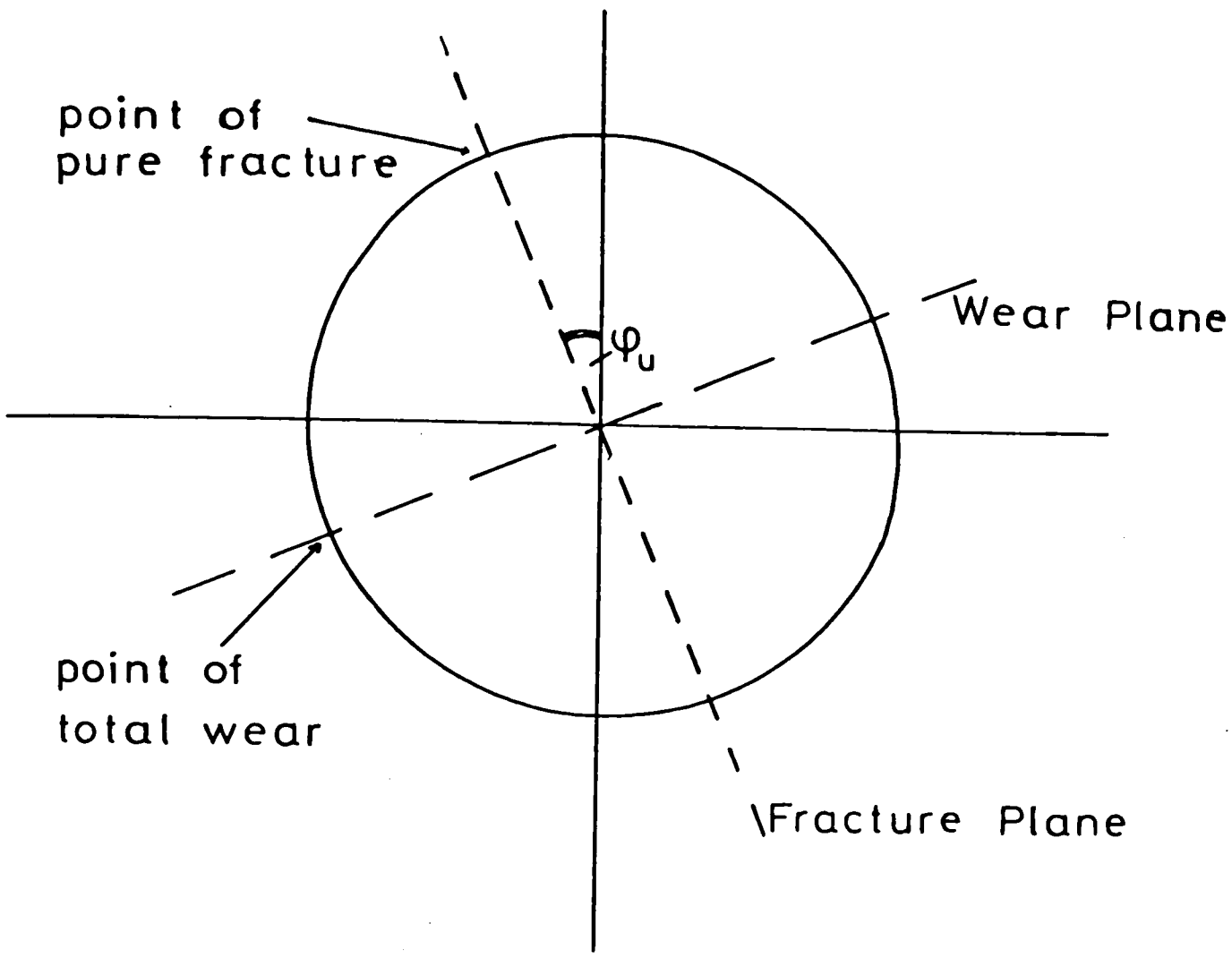


Fig. A.3.a. Fracture and Wear planes on a sphere

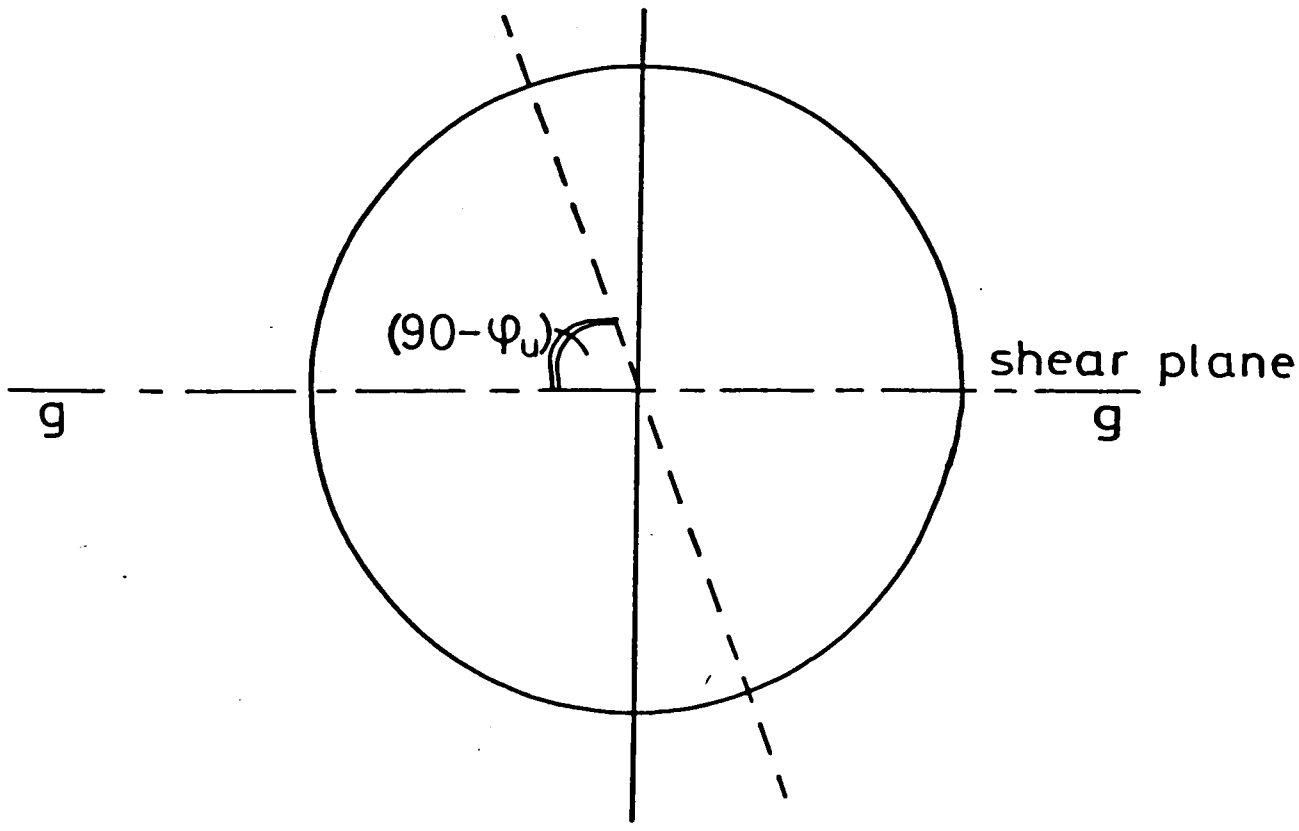


Fig. A.3.b. Relating shear plane $\overline{gg}$ to φ_u

$$\sigma_{zz} = \frac{3c(1-\varepsilon)}{8\pi^2 r^5} \int_0^r d\lambda \int_S F \cos(\phi + \alpha) dS$$

Since it has been shown that $\phi + \alpha = \phi_u$, which is constant for a particular material,

$$\sigma_{zz} = \frac{3c\ F(1-\varepsilon)\ \cos\phi_u}{8\pi^2 r^5} \int_0^r d\lambda \int_S dS$$

Since $dS = \frac{dA_t}{\cos\phi}$ from Fig. A.2b

$$A_t = \pi(r^2 - \lambda^2)$$

and $\lambda = r \cos \phi$

$$dS = \frac{-2\pi\lambda d\lambda}{(\lambda/r)} = -2\pi r d\lambda$$

$$\therefore \quad \sigma_{zz} = \frac{3cF\ (1-\varepsilon)\ \cos\ \phi_u}{8\pi^2 r^5} \int_0^r d\lambda \int_r^\lambda -2\pi r d\lambda$$

$$= \frac{3cF(1-\varepsilon)\ \cos\phi_u}{16\pi r^2}$$

Similarly,

$$\tau = \frac{3cF(1-\varepsilon)\ \sin\phi_u}{16\pi r^2}$$

Thus, the relationship $\tau = \mu\sigma$ is satisfied.

Hence, F can be determined from these equations. For a given value of ϕ, $F_{wear} = F \sin\alpha$ and $F_{fracture} = F \cos\alpha$ where $|\alpha| = \phi_u - \phi$. Thus the distribution of wear and fracture components may be computed over the surface of the sphere where $-\pi < \phi < \pi$.

If a uniform force distribution is assumed around the sphere, the normal force $N(\phi)$ is given by

$$N(\phi) = F \cos \alpha \text{ (fracture force)}$$

Since $\alpha = \phi_u - \phi$

$$N(\phi) = F \cos(\phi_u - \phi)$$

$$= F \cos\phi_u . \cos\phi + F \sin\phi_u . \sin\phi$$

Since uniform stresses are assumed,

$$\sigma_{zz} = \frac{3cF(1-\varepsilon) \cos\phi_u}{16\pi r^2}$$

$$\therefore \quad F \cos\phi_u = \frac{16\sigma_{zz}\pi r^2}{3c(1-\varepsilon)}$$

$$\tau = \frac{3cF(1-\varepsilon) \sin\phi_u}{16\pi r^2}$$

$$\therefore \quad F \sin\phi_u = \frac{16\tau\pi r^2}{3c(1-\varepsilon)}$$

$$\therefore\ N(\phi) = \frac{16\sigma_{zz}\pi r^2 \cos\phi}{3c(1-\varepsilon)} + \frac{16\tau\pi r^2 \sin\phi}{3c(1-\varepsilon)}$$

Since $\tau = \mu\sigma$

$$N(\phi) = \frac{16\sigma_{zz}\pi r^2}{3c(1-\varepsilon)} \left(\cos\phi + \mu \sin\phi\right)$$

$$= \frac{16\sigma_{zz}\pi r^2}{3c(1-\varepsilon)} \left(\frac{\cos\phi . \cos\phi_u + \sin\phi_u . \sin\phi}{\cos\phi_u}\right)$$

$$= \frac{16\sigma_{zz}\pi r^2}{3c(1-\varepsilon)} \cdot \frac{\cos(\phi_u - \phi)}{\cos\phi_u}$$

$$= \frac{16\sigma_{zz}\pi r^2}{3c(1-\varepsilon)} \cdot \frac{\cos\alpha}{\cos\phi_u}$$

The average stress $\sigma(\phi) = N(\phi)/$ area

$$= \frac{16\sigma_{zz}\pi r^2}{3c(1-\varepsilon)} \frac{\cos\alpha}{\cos\phi_u} \cdot \frac{1}{4\pi r^2}$$

$$= \frac{4\sigma_{zz}\cos\alpha}{3c(1-\varepsilon)\cos\phi_u}$$

The shear force $T(\phi) = F \sin\alpha$

$$= F \sin(\phi_u - \phi)$$

$$= F \sin\phi_u \cos\phi - F \cos\phi_u \sin\phi$$

An identical procedure to the above is followed to obtain

$$T(\phi) = \frac{16\pi r^2 \sigma_{zz}}{3c(1-\varepsilon)} \cdot \frac{\sin\alpha}{\cos\phi_u}$$

$$\text{Thus } \tau(\phi) = \frac{4 \sin\alpha \, \sigma_{zz}}{3c(1-\varepsilon)\cos\phi_u}$$

It is now possible to relate these forces to traditional wear theories. When particles fracture, Griffith calculated that the breaking stress P was related to crack length by

$$P = \sqrt{\frac{2Eq}{\pi c}}$$

From the stress equations calculated,

$$P = \sigma(\phi) = \frac{4\sigma_{zz} \cos\alpha}{3c(1-\varepsilon)\cos\phi_u}$$

$$\text{Thus } \frac{4\sigma_{zz} \cos\alpha}{3c(1-\varepsilon)\cos\phi_u} = \sqrt{\frac{2Eq}{\pi c}}$$

Thus if the material properties of the particles are known, it is possible to relate the applied normal stress to breakage.

Archard's wear theory states that the worn volume per unit sliding distance W is given by

$$W = \frac{KN}{p_m}$$

where N is the normal load and p_m the flow pressure of the material. Since N in this case is equal to $T(\phi)$,

$$W = \left(\frac{16\pi r^2 \sigma_{zz}}{3c(1-\varepsilon)} \; \frac{\sin\alpha}{\cos\phi_u} \right) \; \frac{K}{p_m}$$

Again, if material properties are known, then W can be computed.

Holm derived a wear depth h for a material where

$$h = \frac{kPL}{p_m}$$

P is the average normal stress over the nominal contact area and L the sliding distance.

P may be equated to $\tau(\phi)$

where $\tau(\phi) = \dfrac{4\sin\alpha \; \sigma_{zz}}{3c(1-\varepsilon)\cos\phi_u}$

Thus $h = \dfrac{k \; L}{p_m} \left(\dfrac{4\sin\alpha \; \sigma_{zz}}{3c(1-\varepsilon)\cos\phi_u} \right)$

APPENDIX B

Examples of failure zone identification and velocity profiles are shown in Figs. B.1, B.2 and B.3 for glass beads, molecular sieve and granular sodium chloride. The glass beads were only used in preliminary runs to identify the failure zone depth and were not used in any further experiments. It was not possible to rigorously identify the depth of the failure zone for the finer particles (PDV salt, soda ash), as it was very difficult to separate particle layers to accurately locate the position of tracer on account of their size. The smaller particles were also prone to greater attrition at corresponding strains which resulted in a large spread of tracer at the different depths. As a result, the failure zone identification was confined to the larger materials.

The results are presented as a plot of vertical linear position (z) against horizontal displacement (x), the latter being equivalent to the horizontal velocity as a percentage of the cell velocity. This can be regarded as a direct measure of the velocity profile across the failure zone. The linear velocity profile indicates that all the particles are within the failure zone depth for that powder. A depth of approximately twenty particle diameters was obtained for the 1 mm glass beads and about eleven particle diameters for molecular sieve and granular sodium chloride. This would indicate that incomplete velocity profiles have been obtained for the larger materials but they e linear and expected to match those of deeper beds for the same material (Stephens, 1976).

Stephens carried out extensive investigations into the formation of

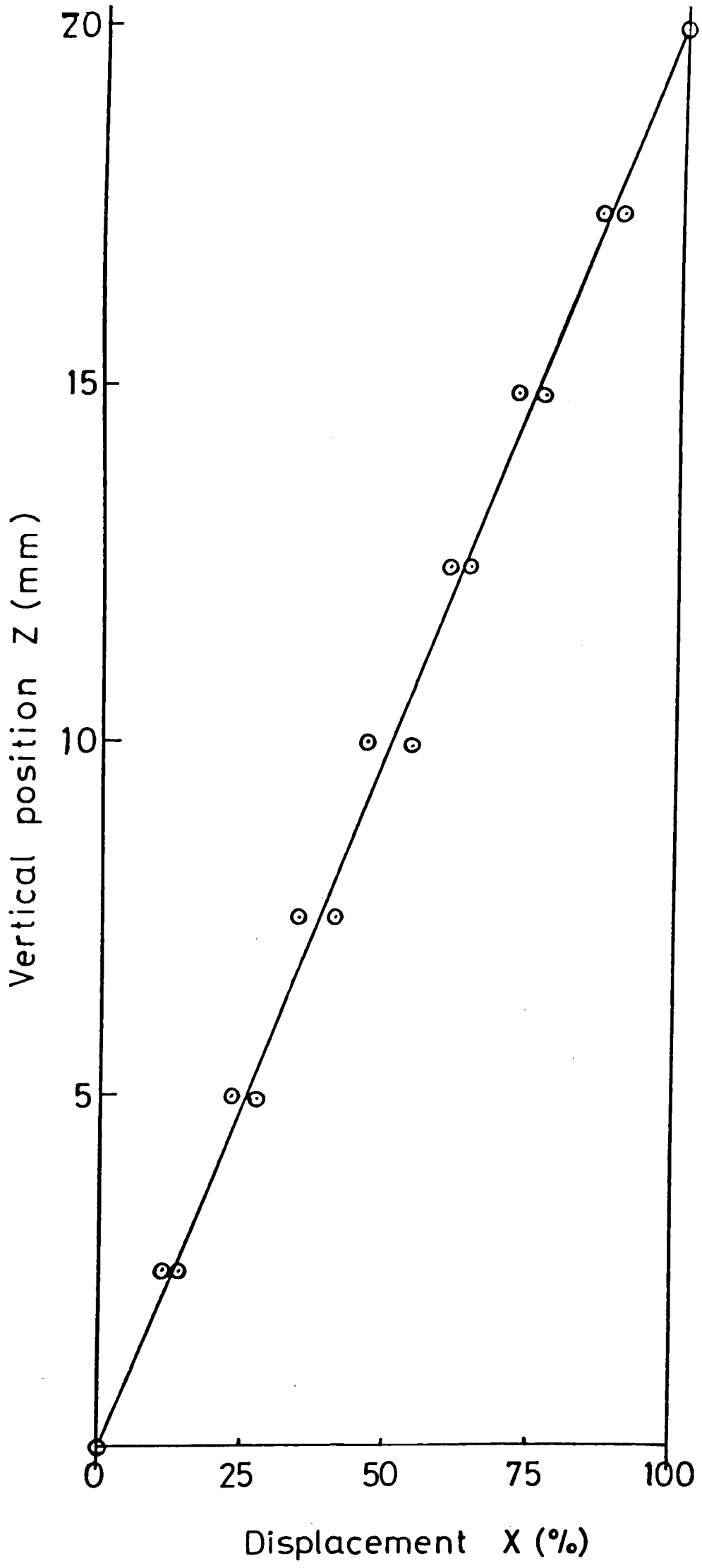


Fig.B.1. Glass Beads

Velocity profile and failure zone identification. Vertical position against circumferential tracer displacement as % of one revolution. Normal stress 20.7 kN/m^2, cell speed 5 r.p.m.

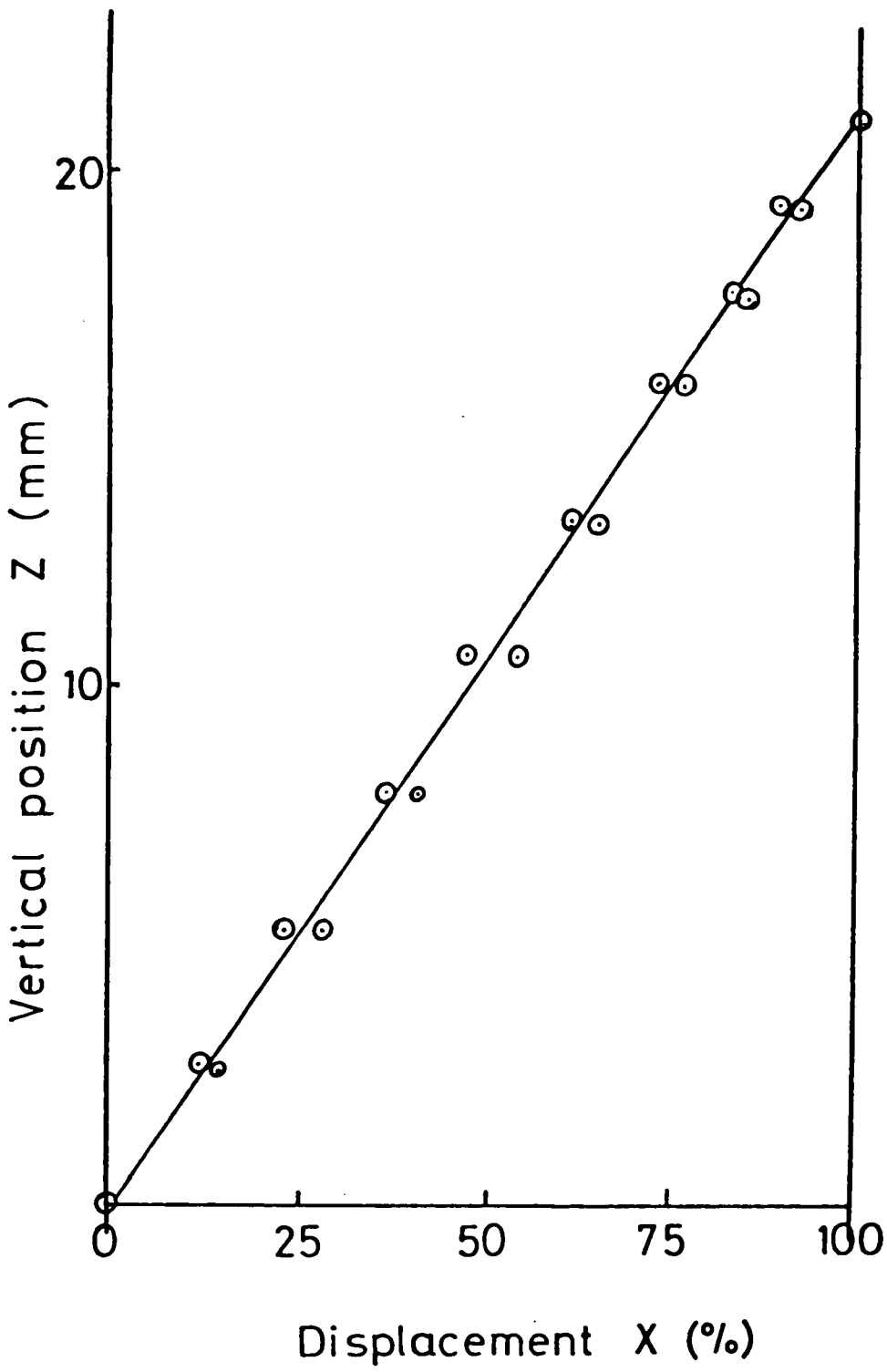


Fig.B.2. Molecular Sieve (175 gm)

Velocity profile and failure zone identification. Vertical position against circumferential tracer displacement as % of one revolution. Normal stress 20.7 kN/m^2, cell speed 5 r.p.m.

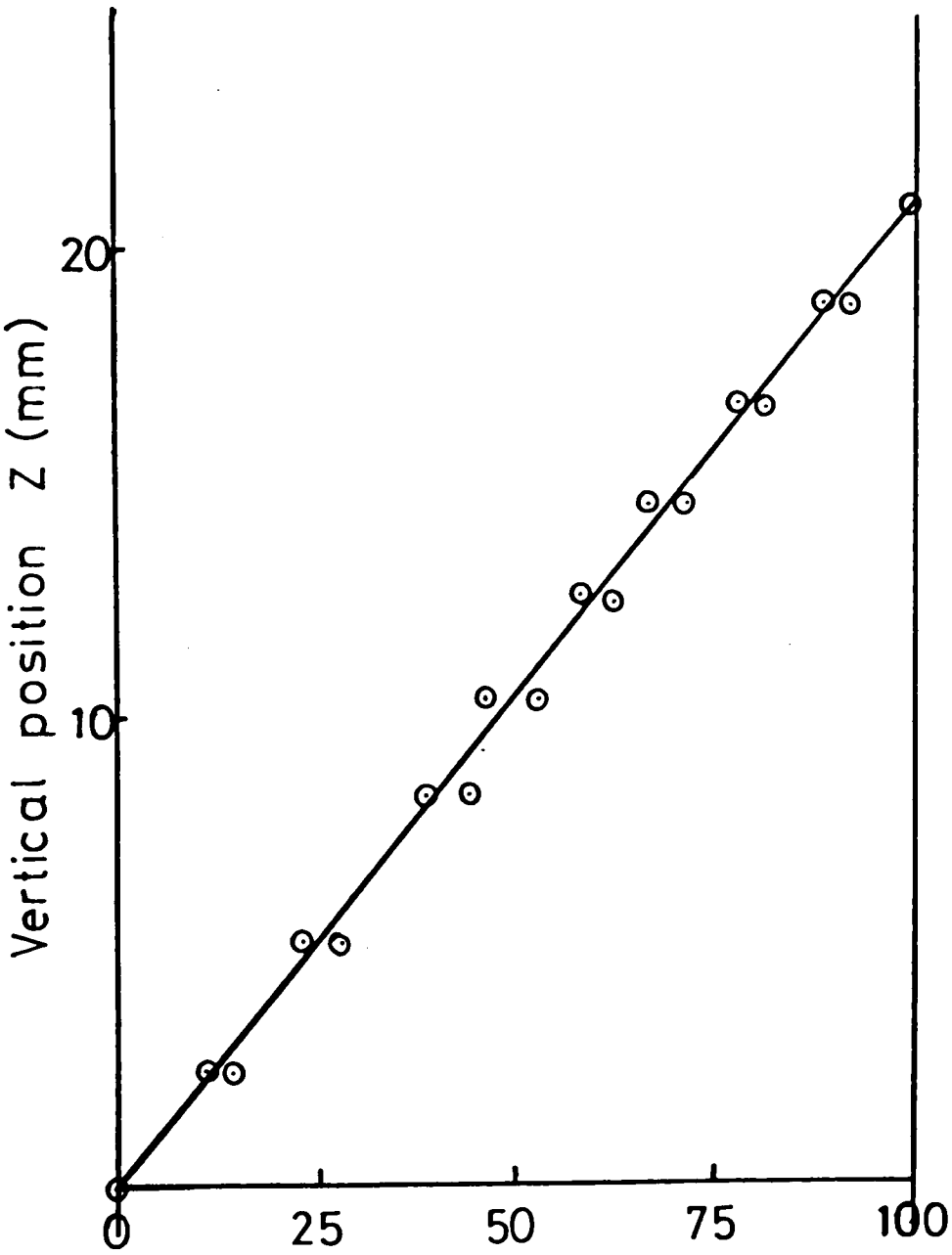


Fig.B.3. Granular Sodium Chloride (175 gm)

Velocity profile and failure zone identification. Vertical position against circumferential tracer displacement as % of one revolution. Normal stress 20.7 kN/m^2, cell speed 5 r.p.m.

failure zones and their behaviour under different process conditions in an annular shear cell, and his work has been useful in evaluating powder behaviour in the attrition cell. He showed that increasing the normal stress slightly reduced the depth of the failure zone. It was not possible to investigate this effect in the grinding cell due to attrition of powder samples. Stephens also showed that, when experiments were carried out under fixed conditions, the failure zone depth remained unchanged for many-fold increases in strain. At constant cell speed, the strain rate is higher for smaller materials and the failure zone depth correspondingly less. The strain rate is highest at the outer wall of the annulus since particle movement is greatest at the larger diameter. Lowering the cell speed caused the average strain rate to fall by the same ratio and the displacements remained unchanged.

From the experimental data, it is possible to calculate the average strain rate using the slope and intercept of the velocity profile.

As an example, for molecular sieve (Fig. B.2)

Gradient (dz/dx) = 21.0 mm for one revolution of the cell (failure zone depth);

Total cell movement = 440 mm in 12 seconds;

Strain per revolution = 21 rev^{-1};

Mean strain rate = 1.75 s^{-1}.

APPENDIX C

The F-test

From a normal distribution with variance σ^2, two random samples of size n_1 and n_2 are drawn and their variances s_1^2 and s_2^2 calculated. As s_1^2 and s_2^2 are both estimates of the same quantity σ^2, the ratio s_1^2/s_2^2 is expected to be close to unity provided that the samples are reasonably large. If repeated pairs of samples, size n_1 and n_2, are taken the ratio $F = s_1^2/s_2^2$ follows a distribution called the F-distribution. The distribution depends on two parameters which are the degrees of freedom of s_1^2 and s_2^2, given by (n_1-1) and (n_2-1).

The F-test is a significance test which is widely used for comparing different estimates of variance. The analysis of variance may either be one-way or two-way. In the one-way analysis of variance, which is used in the present tests, the total variation of the observations is partitioned into two components, one measuring the variability between group means and the other measuring the variation within each group. The two components are then compared by means of an F-test.

Results from experiments may be tabulated in the following way.

OBSERVATIONS		TOTAL	SAMPLE MEAN	SAMPLE VARIANCE
Treatment 1	$x_{11}, x_{12}, x_{13}, \ldots . x_{1n}$	T_1	$\bar{x}_1$	s_1^2
Treatment 2	$x_{21}, x_{22}, x_{23}, \ldots . x_{2n}$	T_2	$\bar{x}_2$	s_2^2
.	. . . . .	.	.	.
.	. . . . .	.	.	.
.	. . . . .	.	.	.
.	. . . . .	.	.	.
.	. . . . .	.	.	.
.	. . . . .	.	.	.
Treatment c	$x_{c1}, x_{c2}, x_{c3}, \ldots . x_{cn}$	T_c	$\bar{x}_c$	s_c^2

where

$$T_i = \sum_{n=1}^{n} x_{ij}$$

$$\bar{x}_i = T_i/n$$

$$s_i^2 = \sum_{j=1}^{n} \frac{(x_{ij} - \bar{x}_i)^2}{n-1}$$

The usual way to obtain the F-ratio is to calculate the following quantities and enter them in an analysis of variance table.

SOURCE OF VARIATION	SUM OF SQUARES	DEGREES OF FREEDOM	MEAN SQUARE
Between groups (between treatments)	$n \sum_{i=1}^{c} (x_i - \bar{x})^2$	c-1	s_B^2
Within groups (residual variation)	$\sum_{i=1}^{c} \sum_{j=1}^{n} (x_{ij} - \bar{x}_i)^2$	c(n-1)	s^2
Total variation	$\sum_{i=1}^{c} \sum_{j=1}^{n} (x_{ij} - \bar{x})^2$	cn-1	

The two mean squares, s_B^2 and s^2, are obtained by dividing the appropriate sum of squares by the appropriate number of degrees of freedom.

Then, the F-ratio $= s_B^2/s^2$

In all cases where reproducibility had to be ascertained, only the variation within groups was considered. Hence, s^2 provided a measure of the reproducibility of the duplicate runs carried out.

As an example, consider the column of results in Table 3.1.2 which gives the weight of ground product larger than 1.7 mm. It can be summarised as follows:

TREATMENT LEVELS (Variation of stress kN/m^2)	OBSERVATIONS (Duplicate runs weight in gm)	
	Run 1	Run 2
41.4	88.2	87.8
82.8	86.4	84.8
124	76.6	76.3
165	72.4	73.5
207	67.8	68.6
248	64.4	67.1

The analysis of variance table can then be formulated as explained above.

SOURCE OF VARIATION	SUM OF SQUARES	DEGREES OF FREEDOM	MEAN SQUARE
Between groups (between treatments)	822.835	5	164.567
Within groups (residual variation)	5.975	6	0.9958
Total variation	828.81	11	

The measure of reproducibility is given by the mean square of variation within groups (0.9958). This results in a standard

deviation of 0.998 for the weights considered, which indicates that the spread of values is small. Values of s for all other columns were obtained in an identical manner. These all showed that duplicate runs were reproducible.

The only instance where the variation between groups was considered was in Table 3.1.3 where it was useful in showing that there was little difference in attrition behaviour when the strain rate was varied. Here, an identical procedure was followed but the variation between groups was used and shown to be insignificant, thus confirming that strain rate did not influence the rate of attrition for that material.

APPENDIX D

The torque exerted by the motor was primarily monitored as an early warning against the cell jamming during experiments and causing damage to the annulus. The torque is a function of the applied normal stress and thus is a dependent variable of the system. It can be related to the normal stress through the internal angle of friction for the powder. It was not possible to measure the angle of friction independently for the different powders used and, as a result, the observed values of torque were not directly related to the normal stress.

However, it is possible to relate the torque to the applied shear stress on the powder. If an annulus of radius r and width δr is considered, the torque δT and shear stress τ are related by

$$T = 2\pi r^2 \delta r \tau$$

If r_1 and r_2 are the cell wall radii which would correspond to the limits of the shearing region

$$T = \int_{r_1}^{r_2} 2\pi r^2 dr \tau$$

If τ is assumed to be constant

$$T = \frac{2\pi}{3} \tau (r_2^3 - r_1^3)$$

Thus

$$\tau = \frac{3T}{2\pi (r_2^3 - r_1^3)}$$

The design of the cell, method of measurement and friction

between the walls and the powder may all affect the shear stress results which should only be regarded as estimates of the actual shear stress.

If the shear stress is plotted against strain (Fig. D.1), horizontal straight lines are obtained for all samples except for molecular sieve. Since the strain values correspond to between one and twenty-five revolutions of the cell, it is seen that the critical state was reached very quickly.

These experiments do not show whether a peak shear stress was reached at a fraction of one revolution of the cell, but it is reasonable to assume the absence of such a peak since the powder sample was loosely packed when initially charged to the cell (as no compacting loads were used). Even if a peak did occur, this would have been very close to the starting point of the runs. Stephens (1976) reports that such a peak occurred within one fifth of one revolution in his experiments and then the shear stress rapidly reached a minimum value. Thus experimental evidence shows that the runs were conducted when the shear stress was constant.

The only exception was molecular sieve material which only reached its critical volume after two revolutions of the cell. The reason for this is unclear; however, this is possibly due to the structure of the particles, since although an identical loading procedure was used, the porous nature of the granules may be significant. This warrants further study.

The variation in bed height before and after straining was measured. The bed height usually decreased after prolonged straining, a reduction

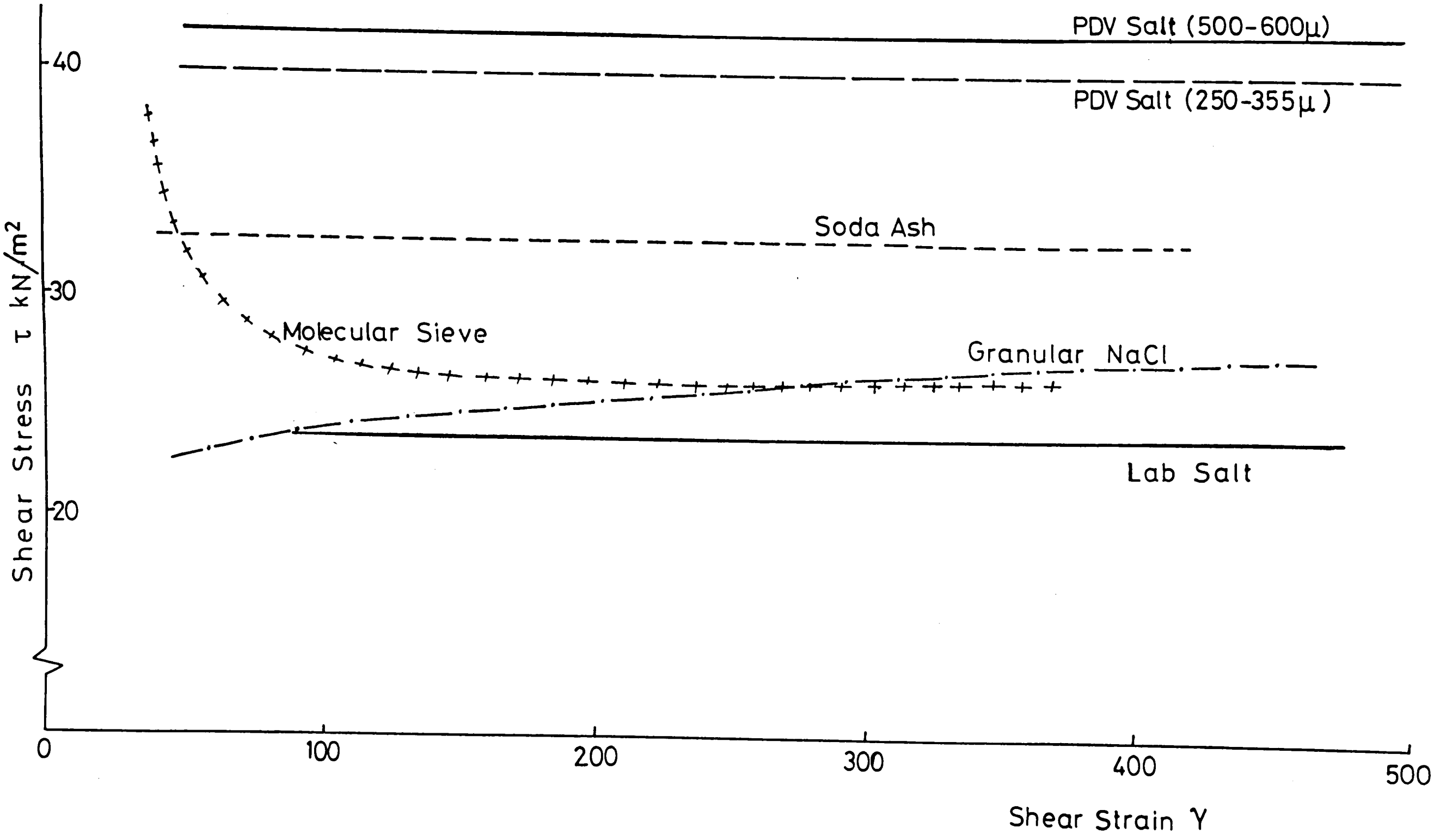
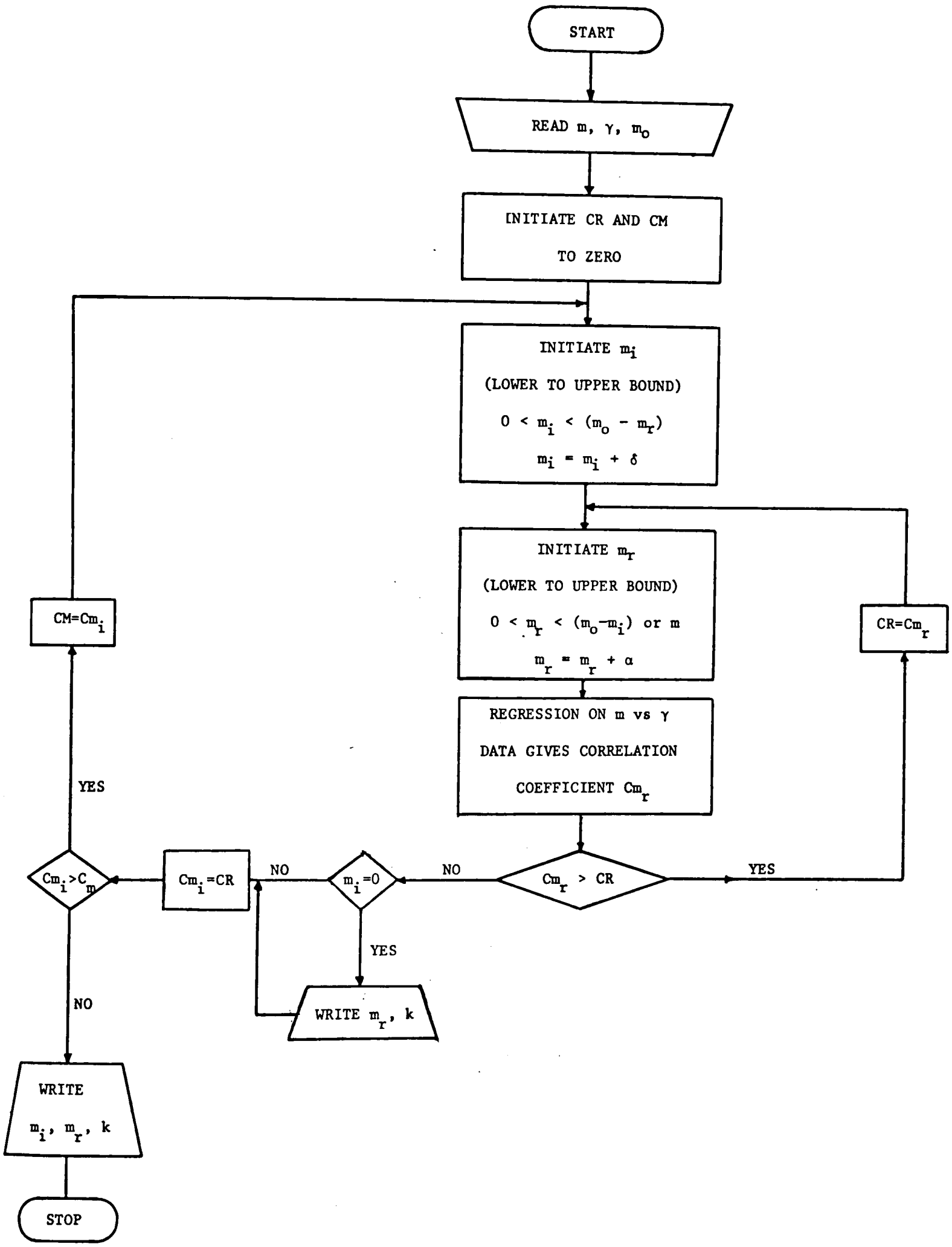


Fig. D.1. Variation of Shear Stress with Strain for materials used

of one particle diameter being observed for molecular sieve and between 0.5 - 0.75 particle diameters for the other material at a normal stress of $41.4 kN/m^2$ and twenty-five revolutions of the cell. This could be thought of as an effect due to particle degradation and repacking.

APPENDIX E



Flow Diagram for the Calculation of m_i, m_r and k.

APPENDIX F

Influence of Moisture Content on Attrition Rates of Silica Gel

Preliminary grinding experiments were carried out to investigate the effect of varying material properties by using silica gel crystals containing different amounts of moisture. 100 gm of sample material of sieve-cut between 1.4-1.7 mm was attrited at 41.4 kN/m^2 normal stress for up to twenty-five revolutions of the cell and the ground product separated using the following nest of sieves: 1.4 mm, 1.0 mm, 850 μm, 600 μm, 425 μm, 300 μm, 106 μm.

Results were plotted according to Gwyn and presented in Fig.F.1. The plot shows that increased moisture content results in greater attrition of the crystals. The gradient and intercept of the line are seen to increase at higher moisture levels, showing that particle attrition is greater when the water content is increased. Normal stress is also seen to increase the attrition rate, in common with observations made previously with other materials. Thus, these exploratory experiments show the potential of the machine to examine particle properties and their effect on attrition rates.

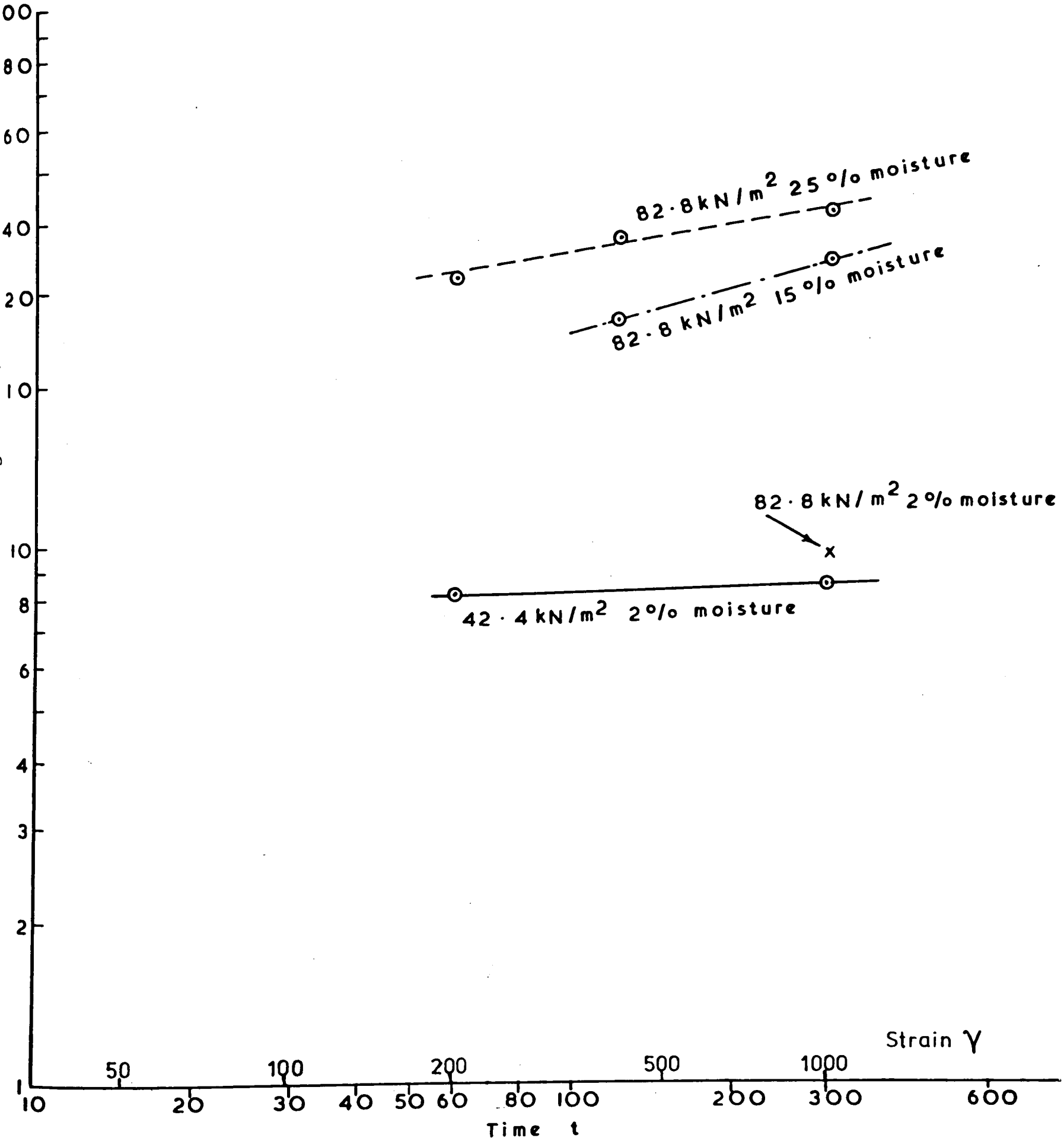


Fig. F.1. Silica Gel - Effect of Shear Strain on Attrition at different moisture levels

REFERENCES

ARCHARD, J.F. (1953), J. Appl. Phys., 24, 981.

ARCHARD, J.F., and HIRST, W. (1956), Proc. Roy. Soc., A 236, 397.

ARCHARD, J.F. (1957), Proc. Roy. Soc., A 243, 190.

AUSTIN, L.G. (1971), Powder Technol., 5, 1.

BILLAM, J. (1972), Stress Strain Behaviour of Soils, Roscoe Memorial Symposium, Univ. of Cambridge.

BISHOP, A.W., GREEN, G.E., GARGA, V.K., ANDRESSEN, A., and BROWN, J.D. (1971), Geotechnique, 21, 273.

BOWDEN, F.P., and TABOR, D. (1950), The Friction and Lubrication of Solids, Oxford University Press.

BRANSBY, P.L., BLAIR-FISH, P.M., and JAMES, R.G. (1971/72), Powder Technol., 5, 1.

BRIDGWATER, J., and BAGSTER, D.F. (1969), 3rd CHISA Congress, Marienbad, Czechoslovakia.

BRIDGWATER, J. (1972), ASME paper 72-MH-21.

BURWELL, J.T., and STRANG, C.D. (1952), J. Appl. Phys., 23, 18.

CAPES, C.E., and DANKWERTS, P.V. (1965), Trans. Inst. Chem. Engrs., 43, T116.

CAPES, C.E. (1976), Can. J. Chem. Eng., 54, 3.

CAPES, C.E. (1980), Particle Size Enlargement, Elsevier, Netherlands.

CARR, J.F., and WALKER, D.M. (1967/68), Powder Technol., 1, 369.

DRAHUN, J.A. (1978), D. Phil. Thesis, Univ. of Oxford.

DYSON, J., and HIRST, W. (1954), Proc. Phys. Soc., B67, 309.

EVANS, I. (1966), 3rd Congress of European Federation of Chem. Engrs., 6, 62.

FORSYTHE, W.L., and HERTWIG, W.R. (1949), Ind. Eng. Chem., 41, 1200.

GRIFFITH, A.A. (1920), Phil. Trans. R. Soc., A221, 163.

GWYN, J.E. (1969), A.I. Chem. E. J., 15, 35.

HERTZ, H. (1881), J. Math., 92, 156.

HOLM, R. (1946), Electrical Contacts, Springer-Verlag, Berlin.

HVORSLEV, M.J. (1937), Ing. Skrf. A., No. 45.

HVORSLEV, M.J. (1939), Proc. Amer. Soc. Test. Matls., 39, 999.

IRWIN, G.R. (1948), Fracturing of Metals, Am. Soc. Metals, Cleveland, 147.

JENIKE, A.W. (1961), Bulletin 108, Utah Engng. Expt. Stn., Univ. of Utah.

KAPUR, P.C., and FUERSTENAU, D.W. (1966), Ind. Eng. Chem. Proc. Des. Dev., 5, 5.

KAPUR, P.C. (1978), Advances in Chemical Engineering, Volume 10, Academic Press, New York.

KARABELAS, A.J. (1976), A.I. Chem. E.J., 22, 765.

KAYE, B.H. (1962), Ph.D. Thesis, Univ. of London.

KENDALL, K. (1978), Nature, 272, 710.

KICK, F. (1885), Das Gesetz der proportionalen Widerstande und seine Anwendung, Leipzig (Arthur Felix Edition).

LACEY, P.M.C. (1954), J. Appl. Chem., 4, 257.

MASON, J.S., and SMITH, B.V. (1972), Powder Technol., 6, 323.

MASON, J.S. (1975), Powtech '75, Heyden Press, London.

MEISSNER, H.P., MICHAELS, A.S., KEISER, R. (1966), Ind. Eng. Chem. Proc. Des. Dev., 5, 10.

MILLS, D., and MASON, J.S. (1978), Pneumotransport 4, California.

MOLERUS, O. (1975), Powder Technol., 12, 259.

NEWITT, D.M., and CONWAY-JONES, J.M. (1958), Trans. Inst. Chem. Eng., 36, 422.

NOVOSAD, J. (1964), Colln. Czech. Chem. Comm., 29, 2697.

OROWAN, E. (1949), Rep. Prog. Phys., 12, 185.

RITTINGER, P.R. (1867), Lebruch der Aufbereitungskunde, Ernst and Korn, Berlin.

ROSCOE, K.H. (1953), Proc. 3rd Int. Conf. Soil Mech., 1, 186.

ROSCOE, K.H., SCHOFIELD, A.N., and WROTH, C.P. (1958), Geotechnique, 8, 22.

ROSCOE, K.H. (1970), Geotechnique, 20, 129.

ROWE, P.W. (1962), Proc. Roy. Soc., A269, 500.

RUMPF, H. (1973), Powder Technol., 7, 145.

SASTRY, K.V.S., and FUERSTENAU, D.W. (1971), Proc. Inst. Briquetting Agglomeration, 12, 113.

SCARLETT, B., and TODD, A.C. (1968), J. Sci. Instrum., Series 2, 1, 655.

SCHÖNERT, K., and LESCHONSKI, K. (1975), Symposium on Communition and Air Classification, Univ. of Bradford.

SCOTT, A.M. (1974), D. Phil. Thesis, Univ. of Oxford.

SHERGOLD, F.A. (1946), Trans. Soc. Chem. Ind., 65, 245.

SHERRINGTON, P.J. (1969), Can. J. Chem. Eng., 47, 308.

SHERRINGTON, P.J., and OLIVER, R. (1981), Granulation, Heyden, London.

STEPHENS, D.J. (1976), D. Phil. Thesis, Univ. of Oxford.

SUH, N.P. (1973), Wear, 25, 111.

TIMOSHENKO, S.P., and GOODIER, J.N. (1970), Theory of Elasticity, McGraw-Hill, New York.

UNITED STATES ENVIRONMENTAL PROTECTION AGENCY (1980), Energy/ Environment Research and Development Program Report.

WEI, J., LEE, W., and KRAMBECK, F.J. (1977), Chem. Eng. Sci., 32, 1211.

GB 2047118 A - PARAMANATHAN, B.K., BRIDGWATER, J., ICI Ltd. Patent on design details of Attrition Cell.

B.S.410 (1976), Specification for Test Sieves.

B.S. 1796 (1976), Method for Test Sieving.

I.S.O.565 (1972), Test Sieves, Woven Metal Wire Cloth and Perforate Plate. Nominal Sizes of Apertures.

I.S.O.2591 (1973), Test Sieving.